DYNAMICS OF HEAVY ION COLLISIONS AT INTERMEDIATE ENERGIES

A THESIS

submitted to the

THAPAR UNIVERSITY, PATIALA

for the degree of

DOCTOR OF PHILOSOPHY

IN THE FACULTY OF SCIENCE

By

Sanjeev Kumar

Regn. No. 90712002

SCHOOL OF PHYSICS AND MATERIALS SCIENCE

THAPAR UNIVERSITY

PATIALA-147004, PUNJAB,

(INDIA)

SEPTEMBER 2010

" Your arms were always open when I needed a hug. Your heart understood when I needed a friend. Your gentle eyes were stern when I needed a lesson. Your strength and love has guided me and gave me wings to fly."- Sarah Malin .

Dedicated to

My Beloved Mother

who left this materialistic world on 17^{th}*, September, 2004.*

CERTIFICATE

This is to certify that the thesis entitled " **DYNAMICS OF HEAVY ION COLLISIONS AT INTERMEDIATE ENERGIES**" being submitted by **Mr. Sanjeev Kumar** for the fulfillment of the requirements for the award of Degree of Doctor of Philosophy in the School of Physics and Materials Science, Thapar University, Patiala, is a record of the candidate's own work carried out by him under my supervision. The matter presented in this thesis has not been submitted in part or full for the award of any degree in any university or institute.

Supervisor

SKumar
20/9/2010

Dr. Suneel Kumar
Assistant Professor
School of Physics and Materials Science
Thapar University, Patiala-147004
Punjab (India)

Acknowledgments

First and foremost, I would like to express my most sincere gratitude to my thesis supervisor **Dr. Suneel Kumar** *Assistant Professor, Thapar University, Patiala.* I started my Ph.D. pursuit four years ago, with absolute no experience in theoretical research. It is the enthusiasm he has toward research that attracted me into the field of heavy-ion reactions in the first place. His intuition and persistency are the key reasons I could successfully finish each of the research topics. He is a unique combination of great intellects and genuine caring for those persons for whom he has some responsibility. I was very fortunate to be one of these people. To me, he is not only a world class advisor, but also an influential mentor. He is the source of endless inspiration even during the most stressful times. His guidance, support, vision, and friendship will be a long-lasting influence in my professional and personal life.

Special thanks go to **Dr. Rajeev K. Puri** *Associate Professor, Panjab University, Chandigarh* for his enthusiasm. He has especially contributed a lot to this thesis during the data analysis and revising my thesis. He is an inexhaustible source of intellectual and creative energy. His good sense in finding general physics laws to explain complicated theoretical data was an excellent lesson to me. I am extremely impressed by his ability to get an intuitive feel of the most difficult ideas. It is a fortunate for me being associated with them in research field.

I offers special thanks to **Prof. O.P. Pandey**, *Head, School of Physics and Materials Science, Thapar University, Patiala*, for providing all the necessary facilities in the department and fellowship as a teaching assistant well in time. Also, I wishes to express thankfulness to all the faculty and staff of the School for their kind support. I am thankful to Prof. K.K. Raina, Deputy Director, and Prof. N.K. Verma, Dean Student Welfare, for their encouragement and constant moral support to accomplish this task. I acknowledges the useful suggestions of the members of my doctoral committee Dr. Rajesh Khanna and Dr. Manoj Kumar Sharma. Thanks to Dr. Susheel Mittal, Dean, research and sponsered projects for providing the possible research facilities here at Thapar University campus. Many thanks are due to head of computer science department, Thapar University, Patiala for providing me the supercomputing facility. Special thanks to **Dr. Kulvir Singh** for providing me useful and valuable tips for research as a PG incharge.

I am fortunate enough to have worked with my lab mates Mrs. Varinderjit Kaur, Mrs. Shefali Kanwar, Rajni Bansal , Gudveen Sawhney, Karan Vinayak and many others research scholars here at Thapar University, Patiala. I am thankful to them for their sincere help

cooperation. I acknowledges with thanks the co-operation and encouragement extended by his friends and colleagues in the Heavy Ion Reactions Theory group at Chandigarh, particularly, Yogesh Vermani, Rajeev Chugh, Ishwar Dutt, Sakshi and Supriya for their fruitful discussions and novel views. I am highly thankful to Dr. Amandeep Sood from Nantes Subatech, France for valuable discussions on IQMD model for studying the isospin dependence of the equation of state.

I would love to mention my close and ever cheerful friends **Amit Awasthi, Dr. Manpreet (now in Hong-Kong) , Dinesh Kumar, Ravi Shukla, Nirankar Singh, Mukesh, Achal, Amar** for moral support and all the fantastic moments we spent together. Here, I will not forgot to thank Dr. Rajesh from school of chemistry for useful suggestions, moral support and joyous company during my entire Ph. D. work.

A special word of thanks to my seniors Dr. Pankaj, Mr. Ankush Pathania, Mr. Vishal, Mr. Akshay Kumar, Santosh Pathak, Kamal, for their help and encouragement.

Of course, none of this could have happened without the support of my grandparents, parents, **Mr. Kamal Raj and Mrs. Tara Devi**, my uncle and aunti, **Mr. Raj Kumar Sharma and Mrs. Sarla Sharma**, my sisters **Mrs. Anjana Sharma, Salini and Rachna**, jiju ji, **Mr. Naresh Kumar Sharma**, my brothers **Sahil**, who always gave me an inspiration to achieve the goal of my life. They have been my backbone in all the difficult phases of my life. The smiling faces and tantrums of kids, Abhi and vaisanavi, have always made me refreshing.

Special thanks are due to my in-laws Mr. Prem Lal, Mrs. Santosh Kumari, Ambika and Ashish for their unconditional love and support.

Last, but not the least, I records a special note of admiration and gratitude for **my loving wife Neelam Kumari** whose interest was ignored during the course of this work. Her patience , corporation and understanding paved the way to achieve this academic goal.

The financial assistance in the form of fellowships from **Council of Scientific and Industrial Research (CSIR)**, New Delhi, Govt. of India and then from **Thapar university, Patiala** is greatly acknowledged.

I feels that the chain of gratitude would be definitely incomplete without thanking the Almighty, the prime mover, for inspiring and guiding me to complete this task successfully.

Date : September 2010
Patiala

(Sanjeev Kumar)
20/9/2010

List of Publications :

A. Journals :

1. Medium mass fragments production due to momentum dependent interactions.
   Sanjeev Kumar, Suneel Kumar, and Rajeev K. Puri,
   Physical Review C 78, 064602 (2008).

2. Effect of symmetry energy on nuclear stopping and its relation to the production of light charged fragments.
   Sanjeev Kumar, Suneel Kumar, and Rajeev K. Puri,
   Physical Review C 81, 014601 (2010).

3. Elliptical flow and isospin effects in heavy ion collisions at intermediate energies.
   Sanjeev Kumar, Suneel Kumar, and Rajeev K. Puri,
   Physical Review C 81, 014611 (2010).

4. A Comparative study of model ingredients: fragmentation in heavy-ion collisions using quantum molecular dynamics.
   Sanjeev Kumar and Suneel Kumar,
   Pramana Journal of Physics 74, 731 (2010).

5. Systematic study of system size dependence of global stopping: Role of momentum dependence interactions and symmetry energy.
   Sanjeev Kumar and Suneel Kumar,
   Chineese Physics Letter 27, 062504 (2010).

6. Experimental balance energies and isospin-dependent nucleon-nucleon cross-sections.
   Sanjeev Kumar, Rajni and Suneel Kumar,
   Physical Review C 82, 024610 (2010).

7. Rapidity distribution as a probe for elliptical flow at intermediate energies.
   Sanjeev Kumar and Suneel Kumar,
   Physical Review C (under review).

8. Influence of coulomb interactions on balance energy and mass-asymmetry in heavy-ion collisions.
   Sanjeev Kumar, Varinderjit Kaur and Suneel Kumar,
   Central European Journal of Physics (under review).

9. Sensitivity of elliptical flow in intermediate energy heavy-ion collisions.
   Sanjeev Kumar and Rajeev Chugh,
   Physica Scripta (under review).

10. Dynamics of multifragmentation at the transition energies for $A \leq 4$ particles.
    Sanjeev Kumar, Suneel Kumar, and Rajeev K. Puri,
    Physical Review C , to be submitted.

B. Symposia/Workshops/Conferences:

11. Effect of equation of state on nuclear matter.
    Sanjeev Kumar and Suneel Kumar,
    National Conference on Emerging Trends in Engineering Materials, Feb. 1-3, Thapar University, Patiala (Punjab), p. 33 (2007).

12. Effect of equation of state on multifragmentation at intermediate energies.
    Sanjeev Kumar and Suneel Kumar,
    International Nuclear Physics Conference, June 3-8, Tokyo, Japan, QW-236 (2007)

13. Simulation of symmetric collisions with momentum dependent interactions.
    Sanjeev Kumar and Suneel Kumar,
    International Conference on Modeling and Simulation, August 27-29, Coimbatore Institute of Technology, Coimbatore (INDIA), **Vol.1**, p. 30 (2007).

14. Large cross section results in production of heavy fragments.
    Sanjeev Kumar and Suneel Kumar,
    52^{nd} DAE Symposium on Nuclear Physics, **Vol. 52**, p. 491 (2007) (2^{nd} Best Poster).

15. Study of elliptical flow at intermediate energies.
    Sanjeev Kumar and Suneel Kumar,
    11^{th} Punjab Science Congress, p. 38 (2008).

16. Isospin effects on the observables in heavy ion collisions.
    Sanjeev Kumar, Suneel Kumar, and Rajeev K. Puri,
    National Seminar on Advances in Physics, Feb 28- March 1, Panjab University, Chandigarh (2008).

17. Isospin effects on the system size dependence of elliptical flow at intermediate energies.
    Sanjeev Kumar, Suneel Kumar, and Rajeev K. Puri,
    Zakopane Conference on Nuclear Physics, September 1-7, Poland (2008).

18. On the role of symmetry energy in nuclear stopping: analysis of systems size effects.
    Sanjeev Kumar, Suneel Kumar, and Rajeev K. Puri,

53^{rd} DAE symposium on Nuclear Physics, **Vol. 53**, p. 571 (2008).

19. Impact Parameter dependence of momentum quadrupole in symmetric reactions.
    Sanjeev Kumar, Suneel Kumar, and Rajeev K. Puri,
    53^{rd} DAE symposium on Nuclear Physics, **Vol. 53**, p. 569 (2008).

20. Effect of Coloumb interactions on Ca isotopes and fragmentation.
    Sanjeev Kumar, Suneel Kumar, and Rajeev K. Puri,
    3^{rd} Chandigarh Science Congress (2009)

21. Isospin effects on $_{44}Ru^{96}$ + $_{44}Ru^{96}$ and $_{40}Zr^{96}$ + $_{40}Zr^{96}$ in intermediate energy heavy-ion collisions.
    Sanjeev Kumar, Suneel Kumar, and Rajeev K. Puri,
    IWND09, August 22-25, Shanghai, China.

22. Light charged particles as a probe for symmetry energy and global stopping.
    Sanjeev Kumar, Suneel Kumar, and Rajeev K. Puri,
    Indian Nuclear Society seminar on Nuclear Technology for Sustainable Development, Oct. 10-11, Thapar University, Patiala, (India)(Best Poster Award) (2009).

23. A comparative study of excitation function of elliptical flow with experimental findings and system size dependence
    Sanjeev Kumar, Suneel Kumar, and Rajeev K. Puri,
    International Symposium on Nuclear Physics, December 08-12, BARC, Mumbai, **Vol. 54**, 446 (2009).

24. Isotropic cross-sections and balance energy.
    Rajni Bansal, Sanjeev Kumar, Suneel Kumar, and Rajeev K. Puri,
    National theme workshop on nuclear reaction mechanism, March 17-19, Panjab University, Chandigarh (2010).

25. Isospin effects on elliptical flow at intermediate energies.
    Sanjeev Kumar, Suneel Kumar, and Rajeev K. Puri,
    National theme workshop on nuclear reaction mechanism, March 17-19, Panjab University, Chandigarh p. 30 (2010).

26. Effect of isospin dependent cross sections on the transverse in-plane flow at intermediate energy.
    Suneel Kumar, Rajni Bansal, Sanjeev Kumar, and Rajeev K. Puri,
    International Nuclear Physics Conference, July 04-09, University of British Colombia, Vancouver, Canada (2010).

Contents

List of Figures

List of Tables

ABSTRACT

The aim of the present work is to study the fragmentation, collective flow and nuclear stopping in heavy-ion collisions using the dynamical microscopic theory and compare the results with experimental data. The theoretical investigations are carried out using microscopic *quantum molecular dynamical* (QMD) and *isospin-dependent quantum molecular* (IQMD) model. We aim to discuss the role of model ingredients, momentum dependent interactions, different nucleon-nucleon cross sections, in fragments distribution for symmetric and asymmetric colliding nuclei. An attempt to understand the role of symmetry energy and momentum dependent interactions on elliptical flow, nuclear stopping and thermalization reached in heavy-ion collisions, will also be discussed.

The present thesis is divided into following seven chapters.

Chapter 1 presents the general introduction of the present work. The importance of heavy-ion collisions at intermediate energies is discussed. It outlines the status of the available experimental attempts for multifragmentation and collective flow by different collaborations, at MSU (USA), GANIL(France), BNL(USA), University of Arizona (USA), Texas (USA), INFN (Italy) and GSI(Germany). The attempts of different theoretical models like Statistical Multifragmentation Model (SMM), Percolation, Lattice Gas Model, Expanding Emitting Source (ESS), Time Dependent Hartree Fock (TDHF) , Vlasov-Uehling-Uhlenbeck (VUU) , QMD and IQMD for multifragmentation and collective flow are also presented.

Chapter 2 gives the detail of various theoretical models used in literature to study the phase space of nucleons in heavy-ion reactions and clusterization algorithms. This chapter is divided mainly in three parts. In the first part, the different theoretical models used to study heavy-ion reactions without isospin effect, are discussed. On the other hand, second part consists of different theoretical models used to study heavy-ion collisions with isospin effects. These models are the primary models which gives the phase space of the nucleons. The third part presents the different secondary models used to analyze the phase space of

nucleons generated by the primary models. We shall discuss the QMD, IQMD model in detail, while, MST, MSTM and SACA are discussed in brief. The detail of MST, MSTP and SACA is given where they are used.

In **chapter 3**, we discuss the importance of momentum dependent interactions in explaining the multifragmentation in symmetric reactions of $_{20}Ca^{40} + _{20}Ca^{40}$, $_{28}Ni^{58} + _{28}Ni^{58}$, $_{41}Nb^{93} + _{41}Nb^{93}$, $_{54}Xe^{131} + _{54}Xe^{131}$, $_{68}Er^{167} + _{68}Er^{167}$, $_{79}Au^{197} + _{79}Au^{197}$ and $_{92}U^{238} + _{92}U^{238}$ by comparing our results with static equation of state in QMD model. We find that the inclusion of momentum dependent interactions leads to less freeze-out density and number of collisions in all colliding systems as well as at all colliding geometries. This is due to the repulsive nature of the momentum dependent interactions, which further leads to the radial expansion of the matter. Moreover, it is also observed that at higher incident energies momentum dependent interactions are able to break-up the initial correlations among nucleons, which was earlier not possible with static equation of state. This leads to the decrease in the production of heaviest fragment A_{max} and enhancement in the production of medium mass fragments in the presence of momentum dependent interactions.

The system size effects are found to vary with reaction parameters, incident energies and momentum dependent interactions. The multiplicity of medium mass fragments can be parameterized in term of a power law. This is true for a wide range of impact parameters and incident energies considered here. However, the parameter τ does not have unique value. At low incident energies, the parameter τ is close to 2/3 suggesting the dominance of mean field that scales as $A^{2/3}$. On the other hand, no physical correlation is observed at higher incident energies for central collisions.

In **chapter 4**, we discuss the importance of different nucleon-nucleon cross sections in multifragmentation by comparing our theoretical results of QMD model with the experimental findings of ALADIN (for $_{79}Au^{197} + _{79}Au^{197}$ at incident energies of 100, 400, 600 and 1000 MeV/nucleon) and NSCL collaborations (for $_{10}Ne^{20} + _{13}Al^{27}$, $_{18}Ar^{40} + _{21}Sc^{45}$, $_{36}Kr^{84} + _{41}Nb^{93}$ and $_{54}Xe^{131} + _{57}La^{139}$ at incident energies between 20 and 150 MeV/nucleon)

in the presence of MDI. We also employ different technical model ingredients such as Gaussian width (L), Clusterization distance (R_{Clus}), equations of state (soft [S] and hard [H]) and different clusterization algorithms etc. We find that both the MDI and the large nucleon-nucleon cross-sections help to improve the agreement with experimental data. Interestingly, the same conclusion is also observed when one consider the different model ingredients like Gaussian width (L), Clusterization distance (R_{Clus}), clusterization method as well as different equations of state. It means that the effect of different NN cross sections is of the order of one obtained with different model ingredients. All model ingredients are found to affect the fragmentation process in a similar pattern.

In **chapter 5**, we study the isospin effect in term of symmetry energy on the elliptical flow and in-plane to out-of-plane emission of elliptical flow in mid-rapidity region by using IQMD model. For this, in the first instance, we analyzed the transverse momentum dependence of elliptical flow for different fragments for the reactions of ${}_{20}Ca^{40} + {}_{20}Ca^{40}$, ${}_{54}Xe^{131} + {}_{54}Xe^{131}$ and ${}_{79}Au^{197} + {}_{79}Au^{197}$. To see the isospin effect due to symmetry energy, we discussed the detailed transverse momentum dependence of elliptical flow for the reactions of ${}_{40}Zr^{96} + {}_{40}Zr^{96}$ and ${}_{44}Ru^{96} + {}_{44}Ru^{96}$ (having same mass number and different proton number) in the presence of Coulomb interactions and symmetry energy. Moreover, to observe the transition from in-plane to out-of-plane emission, excitation function of the elliptical flow is elaborated for the reactions mentioned above and the results are also compared with the experimental findings of the INDRA, FOPI and PLASTIC BALL collaborations. Our results shows that LCP's exhibit isospin effects in the mid-rapidity region. The elliptical flow is found to show a transition from in-plane to out-of-plane at a certain beam energy in mid-rapidity region, while no such transition is observed when integrated over entire rapidity region. The results are found in better agreement with the experimental findings of INDRA, FOPI and PLASTIC BALL collaborations in the presence of static hard equation of state for Z $\leq$ 2 particles. The need of momentum dependent interactions is discussed for the protons. This transition energy is found to decrease with the composite mass as well as with the size of the fragment. The transition energy is further parameterized in term of mass power law.

The nuclear stopping as well as multifragmentation are studied in the literature separately as two processes, many times. A very few attempts were made to correlate the nuclear stopping and fragmentation process. In **chapter 6**, we try to correlate the production of fragments with nuclear stopping in the presence of symmetry energy and study the effect of MDI in the presence of symmetry energy on nuclear stopping by using IQMD model. We observe that the degree of stopping depends weakly on the symmetry energy and strongly on the isospin-dependent cross section. On the other hand, the symmetry energy and isospin-dependent cross section has an effect of the order of more than 10% on the emission of LCP's. It means that nuclear stopping and LCP's can be used as a tool to get the information of isospin-dependent cross section. Interestingly, the LCP's emission in the presence of symmetry energy is found to be highly correlated with the global stopping. It is also observed that the maximum stopping is obtained for heavier systems in central collisions in the presence of symmetry energy and isospin dependent cross section, without momentum dependent interactions. This is due to the suppression in binary collisions in the presence of momentum dependent interactions.

Finally, we will summarize our results along with an outlook in chapter 7.

Chapter 1

Introduction

" When you see something that is technically sweet, you go ahead and do it and you argue about what to do about it only after you have had your technical success. That is the way it was with the atomic bomb.".....*Julius Robert Oppenheimer* (1904-1967).

1.1 Importance of the heavy-ion collisions at intermediate energies

The science of nuclear physics deals with the properties of "nuclear matter" which makes up the massive centers of the atoms accounting 99.95 percent of the matter. The main interest revolves around the structure of nucleus. One is also interested to understand the interactions among nucleons (protons and neutrons). The understanding of various nuclear phenomena is also vital for the understanding of the mechanism behind the nuclear reactions that fuel the stars, including our sun.

Another domain of the interest in nuclear physics is the properties of nuclear matter at high densities, that is of magnitude higher than the ordinary matter we encounter everyday. The typical baryon density of nuclear matter is of the order of $\rho = 0.17\ fm^{-3}$, which, when converted into mass density, is about $10^{27}\ g/cm^3$. For comparison, the density of water is $\rho(water) = 1\ g/cm^3$, and even the density of the most dense metal is $\rho(Os) = 22.5\ g/cm^3$ only. When high density is generated in reactions, the temperature of the matter is also often quite high. The temperature often reaches the level of hundreds of MeV. Again this is not the ordinary temperature. For example, if we convert the scale of MeV to regular temperature scale, 1 MeV is equivalent to about 10 billion degree Kelvin. Room temperature oftenly is about 300 K and even the surface of the sun is only 6000 K.

Fig.1.1 shows schematic phase diagram of hot dense nuclear matter. The X-axis represents the normal density, whereas temperature is shown on Y-axis. The normal nuclear matter (at $\rho = \rho_0$, T = 0) represents a liquid phase. The liquid-gas phase (LGP) transition region at the lower left corner of the figure is characterized by the temperature below $\approx$ 15 MeV and densities ($\frac{\rho}{\rho_0} < 1$)[1]. The region of very high density and temperature corresponds to the Quark-Gluon Plasma phase (QGP)[2, 3, 4]. The hadron gas (HG) phase exists at intermediate temperatures and densities. The neutron star (NS) density region extends from the low density upto more than 10 times the normal nuclear matter density. The typical temperatures are less than 10 MeV for newly born neutron stars and less than 0.01 MeV for cold neutron stars. The two lines that separates the QGP phase from the HG phase is the phase co-existence and/or transition region[5]. One of the theories predicts a cross-over phase transition at lower densities, a first order phase transition at higher density and a critical point (the solid square symbol) that separates the two phase transitions [5]. The chemical freeze out points reached at SPS and RHIC experiments[5] are plotted here as open symbols. The head-on collisions are likely to follow the arrows on the solid line, starting at cold normal nuclear matter ($\rho = \rho_0$, T = 0 MeV)[6]. The maximum density and temperature achieved are determined by the incident energy. After the maximum compression, the compressed matter expands and cools down as indicated by the dashed lines. Some of the low energy reactions will dive into the liquid-gas phase transition. The high energy systems, on the other hand, could enter the phase of QGP.

In the study of hot dense matter, heavy-ion reactions offer excellent opportunities compared to other methods. Though, the dense matter exists in the neutron stars, unfortunately, only indirect information can be extracted from the astrophysical observations. The QGP and dense hadron gas phases existed in the early stage of the evolution of universe (about 15 billion years ago) are inaccessible today. The nuclear structure studies have provided vital information about the nuclear interactions[8, 9], fusion-fission[8, 10], cluster radioactivity[11] as well as halo nuclei [12]. These studies take place around normal densities and at low temperatures. The heavy-ion reaction, during which the matter undergoes through compression and expansion stages, are true testing grounds for the hot and dense nuclear matter. The maximum compression in a heavy-ion reaction could be few times the normal nuclear matter

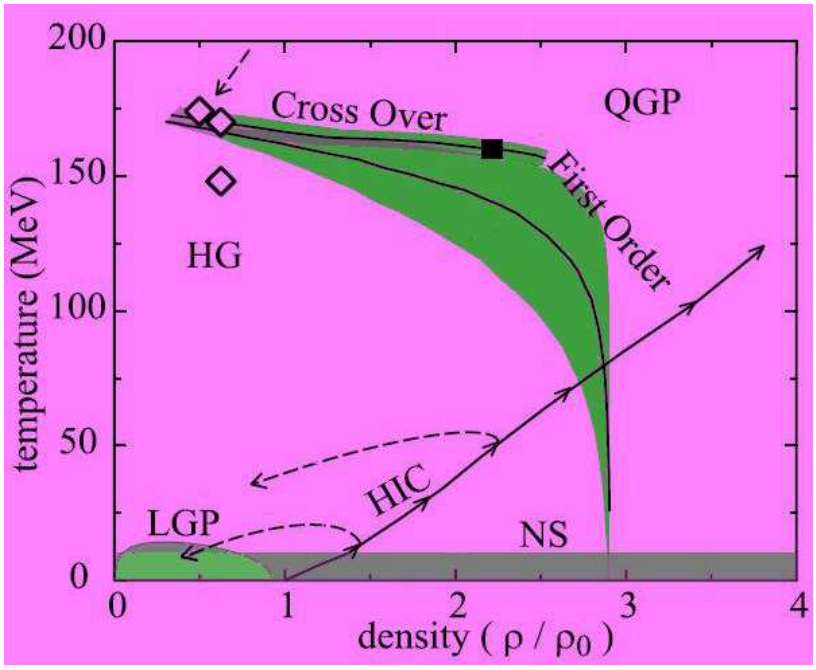

Figure 1.1: Schematic phase diagram for the hot dense matter. The theoretical predictions are also displayed at all temperatures. The only experimentally known point is $\rho = \rho_0$, T = 0. The head-on heavy-ion collisions will likely follow the arrows on the solid line. The maximum density and temperature achieved are determined by the incident energy. After the compression to maximum density, the reaction system expands and cools as indicated by dashed lines. This figure is taken from Ref. [7].

density in head-on collision, and could possibly produce QGP at higher incident energies. The expansion of nuclear matter (after compression stage) usually leads to freeze out for the interactions at sub-normal densities ($\rho < \rho_0$). The freeze-out temperature and density could be in the phase transition region (QGP to HG phase transition, or LGP), or in HG phase.

The specific region of the phase-diagram and corresponding physics depends crucially on the incident energy. Thus, the highest energy reaction experiments at Relativistic heavy-ion collider (RHIC) and Large Hadron Collider (LHC) explore the most dense matter, where quarks and gluon's become the elementary degree of freedom and quantum chromodynamics (QCD) is the basic theory. The reactions at intermediate energies are violent enough to excite the system to a very high temperature leading to the break-up of the initial correlations among nucleons, but not enough to break the internal structure of nucleons or hadrons. The description of the interactions with only hadrons and mesons is sufficient for

the intermediate energy reactions. The work in this thesis is concentrated on the heavy-ion reactions at intermediate energies.

The reactions at intermediate energies involve many topics of interest including nuclear equation of state (NEOS), multifragmentation, collective flow and lately, the isospin physics. The nuclear equation of state describes the energy-density relation in nuclear matter. The prediction of nuclear equation of state is an important question. The multifragmentation, collective flow and the isospin physics are the primary tools for studying the EOS. Here, I will discuss briefly each of these phenomena, which are the primary phenomena at intermediate energies.

1.2 Nuclear Equation Of State(NEOS)

An equation of state (EOS) is a nontrivial relation between thermodynamic variables characterizing a medium. While the term is used in its singular form in nuclear physics, actually different relations are of interest, such as between pressure P and baryon density ρ and temperature T, P(ρ,T), or chemical potential and T, P(μ,T), between energy density e and ρ and T, e(ρ,T), etc. Some of the relations are fundamental under certain conditions, i.e. all other relations may be derived from them (such as from e(ρ) at T =0).

The nuclear EOS is of interest because it affects the fate of the Universe at times t $\geq 1\mu$s from the Big Bang and because its features are behind the supernova explosions. Moreover, its features ensure the stability of neutron stars[13]. Through its effects on the evolution of the Universe, on supernovae explosions, and on neutron-star collisions, the EOS affects nucleosynthesis. Moreover, the EOS impacts central reactions of heavy nuclei. Finally, the form of the EOS constraints hadronic interactions and the non-perturbative quantum chromodynamics (QCD).

The advances in the determination of the nuclear EOS have been, generally, difficult. The elementary information comes from the Weizsäcker binding-energy formula and from the systematics of nuclear density profiles. The Weizsäcker formula separates out the contributions to the energy associated with nuclear interactions, the interior and surface of nuclei, the contributions associated with isospin asymmetry and with Coulomb interactions, and

the shell correction, given as:

$$-B(A,Z) = \quad -16MeV/nucleon + a_s A^{2/3} + a_a \frac{(A-2Z)^2}{A} + a_c \frac{Z(Z-1)}{A^{1/3}} - B_{p,s}. \quad (1.1)$$

Nuclear densities, obtained from charge densities multiplied by mass to charge number ratio, are seen to reach the same value, $\rho_0 = 0.17\ fm^3 \simeq 1/(6fm^3)$, for a wide range of nuclear masses[14]. We conclude that the energy per nucleon in a uniform symmetric nuclear matter at T = 0, in the absence of Coulomb interactions, has a minimum at the normal density ρ_0 with the energy value, relative to nucleon mass, of -16 MeV, from the volume term in the binding energy formula, see Fig.2.2.

The next nontrivial feature of the energy per nucleon is its curvature in the dependence on ρ, around ρ_0. This curvature is commonly quantified in terms of the so-called nuclear incompressibility, with an unusual numerical factor[14]:

$$\kappa \ = \ 9\rho_o^2 \frac{d^2}{d\rho^2}\left(\frac{E}{A}\right). \quad (1.2)$$

The factor stems from the fact that the nuclei were first considered as sharp-edged spheres with the energy changing as a function of the radius. To get an idea of what might be expected for the incompressibility, one might just run a parabola through the two known points on the curve of $\frac{E}{A}(\rho)$. Then the resulting incompressibility has a value of $\kappa \approx 290$ MeV. If the actual incompressibility turns out to be below this benchmark value, we may consider the nuclear EOS to be soft, and stiff if the opposite is the case.

Features of EOS in intermediate energy heavy-ion collisions can be inferred from multifragmentation, collective flow and isospin physics processes. On the other hand, NEOS at higher incident energies is characterized by the production of sub-threshold particles[15] and their isospin dependence[16].

1.3 Different phenomena affecting NEOS at intermediate energies

1.3.1 Multifragmentation

The multifragmentation process refers to the process where large number of particles are produced in a energetic heavy-ion reaction. The produced particles include the free particles,

light charged particles as well as very heavy clusters. The pictorial view of multifragmentation process is shown in Fig.1.2. This production of particles is linked with the incident energy and collision geometry. A increase in the incident energy leads to more compressed zone and hence as a result gives insight into the nuclear equation of state (EOS). Similarly, the variation in the collision geometry is also observed to vary the compressed zone. Moreover, the momentum dependence of the equation of state in multifragmentation have also attracted a lot of considerations[17, 18, 19]. These momentum dependent interactions (MDI) are found to affect transverse momentum drastically. The importance of MDI is clear from the Refs. [20, 21] where static equation of state is badly failed to reproduce the experimental findings. The nucleon-nucleon cross sections which are found to affect the collisions and mean field are also an important candidate for the study of the nuclear equation of state. In Ref.[17, 22] requirement of large cross section is also indicated. The detailed analysis of multifragmentation in the presence of momentum dependent interactions and nucleon-nucleon cross sections is performed in chapter 3 and 4, respectively.

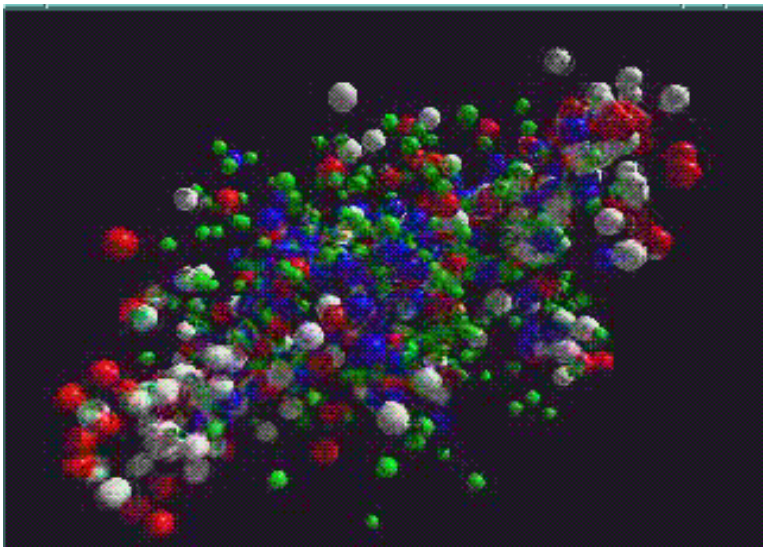

Figure 1.2: Schematic view of the multifragmentation process, clearly indicating the production of lighter and heavier fragments

1.3.2 Collective flow

The Collective flow is a measure of the transverse motion imparted to particles and fragments during the collision of two nuclei. The development of collective flow is closely related to the pressure build-up during the compression stage of the reaction, and gives us information about the pressure and particle density relation (that is, the EOS). Generally, there are three types of flows, namely, radial, directed, and elliptical flows. The radial flow arises in central collisions and is characterized by the increased yields in the kinetic energy spectra of the particles emitted near $\theta_{c.m.} = 90^0$ relative to the beam axis. On the other hand, directed flow, also called "in-plane" or "sidewards" flow in the literature, refers to the preferential emission of particles within, and to a particular side of, the reaction plane (reaction plane is defined as the plane which contains the beam axis and a line joining the centers of two nuclei). When the experimental data of different collaborations is compared with the theoretical calculations[23], the simulations with EOS characterized by the incompressibility $\kappa = 167$ MeV yield adequate directed flow at lower beam energies, but too low at higher energies. On the other hand, with the EOS characterized by $\kappa = 380$ MeV, the directed flow appears to be too high at virtually all energies.

Whereas, directed flow is anti-symmetric with respect to the ϕ distribution for forward rapidity ($y_{c.m} > 0$) and backward rapidity ($y_{c.m.} < 0$), elliptical flow has the same distribution in both rapidity regions, at least for symmetric reactions. The elliptical flow refers to the anisotropy of the ϕ distribution at mid-rapidity and its value indicates whether the particle emission is in-plane or out-of-plane. Azimuthal distribution which are peaked at 0^0 and 180^0 exhibit predominantly in-plane emission, while ϕ distribution peaked at $\pm 90^0$ signify out-of-plane emission. The term elliptical flow has replaced old naming such as "squeeze out", "rotational motion", or "anisotropic flow" because the shape of ϕ distribution at mid-rapidity resembles ellipse with a major axis along the x-axis (in-plane emission) or y-axis (out-of-plane emission). Fig.1.3 illustrate the formation of compressed region in a non-central nuclear collision and the subsequent emission of particles from the mid-rapidity participant region. Again in Ref.[23], we see that without interaction contributions to pressure, simulations cannot reproduce the measurements. The simulations with $\kappa = 167$ MeV give too little pressure at high energies, and those with $\kappa = 380$ MeV generally too much. A

label of discrepancy is seen between data from different experiments. The extensive study is reported on the radial and directed flows in the literature. The systematic study of elliptical flow is carried out in chapter 5 to explain the data i.e. to know th nature of equation of state.

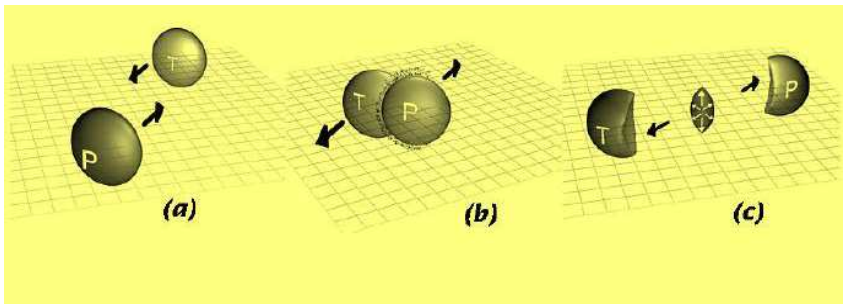

Figure 1.3: Schematic illustration of the collision of two Au nuclei and the resulting elliptical flow of the participant zone. Time shots are shown for an instant before the collision (a), early in the collision (b), and late in the collision (c), taken from Ref. [24].

1.3.3 Isospin physics

The recent progress in rare isotopes facilities has also raised interest in the isospin degree of freedom at high densities. The term isospin refers to the pair of similar particles, the protons and neutrons, which are almost identical in the nuclear matter when electric charge difference is ignored. In many transport simulations, the nuclear interactions difference between protons and neutrons are simply ignored. In other words, these simulations explore the reactions in symmetric nuclear matter limit only. Such simplification is used because of the limited beam and target combinations, but needs to be refined in view of the rare isotopes beam reactions offer by many facilities. The isospin dependence of the nuclear equation of state is often expressed in terms of symmetry energy. An elementary illustration of concept of symmetry energy is shown in Fig.1.4. the symmetric matter is represented by the lower line, while pure neutron matter is represented by the upper line. The difference between the two lines is the symmetry energy, which express the effect of the isospin on nuclear matter

energy density. These isospin effects comes into picture in term of symmetry energy and cross section, which are supposed to affect the multifragmentation as well as collective flow and related phenomena to great extent[26]. We have tried to study the isospin effects on elliptical flow, nuclear stopping as well as on fragmentation in chapter 5 and 6 in term of symmetry energy, cross section and momentum dependent interactions..

The extensive experimental and theoretical efforts have been made during last 20 years

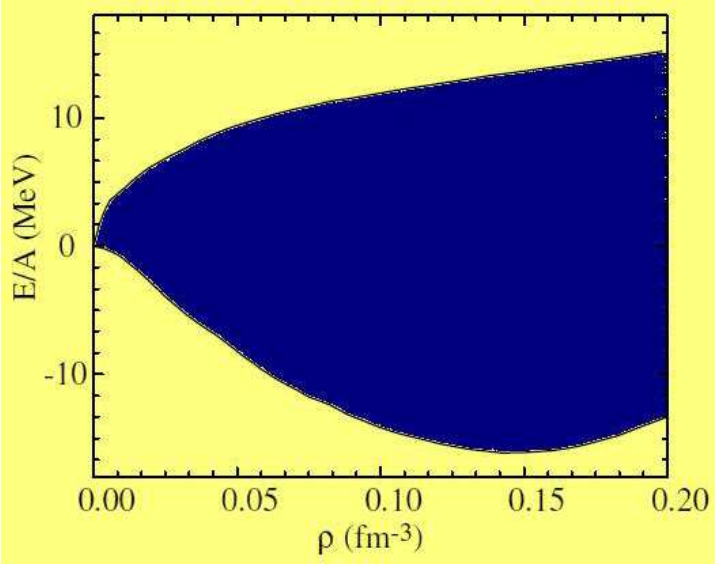

Figure 1.4: The concept of symmetry energy: The top line is the energy density for pure neutron matter and lower line is that for symmetric nuclear matter. The difference of two lines is the symmetry energy.(from[25]).

to understand the mechanism of multifragmentation, collective flow; while isospin physics is a newly burning topic in the community of nuclear physics. These efforts are discussed in the next sections.

1.4 Review of the experimental attempts for multi-fragmentation

Nuclear fragmentation was discovered nearly seventy three years ago[27] in cosmic ray studies as a puzzling phenomena accompanying the collision of relativistic protons with a heavy target and consisted of the emission of slow nuclear fragments. These fragments were in the range of $3 \leq Z \leq 30$, dubbed as intermediate mass fragments. Using the radiochem-

ical methods, total cross-section of the fragmentation could not be determined and process was considered as very rare and exotic. In 1980's, Jakobsson *et.al.*[28], observed the multiple emission of IMF's in the emulsion irradiated by the carbon beam of 250 MeV/nucleon. This result created the interest of the nuclear community toward multifragmentation. Warwick *et.al.*[29] found that multifragmentation is a dominant reaction channel at beam energies higher than 35 MeV/nucleon. Further, the Purdue group [30] conjectured that multifragmentation is a clear signature for the phase transition between a gaseous and liquid phase of nuclear matter, which occurs around a density of $0.4\rho_0$; ρ_0 is the normal nuclear matter density. Since then, the study of multifragmentation has been considered of great interest. Lots of detectors included the forward and 4π designed to understand the each and every aspect in detail.

First accelerator in this series was the *BEVALAC* accelerator at Lawrence Berkeley

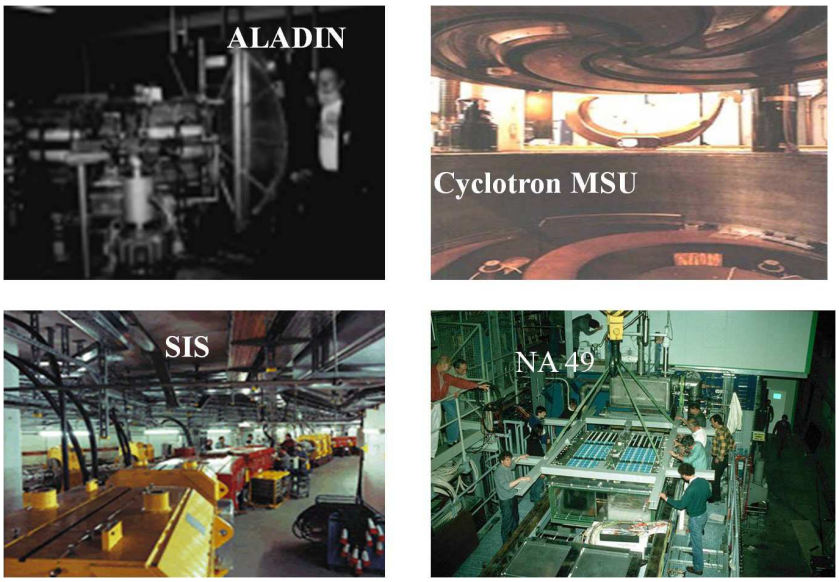

Figure 1.5: The pictorial view of different accelerators used by ALADIN, NSCL, SIS and NA49 collaborations to generate the beam in intermediate energy range.

Laboratory that led way to high energy accelerators built at the Michigan state university *(MSU)(USA)*. With the passage of time, the Grand Accelerateur National D'ions Lourds *(GANIL)(France)*, Relativistic Heavy-Ion Collider *(RHIC) (USA)*, Superconducting Super-Collider *(SSC)* at *BNL (USA)*, *NSF-Arizon* accelerator at the university of *Arizona (USA)*, *Vivitron* Accelerator in *Strasbourg (France)*, Superconducting Cyclotron *(SC)* at *Texas*

(USA), Superconducting Cyclotron *(SC)* and *CHIMARA* detector at Laboratori Nazionali del Sud in *INFN, Catania (Italy)* and Heavy-ion Synchrotron *SIS* accelerator at *GSI (Germany)* etc. has contributed lot in the field of multifragmentation. Recently many of them are upgraded to study the isospin physics. For the better understanding, the pictures of different accelerators used by the respective collaborations is shown in Fig.1.5.

In actual heavy-ion experiment, the crucial part of the analysis is sorting of "well measured" events as a function of the violence of the collision (i.e. impact parameter). This analysis is meant for comparing the results with experimental findings. The *INDRA* group at *GANIL* used total transverse energy E_{tr}^{TOT} [31] and transverse energy of light charged particles (LCP's, Z = 1,2) i.e. $E_{trans12}$[32]. The multiplicity of charged particles denoted by PM has often been used by the *FOPI* group at *GSI* to characterize the events [33]. This group also used a new quantity called ERAT for sorting which is discussed in Ref.[33]. The correlation of the charged particle multiplicity (M_{cp}) and neutron multiplicity (M_n) was used by the *NIMROD* group [34] at *Texas A & M University*. The *Superconducting Cyclotron group (SC)* at *INFN (Italy)* sorted data according to the kinematic variable- total kinetic energy loss (TKEL) [35]. All the above methods are employed by various experimental groups to sort out the data are based on the cuts in global variables distributions. It mean that all experimental results are subjected to various filters and in order to make comparison with the findings, theoretical results must also be subjected to the same filters.

The Emulsion experiment [28, 36] was among the first attempts to study the multifragmentation. They provided an unique possibility to study the fusion, multifragmentation as well as vaporization at intermediate energies.

The *Berkeley* group focus mainly on the asymmetric reactions between the incident energy 50 to 110 MeV/nucleon [37-41], with an aim to investigate the role of entrance-channel mass asymmetry reaction dynamics. The emphasis was on the different parameters like excitation energy, angular distribution, cross-section as well as velocity distribution. The aim of the *EOS* collaboration at *BEVALAC* was to study phase transition in nuclear matter. Through the process of multifragmentation, critical exponents like surface energy, volume energy, symmetry energy, entropy etc. [42] are extracted for the asymmetric reactions in the energy region of 1 GeV/nucleon. In the earlier studies, similar exponents were extracted

for symmetric Au^{197} + Au^{197} collisions[43].

Like *Berkeley* group, *National Superconducting Cyclotron Laboratory (NSCL)* of *Michigan State University (MSU)* focus on the asymmetric reactions like Xe^{129} + C^{12}, Al^{27}, V^{51}, Cu^{64}, Y^{89} (50 MeV/nucleon), Ar^{36} + Au^{197}, Xe^{129} + Au^{197} (50-110 MeV/nucleon), Ar^{40} + Cu^{64}, Ag^{108}, Au^{197} (at 17-115 MeV/nucleon) [44, 45]. The average multiplicity as well as mass of the heaviest fragments are investigated. Apart from asymmetric reactions, nearly symmetric channels Ne^{20} + Al^{27}, Ar^{40} + Sc^{45}, Kr^{84} + Nb^{93}, Xe^{129} + La^{139} (15-135 MeV/nucleon) are also investigated [46]. In the experiment of Cd^{114} ion with Mo^{92} at $E = 50$ MeV/nucleon, the charge correlations, average relative velocities for mid-velocity fragments emission [47] and the size, density, N/Z, E^*/A , E_{flow}/A of the emitted source on the measured isotope ratio was explored [48]. The work on the isospin dependence of nuclear matter is carried out by colliding Sn^{112} + Sn^{112} and Sn^{124} + Sn^{124} nuclei at 50 MeV/nucleon [49-53]. The isospin effects are studied by neutron-proton spectra double ratio [50], cross-section and binding energy [51], rapidity distribution, transverse momentum and impact parameter dependence of isospin diffusion [52]. In a recent communication, constraints on the density dependence of symmetry energy are also put forward [53].

The symmetric collisions are studied by the *Superconducting Cyclotron* of the Laboratori Nationali del Sud of *INFN (Italy)*. They considered the reactions of Nb^{93} + Nb^{93} (at 17, 23, 30 and 38 MeV/nucleon) and Sn^{116} + Sn^{116} (at 29.6, 38 MeV/nucleon) [35]. The multiplicity of LCP's and IMF's in peripheral and semi-peripheral collisions as a function of excitation energy of emitting source, mass of the system and beam energy have been presented[35]. The difference in isotropic composition of fragments emitted from statistical and dynamical production process [54, 55] has also been observed. Recently *Isospin collaboration* at *INFN (Italy)* studied the isospin effects for neutron-rich Sn^{124} + Ni^{64} and neutron-deficient Sn^{112} + Ni^{68} systems for non-central collisions at 35 MeV/nucleon [56].

The *FOPI* and *ALADIN* groups at GSI studied the multifragmentation process over a wide range of masses from C^{12} to Pb^{208} with incident energies ranging from 100 to 1000 MeV/nucleon [57-59]. These groups studied the particle evaporation to multi fragment emission and at last total disassembly of the nuclear matter. A rise and fall in the multifragmentation is also reported by *ALADIN* collaboration for the reaction of Au^{197} + Au^{197}

[57]. Moreover, the fragment multiplicities and correlations are found to obey the universal behavior [57]. With the passage of time, secondary beams has also been generated extending the domain of the study to isospin plane[60, 61].

The *NIMROD* collaboration at *TAMU* focuses on the reaction dynamics in Fermi energy domain of the heavy-ion collisions [62-66]. An extensive study on the critical behavior in the disassembly of nuclei with $A \approx 36$ produced in reactions of $Ar^{20} + Al^{27}$, Ti^{48} and Ni^{58} at 47 MeV/nucleon has been carried out [62]. The multiplicity and charge distribution, energy and velocity spectra has been observed for $Zn^{64} + Ni^{58}$ (26 MeV/nucleon), Au^{197} (at 47 MeV/nucleon), Mo^{92} (at 35 and 47 MeV/nucleon), $Ar^{40} + Sn^{112}$ (40 MeV/nucleon) and $Al^{27} + Sn^{124}$ (at 55 MeV/nucleon) collisions [63]. The hot topic of recent years, the study of equation of state of isospin asymmetric nuclear matter [64] has also been studied by this collaboration. A number of observables such as symmetry energy, isotropic and isobaric yield ratio, average N/P ratio for the reactions of $Sn^{124} + Sn^{124}$, $Xe^{124} + Sn^{124}$, $Sn^{112} + Sn^{112}$ at 28 MeV/nucleon has been explored [64, 65]. These properties are also studied by using different beams of Ar^{40}, Ca^{40}, Fe^{58} and Ni^{58} on Fe^{58} and Ni^{58} targets at 25, 30, 33, 40, 45, 47 and 53 MeV/nucleon [64, 65]. These findings showed that the isotopic distribution of the hot primary fragments are found to vary wide and extended towards the neutron drip line. Moreover, the form of symmetry energy for the heavy-ion studies favour a dependence of the form $E_{Sym} = 31.6(\rho/\rho_0)^{\gamma}$, where $\gamma = 0.6$-1.05. Recently, this group has studied the mass dependence of the nuclear caloric curve [66].

The last, but not least, *INDRA* group at *GANIL (France)* is also one of the leading group in this field. They analyze a variety of parameters in multifragmentation. The system size effects, the role of system size in entrance channel as well as Coulomb instabilities, kinetic energy spectra and fragment velocity correlation are studied in nearly asymmetric reactions of $Ar^{36} + Ni^{58}$, $Gd^{155} + U^{238}$ and $Xe^{129} + Sn^{nat}$ (at 30-95 MeV/nucleon), $Ni^{58} + Ni^{58}$ (32-90 MeV/nucleon), $Pb^{208} + Au^{197}$ (at 29 MeV/nucleon) and $Ar^{36} + KCl$ [67]. The entrance channel effects are also studied for different asymmetric reactions in the mass range 58 to 181 and beam energy between 24 to 90 MeV/nucleon [68]. The symmetric reaction of $Au^{197} + Au^{197}$ was also studied between 40 and 150 MeV/nucleon [69]. It is also observed that mutifragmentation is responsible for fragment production around the excitation

energy of 3 MeV/nucleon [70]. In the collaborative work of *ALADIN-INDRA* collaboration, bimodal behavior of heaviest fragment distribution in projectile fragmentation has been studied [71]. Recently, isospin effects are observed in semi-peripheral Ni^{58} + Au^{197} collisions at intermediate energies [72].

1.5 Review of the experimental attempts for collective flow

The collective flow has attracted a wide attention in in recent times. As discussed earlier, collective flow can be classified as: radial, directed and elliptical flows. Lots of findings are presented in the literature on the radial and directed flows [73-79], while elliptical flow is yet to be fully explored in the nuclear science community at intermediate as well as high energies. The elliptical flow term was introduced in 1997 by H. Sorge [80]. The review of experimental findings on elliptical flow by different collaborations (discussed in the review of multifragmentation) is presented as follow:

Experimentally out-of-plane emission, termed as squeeze-out was first observed in 1989 at nearly the same time by two competing collaborators. The *Diogene* collaboration at *Saturne Synchrotron in Saclay (France)* observed few peaks in the azimuthal distribution of the particles at mid-rapidity in 800 MeV/nucleon Ne-induced reactions [81]. At *BEVALAC* in *Berkeley*, the *Plastic Ball/Wall* group observed out-of-plane emission in Au^{197} + Au^{197} collisions at 400 MeV/nucleon [82]. The *BEVALAC* group also characterize the squeeze-out as a function of projectile energy, mass as well as the rapidity dependence by using a novel ratio of out-of-plane/in-plane emission [83]. The transition from the in-plane to out-of-plane emission was first observed using the Zn^{64} + Ni^{58} reaction at *GANIL* facility by the NAUTILUS collaboration in 1994 [84]. The energy of transition increases with impact parameter. Moreover, the *MINIBALL/ALADIN* collaboration observed the onset of out-of-plane emission (GSI) in Au^{197} + Au^{197} collisions at 100 MeV/nucleon [85], where out-of-plane emission is seen for central collisions, while peripheral collisions clearly show in-plane emission.

The *NSCL* at *MSU (USA)* focused on the disappearance of elliptical flow for symmetric Au^{197} + Au^{197} reactions (at 500 MeV/nucleon to 11 GeV/nucleon) [86, 87]. The excitation

function shows a transition from negative to positive elliptical flow at a beam energy, $E \approx 4$ GeV/nucleon. Later on, *NSCL* in collaboration with *STAR*, investigated the elliptical flow at $\sqrt{S_{NN}} = 130$ and 200 GeV [88]. They presented the pseudo rapidity, transverse momentum dependence and centrality dependence of elliptical flow. Recently, the elliptical flow and nuclear stopping is used as a tool to determine NN cross-section in heavy-ion collisions at intermediate energies [89].

Other collaborations: *FOPI, ALADIN* at *GSI*, and *INDRA* at *GANIL* emphasis on the transition of elliptical flow for different kind of fragments from in-plane to out-of-plane in intermediate energy heavy-ion collisions [74, 75, 76, 90]. The $Au^{197} + Au^{197}$ reaction is studied for incident energies ranging from 40 to 800 MeV/nucleon. The transition from in-plane to out-of-plane is observed around 100 MeV/nucleon. The *FOPI* collaboration also got success in correlating the global stopping with flow [91] as well as with cluster formation during expansion [92]. A total of 25 system-energies are analyzed for this work: $Ca^{40} + Ca^{40}$ (at 0.4, 0.6, 0.8, 1.0, 1.5, 1.93 GeV/nucleon), $Ni^{58} + Ni^{58}$ (at 0.09, 0.15, 0.25, 0.4 GeV/nucleon), $Ru^{96} + Ru^{96}$ (at 0.4, 1.5 GeV/nucelon), $Xe^{129} + Cs^{133}I^{127}$ (at 0.15, 0.25, 0.4 GeV/nucleon) and $Au^{197} + Au^{197}$ (at 0.09, 0.12, 0.15, 0.25, 0.4, 0.6, 0.8, 1.0, 1.2, 1.5 GeV/nucleon). The findings related to the stopping-flow relation are also obtained by the *INDRA* and *ALADIN* groups [93]. The *FOPI* collaboration reported new method to study the analysis of anisotropic flow with different methods like the event plane reconstruction, on Lee-Jang Zeros and on multi-particle cumulants [94]. On the other hand, *INDRA and ALADIN* collaborations presented new results of flow analysis for the set of reactions $Xe^{124,129}$ and $Sn^{112,124}$ (at 100 and 150 MeV/nucleon) [95]. The dependence on the centrality and p_t of the directed and elliptical flow are determined for isotropically selected reaction products with $Z \leq 3$.

The recent study in the field of elliptical flow in intermediate energy heavy-ion collisions is by J.Y. Ollitrault and co-workers [96]. They discussed how the different estimates of elliptical flow are influenced by the flow fluctuations and non-flow effects. It is argued that non-flow effects and fluctuations can not be disentangled without any assumptions. In the presence of reasonable assumptions, the all measured values of elliptical flow are converges to a unique mean value in respective plane.

1.6 Review of the theoretical models used to study various phenomena at intermediate energies in heavy-ion collisions

Before looking for the different theoretical models and algorithms suitable at intermediate (and relativistic) energies, we have to keep in the mind the dynamics involved at these incident energies. The key point to remember is that the heavy-ion collisions involve very complicated non-equilibrium physics, therefore, its numerical modeling is not straight forward. Due to the lack of free phase space at low incident energy, about 98 % of the attempted collisions are blocked. The whole dynamics at low energies is governed by the mean field or by the mutual two and three body interactions. On the contrary, the availability of large phase space at relativistic energies ($\geq$ GeV/nucleon) makes the Pauli-blocking [97] quite small (roughly 4% collisions are blocked) and hence the dynamics of a reaction is governed by cascade picture. On the other hand, both cascade and mean field pictures emerges at intermediate energies. Beside cascade and mean field picture, isospin picture (to extract the information of the EOS of neutron rich matter, especially the density dependence of the nuclear symmetry energy) also comes into existence in this energy range. Isospin is a factor which differentiate between the neutron and proton inside the nucleus on the basis of the charges and make possible interactions between the n-n, p-p and n-p. This isospin degree of freedom enters in term of isospin-dependent physical quantities such as the iso-vector (symmetry) potential, and isospin-dependent in-medium nucleon-nucleon (NN) cross-sections and Pauli blocking.

A native picture of nuclear reactions at intermediate energies undergoes three important steps: Initial stage where the target and projectile are boosted toward each other with proper center of mass energy: compression and expansion stage, after which a pre-fragment source is formed and reaches equilibrium; a secondary decay process of various emitted fragments.

The theoretical models for the processes at intermediate energies can be divided into two categories: Statistical and Dynamical model. Example of statistical models include multi-

particle phase space models, such as the *Statistical Multifragmentation Model (SMM)* [98, 99] and the *Berlin Multifragmentation Model* [100], which can incorporate specific nuclear properties directly. Accordingly, *a semi- micro canonical version of SMM* [99] that incorporates detailed nuclear structure information relevant to the population and secondary decay of the excited fragments was developed [101]. Additional static models include *Percolation* [102], *Lattice Gas Approach* [103] and *Expanding Emitting Source (EES) model* [104]. These approaches have the virtue of providing relatively simple schematic algorithms suitable for the exploration of critical phenomena in finite systems. The limitation of the statistical models are: (i) The situation at the start of reaction is based on some assumption for the degree of thermalization [99] and (ii) The statistical models give a better description only of the later/final stage of the reaction. Our aim is to study all the stages discussed earlier: initialization, compression and expansion. Hence the statistical models are neglected in this study. This study is possible by the dynamical models only.

The dynamical approaches such as the Time Dependent Hartree Fock (TDHF) [105, 106] or its semi-classical version called *Vlasov equation* (in phase space) [107, 108] are suitable at low incident energies where nucleon-nucleon collisions are negligible. However, a suitable and reasonable approach for the intermediate energy heavy-ion physics should treat the nucleon-nucleon scattering and mean field on equal footing. Some attempts were made in the literature to extend the *TDHF* theory to take care of the residual n-n interactions, which are responsible for the two-body collisions. This was dubbed as *Extended Time dependent Hartree-Fock (ETDHF)* theory [109]. However its numerical implementation prohibited its use for large scale investigations of heavy-ion collisions.

In the first attempt, semi-classical version of *ETDHF* theory i.e. *Vlasov equation* [107] was coupled with nucleon-nucleon collisions and thus, a new realization, *named as Boltzmann -Uehling - Uhlenback equation (BUU)*, was developed to study the large deviation problems of low, intermediate and relativistic heavy-ion collisions. The *BUU* equation was solved by test particle method. The one body distribution function is described as a collection of NA test particles, where A is the mass number and N is event number. All possible collisions between the test particles are considered, i.e., there is no division of test particles. In other words, N parallel runs communicate with each other, therefore, event by event correlation

can not be analyzed. However, Bonasara *et.al.* [110], solved the collision integral using the concept of mean free path. In this method, N parallel events are performed and the average physical values of various quantities are calculated over large number of events. Since N parallel runs do not communicate with each other, event by event correlations are preserved.

Keeping in mind the requirement of intermediate energy region, one would like to have those methods where correlations and fluctuations among nucleon can be preserved. The *Classical Molecular Dynamics (CMD)* [111] approach (or the equation of motion), in principle, is capable of predicting the fragments production. It also incorporate the complete classical N-body dynamics which is necessary to describe the formation of the fragments. The simple Classical Molecular Dynamics, however, needs major refinements (including quantum features). The quantum features play a very important role at low incident energies. The above approach was later extended to incorporate the quantum features by Aichelin and Stocker [105, 112]. This new approach, *which explicitly incorporates the N-body correlations as well as nuclear matter equation of state and important quantum features (like the Pauli principle, Stochastic scattering and particle production), was dubbed as Quantum Molecular Dynamics (QMD)* model [14, 105, 112, 113].

To extract the information of the EOS of neutron-rich matter, especially the density dependence of the nuclear symmetry energy, from heavy-ion reactions induced by neutron rich (stable and/or radioactive) beams, one needs reliable theoretical tools. For this purpose, one must have transport models that include explicitly the isospin degree of freedom and thus the isospin-dependent physical quantities such as the iso-vector (symmetry) potential and isospin-dependent in-medium nucleon-nucleon (NN) cross -sections and Pauli-blocking. As discussed above, the semi-classical models include mainly the two types: the BUU and the QMD model. With the development of radioactive ion-beam physics, several rather comprehensive isospin-dependent, but mostly semi-classical transport model such as IBUU[114], SMF[116] and IQMD[117] have been successfully developed in recent years to describe nuclear reactions induced by neutron-rich nuclei at intermediate energies.

The *isospin- dependent Boltzmann-Uehling-Uhlenback (IBUU)* transport model has successfully explained several isospin dependent phenomena in heavy-ion collisions at intermediate energies [114]. In this model, the isospin dependence was included in the dynam-

ics through nucleon-nucleon collisions by using isospin-dependent cross-sections and Pauli blocking factors, the symmetry potential $V_{sym}(\rho, \delta)$, and the coulomb potential. This model was used to calculate the ratio of yield of neutron and protons in pre-equilibrium emission [115]. The *BUU* equation provides an accurate description of the time dependence of the one body distribution function. Accurate solution of the *BUU* equation average away fluctuations in the density that might lead to the formation of fragments in an individual collision. This is usually achieved by solving the *BUU* equation with a large number of test particles per nucleon N_{test}. The density fluctuations that lead to the fragment production are suppressed in the *BUU* equation, so the calculation of fragment yield directly via *BUU* model is not feasible. Therefore, alternate model such as, *Stochastic Mean Field (SMF)* model [116] and *Isospin Quantum Molecular Dynamics (IQMD)* model [117] has been developed to address the density fluctuations.

The *SMF*, like *IBUU*, describes the time evolution of the collision using self-consistent mean field. The application of the *SMF* model to the unstable situations relies on the knowledge of the most important unstable modes, which may be difficult to identify in case where the modes are not known a priori.

The *IQMD* model [117] treats different charged states of nucleons, deltas and pions explicitly [118], as inherited from the *VUU* model[108]. The isospin degree of freedom enters into the calculations via symmetry potential and cross-sections[108, 119]. This model is proven successful to study the isospin effects in intermediate energy heavy-ion collisions. The model incorporate the N-body correlations, reduces the fluctuations to minimum extent, explains the nuclear equation of state and includes the many quantum features like Pauli blocking, Stochastic scattering, particle production and isospin.

All these dynamical models can follow the time evolution of nucleons only. These models are termed as "primary model" which generate the phase-space of nucleons. One needs a procedure to define clusters. These algorithms are termed as " secondary models". In a very simple picture, nucleons are connected to a cluster using space correlation method. This method identifies the two nucleons in the same fragment if their centroids are less than some distance [120]. This method is known as *Minimum Spanning Tree (MST)* method.. Till today, it is one of the most extensively used methods. Several refinements to this method have

been proposed including momentum cut and binding energy cut [121]. One more and newly developed secondary model is "*Simulated Annealing Clusterization Algorithm*, developed by Puri, Hartnack and Aichelin [122], which is based on the minimization of energy of the system.

As discussed in the above paragraphs, we have several theoretical models that are available to study the heavy-ion collisions at intermediate energies. We shall study the phenomena of multifragmentation and elliptical flow using primary models *QMD* and *IQMD* and then analyze by secondary models MST, MSTP and SACA.

1.7 Organization of thesis

The thesis is organized as follows:

In chapter 2, we will describe various theoretical models in brief. The primary models, Quantum Molecular Dynamics *(QMD)* and Isospin-dependent Quantum Molecular Dynamics *(IQMD)* will be discussed in detail.

In **chapter 3**, we shall study the influence of momentum dependent interactions (MDI) on the production of different kind of fragments like free particles, light charged particles (LCP's) and medium mass fragments (MMF's) by taking into account the composite system mass ($A_{tot} = A_T + A_P$) from 80 to 394, using QMD model. The reactions are analyzed with MST method. We shall show that the decrease is observed in the the density profile, number of allowed collisions as well as heaviest fragment (A_{max}) in the presence of MDI. We shall also show that enhanced production of MMF's will take place in the presence of momentum dependent interactions at semi-peripheral geometries. It will also be shown that multiplicity of MMF's can be parameterized in term of power law[21].

The experimental attempts of *ALADIN* and *NSCL* collaborations exists in the literature to study the rise and fall of intermediate mass fragments (IMF's) with impact parameter and incident energies[46, 123]. The results of *ALADIN* collaboration is available for ${}_{79}Au^{197}$ + ${}_{79}Au^{197}$ at different incident energies and impact parameters. On the other hand, the asymmetric systems data is available from *NSCL* collaborations at different energies. In the **chapter 4**, we shall try to compare the results with our theoretical results in the presence of momentum dependent interactions by varying the N-N cross-sections. Moreover, we shall also observe the effect of technical model ingredients such as Gaussian width (L), Clusterization distance (R_{Clus}), equations of state (Soft[S], Hard[H] and S with momentum dependence [SM]) and different clusterization algorithms on the production of IMF's. We shall show, first time, that the effect of different NN cross-sections and model ingredients on the process of multifragmentation is of same order. [22]

Recently, the elliptical flow has attracted the nuclear community a lot due to its nature of in-plane to out-of-plane emission. In **chapter 5**, we shall study the elliptical flow in detail by using the IQMD model. The transverse momentum, excitation function, impact parameter and composite mass of the system, dependence will be studied in detail for different kind of fragments. We shall show the excitation function of elliptical flow for the reactions of ${}_{20}Ca^{40}$ + ${}_{20}Ca^{40}$, ${}_{54}Xe^{131}$ + ${}_{54}Xe^{131}$ and ${}_{79}Au^{197}$ + ${}_{79}Au^{197}$ at entire rapidity as well as mid-rapidity range. We shall also show the comparison of excitation function of elliptical flow with the findings of INDRA, FOPI and PLASTIC BALL collaborations for ${}_{79}Au^{197}$ + ${}_{79}Au^{197}$ nuclei in mid-rapidity region. Moreover, we shall made an attempt to parametrized the system mass dependence of elliptical flow in term of power law for different kind of fragments.[124]

The nuclear stopping as well as multifragmentation are studied in the literature separately as two processes, many times. A very few attempts were made to correlate the nuclear stopping and fragmentation process. In **chapter 6**, we shall also correlate the production of fragments with nuclear stopping in the presence of symmetry energy by using IQMD model. We shall study all the possible variations like impact parameter, system size, cross-section, symmetry energy and equations of state. We shall show that the light charged particles (LCP's) production in the presence of symmetry energy can acts as a better indicator for the nuclear stopping (R and Q_{zz}). Moreover, we shall also show that maximum stopping is obtained for heavier systems in central collisions in the presence of symmetry energy and isospin dependent cross-section, without momentum dependent interactions. This is due to the destabilizing nature of momentum dependent interactions.[125]

Our results are summarized in **chapter 7**, which also contains an outlook of the work.

Bibliography

[1] H. Muller and B. D. Serot, Phys. Rev. C **52**, 2072 (1995).

[2] A. Bonasera, Phys. Rev. C **60**, 065212 (1999); S. Terranova and A. Bonasera, Phys. Rev. C **70**, 024906 (2004).

[3] P. Wang, V. E. Lyubovitskij, T. Gutsche and A. Faessler, Phys. Rev. C **67**, 015210 (2003); F. Giacosa, T. Gutsche, and A. Faessler, Phys. Rev. C **71**, 025202 (2005).

[4] P. Czerski *et al.,* J. of phys. G: Nucl. and Part. **36**, 025008 (2009).

[5] S. E. Jiri *et al.,* Nucl. Phys. B **119**, 538 (2003); F. Csikor *et al.,* Strong and Electroweak Matter 2002 **1**, hep-lat/0301027 (2003); P. Braun-Munzinger and J. Stachel, Nucl. Phys. A **606**, 320 (1996).

[6] P. Danielewicz, Phys. Rev. C **51**, 716 (1995).

[7] L. Shi, Ph.D thesis (2003) MSU, USA.

[8] J. R. Birkelund, J. R. Huizenga, J. N. De, and D. Sperber, Phys. Rev. Lett. **40**, 1123 (1978); A. Bonasera, Phys. Rev. C **34**, 740 (1986); J. N. De and W. Stocker, Phys. Rev. C **42**, R819 (1990); M. M. Majumdar, J. N. De, C. Samanta, and S. K. Sammander, Phys. Rev. C **48**, 2093 (1993); K. P. Singh, D. C. tayal, G. Singh and H. S. hans, Phys. Rev. C **31**, 1726 (1985); K. P. Singh *et al.,* Acta. Phys. Slov. **37**, 316 (1987).

[9] N. Bhatia, S. S. Malik, and A. K. Jain, Eur. Phys. J A **26**, 241 (2005); S. S. Malik, P. Agarwal, and A. K. Jain, Nucl. Phys. A **732**, 13 (2004); A. K. Jain *et al.,* Review of Modern Physics **70**, 843 (1998); *ibid.* **62**, 393 (1990); S. Singh, S. S. malik, and A. K. Jain, phys. rev. C **75**, 067301 (2007); A. K. Jain *et al.,* Eur. Phys. J. A **27**, 33 (2006).

[10] S. V. S. Sastry, S. Kailas, A. K. Mohanty, and A. Saxena, Pramana J. of Physics **64**, 47 (2005); M. Sinha *et al.,* Phys. Rev. C **78**, 027601 (2008); A. Mukherjee *et al.,* phys. Lett. B **636**, 91 (2006); D. Bandyopadhyay *et al.,* Phys. Rev. C **59**, 1179 (1999).

[11] P. B. Price *et al.,* Phys. Rev. C **46**, 1939 (1992); Z. Ren, C. Xu, and Z. Wang, Phys. Rev. C **70**, 034304 (2004).

[12] C. Yanhuang, A. Smerzi, and M. D. Toro, Phys. Rev. C **50**, 2809 (1994); Z. H. Liu, X. Z. Zhang, and H. Q. Zhang, Phys. Rev. C **68**, 024305 (2003); C. Beck, N. Keeley, and A. Diaz-Torres, Phys. Rev. C **75**, 054605 (2007).

[13] B. K. Agrawal, R. Kumar, and S. K. Dhiman, Phys. Rev. D **77**, 087301 (2008); S. K. Dhiman, R. Kumar, and B. K. Agrawal, Phys. Rev. C **76**, 045801 (2007); R. Kumar, B. K. Agrawal, and S. K. Dhiman, Phys. Rev. C **74**, 034323 (2006); B. K. Agrawal, S. K. Dhiman, and R. Kumar, phys. Rev. C **73**, 034319 (2006).

[14] J. Aichelin *et al.,* Phys. Rev. Lett. **58**, 1926 (1987); J. Aichelin *et al.,* Phys. Rev. C **37**, 2451 (1988); A. Bohnet *et al.,* Phys. Rev. C **44**, 2111 (1991); P. B. Gossiaux, D. Keane, S. Wang, and J. Aichelin, Phys. Rev. C **51**, 3357 (1995); L. Zhuxia, C. Hartnack, H. Stocker, and W. Greiner, Phys. Rev. C **44**, 824 (1991); D. T. Khoa *et al.,* Nucl. Phys. A **529**, 363 (1991); G. Q. Li *et al.,* Nucl. Phys. A **534**, 697 (1991); D. T. Khoa *et al.,* Nucl. Phys. A **542**, 671 (1992); G. Q. Li *et al.,* Nucl. Phys. A **537**, 631 (1992); S. Huber and J. Aichelin, Nucl. Phys. A **573**, 587 (1994); C. Fuchs, A. Faessler, E. Zabrodin, and Y. M. Zheng, Phys. Rev. Lett. **86**,1974 (2001); E. Lehmann *et al.,* Phys. Rev. C **51**, 2113 (1995); A. Bohnet *et al.,* Nucl. Phys. A **494**, 349 (1989); J. Jaenicke *et al.,* Nucl. Phys. A **536**, 201 (1992); E. Lehmann *et al.,* Z. Phys. A **355**, 55 (1996).

[15] T. Branz, L. S. Geng, and E. Oset, Phys. Rev. D **81**, 054037 (2010); L. Tolos, A. Ramos, and E. Oset, Prog. theo. Phys. Suppl. **168**, 635 (2007); E. Oset and H. Toki, Phys. Rev. C **74**, 015207 (2006); S. Hirenzaki and E. Oset, Phys. Lett. B **527**, 69 (2002); A. ramos and E. Oset, Nucl. Phys. A **671**, 481 (2000).

[16] D. Gamermann and E. Oset, Phys. Rev. D **80**, 014003 (2009).

[17] J. Aichelin, Phys. Rep. **202**, 233 (1991).

[18] S. Kumar and R. K. Puri, Phys. Rev. C **60**, 054607 (1999).

[19] L.W. Chen, C. M. Ko, and B. A. Li, Phys. Rev. C **69**, 054606 (2004).

[20] J. Singh, S. Kumar and R. K. Puri, Phys. Rev. C **63**, 054603 (2001);*ibid*, Phys. Rev. C **62**, 044617 (2000); Y. K. vermani, S. Goyal, and R. K. Puri, Phys. Rev. C **79**, 064613 (2009).

[21] S. Kumar, S. Kumar, and R. K. Puri, Phys. Rev. C **78**, 064602 (2008); NCETEM2007, Thapar University, Patiala (Punjab), **p33**, Feb 1-3, (2007); INPC2007, Tokyo, Japan, **QW-236**, June 3-8, (2007); CITICOMS2007, CIT, Coimbatore, Vol.1, 30, Aug. 27-29 (2007).

[22] S. Kumar and S. Kumar , Pramana J. of Phys. **74**, 731 (2010); 52^{nd} DAE Symposium on Nuclear Physics, Sambalpur University, Orissa **52**, 491 (2007).

[23] P. Danielwicz *et al.,* Science **298**, 1592 (2002).

[24] P. Danielewicz *et al.,* Phys. Rev. Lett. **81**, 2438 (1998).

[25] B. A. Li, C. M. Ko, and W. Bauer, Int. J. of Mod. Phys. E **7**, 147 (1998).

[26] G. Souliotes *et al.,* Phys. Rev. C **75**, 011601 (R) (2007); A. R. Raduta and F. Gulminelli, Phys. Rev. C **75**, 024605 (2007); B. A. Li, Phys. Rev. Lett. **85**, 4221 (2000); B. A. Li, P. Danielewicz and W. G. Lynch, Phys. Rev. C **71**, 054603 (2005); J. Y. Liu *et al.,* Phys. Rev. Lett. **86**, 975 (2001), L. Q. Feng, L. Z. Xia, Chin. Phys. Lett. **19**, 321 (2002).

[27] E. Schopper, Naturwissenschaftler **5**, 557 (1937); I. I. Gurevich *et al.,* Dokl. Akad. Nauk SSSR 18, 169 (1938).

[28] B. Jakobsson *et al.,* Z. Phys. A **307**, 293 (1982).

[29] A. I. Warwick *et al.,* Phys. Rev. C **27**, 1083 (1983).

[30] J. E. Finn *et al.,* Phys. Rev. Lett. **49**, 1321 (1982).

[31] T. Lefort *et al.,* Nucl. Phys. A **662**, 397 (2000); A. Le Fevre *et al.,* Phys. Rev. Lett. **94**, 162701 (2005); S. Hudan *et al.,* Phys. Rev. C **67**, 064613 (2003).

[32] E. Plagnol *et al.,* Phys. Rev. C **61**, 014606 (1999).

[33] J. P. Alard et al., Phys. Rev. Lett. **69**, 889 (1992).

[34] Y. G. Ma *et al.,* Phys. Rev. C **71**, 054606 (2005).

[35] S. Piantelli et al., Phys. Rev. C **74**, 034609 (2006); S. Piantelli *et al.,* Phys. Rev. C **78**, 064605 (2008).

[36] S. R. Souza *et al.,* Phys. Rev. C **50**, 257 (1994).

[37] L. G. Moretto, D. N. Delis, and G. J. Wozniak, Phys. Rev. Lett. **71**, 3935 (1993).

[38] L. Phair *et al.,* Phys. Rev. Lett. **75**, 213 (1995); L. Phair *et al.,* Phys. Rev. Lett. **77**, 822 (1996).

[39] T. C. Sangster *et al.,* Phys. Rev. C **46**, 1404 (1992).

[40] D. R. Bowman *et al.,* Nucl. Phys. A **523**, 386 (1991).

[41] P. R. Chomaz *et al.,* Nucl. Phys. A **552**, 508 (1993).

[42] N. T. Porlie, Nucl. Phys. A **681**, 253 (2001); B. K. Srivastva *et al.,* Phys. Rev. C **65**, 054617 (2002); J. B. Elliott *et al.,* Phys. Rev. C **71**, 024607 (2005); L. G. Moretto, C. O. Dorso, J. B. Elliott, and L. Phair, Phys. Rev. C **77**, 037603 (2008).

[43] A. Insolia *et al.,* Phys. Rev. C **61**, 044902 (2000).

[44] R. T. de Souza *et al.,* Phys. Lett. B **268**, 6 (1991); T. Li *et al.,* Phys. Rev. Lett. **70**, 1924 (1992); L. Phair **et al.,** Phys. Lett. B **285**, 10 (1992); D. R. Bowman *et al.,* Phys. Rev. C **46**, 1834 (1992); M. B. Tsang *et al.,* Phys. Rev. Lett. **71**, 1502 (1993); T. Li *et al.,* Phys. Rev. C **49**, 1630 (1994); C. Williams *et al.,* Phys. Rev. C **55**, R2132 (1997).

[45] R. Sun *et al.,* Phys. Rev. C **61**, 06160 (2000).

[46] W. J. Llope *et al.,* Phys. Rev. C **51**, 1325 (1995); N. T. B. Stone, W. J. Llope, and G. D. Westfall, Phys. Rev. C **51**, 3157 (1995); D. Sisan *et al.,* Phys. Rev. C 63, 027602 (2001).

[47] B. Davin *et al.,* Phys. Rev. C **65**, 064614 (2002).

[48] H. Xu *et al.,* Phys. Rev. C **65**, 061602 (2002).

[49] M. B. Tsang *et al.,* Phys. Rev. Lett. **92**, 062701 (2004).

[50] Y. Zhang *et al.,* Phys. Lett. B **664**, 145 (2008).

[51] M. B. Tsang *et al.,* Phys. Rev. C **76**, 041302 (R) (2007); M. Mocko *et al.,* Eur. Phys. Lett. **79**, 12001 (2007).

[52] T. X. Liu *et al.,* Phys. Rev. C **76**, 034603 (2007).

[53] M. B. Tsang *et al.,* Phys. Rev. Lett. **102**, 122701 (2009).

[54] P. M. Milazzo *et al.,* Phys. Lett. B **509**, 204 (2001).

[55] P. M. Milazzo *et al.,* Nucl. Phys. A **703**, 466 (2002).

[56] R. Planeta *et al.,* Phys. Rev. C **77**, 014610 (2008).

[57] C. A. Ogilvie *et al.,* Phys. Rev. Lett. **67**, 1214 (1991); J. Hubele *et al.,* Phys. Rev. C **46**, R1577 (1992); M. Begemann-Blaich *et al.,* Phys. Rev. C **48**, 610 (1993); G. F. Peaslee *et al.,* Phys. Rev. C **49**, R2271 (1994); A. S. Botvina *et al.,* Nucl. Phys. A **584**, 737 (1995); A. Schuttauf *et al.,* Nucl. Phys. A **607**, 457 (1996); N. T. B. Stone *et al.,* Phys. Rev. Lett. **78**, 2084 (1997); A. S. Botvina *et al.,* Phys. Rev. C **74**, 044609 (2006).

[58] B. de Schauenburg, et al., GSI Rep. **98-1**, p. 56 (1997); W. Reisdorf, Nucl. Phys. A **630**, 15c (1998); W. Reisdorf, *et al., ibid.* **2000-1**, p. 45 (1999); W. Reisdorf, Hirschegg, p. **82** (1999); B. Hong *et al.,* Phys. Rev. C **66**, 034901 (2002).

[59] G. Poggi *et al.,* Nucl. Phys. A **586**, 755 (1995); J. Konopka, *et al.,* GSI Rep. **96-1**, p. 65 (1995); J. P. Alard, *et al., ibid.* **97-1**, p. 54 (1996); N. Bastid, *et al., ibid.* **98-1**, p. 54 (1997); A. Andronic, *et al., ibid.* **98-1**, p. 55 (1997).

[60] W. Trautmann *et al.,* Int. J. Mod. Phys. E **17**, 1838 (2008); W. Trautmann *et al.,* Nucl. Phys. A **787**, 575 (2007).

[61] C. Sfienti *et al.,* Phys. Rev. Lett. **102**, 152701 (2009).

[62] Y. G. Ma *et al.,* Phys. Rev. C **69**, 031604 (2004).

[63] R. Wada *et al.,* Phys. Rev. C **69**, 044610 (2004); J. Wang *et al.,* Phys. Rev. C **72**, 024603 (2005); R. Wada *et al.,* Phys. Rev. C **71**, 054608 (2005).

[64] D. V. Shetty *et al.,* Phys. Rev. C **68**, 054605 (2003); D. V. Shetty, S. J. Yennello and G. A. Souliotis, Phys. Rev. C **75**, 034602 (2007).

[65] D. V. Shetty *et al.,* J. Phys. G: Nucl Part. Phys. **36** , 075103 (2009).

[66] D. V. Shetty, G. A. Souliotis, S. Galanopoulos, and S. J. Yennello, Phys. Rev. C **79**, 034603 (2009).

[67] N. Marie *et al.,* Phys. Rev. C **58**, 256 (1998); W. Loveland *et al.,* Phys. Rev. C **59**, 1472 (1999); J. D. Frankland *et al.,* Nucl. Phys. A **689**, 940 (2001); S. Hudan *et al.,* Phys. Rev. C **67**, 064613 (2003); J. D. Frankland *et al.,* Phys. Rev. C **71**, 034607 (2005).

[68] J. Colin *et al.,* Phys. Rev. C **67**, 064603 (2003).

[69] J. Lukasik *et al.,* Phys. Rev. C **66**, 064606 (2002).

[70] L. Manduci *et al.,* Nucl. Phys. A **811**, 93 (2008).

[71] E. Bohnet *et al.,* Phys. Rev. Lett. **103**, 072701 (2009).

[72] E. Galichet, M. Colonna, B. Borderie and M. F. Rivet, Phys. Rev. C **79**, 064615 (2009); E. Galichet *et al.,* Phys. Rev. C **79**, 064614 (2009).

[73] G. D. Westfall *et al.*, Phys. Rev. Lett.**71**, 1986 (1993); M. B. Tsang *et al.*, Phys. Rev. C **53**, 1959 (1996); Y. M. Zheng, C. M. Ko, B. A. Li, and B. Zhang, Phys. Rev. Lett. **83**, 2534 (1999); A. B. Larionov, W. Cassing, C. Greiner, and U. Mosel, Phys. Rev. C **62**, 064611 (2000); B. A. Li, A. T. Sustich, and B. Zhang, *ibid.* **64**, 054604 (2001); C. Alt *et al.*, *ibid.* **68**, 034903 (2003).

[74] J. Lukasik, G. Auger, and M. L. Begemann-Blaich *et al.*, Phys. Lett. B **608**, 223 (2005).

[75] A. Andronic *et al.*, Nucl. Phys. A **679**, 765 (2001); Phys. Lett. B **612**, 173 (2005).

[76] J. Lukasik, *et.al.,* INDRA Collaborations, Int. Workshop on Multifragmentation and related topics (IWM 2003) Caen, France (2003).

[77] S. Kumar, M. K. Sharma, R. K. Puri, K. P. Singh, and I. M. Govil, Phys. Rev. C **58**, 3494 (1998); A. D. Sood, R. K. Puri, and J. Aichelin, Phys. Lett. B **594**, 260 (2004).

[78] A. D. Sood and R. K. Puri, Phys. Rev. C **69**, 054612 (2004); *ibid.* **73**, 067602(2006); Eur. Phys. A **30**, 571 (2006).

[79] L. W. Chen and C. M. Ko, Phys. Lett. B **634**, 205 (2006); Phys. Rev. C **73**, 014906 (2006).

[80] H. Sorge, Phys. Rev. Lett. **78**, 2309 (1997).

[81] M. Demoulins *et al.,* Phys. Lett. B **241**, 476 (1990).

[82] H. H. Gutbroad *et al.,* Phys. Lett. B **216**, 267 (1989).

[83] H. H. Gutbroad *et al.,* Phys. Rev. C **42**, 640 (1990).

[84] R. Popescu *et al.,* Phys. Lett. B **331**, 285 (1994).

[85] M. B. Tsang *et al.,* Phys. Rev. C **53**, 1959 (1996).

[86] P. Danielewicz *et al.,* Phys. Rev. Lett. **81**, 2438 (1998).

[87] C. Pinkenburg *et al.,* Phys. Rev. Lett. **83**, 1295 (1999).

[88] K. H. Ackermann *et al.,* Phys. Rev. Lett. **86**, 402 (2001); C. Adler *et al., ibid.* **87**, 182301 (2001); C. Adler *et al.,* Phys. Rev. C **66**, 034904 (2002); J. Adams *et al., ibid.* **72**, 014904 (2005).

[89] Y. Zhang, Z. Li, and P. Danielewicz, Phys. Rev. C **75**, 034615 (2007).

[90] P. Crochet *et al.,* Nucl. Phys. A **624**, 755 (1997).

[91] W. Reisdorf *et al.,* Phys. Rev. Lett. **92**, 232301 (2004).

[92] W. Reisdorf *et al.,* Phys. Lett. B **595**, 118 (2004).

[93] A. Andronic, J. Lukasik, W. Reisdorf, and W. Trautmann, Eur. Phys. J. A **30**, 31 (2006); C. Escano-Rodriguez *et al.,* nucl-ex **0503007** (2005) submitted to Phys. Rev. Lett.

[94] N. Bastid *et al.,* Phys. Rev. C **72**, 011901 (2005).

[95] J. Lukasik *et al.,* Proc. of INPC **2**, 513 (2007).

[96] J. Y. Ollitrault, A. M. Poskanzer, and S. A. Voloshin, Phys. Rev. C **80**, 014904 (2009).

[97] E. Schiller, H. Muther, P. Czerski, Phys. Rev. C **59**, 2934 (1999); P. Bozek, P. Czerski, Acta. phys. Polo. B **34**, 2759 (2003).

[98] J. P. Bondorf, A.S. Botvina, A.S. Iljinov, I.N. Mishustin, and K. Sneppen, Phys. Rep. **257**, 133 (1995). S. Pal, S. K. Samaddar, and J. N. De, Nucl. Phys. A **608**, 49 (1996), D. K. Srivastava *et al.,* Nucl-th/0506075 (2005); L. Satpathy, M. Mishra, A. Das, M. Satpathy, Phys. Lett. B **237**, 181 (1990); C. B. Das, A. Das, L. Satpathy, M. Satpathy, Phys. Rev. C **53**, 1833 (1996).

[99] J. P. Bondorf, R.Donangelo, I.N. Mishustin, C.J. Pethick, H. Schulz, and K. Sneppen, Nucl. Phys. A **443**, 321 (1985); *ibid* **444**, 460 (1985); *ibid* **448**, 753 (1986). G. A. Souliotis *et al.,* Phys. Rev. C **75**, 011601 (2007); S. Pal, S. K. Samaddar, J. N. de, and B. Djerroud, Phys. Rev. C **57**, 3246 (1998); A. Das, M. Mishra, M. Satpathy, and L. Satpathy, J. Phys. G: Nucl. and Part. **19**, 319 (1993).

[100] D. H. E. Gross, Rep. Prog. Phys. **53**, 605 (1990).

[101] S.R. Souza, W.P. Tan, R. Donangelo, C.K. Gelbke, W.G. Lynch, and M.B. Tsang, Phys. Rev. C **62**, 064607 (2000).

[102] W. Bauer, D. R. Dean, U. Mosel, and U. Post, Phys. Lett. B **150**, 53 (1985); W. Bauer, U. Post, D. R. Dean, and U. Mosel, Nucl. Phys. A **452**, 699 (1986).

[103] J. Pan, S. Das Gupta, Phys. Lett. B **344**, 29 (1995); J. Pan, S. D. Gupta, Phys. Rev. C **51**, 1384 (1995); S. D. Gupta and J. Pan, Phys. Rev. C **53**, 1319 (1996).

[104] W.A. Friedman, Phys. Rev. C **42**, 667 (1990).

[105] H. Stocker and W. Greiner, Phys. Rep. **137**, 277 (1986); J. Aichelin, Phys. Rep. **202**, 233 (1991).

[106] A. K. Kerman and S. E. Koonin, Ann. of Phys. **100**, 332 (1976); P. Bonche, S. Koonin and J. W. Negele, Phys. Rev. C **13**, 1226 (1976); K. T. R. Davies and S. E. Koonin, Phys. Rev. C **23**, 2042 (1981); M. D. Toro, G. Russo, and F. Duggan, Phys. Rev. C **21**, 2054 (1980).

[107] G. F. Bertsch, H. Kruse and S. D. Gupta, Phys. Rev. C **29**, R673 (1984); J. J. Molitoris, H. Stocker, and B. L. Winer, Phys. Rev. C **36**, 220 (1987); C. Gale *et al.,* Phys. Rev. C **41**, 1545 (1990); W. Cassing, W. Metag, U. Mosel, and K. Nitta, Phys. Rep. **188**, 363 (1990).

[108] H. Kruse, B. V. Jacak, and H. Stocker, Phys. Rev. Lett. **54**, 289 (1985); J. J. Molitoris, A. Bonasera, B. L. Winer, and H. Stocker, Phys. Rev. C **37**, 1020 (1988).

[109] E. Suraud, C. Gregoire, and B. Tamain, Prog. Part. Nucl. Phys. **23**, 357 (1989).

[110] A. Bonasera, G. F. Burgio, and M. D. Toro, Phys. Lett. B **221**, 233 (1989); A. Bonasera, G. Russo, and H. H. Wolter, Phys. Lett. B **246**, 337 (1990).

[111] L. Wilets, Y. Yariv, and R. Chestnut, Nucl. Phys. A **301**, 359 (1978); A. R. Bodmer, C. N. Panos, and A. D. MacKellar, Phys. Rev. C **22**, 1025 (1980); A. Vicentini, G. Jacucci and V. R. Pandharipande, Phys. Rev. C **31**, 1783 (1985).

[112] J. Aichelin and H. Stocker, Phys. Lett. B **176**, 14 (1986).

[113] G. Peilert, H. Stocker, W. Griener, A. Rosenhauer, A. Bohnet, and J. Aichelin, Phys. Rev. C **39**, 1402 (1989).

[114] B. A. Li *et al.,* Phys. Rev. C **52**, R1746 (1995).

[115] B. A. Li, Phys. Rev. Lett. **88**, 192701 (2002) and refs. therein

[116] M. Colonna *et al.,* Phys. Rev. C **57**, 1410 (1998).

[117] C. Hartnack *et al.,* Nucl. Phys. A **495**, 303 (1989); C. Hartnack Ph.D thesis, GSI-Report **93-5** (1993); C. Hartnack, J. Aichelin, H. Stöcker, and W. Greiner, Mod. Phys. Lett. A **9**, 1151 (1994); Phys. Lett. B **336**, 131 (1994); S. Soff *et al.,* Phys. Rev. C **51**, 3320 (1995); C. Hartnack *et al.,* Eur. Phys. J. A **1**, 151 (1998).

[118] C. Hartnack, H. Oeschler, and J. Aichelin, Phys. Rev. Lett. **90**, 102302 (2003); J. Phys. G: Nucl. and Part. Phys. **35**, 044021 (2008).

[119] S. A. Bass, C. Hartnack, H. Stöcker, and W. Greiner, Phys. Rev. C **51**, 3343 (1995); B. J. VerWest and R. A. Arndt, Phys. Rev. C **25**, 1979 (1982); J. Y. Liu *et al.,* Phys. Rev. Lett. **86**, 975 (2001).

[120] J. Singh, S. Kumar, and R. K. Puri, Phys. Rev. C **62**, 044617 (2000); *ibid.,* **65**, 024602 (2002).

[121] S. Kumar, Ph.D Thesis 1999, Punjab University, Chandigarh (India).

[122] R. K. Puri, C. Hartnack, and J. Aichelin, Phys. Rev. C **54**, R28 (1996); P. B. Gossiaux, R. K. Puri, C. Hartnack, and J. Aichelin, Nucl. Phys. A **619**, 379 (1997).

[123] A. Schuttauf *et al.,* Nucl. Phys. A **607**, 457 (1996).

[124] S. Kumar, S. Kumar and R. K. Puri, Phys. Rev. C **81**, 014611 (2010); 11^{th} Punab Science Congress, Thapar University, Patiala **p38**, Feb. 7-9, (2008); National Seminar on Advances in Physics, Panajb University, Chandigarh (India), Feb 28-March 1, (2008); Zakopane Conference on Nuclear Physics, Poland, Sep. 1-7, (2008); Int. Symposium on Nuclear Physics, BARC, Bombay Dec. 8-12, (2009).

[125] S. Kumar and S. Kumar, Chin. Phys. Lett. **27**, 062504 (2010); S. Kumar, S. Kumar, R. K. Puri, Phys. Rev. C **81**, 014601 (2010); 53^{rd} DAE Symosium on Nuclear Physics, IIT, Roorkee (India) 53, 569 (2008); *ibid* 571 (2008); INS Seminar NSTD2009, Thapar University, Patiala, Oct. 10-11, (2009).

Chapter 2

Methodology

2.1 Introduction

As discussed in chapter 1, the conventional mean field theory [1] like the Hartree-Fock and Schröedinger equation are suitable for the low energy reactions. On the other hand, contrary to the TDHF approach, the cascade model [2] describes very high energy heavy-ion collisions. It neglects mean field completely and take only nucleon-nucleon collisions without Pauli-blocking into account. The dynamics at intermediate energies, however, requires the equal weightage to nucleon-nucleon binary and mean field. This demands exact information about the real (trajectory of nucleons) and imaginary (nucleon-nucleon collisions) parts of the potential. Furthermore, to extract the information of the equation of state (EOS) of neutron-rich matter at intermediate energies from heavy-ion reactions induced by neutron-rich (stable and/or radioactive) beams, one must include explicitly the isospin degree of freedom. This isospin degree of freedom enter into real and imaginary part in term of iso-vector (symmetry) potential, and isospin-dependent in-medium nucleon-nucleon cross-sections, Pauli-blocking, respectively. In addition, one also has to deal from the start (where matter is non-equilibrated) to the final state (where matter is cold and fragmented). The dynamical transport models employed at intermediate energies are supposed to be including the essential collision physics. These dynamical models at intermediate energies can be subdivided into two classes: Those which follow the time evolution of the one-body phase space distribution i.e. VUU type, IBUU and SMF and those which are based on N-body molecular dynamics or cascade schemes i.e QMD and IQMD. In the present chapter, we shall study QMD and IQMD models in detail.

2.2 Various models used to study the heavy-ion collisions without isospin effects

2.2.1 VUU-type Models

The microscopic transport models for the one-body Wigner phase space density distribution obtained different names although they solve the same equation. They differ in the technical realization, i.e. the computer program, and are known as Vlasov Uehling-Uhlenbeck (VUU) model [3] (or BUU[4], LV [5]). They solve the following transport equation for the one-body Wigner density $f(r,p,t)$ in the limit $\hbar \to 0$:

$$\begin{aligned}\frac{\partial f}{\partial t} \; + \; v \cdot \nabla_r f - \nabla_r U \cdot \nabla_p f \;\; &= \;\; -\frac{4\pi^3(\hbar c)^4}{\hbar (mc^2)^2} \int \frac{d^3\acute{p_1}}{(2\pi\hbar)^3} \; \frac{d^3\acute{p_2}}{(2\pi\hbar)^3} \; d^3p_2 \; \frac{d\sigma}{d\Omega} \\ &\times \Big[f \; f_2 (1-\acute{f_1})(1-\acute{f_2}) \; - \; \acute{f_1}\acute{f_2}(1-f)(1-f_2) \Big] \\ &\times \delta^4(p \; + p_2 \; - \acute{p_1} - \acute{p_2}). \end{aligned} \tag{2.1}$$

The l.h.s. of this equation is the total differential of f with respect to the time assuming a momentum independent potential U. This potential is calculated self consistently and corresponds to the real part of the Brückner G-matrix. Usually a Skyrme-parametrization

$$U \;\; = \;\; \alpha \left(\frac{\rho}{\rho_0} \right) \; + \; \beta \left(\frac{\rho}{\rho_0} \right)^{\gamma} \tag{2.2}$$

of the real part of the G-matrix is employed, where ρ is the nuclear density which is frequently measured in units of the saturation density ρ_0 of cold nuclear matter.

The r.h.s. of eqn. 2.1 contains a Boltzmann collision integral, which is identified with the imaginary part of the G-matrix. This part describes the influence of binary hardcore collisions, where the term with ff_2 describes the loss of particles (in a phase space region) and the terms with $f_1 f_2$ the gain term due to collisions feeding the considered phase space region. It is supplemented with the Nordheim-Uehling-Uhlenbeck modifications in order to obey the Pauli-principle in the final state of the collisions[6]. The δ-functions assure the conservation of the four momentum. The cross section σ is normally adjusted to the free nucleon-nucleon scattering. The differences from cross sections calculated from the imaginary part of the Brückner G-matrix are minor [7] and influence little the observables of a heavy ion collision. For a derivation of this eqn. see [8].

The equation is solved by the use of the test particle method. Here the continuous one-body distribution function f at $t = 0$ is represented by an ensemble of $n \cdot (A_p + A_t)$ point like

particles. The recent calculations, however, use Gaussian wave packets for test particles[9]. This is often viewed as an ensemble of n parallel events with $A_p + A_t$ physical particles each, where A_p and A_t denote the number of nucleons in projectile and target, respectively. The l.h.s. of eqn.2.1 can be regarded as the transport equation (Vlasov-equation) for a distribution of classical particles whose time evolution is governed by Hamilton's equations of motion.

$$\dot{p_i} \;=\; -\;\frac{\delta\langle\; H\;\rangle}{\delta r_i};\;\; \dot{r_i} \;=\; \frac{\delta\langle\; H\;\rangle}{\delta p_i}, \tag{2.3}$$

The test particles move due to their own, self consistently generated mean field. The r.h.s. is taken into account by additional stochastic scattering similar to the collisions in cascade models [10].

More explicitly the test particle method corresponds to the replacement of the expectation value of a single particle observable

$$\langle O(t)\rangle \;=\; \int\; f(r,p,t)\; O(r,p)\; d^3r\; d^3p, \tag{2.4}$$

by a Monte Carlo integration

$$\langle O(t)\rangle \;=\; \frac{1}{n(A_T\;+A_P)}\;\;\sum_{i=1}^{n(A_T+A_P)}\;\; O(r_i(t),\; p_i(t)), \tag{2.5}$$

Where the $r_i(t)$ and $p_i(t)$ are point in phase space which are distributed according to $f(r,p,t)$, i.e.,

$$f(r,\;p,t) \;=\; \lim_{n\to\infty}\frac{1}{n(A_T\;+\;A_P)}\;\;\sum_{i=1}^{n(A_T\;+\;A_P)}\;\;\delta(r\;-\;r_i(t))\delta(p\;-\;p_i(t)). \tag{2.6}$$

It is evident that a large number n is necessary to avoid numerical noise. Predictions beyond the one-body level are not feasible although several attempts have been made to relate the (unphysical) numerical noise to physical fluctuations. In practice the number n lies in the range between 15 and 500 and one employs a grid to obtain a smooth phase space density distribution.

The numerical realization can be achieved in various ways. VUU uses a phase space sphere around each particle in order to determine f and a coordinate space sphere to determine ρ and thus $U(\rho)$. This corresponds to a Lagrangian method. On the contrary, BUU uses a fixed grid corresponding to an Eulerian method in hydrodynamics. In both models collisions

are treated in a parallel event method, only test particles of the same events, i.e. the $A_p + A_t$ test particles with the same index n, can collide. The Landau-Vlasov model determines f by the overlap of several Gaussians. The collisions are performed in a crossed event (or full ensemble) method where all $n(A_p + A_t)$ may collide with each other particle with a scaled cross section.

For a solution of (eqn. 2.1) proper boundary conditions have to be specified. In the case of heavy ion reactions, the test particles are distributed according to the density- and Fermi-momentum distribution of ground state nuclei. The latter are then boosted onto every other with the proper relative momentum. Initially the test particles are randomly distributed in a coordinate space sphere of the radius $R = 1.12A^{1/3}$ fm (where A is the atomic number of the nucleus) and in a momentum space sphere of the radius of the corresponding Fermi momentum.

One should keep in the mind that the forces acting on the test particles are calculated from the entire distribution including test particles from all events, hence the n parallel events are not independent and event-by-event correlations cannot be analyzed within this one-body transport models. In the limit $n \to \infty$ the distribution of these propagated test particles at the time t represents the one-body distribution function at this time.

Another method to solve the collision integral of eqn. 2.1 was developed by Bonasera *et al.* [11]. In this method, concept of mean free path was used to solve the collision integral where mean free path was defined as:

$$\lambda \; = \; \frac{1}{\sigma_{NN}\rho_{test}/N} \tag{2.7}$$

Where σ_{NN} is the free nucleon-nucleon cross-section and N is the number of test particles per nucleon. The test particle density is represented by ρ_{test}. One can have (i) Parallel ensembles approximation in which N = 1 and $\rho_{test} = \rho_0$ (normal nuclear matter density). Since single ensemble is not enough to avoid numerical noise, one needs to perform n parallel events and (ii) Full phase-space evaluation of the collision integral which is similar to the method described above in the BUU model. In this case $N >> 1$ and $\rho_{test} = N\rho_0$. Only one ensemble is necessary to calculate the average physical quantities. Note that in both cases, mean free path remains the same, i.e., if one increase the test particle density, accordingly one reduces the nucleon-nucleon cross section.

Any one-body observable can be calculated by averaging the values weighted with the distribution function. In brief, the $VUU - type$ model is able to explain the one-body observables like the collective flow, stopping as well as particle spectra [9], but, fluctuations and correlations, such as the formation of fragments or the description of two-particle correlations in relativistic heavy ion collisions, are beyond the scope of a transport model based on a one-body distribution function [12]. In the following, we describe in detail the *Quantum Molecular Dynamics (QMD)* model [13, 14], which is an N-body model. The recent developments in the $VUU - type\ i.e\ BUU$ model incorporate the momentum dependent potential [15], isospin dependent potential as well as isospin dependent nucleon-nucleon scattering cross section [16]. In order to study, isospin effects in neutron-rich systems, for one-body distribution function, the BUU model with isospin effects and *Stochastic Mean Field (SMF)* [17] is used in literature. Additionally, for N-body distribution, *isospin dependent quantum molecular model (IQMD)* [18] is used. These models are discussed later in the coming sections.

2.2.2 Quantum Molecular Dynamics (QMD) Model

The classical molecular dynamics (CMD) approach, which is a true N-body theory, is capable of treating both the compression and fragments formation, but on a completely classical level: the Hamilton's equation of motion are integrated for N classical point particles, with finite range nucleon-nucleon potential. Based on the CMD approach, Aichelin and Stocker[19], designed a novel method that incorporates N-body correlations, an equation of state and most important quantum features, namely, the Pauli-principle, Stochastic scattering as well as particle production. It is based on an event by event method. Here each event is simulated independent of other events. In contrast to BUU model, no averaging is done over various events and hence, the correlations among nucleons can be preserved. The simulation models like BUU, QMD [13, 14] etc. need three steps. First, one has to generate the nuclei. This procedure is called as *initialization*. It becomes very important to make sure that our initialization do not destabilize the cold nuclei. For this, we will discuss some *initial checks for stability of nuclei.* Then propagate under the influence of surrounding mean field. This is termed as *propagation*. Finally, nucleons are bound to collide if they

come too close to each other. This part is dubbed as *nucleon-nucleon collisions*. These nucleon-nucleon collisions and mean field effects make uni-important to check the role of *Pauli blocking*. In the following, we shall discuss all of these parts in detail.

Initialization

The fact that the TDHF (Slater determinant is used for initialization) and classical Vlasov (Point-like nucleons used in initialization) yield nearly the same results, depicts [20] that different initialization does not influence the nuclear dynamics. Therefore, detailed form of the wave function has only minor influence on the time evolution of the bulk properties of the system, provided it fulfills the minimal requirements, like approximate constant density over the proper region in coordinate space. In QMD model, the nucleons are represented by Gaussian wave packets which interact by mutual two- and three-body forces. The model simulates the heavy ion collisions on an event by event basis and as a consequences, preserve the correlations and fluctuations. Each nucleon is represented by a coherent state of the form

$$\psi_i(r,\ p_i(t),\ r_i(t)) \ = \ \frac{1}{(2\pi L)^{3/4}} exp\left[\frac{i}{\hbar}\ p_i(t)\cdot r \ - \ \frac{(r \ - \ r_i(t))^2}{4L}\right]. \tag{2.8}$$

The parameter L, which is related to the extension of the wave packet in phase-space. For more details related to L value, reader is refered to Ref.[18]. The total N-body function is assumed to be the direct product of coherent states (eqn. 2.8)

$$\Phi \ = \ \prod_i \psi_i(r,\ r_i, p_i, t). \tag{2.9}$$

As discussed earlier, we do not use a Slater determinant (with $(A_P \ + A_T)!$ summation terms) and thus, neglect the anti-symmetrization. First successful attempts to simulate the heavy ion reactions with anti-symmetrized states have been performed for smaller systems [21, 22]. As the model is semi-classical, so, in order to transit from quantum mechanical wave function to classical distribution function in phase space, the Wigner distribution function is used. The Wigner transforms of the coherent states are Gaussian in momentum and coordinate space. The Wigner density reads as

$$f_i(r,\ p, r_i(t),\ p_i(t)) \ = \ \frac{1}{(2\pi\hbar)^3} \int e^{-\frac{i}{\hbar}p\cdot r_{12}} \psi_i(r+\frac{r_{12}}{2},\ t)\ \psi_i^*(r-\frac{r_{12}}{2},\ t) d^3 r_{12}$$

$$= \frac{1}{(\pi\hbar)^3} e^{-(r\ -r_i(t))^2/2L}\ e^{-(p\ -p_i(t))^2 2L/\hbar^2}, \tag{2.10}$$

where $r_i(t),\ p_i(t)$ define the classical orbit or the center of the Gaussian wave packet in phase-space, whereas the squared width L is assumed to be independent of the time. The density of i^{th} particle is

$$\begin{aligned} \rho_i(r) &= \int f_i(r,p,r_i(t),p_i(t))\ d^3p \\ &= \frac{1}{(2\pi L)^{3/2}}\ e^{-[r\ -\ r_i(t)]^2/2L}. \end{aligned} \tag{2.11}$$

To initialize a nucleus, we have to assign the coordinates and momenta to all nucleons. In three dimensional space [inside a sphere of radius $R = 1.14\ A^{1/3}$, where A is the mass number of the nucleus under consideration], the centers of Gaussian wave packet r_i are uniformly distributed in polar coordinate by:

$$\begin{aligned} r &= R\ x_1^{1/3}, \\ cos\theta &= 1\ -\ 2x_2, \\ \phi &= 2\pi\ x_3, \end{aligned} \tag{2.12}$$

where $x_1,\ x_2,\ x_3$ are the random numbers. The coordinates of nucleons are rejected if the distance between them is less than 1.5 fm. The local Fermi momentum is determined by the relation

$$p_F(r_i) = \sqrt{-2mU(r_i)}, \tag{2.13}$$

where $U(r_i)$ is the local potential. The center of each Gaussian wave packet p_i are uniformly distributed in polar coordinate

$$\begin{aligned} p_i &= p_F(r_i)x_4^{1/3}, \\ cos\theta &= 1\ -\ 2x_5, \\ \phi &= 2\pi x_6. \end{aligned} \tag{2.14}$$

where x_4, x_5 and x_6 are again random numbers. We reject those distributions where two particles are closer than some distance d_{min}. In other words, we demand

$$(r_i\ -\ r_j)^2\ (p_i\ -\ p_j)^2 \geq d_{min}. \tag{2.15}$$

Typically 1 out of 50,000 initializations is accepted under the present criteria. As noted from Ref.[23], the initial phase-space distribution for the colliding nuclei in QMD agrees fairly well with the experiments as well as with PPW+RPA approach.

Numerical tests for the stability of nuclei

The nuclei prepared within transport model may start emitting nucleons after the lapse of hundred fm/c. Therefore, it is very important to make sure that our initialization does not destabilize the cold nuclei. The stable fragments formation take place if the interaction among the nucleons ceases to exist. Extensive tests were conducted by *Heidelberg-Nantes-Frankfurt-Tubingen* groups to study the properties of different single nuclei. The nucleons inside a nucleus move under the influence of the mean field of their neighbors. During the motion whenever a nucleon come close to the surface of the nucleus, it is pulled back by other nucleons. Thus every nucleon remains confined in a sphere as shown in Ref. [13, 24]. Due to the local density approximation used here, the light nuclei are unstable compared to heavier one. Frankfurt group [25] showed that inclusion of Pauli-potential in the mean field keeps the nucleon stable for several thousand fm/c. Nantes Group[13] checked the stability in term of root mean square (r.m.s) radius as well as binding energy. We have also carried out various checks by calculating the binding energy and r.m.s radius of different nuclei as well as propagation of heaviest fragment. Most of the nuclei were found to be stable for couple of hundred fm/c, which is long enough for the present purpose.

Once the target and projectile are generated with proper initialization, we boost them with proper center of mass velocity. In the following, we shall first discuss the propagation and then shall discuss the nucleon-nucleon scattering/collision with Pauli-blocking effects.

Propagation

The successfully initialized nuclei are then boosted towards each other with proper center of mass velocity using relativistic kinematics. The center of each distribution moves along the Coulomb trajectories. This distribution is kept fixed until the distance between surfaces of the nuclei is 2 fm. The equation of motion of many-body system is, then, calculated by

means of a generalized variational principle: we start from the action

$$S = \int_{t_1}^{t_2} \mathcal{L}[\Phi, \Phi^*] d\tau, \tag{2.16}$$

with the Lagrange functional

$$\mathcal{L} = \langle \Phi | i\hbar \frac{d}{dt} - H | \Phi \rangle, \tag{2.17}$$

Where the total time derivative includes the derivation with respect to the parameters. The time evolution is obtained by the requirement that the action is stationary under the allowed variation of the wave function

$$\delta S = \delta \int_{t_1}^{t_2} \mathcal{L}[\Phi, \Phi^*] dt = 0. \tag{2.18}$$

The Hamiltonian H contains a kinetic term and mutual interactions V_{ij}, which can be interpreted as the real part of the Brückner G-matrix supplemented by the Coulomb interaction. The time evolution of the parameters is obtained by the requirement that the action is stationary under allowed variation of the wave function. This yields an Euler-Lagrange equation for each parameter. We obtain for each parameter λ an Euler-Lagrange equation:

$$\frac{d}{dt} \frac{\partial \mathcal{L}}{\partial \dot{\lambda}} - \frac{\partial \mathcal{L}}{\partial \lambda} = 0. \tag{2.19}$$

If the true solution of the Schrödinger equation is contained in the restricted set of wave function $\psi_i(r,\ p_i(t),\ r_i(t))$, this variation of the action gives the exact solution of the Schrödinger equation. If the parameter space is too restricted, we obtain that wave function in the restricted parameter space which comes closest to the solution of the Schrödinger equation. Note that the set of wave functions which can be covered with special parameterizations is not necessarily a subspace of Hilbert-space, thus the superposition principle does not hold.

For the coherent states and a Hamiltonian of the form $H = \sum_i T_i + \frac{1}{2}\sum_{ij} V_{ij}$ ($T_i =$ kinetic energy, $V_{ij} =$ potential energy, the Lagrangian and the variation can easily be calculated and we obtain:

$$\mathcal{L} = \sum_i \dot{r}_i p_i - \sum_{j \neq i} < V_{ij} > - \frac{3}{2Lm}, \tag{2.20}$$

$$\dot{r}_i = \frac{p_i}{m} + \nabla_{p_i} \sum_j < V_{ij} > \ = \ \nabla_{p_i} < H >, \tag{2.21}$$

$$\dot{p}_i = -\nabla_{r_i} \sum_{j \neq i} < V_{ij} >= -\nabla_{r_i} < H >, \tag{2.22}$$

with $r_i = r_i + \frac{p_i}{m} t$ and $\langle V_{ij} \rangle = \int d^3r_1 d^3p_2 \langle \psi_i^* \psi_j^* | V(r_1, r_2) | \psi_i \psi_j \rangle$.

These equations represent the time evolution and can be solved numerically. Thus, the variational principle reduces the time evolution of the n-body Schrödinger equation to the time evolution equations $6 \cdot (A_P + A_T)$. The equations of motion now show a similar structure like classical Hamiltonian equations.

$$\dot{p}_i = -\frac{\partial \langle H \rangle}{\partial r_i} \; ; \; \dot{r}_i = \frac{\partial \langle H \rangle}{\partial p_i}. \tag{2.23}$$

The numerical solution can be achieved in the spirit of the classical molecular dynamics [26]. The expectation value of total Hamiltonian reads as:

$$\begin{aligned} \langle H \rangle &= \langle T \rangle + \langle V \rangle \\ &= \sum_i \frac{p_i^2}{2m_i} + V_{Skyrme} + V_{Yuk} + V_{Coul} + V_{MDI}. \end{aligned} \tag{2.24}$$

where V_{Skyrme}, V_{Yuk}, V_{Coul} and V_{MDI} are, respectively, the local (two and three body) Skyrme, Yukawa, Coulomb and momentum dependent potentials. The momentum dependent interactions will be discussed in chapters 3 and 4. The local Skyrme interaction is written as:

$$V_{Skyrme} = \frac{1}{2!} \sum_{j;i \neq j} V_{ij}^{(2)} + \frac{1}{3!} \sum_{j,k;i \neq j \neq k} V_{ijk}^{(3)}, \tag{2.25}$$

Here, $V_{ij}^{(2)}$ and $V_{ijk}^{(3)}$ are the two and three-body interactions. The two-body interactions $V_{ij}^{(2)}$ is obtained by folding the two-body interactions with the densities of both particles.

$$\begin{aligned} \sum_{j;i \neq j} V_{ij}^{(2)} &= \sum_{j;i \neq j} \int f_i(r_i, p_i, t) \; f_j(r_j, p_j, t) \; V(r_i, r_j) \\ &\quad \times d^3r_i \; d^3r_j \; d^3p_i \; d^3p_j, \\ &= \sum_{j;i \neq j} \int f_i(r_i, p_i, t) \; f_j(r_j, p_j, t) \; t_1 \\ &\quad \times \delta(r_i - r_j) d^3r_i \; d^3r_j \; d^3p_i \; d^3p_j, \\ &= \sum_{j;i \neq j} t_1 \int f_i(r_i, p_i, t) \; f_j(r_j, p_j, t) \\ &\quad \times d^3r_i \; d^3p_i \; d^3p_j, \\ &= \sum_{j;i \neq j} t_1 \int \frac{1}{(\pi\hbar)^3} e^{-(r - r_i(t))^2/2L} e^{-(p - p_i(t))^2 2L/\hbar^2} \end{aligned} \tag{2.26}$$

$$
\begin{aligned}
&\times \frac{1}{(\pi\hbar)^3} e^{-(r-r_j(t))^2/2L}\ e^{-(p-p_j(t))^2 2L/\hbar^2}\ d^3r_i\ d^3p_i\ d^3p_j, \\
&= \sum_j\ t_1 \frac{1}{(4\pi L)^{3/2}} e^{-(r_i-r_j)^2/4L}, \\
&= t_1 \sum_{j;i\neq j} \rho_{ij}. \qquad (2.27)
\end{aligned}
$$

where

$$
\rho_{ij} = \int d^3r\ \rho_i(r)\ \rho_j(r) = \frac{1}{(4\pi L)^{3/4}} e^{-(r_i-r_j)^2/4L}. \qquad (2.28)
$$

The three-body interaction can be calculated as follows

$$
\begin{aligned}
\sum_{j,k;i\neq j\neq k} V^{(3)}_{ijk} &= \sum_{j,k;i\neq j\neq k} \int f_i(r_i,p_i,t)\ f_j(r_j,p_j,t)\ f_k(r_k,p_k,t)\ V(r_i,r_j,r_k) \\
&\quad \times\ d^3r_i\ d^3r_j\ d^3r_k\ d^3p_i\ d^3p_j\ d^3p_k, \\
&= \sum_{j,k;i\neq j\neq k} \int f_i(r_i,p_i,t)\ f_j(r_j,p_j,t)\ f_k(r_k,p_k,t)\ t_2 \\
&\quad \times \delta(r_i-r_j)\ \delta(r_i-r_k) d^3r_i\ d^3r_j\ d^3r_k\ d^3p_i\ d^3p_j\ d^3p_k, \\
&= \frac{t_2}{(2\pi L)^3 \cdot 3^{3/2}} \sum_{j,k;i\neq j\neq k} e^{-\left[(r_i-r_j)^2+(r_i-r_k)^2+(r_k-r_j)^2\right]/6L}, \\
&= \frac{t_2}{(2\pi L)^3 3^{3/2}} \sum_{j,k;i\neq j\neq k} e^{-\left[(r_i-r_j)^2+(r_i-r_k)^2\right]/6L\times\frac{3}{2}}, \\
&= \frac{t_2\ (4\pi L)^{3/2\times 2}}{(2\pi L)^3 \cdot 3^{3/2}} \left[\sum_{j\neq i} \frac{1}{(4\pi L)^{3/2}} e^{-(r_i-r_j)^2/4L}\right]^2, \\
&= \frac{t_2\ 2^3}{3^{3/2}} \left[\sum_{j\neq i} \rho_{ij}\right]^2. \qquad (2.29)
\end{aligned}
$$

From above derivation, we see that the three-body term reduces to two body term. The finite range Yukawa term V_{Yuk} and an effective Coulomb interaction V_{Coul} are also included to account for various effects, can be, read as:

$$
V_{Yuk} = t_3 \frac{exp\{-|r_i-r_j|\}/\mu}{|r_i-r_j|/\mu}. \qquad (2.30)
$$

$$
V_{Coul} = \frac{Z^2_{eff}\ e^2}{|r_i-r_j|}. \qquad (2.31)
$$

The Yukawa term (with t_3= -6.66 MeV and μ=1.5 fm) has been added to improve the surface properties of the interaction which are very important for multi-fragmentation. In nuclear matter where the density is constant, the interaction density coincides with the single particle density, and $V^{(2)}_{loc}$, as well as $V^{(2)}_{Yuk}$, are directly proportional to $(\frac{\rho}{\rho_o})$. The three-body part $V^{(3)}_{loc}$ of the interaction is proportional to $(\frac{\rho}{\rho_o})^2$. In nuclear matter, the local

Table 2.1: Parameters of static potentials [13]

K(MeV)	$\alpha(MeV)$	$\beta(MeV)$	γ	EOS
200	-356	303	1.17	Soft(S)
380	-124	70.5	2	Hard(H)
200	-390	320	1.14	SMD
380	-130	59	2.09	HMD

potential energy has the form

$$V_{loc} = \frac{\alpha}{2}\left(\frac{\rho}{\rho_o}\right) + \frac{\beta}{\gamma+1}\left(\frac{\rho}{\rho_o}\right)^2. \tag{2.32}$$

The above potential has two free (α and β) parameters, which can be fixed by the requirement that at normal nuclear matter density the average binding energy should be -16 MeV and total energy should have a minimum at ρ_o. In order to investigate the influence of different compressibilities, one can generalize the above potential energy (eqn.2.32) to

$$V_{loc} = \frac{\alpha}{2}\left(\frac{\rho}{\rho_o}\right) + \frac{\beta}{\gamma+1}\left(\frac{\rho}{\rho_o}\right)^\gamma. \tag{2.33}$$

This equation leads to the nuclear matter equation of state which connect the pressure and energy[13]. In the study of heavy-ion collisions one usually uses the so-called the Skyrme parameterization of nuclear equation of state (EOS), which contains two sets of parameter giving the same correct binding energy and saturation density, but, two different incompressibility K(one corresponds to soft EOS with $K = 200$ MeV(at smaller value of γ), another corresponds to hard EOS with $K = 380$ MeV(at larger value of γ)). The density dependence of the compressional energy per nucleon is shown in Fig.2.1 for the soft and hard interactions.

When the momentum dependent is introduced, we have to readjust the parameters of Skyrme force to have correct saturation properties for normal nuclear matter and the same incompressibilities as those of the soft and hard EOS. The new parameter sets with the momentum dependence are called SMD and HMD, respectively. These four sets of parameters are listed in table 2.1 together with the incompressibilities.

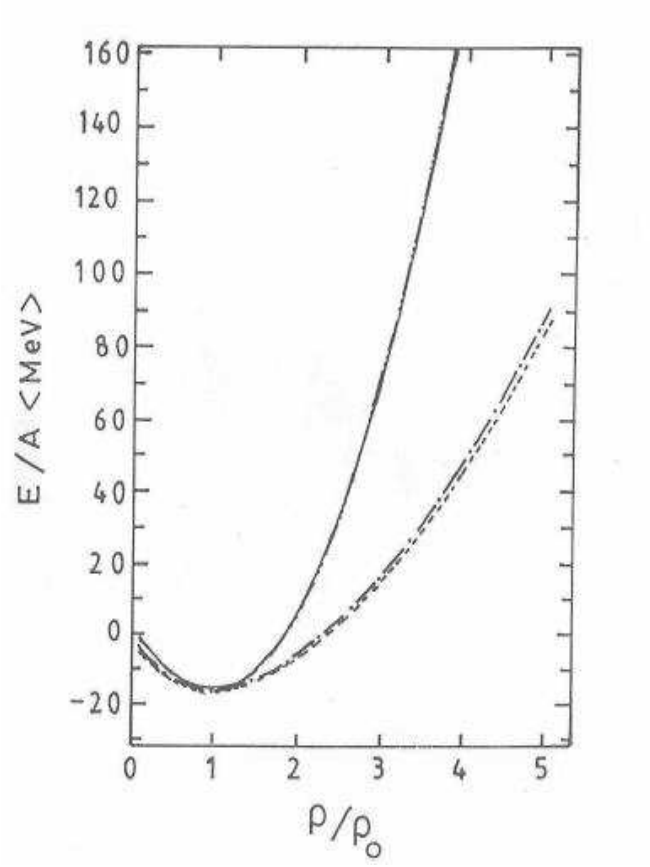

Figure 2.1: The density dependence of compression energy per nucleon. The soft and Hard interactions are shown by dash-dot-dash and solid lines, respectively. The other two lines are with momentum dependent interactions, will be discussed in detail in chapter 3. The figure is taken from Ref.[13].

The Nucleon-Nucleon(NN) Collisions

During the propagation, two nucleons can collide if they come close to each other. The effect of N-body collision is found to be rather small, therefore, we neglect the N-body collisions [27]. The collisions in QMD are treated in the same way as in BUU model. Two particles undergo scattering if they are closer than a distance $\sqrt{\frac{\sigma^{tot}(\sqrt{s})}{\pi}}$. This scattering is further subjected to the fulfillment of Pauli-principle. If the final state of scattered nucleons violate the Pauli-principle, the collision is neglected. Here the $\sigma^{tot}(\sqrt{s})$ represents the total NN cross section and '$\sqrt{s}$' is the center-of-mass energy. The detailed form of various NN cross-sections shall be discussed in chapter 4.

Pauli-blocking

The Pauli-blocking is very important quantum feature of any dynamical model, to, understand the exact reaction mechanism. Whenever a collision occurs, the phase space around the scattering partners is checked. For simplicity, we assume that each nucleon occupies a sphere in coordinate and momentum space. This trick yields the same Pauli blocking ratio as an exact calculation of the overlap of the Gaussians, will yield. We calculate the fractions P_1 and P_2 of final phase spaces for each of the two scattering partners that is already occupied by other nucleons. The collision is blocked with a probability

$$P_{block} \;=\; 1 \;-\; [1 \;- min(P_1, 1)]\,[1 -\; min(P_2, 1)]\,, \tag{2.34}$$

and, correspondingly, is allowed with probability $1 \;- P_{block}$. For a nucleus in its ground state, we obtain an averaged blocking probability $< P_{block} >$ of 0.96. For absolute blocking, this factor should be one. From above description, it is clear that the Pauli factor will be

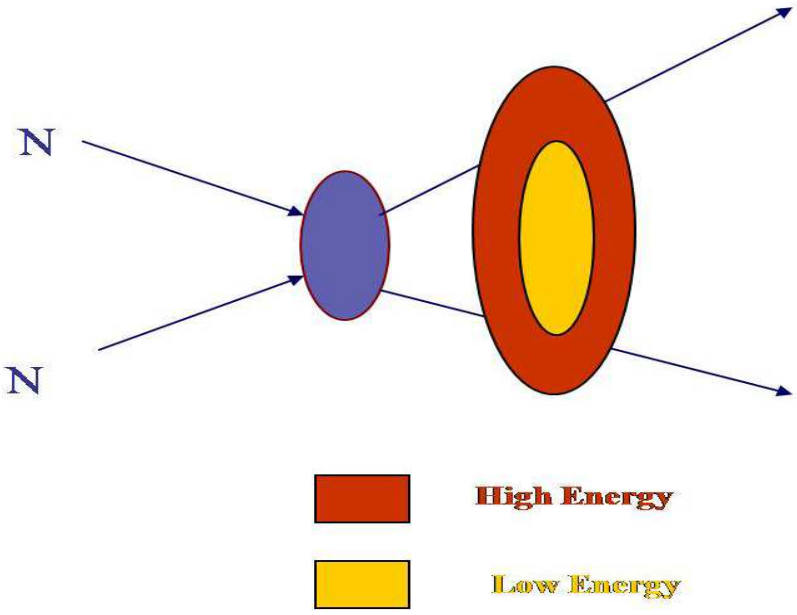

Figure 2.2: Pictorial view of Pauli-blocking at low and high incident energies.

zero or one depending whether the final phase-space is occupied or not. This sharp occupancy is valid for the cold nuclear matter only. With the passage of time, Faessler *et al.* [28] first time included the temperature by smearing the Fermi spheres for Pauli-operator. The impact of in-medium corrections is drastic at low energies. With an increase in the incident

energy, these effects start washing out and thus, the in-medium cross section approaches the free nucleon-nucleon cross section. The pictorial view of Pauli- blocking is shown in Fig.2.2, indicating the more Pauli-blocking effect at low incident energies as compared to high incident energies. On the other hand, with an increase in the bombarding energy, the velocity of particles becomes comparable to the velocity of light, therefore, the relativistic effects become very important. The relativistic versions of QMD/BUU models (RQMD and RBUU) are also available in recent years [24, 29, 30, 31]. Frankfurt group reported a new version (named UrQMD) [32], which is designed specifically for ultra-relativistic collisions, is further improved by Ref.[33] by incorporating momentum dependent Pauli potential, in-medium $NN \rightarrow N\Delta$ angular distribution and clusterization procedure.

As our present interest is to look for the various phenomena at intermediate energies(below 1 GeV/nucleon), the intensity of relativistic effect is assumed to be small [34]. If one wants to go beyond 1 GeV/nucleon, one needs to take care of the proper relativistic tools. We discuss here briefly the relativistic version of the QMD model.

2.2.3 Relativistic Quantum Molecular Dynamics (RQMD) Model

The Relativistic Quantum Molecular Dynamics [RQMD] [24, 29, 30, 31] model describes the propagation of all kinds of baryons and mesons in a Lorentz-invariant fashion. The Hamiltonian for an N-particle system is expressed in terms of 8N variables (4N position coordinates $q_{i\mu}$ and 4N momentum coordinates $p_{i\mu}$). This means that here each particle carries its own energy and time. Since the physical events are described as world lines in a 6N dimensional phase-space, extra 2N-1 degrees of freedom have to be eliminated and a global evolution parameter τ has to be defined. This can be achieved with the help of 2N constraints. In our approach, the first N constraints are chosen as Poincaré invariant mass-on shell constraints [24].

$$\xi_i = p_i^{\mu} p_{i\mu} - m_i^2 - \tilde{V}_i = 0 \qquad ; \qquad i = 1, ..., N. \tag{2.35}$$

This choice of Poincaré invariant constraints requires that the potential part $\tilde{V}_i$ should be a Lorentz the scalar and therefore, function of the Lorentz scalars only. Since in RQMD, a system with mutual two- and three-body interactions (like in QMD) has to be defined, $\tilde{V}_i$

should be given by the sum of these two-body interactions. Further, as we want to look for the relativistic effects in the dynamics, we have to generalize the non-relativistic Skyrme force in such a way that the force is covariant and reduces also to the usual Skyrme force in non-relativistic limit. This can be done as [24]

$$\tilde{V}_i = \sum_{j\neq i}^{N} \tilde{V}_{ij}(q_{Tij}^2). \tag{2.36}$$

This shows that the two-body interactions depend only on the Lorentz invariant squared transverse distance

$$q_{Tij}^2 = q_{ij}^2 - \frac{(q_{ij}^\mu p_{ij\mu})^2}{p_{ij}^2}, \tag{2.37}$$

with $q_{ij}^\mu = q_i^\mu - q_j^\mu$ being the simple four dimensional distance and $p_{ij}^\mu = p_i^\mu + p_j^\mu$ the sum of the momenta of the two interacting particles i and j.

The next set of the constraints (which fix the relative times of all particles) should be chosen in such a way that these constraints must respect the principle of causality and N-1 of these constraints should be Poincaré invariant so that the world line invariance can also be fulfilled. Another feature which these constraints has to fulfill is the cluster separability. This means that the system can be divided into single particles or clusters as soon as their Minkowski distances are space-like. Furthermore, a global evolution parameter should also be defined. These features can be fulfilled by choosing the following set of time constraints:

$$\chi_i = \sum_{j(\neq i)} \frac{1}{q_{ij}^2/L_C}\exp(q_{ij}^2/L_C) \;\; p_{ij}^\mu q_{ij\mu} = 0 \qquad ; \qquad i = 1, ..., N-1, \tag{2.38}$$

$$\chi_{2N} = \hat{P}^\mu Q_\mu - \tau = 0. \tag{2.39}$$

with $\hat{P}^\mu = P^\mu/\sqrt{P^2}$, $P^\mu = \sum_i p_i^\mu$, $Q^\mu = \frac{1}{N}\sum_i q_i^\mu$.

These time fixations take care that the time coordinates of the interacting particles should not be much dispersed in the center-of-mass system of two particles. The Hamiltonian is a linear combination of the Poincaré invariant constraints:

$$H = \sum_{i=1}^{2N-1} \lambda_i \Psi_i, \tag{2.40}$$

with

$$\Psi_i = \begin{cases} \xi_i & ; \;\; i \leq N \\ \chi_{i-N} & ; \;\; N < i \leq 2N-1. \end{cases} \tag{2.41}$$

This Hamiltonian then generates the equations of motion

$$\frac{dq_i^\mu}{d\tau} = [H, q_i^\mu], \tag{2.42}$$

$$\frac{dp_i^\mu}{d\tau} = [H, p_i^\mu]. \tag{2.43}$$

Here square brackets represent the Poisson brackets. The unknown Lagrange multipliers λ_i in eqn. 2.40 are determined by the condition that all constraints must be fulfilled for all times during the simulations. These equations of motion are used to propagate the baryon during the reaction.

The propagation and the "soft interaction" between baryons is combined with the quantum effects like stochastic scattering and the Pauli-blocking etc.. In RQMD, the collision part is treated in a covariant fashion. Therefore, all quantities which determine the collision must be Lorentz invariant. In RQMD, two baryons are allowed to collide if their distance $\sqrt{-q_{Tij}^2} \leq \sqrt{\sigma(\sqrt{s})/\pi}$ where q_{Tij}^2 is the Lorentz-invariant squared transversal distance (eq.2.48) and $\sigma(\sqrt{s})$ is the cross section depending on the available invariant mass $\sqrt{s}$.

In recent years, several refinement and improvements were made over original QMD model. The new versions were named as *MQMD*[35], *HQMD*[18], *PQMD*[25], *BQMD*[18], *Urqmd*[32], *IQMD*[18], *G-Matrix QMD*[36], *Glauber plus QMD(DQMD)*[37] etc. We will discuss IQMD in the coming section. Apart from QMD and its modified versions, there are other dynamical models, which can also used for the study of heavy-ion collisions at intermediate energies. The crucial quantum features like the antisymmetrisation were implemented in approaches like *FMD* [21] and *AMD* [22], which is further modified by including the stochastic incorporation of the diffusion and the deformation of wave packet [38]. Recently the improved version of AMD [39] was used to show the cluster-shell competition of these nuclei. However the use of AMD and FMD models are restricted, due to serious numerical problems, to light systems only. To study the fermionic nature of N-body system, new microscopic mode, dubbed as *Constrained molecular dynamics (CoMD)*, was also proposed in Ref.[40]. To study hadrons and quarks, new formalism *quark molecular dynamics (qMD)* was put forward by Hoffmann *et al.*[41].

In between the two approaches described above, namely, the statistical and dynamical,

there is a possibility for statistical-dynamical phenomenology, known as *"Hybrid Models"*. In these models, the internal dynamics is described by dynamical models and the later stage by a statistical model. The heavy-ion phase space exploration (HIPSE) account for hybrid models[42].

2.3 Various models used to study the heavy-ion collisions including isospin effects

2.3.1 Isospin-dependent Boltzmann-Uehling-Uhlenbeck (IBUU) Model

In IBUU model[16], just like, BUU model[4], the Boltzmann-Uehling-Uhlenbeck equation describes the time evolution of the single particle phase-space distribution function and reads as follow:

$$\begin{aligned}\frac{\partial f_1}{\partial t} + v \cdot \nabla_r f_1 - \nabla_r U \cdot \nabla_p f_1 &= \int \frac{d^3p_1' d^3p_2 d^3p_2'}{(2\pi)^9} \sigma_{12} v_{12} (2\pi)^3 \delta^3(p_1 + p_2 - p_1' - p_2') \\ &\times \left[f_1' f_2' (1 - f_1)(1 - f_2) - f_1 f_2 (1 - f_1')(1 - f_2') \right].\end{aligned} \tag{2.44}$$

Here σ_{12} is the differential cross-section for a certain change of momentum $(p_1, p_2) \rightarrow (p_1', p_2')$ and v_{12} is the relative velocity for the colliding nucleons.

The isospin dependence comes into the model by both the elementary nucleon-nucleon cross-section σ_{12} and the nuclear mean field U. In this model, experimental nucleon-nucleon cross-sections with the explicit isospin dependence are taken into account [43]. The isospin dependence is due to the fact that the cross-section of neutron-proton is about tree times that of the neutron-neutron or proton-proton collisions. In this model, U is the mean field, which will be a function of the local density. It can be parametrized as an arbitrary function of density, making possible to model a variety of equations of state. Typically, it can be written as, the sum of three terms:

$$U = V_{Coul} + V_n + V_{Asy}, \tag{2.45}$$

where V_{Coul}, V_n and V_{Asy} represents the Coulomb, iso-scaler nucleon potential and the symmetry energy, respectively. The nuclear mean field U including the isospin symmetry

term is parametrized as:

$$U(\rho,\tau_z) \;=\; \alpha\left(\frac{\rho}{\rho_0}\right)+\beta\left(\frac{\rho}{\rho_0}\right)^{\gamma}+(1-\rho_z)V_{Coul}+C\frac{\rho_n-\rho_p}{\rho_0}\tau_z. \tag{2.46}$$

Here ρ_0 is the normal nuclear matter density, ρ, ρ_n and ρ_p are the nucleons, neutron and proton densities, respectively. τ_z equals to +1 or -1 for neutrons or protons, respectively. The V_{Coul} as discussed above is the Coulomb potential. Other forms of the parametrization for mean fields which corresponds to probably more complete form of Skyrme forces are also possible [44]. The Skyrme term comes from averaging over the constituent two-body forces with Heisenberg component proportional to $(\tau_i,\ \tau_j)$ [45]. Its strength C can be deduced from experiments (e.g. nuclear symmetry energies, optical potentials for nucleon scatterings, excitation of analog states in (p,n) reactions). However, the strength deduced vary significantly from reaction to reaction and also depends on the energy of nucleon[45]

This model provides an accurate description of the time dependence of the one-body distribution function. Accurate solution of the *BUU* equation average away fluctuations in the density that might lead to the formation of fragments in an individual collision. This is usually achieved by solving the *BUU* equation with a large number of test particles per nucleon N_{test}. The density fluctuations that lead to the fragment production are suppressed in the *BUU* equation, so the calculation of fragment yield directly via *IBUU* model is not feasible. Therefore, alternate model such as, *Stochastic Mean Field (SMF)* model [17] and *Isospin Quantum Molecular Dynamics (IQMD)* model [18] has been developed to address the density fluctuations.

2.3.2 Stochastic Mean Field (SMF)Model

SMF[17], like, IBUU[16] describes the time evolution of the collision using a self-consistent mean field. In this model, fluctuations and asymmetry effects [46] are included. A density-dependent symmetry term is also used in the ground state construction of the initial condition i.e. isospin effects on the nucleon-nucleon cross-section and Pauli-blocking are consistently evaluated. The nucleon-nucleon mean field including the isospin asymmetry is parametrized as:

$$U(\rho) \;=\; \alpha\left(\frac{\rho}{\rho_0}\right) \;+\; \beta\left(\frac{\rho}{\rho_0}\right)^{\gamma} \;+\; C(\rho)\left(\frac{\rho_n-\rho_p}{\rho_0}\right)\tau_z, \tag{2.47}$$

Here, α, β and γ have their usual meanings as in QMD model. In this model, two different choices for the density dependence of symmetry term is used:

$C = 32\ MeV$; ASY-STIFF choice,

$C/\rho_0 = a + b\rho$ with $a = 481.7$ MeV fm^3, $b = -1638.2$ MeV fm^6: ASY-SOFT choice. These two parameterization give close values for the symmetry at normal nuclear matter density $\rho_0 = 0.17\ fm^{-3}$. In the lower density region, they are quite similar, while, at higher densities, the difference is observed. The asy-soft symmetry energy shows a decrease and it changes sign at density $\rho \approx 2\rho_0$. Moreover, the difference between the asy-stiff and asy-soft increases for large asymmetries [17].

For the reaction mechanisms like fragmentation and deep inelastic scattering, it is quite important to have a dynamical approach which includes fluctuations in a consistent way. In this SMF approach, fluctuations are introduced in two different approaches just starting from a local equilibrium assumption in a phase space cell[46]. In the first approach, a fluctuation term is added to the standard Boltzmann-Nordeim-Vlasov (BNV) equation to account for the stochastic force, the strength of which is adjusted to reproduce the growth of the most important unstable mode in the system. In practical term, the stochastic force is a type of stochastic noise. The second approach uses this fact by approximating it with numerical noise caused by solving BUU with a small number of test particles (i.e. $N_{test} = 50$) per nucleon.

Keeping in mind the requirement of intermediate energy region, one would like to have method where correlations and fluctuations among nucleon can be preserved. SMF, like, IBUU model is stable to explain one-body observables like collective flow etc. indicating correlation is not preserved among the nucleons. Moreover, SMF model have the advantage to account for the fluctuations among the nucleons. In order to include both correlations and fluctuations with isospin effects, one must have some other dynamical model. This dynamical model, which explicitly incorporates the N-body correlations as well as nuclear mater equations of state and important quantum features(like Pauli Blocking, Stochastic scattering, particle production and isospin effects) is dubbed as *Isospin-dependent quantum molecular dynamics (IQMD)* model[18]. This model is developed by Ch. Hartnack and co-workers in 1998. In the following section, we will explained this model in detail.

2.3.3 Isospin-dependent Quantum Molecular Dynamics (IQMD) Model

The most widely used microscopic models for the description of heavy-ion collisions were based on the Vlasov- Uehling-Uhlenbeck (VUU) theory [3, 20], which explicitly treats non-equilibrium and (stochastic) quantum effects in the framework of one particle quantities, as well as nuclear potential (nuclear equation of state). However, certain fluctuations and correlations, such as the formation of fragments in heavy-ion collisions, can not be studied with a transport model based on a single particles distribution function. This was one of the motivations for the development of the Quantum Molecular Dynamics (QMD) model[13, 14].

Isospin is treated explicitly (in the so called QMD version), a symmetry potential (to achieve corrected distributions of protons and neutrons in the nucleus) and explicit Coulomb forces between the Z_P and Z_T protons are included. The isospin-dependent quantum molecular dynamics (IQMD)[18] model treats different charge states of nucleons, deltas and pions explicitly[47], as inherited from the VUU model [3, 20]. The IQMD model has been used successfully for the analysis of large number of observables from low to relativistic energies [18, 47, 48]. The isospin degree of freedom enters into the calculations via both cross-sections and mean field[3, 49]. This model also includes three important steps: First, one has to generate the nuclei. This procedure is called as *initialization*. Then propagate under the influence of surrounding mean field. This is termed as *propagation*. Finally, nucleons are bound to collide if they come too close to each other. This part is dubbed as *collisions*. The elastic and inelastic cross-sections for proton-proton, neutron-neutron as well as proton-neutron are supposed to be affected in the presence of isospin. The details for these cross-sections will also be discussed in the last step. In the following, we shall discuss all of these parts in detail.

Initialization

In this model, baryons are represented by Gaussian-shaped density distributions

$$f_i(r,p,t) = \frac{1}{\pi^2\hbar^2}\ e^{-(r-r_i(t))^2\frac{1}{2L}}\ e^{-(p-p_i(t))^2\frac{2L}{\hbar^2}}. \tag{2.48}$$

Here Gaussian width L is regarded as a description of the interaction range of particle. The system dependence of L has been introduced in IQMD in order to obtain maximum stability of the nucleonic density profiles. For the heavier system (e.g. Au + Au), its value is chosen 8.66 fm^2, while for lighter one (i.e. Ca + Ca), the value is 4.33 fm^2.

Nucleons are initialized in a sphere with radius $R = 1.12A^{1/3}$ fm, in accordance with the liquid drop model. Each nucleon occupies a volume of h^3, so that phase space is uniformly filled. The initial momenta are randomly chosen between 0 and Fermi momentum(p_F), without any further local constraints.. The Fermi momentum p_F depends on the ground state density. For $\rho_0 = 0.17\ fm^{-3}$, it has a value of about 268 MeV/c. This possibility, however, gives a reduced binding energy per nucleon as compared to Weizsacker mass formula. Hence the initialized nuclei are less stable. On the other hand, this situation makes available the full Fermi-energy calculated from the Skyrme ansatz. The full Fermi pressure yields a stronger (as compared to IBUU and SMF) stability of the density profile against vibration modes. Moreover, the IQMD model performs a Lorentz contraction of the nucleus coordinate distribution, which becomes important at the higher energies.

Propagation

The successfully initialized nuclei are then boosted towards each other with proper center of mass velocity using relativistic kinematics. The nucleons of target and projectile interact via two and three-body Skyrme forces, a Yukawa potential and momentum dependent interactions. The isospin degree of freedom is treated explicitly by employing a symmetry potential and explicit Coulomb forces between protons of colliding target and projectile. This helps in achieving correct distribution of protons and neutrons within nucleus.

The hadrons propagate using Hamilton equations of motion:

$$\frac{dr_i}{dt} = \frac{d\langle\ H\ \rangle}{dp_i}\ ;\ \frac{dp_i}{dt} = -\frac{d\langle\ H\ \rangle}{dr_i}, \tag{2.49}$$

with

$$\begin{aligned}\langle\ H\ \rangle &= \langle\ T\ \rangle + \langle\ V\ \rangle \\ &= \sum_i \frac{p_i^2}{2m_i} + \sum_i \sum_{j>i} \int f_i(r,p,t) V^{ij}(\vec{r}', r) \\ &\quad \times f_j(r',p',t) dr dr' dp dp'. \end{aligned} \tag{2.50}$$

The baryon-baryon potential V^{ij}, in the above relation, reads as:

$$\begin{aligned} V^{ij}(r'-r) &= V^{ij}_{Skyrme} + V^{ij}_{Yukawa} + V^{ij}_{Coul} + V^{ij}_{mdi} + V^{ij}_{sym} \\ &= \left(t_1\delta(r'-r) + t_2\delta(r'-r)\rho^{\gamma-1}\left(\frac{r'+r}{2}\right)\right) \\ &\quad + t_3\frac{exp(|r'-r|/\mu)}{(|r'-r|/\mu)} \; + \; \frac{Z_iZ_je^2}{|r'-r|} \\ &\quad + t_4\ln^2[t_5({p_i}'-p)^2+1]\delta(r'-r) \\ &\quad + t_6\frac{1}{\varrho_0}T_3^iT_3^j\delta({r_i}'-r_j). \end{aligned} \tag{2.51}$$

Here Z_i and Z_j denote the charges of i^{th} and j^{th} baryon, and T_3^i, T_3^j are their respective T_3 components (i.e. 1/2 for protons and -1/2 for neutrons). Meson potential consists of Coulomb interaction only. The parameters μ and $t_1, ..., t_6$ are adjusted to the real part of the nucleonic optical potential. Other baryonic potentials like V^{ij}_{Skyrme} and V_{mdi} are isospin-independent. For the density dependence of nucleon optical potential, standard Skyrme-type parameterization is employed as displayed in eqn.2.33.

Two different equation of states using this ansatz have been implemented (as discussed in QMD also): A hard equation of state with a compressibility of 380 MeV and a soft equation of state with a compressibility of 200 MeV[13]. The Yukawa potential in IQMD V^{ij}_{Yuk} is very short ranged ($\mu = 0.4$ fm in contrast to $\mu = 1.5$ fm in QMD) and weak. The modification of the α term of the static potential is done in an particle independent way. This corresponds to the interpretation that an additional term in the Skyrme ansatz which is proportional to $(\nabla\rho)^2$ can be expended in first order to a term linear in density (which reduces α effectively) plus Yukawa potentials. Additional attractive Yukawa forces hence modify the EOS (and therefore the α term has to be modified to obtain the same EOS). Yukawa forces stabilize the nuclei because of the increase of the interaction range as compared to a δ-like Skyrme potentials. This results in the reduction of fluctuations.

Collisions

The binary nucleon-nucleon collisions are included by employing the collision term of well known VUU-BUU equation [3, 20]. The binary collisions are done stochastically, in a similar way as are done in all CASCADE models[10]. During the propagation, two nucleons are

supposed to suffer a binary collision if the distance between their centroids

$$|r_i - r_j| \leq \sqrt{\frac{\sigma_{tot}}{\pi}}, \sigma_{tot} = \sigma(\sqrt{s}, type), \tag{2.52}$$

"type" denotes the ingoing collision partners (N-N, N-Δ, N-π,..). In addition, Pauli blocking (of the final state) of baryons is taken into account by checking the phase space densities in the final states. The final phase space fractions P_1 and P_2 which are already occupied by other nucleons are determined for each of the scattering baryons. The collision is then blocked with probability

$$P_{block} \;=\; 1 - (1 - P_1)(1 - P_2). \tag{2.53}$$

Furthermore, parametrized free *pn* and *pp* cross-sections are used instead of an averaged nucleon-nucleon cross-sections. The respective strength of different cross-sections in shown in Fig.2.3. The total cross-section is the sum of the elastic and all inelastic cross-sections.

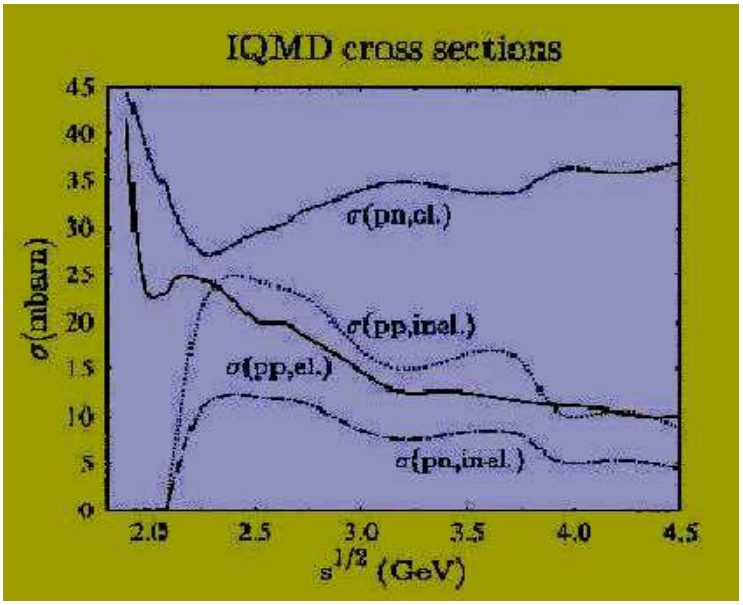

Figure 2.3: The elastic and inelastic cross-sections for proton-proton (pp)and proton-neutron (nn) used in IQMD. The neutron-neutron (nn) cross-section is assumed to be equal to pp. The total cross-section is equal to sum of elastic and inelastic cross-section. This figure is taken from Ref.[18].

$$\sigma_{tot} \;=\; \sigma el \;+\; \sigma_{inel} \;=\; \sigma_{el} \;+\; \Sigma_{channels}\sigma_i \tag{2.54}$$

The following inelastic reactions might influence the dynamics of the collision and are explicitly taken into account:

$$\begin{aligned} N\ N &\rightarrow\ \Delta\ N\ (hard-delta\ production) \quad (a),\\ \Delta &\rightarrow\ N\ \pi\ (delta\ decay) \quad (b),\\ \Delta\ N &\rightarrow\ N\ N\ (delta\ absorption) \quad (c),\\ N\ \pi &\rightarrow\ \Delta\ (soft-delta\ production) \quad (d). \end{aligned} \tag{2.55}$$

Elastic $\pi\ -\ \pi$, $\pi\ -\ N$, $\pi\ -\ \Delta$, $\Delta\ -\ \Delta$, $\Delta\ -\ N$ scattering is not taken into account. Experimental cross-sections are used for processes (a) and (d)[49], as well as for the elastic N-N collisions. Inaccessible reactions like ΔN$\rightarrow\ \ NN$ are calculated from their reverse reactions(here $NN\ \rightarrow\ \Delta N$) using modified detailed balance formula[50]. The conventional detailed balance formula is only correct for particles with infinite lifetimes (zero width). The elastic nucleon-nucleon scattering angular distribution is taken to be [51]

$$\frac{d\sigma_{el}}{d\Omega}\ \approx\ exp\left[A(s)t\right], \tag{2.56}$$

where t is $-q^2$, the transverse momentum transfer and

$$A(s)\ =\ 6\frac{\left[3.65\left(\sqrt{s}-1.8766\right)\right]^6}{1+\left[3.65\left(\sqrt{s}-1.8766\right)\right]^6}. \tag{2.57}$$

$\sqrt{s}$ is the c.m energy in GeV and A is given in $(GeV/c)^{-2}$.

The isospin degree of freedom play an important role especially for the particle production. The employed inelastic channels $NN\ \rightarrow\ NN^*,\ N\Delta\ and\ \Delta\Delta$ are treated in an analogous fashion. The parameterization is suggested by Huber and Aichelin[52] is used: fitted differential cross-sections are extracted from one-boson- exchange (OBE) calculations:

$$\frac{d\sigma_{in}}{d\Omega}\ \approx\ a(s)exp\left[b(s)cos\theta\right]. \tag{2.58}$$

The $a(s)$ and $b(s)$ are functions of $\sqrt{s}$ and vary in their definition for different intervals of $\sqrt{s}$ (see table 2.2). θ is the polar angle.

These isospin effects in the IQMD are found to vary the results, one obtained with QMD model. In the following, the importance of IQMD over QMD model is discussed.

Table 2.2: a(s) and b(s) as a function of the c.m. energy

$x = \sqrt{s}\ (GeV)$	$a\ (fm)$	b
2.104 - 2.12	$294.6(x-2.014)^{2.578}$	$19.71(x-2.014)^{1.551}$
2.12 - 2.43	$\frac{0.01224}{(x-2.225)^2\ +\ 0.004112}$	$19.71(x-2.014)^{1.551}$
2.43 - 4.50	$\left(\frac{2.343}{x}\right)^{43.17}$	$33.14\ arctan(0.5404(x-2.146)^{0.9784})$

Importance of IQMD over QMD

The importance of explicit isospin treatment can be seen in Fig.2.4[53]: The dotted line depicts the results of a QMD calculations without explicit isospin treatment: Average charges are distributed over all nucleons and the inelastic $NN \rightarrow\ N\Delta$ channel is also isospin averaged. Therefore, the neutron to proton ratio must remain constant at 1.5 for $Au\ +\ Au$ independent of transverse momentum and beam energy. The respective IQMD calculations, however, yield a totally different results: The neutron to proton ratio decreases with increasing transverse momentum due to Coulomb interactions. Apart from the p_t dependence also a strong dependence on the incident energy is observed: Due to the explicit inclusion of isospin into the inelastic channels with energy dependent branching ratios, the n/p ratio decreases with increasing beam energy.

The above mentioned models are "primary models" that are used to generate the phase-space of nucleons. As mentioned in chapter 1, we need to have "secondary models" to clusterize the nucleons into fragments. These clusterization methods are discussed briefly in the following section, while, detail is given in the respective chapter, where they are used.

2.4 Secondary models: methods of clusterization

The Minimum Spanning Tree (MST) method is the most extensively used to clusterize the nucleons[13, 54, 55]. In *MST* method, two nucleons share the same fragment if their centroids are closer than a certain distance. The method is discussed in detail in chapter 3. An improvement over the *MST* algorithm, is to put additional cut in momentum space [56]. This method is dubbed as MSTM. It will help to get rid of fragments that although close in spatial space are far in momentum space. As mentioned in the above clusterization methods,

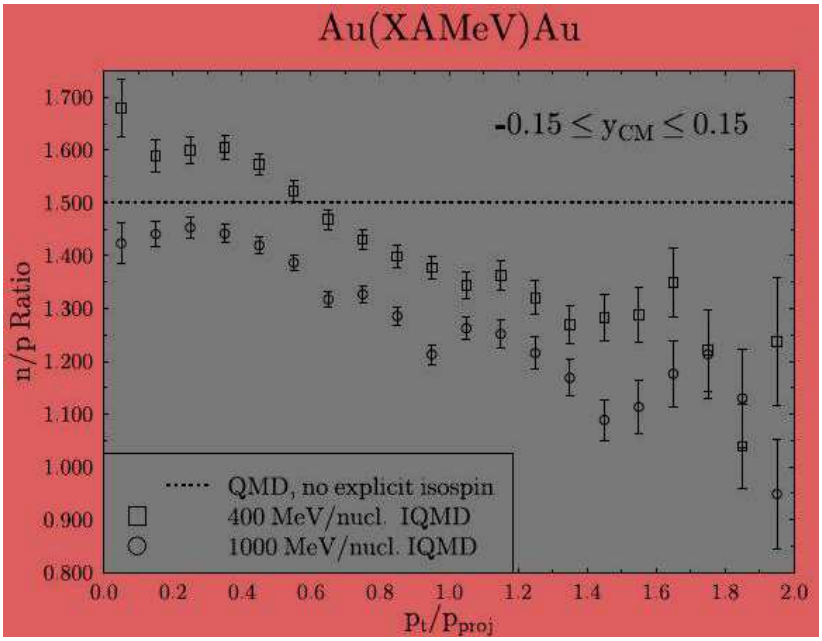

Figure 2.4: Ratio of free neutron to free protons versus transverse momentum p_t at mid-rapidity for $Au + Au$ collisions between 3 and 9 fm impact parameter at 400 and 1000 MeV/nucleon incident beam energy calculated with a hard equation of state (without momentum dependent interactions). This figure is taken from Ref.[53]

it is fairly straightforward to determine the cluster structure of a system, i.e. the particle number and velocity of each product. In practice, however, the additional running time required to reach this stage limits the practical utility of the model. It has been, therefore, of interest to devise methods for recognizing the clusters as early as possible. It is worth mentioning that it may also help to elucidate the mechanism of fragment production. A novel algorithm, namely, *Simulated Annealing Clusterization Algorithm (SACA)*, developed by Puri *et al.* [57] was based on the fact that at any given moment of the reaction, the configuration corresponding to largest binding energy is realized in nature. The detailed description of MSTM and SACA is given in chapter 4.

In summary, we discussed the details of various models in this chapter. In the following chapters, we shall present the detailed analysis of multifragmentation in the presence of momentum dependent interactions using these secondary analysis methods in the presence of *QMD* model. Apart from this, effect of symmetry energy, within *IQMD* model, on the elliptical flow, fragmentation process as well as nuclear stopping will be discussed. Our

results are also compared with experimental data of mutifragmentation and flow, whenever needed.

Bibliography

[1] J. W. Negele, Rev. Mod. Phys. **54**, 913 (1982); H. Stocker and W. Greiner, Phys.Rep. **137**, 277 (1986); F. Sakata *et al.,* Phys. Rev. C **50**, 138 (1994); D. Lacroix. and P. Chomaz, Phys. Rev. C **58**, 1604 (1998); A. S. Umar and D. Oberacker, Phys. Rev. C **74**, 024606 (2006); S. S. Chandel, S. K. Dhiman, R. Shyam, Phys. Rev. C **68**, 054320 (2003).

[2] J. Cugnon and C. Volant, Z. Phys. A **334**, 435 (1989); J. Cugnon, D. Kinet, and J. Vandermeulen, Nucl. Phys. A **379**, 553 (1982); J. Cugnon, Phys. Rev. C **22**, 1885 (1980); J. Cugnon and D. L. Hote, Phys. Lett. B **149**, 35 (1984); H. Duarte, Phys. Rev. C **75**, 024611 (2007).

[3] H. Kruse, B. V. Jacak, and H. Stocker. Phys. Rev. Lett. **54**, 289 (1985); J. J Molitoris and H. Stocker, Phys. Rev C **32**, R346 (1985).

[4] G.F. Bertsch, H. Kruse, and S. D. Gupta. Phys. Rev. C **29**, R673 (1984); J. Aichelin and G. Bertsch. Phys. Rev. C **31**, 1730 (1985).

[5] C. Gregoire, B. Remaud, F. Sebille, L. Vinet, and Y. Raffray, Nucl. Phys. A **465**, 317 (1987).

[6] E. A. Uehling and G. E. Uhlenbeck. Phys. Rev. **43**, 552 (1933); *ibid.* **44**, 917 (1934).

[7] A. Bohnet *et al.,* Phys. Rev. C **44**, 2111 (1991).

[8] W. Botermanns and R. Malfliedt, Phys. Lett. B **215**, 617 (1988); Phys. Rep. **198**, 115 (1990); W. Cassing and U. Mosel, Prog. Nucl. Part, Phys. **25**, 1 (1990).

[9] P. Ring and P. Schuk, The nuclear many-body problem, (Springer-Verlog, 1980); G. F. Bertsch and S. D. Gupta, Phys. Rep. **160**, 189 (1988); C. Gregoire, B. Remaud,

F. Sebille, L. Vincet, and Y. Raffay, Nucl. Phys. A **465**, 317 (1987); W. Bauer, Prog. Part. Nucl. Phys. **30**, 45 (1993); T. Reposeur, V. de la Mota, F. Sebille, and C. O. Dorso, Z. Phys A **357**, 79 (1997).

[10] Y. Yariv and Z. Frankel, Phys. Rev. C **20**, 2227 (1979); J. Cugnon. Phys. Rev. C **22**, 1885 (1980).

[11] A. Bonasera, G. F. Burgio, and M. D. Toro, Phys. Lett. B **221**, 233 (1989); A. Bonasera, G. Russo, and H. H. Wolter, Phys. Lett. B **246**, 337 (1990).

[12] P.B. Gossiaux, D. Keane, S. Wang, and J. Aichelin, Phys. Rev. C **51**, 3357 (1995).

[13] J. Aichelin, Phys. Report **202**, 233 (1991); G. Peilert, H. Stocker, W. Greiner, A. Rosenhauer, A. Bohnet, and J. Aichelin, Phys. Rev. **C 39**, 1402 (1989); A. Bohnet, N. Ohtsuka, J. Aichelin, R. Linden, and A. Faessler, Nucl. Phys. A **494**, 349 (1989); L. Neise, M. Berenguer, C. Hartnack, G. Peilert, H. Stocker and W. Greiner, Nucl. Phys. A **519**, 375 (1990); M. Berenguer, C. Hartnack, G. Peilert, H. Stocker, and W. Greiner, J. Phys. G **18**, 655 (1992).

[14] D. T. Khoa *et al.,* Nucl. Phys. A **542**, 671 (1992); D. T. Khoa *et al.,* Nucl. Phys. A **529**, 363 (1991); G. Q. Li *et al.,* Nucl. Phys. A **534**, 697 (1991); G. Peilert *et al.,* Mod. Phys. Lett. A **3**, 459 (1988); C. Hartnack *et al.,* Nucl. Phys. A **495**, 303c (1989).

[15] C. Gale, G. F. Bertsch, and S. D. Gupta, Phys. Rev. C **35**, 1666 (1987); C. Gale, G. M. Welke, M. Prakash, S. J. Lee, and S. D. Gupta, Phys. Rev. C **41**, 1545 (1990); Q. Pan and P. Danielewicz, Phys. Rev. Lett. **70**, 2062 (1993); J. Zhang, S. D. Gupta, and C. Gale, Phys. Rev. C **50**, 1617, (1994); V. Greco, A. Guarnera, M. Colonna, and M. D. Toro, Phys. Rev. C **59**, 810 (1999).

[16] B. A. Li and S. J. Yennello, Phys. Rev. C **52**, R1746 (1995); B. A. Li *et al.,* Phys. Rev. Lett. **76**, 4492 (1996).

[17] M. Colonna *et al.,* Phys. Rev. C **57**, 1410 (1998).

[18] C. Hartnack *et al.,* Eur. Phys. J A **1**, 151 (1998); C. Hartnack, L. Zhuxia, L. Neise, G. Peilert, A. Rosenhauer, H. Sorge, J. Aichelin, H. Stocker, and W. Greiner, Nucl. Phys. A **495**, 303 (1989); C. Hartnack, J. Aichelin, H. Stocker, and W. Greiner, Mod. Phys. Lett. A **9**, 1151 (1994); Phys. Lett. B **336**, 131 (1994); S. Soff, S. A. Bass, C. Hartnack, H. Stocker, and W. Greiner, Phys. Rev. C **51**, 3320 (1995).

[19] J. Aichelin and H. Stocker, Phys. Lett. B **176**, 14 (1986).

[20] J. Aichelin and G. F. Bertsch, Phys. Rev. C **31**, 1730 (1985); J. Aichelin, Phys. Rev. C **33**, 537 (1986); J. Aichelin and H. Socker, Phys. Lett. B **163**, 59 (1985).

[21] H. Feldmeier and J. Schnack, Prog. Part. Nucl. Phys. **39**, 393 (1997); H. Feldmeier, Nucl. Phys. A **515**, 147 (1990).

[22] A. Ono, H. Horiuchi, T. Maruyama, and A. Ohnishi, Phys. Rev. Lett. **68**, 2898 (1992); A. Ono and H. Horiuchi, Phys. Rev. C **51**, 299 (1995).

[23] M. Jaminan, C. Mahaux, and H. Ngo, Nucl. Phys. A **440**, 228 (1985); *ibid* **452**, 445 (1986). S. W. Huang, Ph. D thesis, Univ. of Tubingen, Tubingen, Germany (1994).

[24] E. Lehmann *et al.,* Phys. Rev. C **51**, 2113 (1995); H. Sorge, Phys. Rev. C **52**, 3291 (1995).

[25] G. Peilert *et al.,* Phys. Lett. B **260**, 271 (1991); G. Peilert *et al.,* Phys. Rev. C **46**, 1457 (1992).

[26] J. Molitoris, J. B. Hoffer, H. Kruse, and H. Stocker, Phys. Rev. Lett. **53**, 899 (1984); S. M. Kiselew and Y. E. Polrowskil, Sov. Journ, Nucl. Phys. **38**, 46 (1983).

[27] G. Batko, J. Randrup, and T. Vetter, Nucl. Phys. A **536**, 786 (1992); G. Batko, J. Randrup, and T. Vetter, Nucl. Phys. A **546**, 761 (1992).

[28] R. K. Puri *et al.,* Nucl. Phys. A **575**, 733 (1994).

[29] R. K. Puri, E. Lehmann, A. Faessler, and S. W. Huang, J. Phys. G **21**, 583 (1995); H. Sorge, H. Stocker, and W. Greiner, Ann. Phys. **192**, 266 (1989); J. L. Klay *et al.,* Phys. Rev. C **68**, 054509 (2003).

[30] T. Maruyama, S. W. Huang, N. Ohtsuka, G. Q. Li, A. Faessler, and J. Aichelin, Nucl. Phys. A **534**, 720 (1991); T. Maruyama, G. Q. Li, and A. Faessler, Phys. Lett. B **268**, 160 (1991); S. W. Huang, A. Faessler, G. Q. Li, R. K. Puri, E. Lehmann, D. T. Khoa, and M. A. Matin, Phys. Lett. B **298**, 41 (1993).

[31] A. Lang, Blättel, W. Cassing, V. Koch, U. Mosel, and K. Weber, Z. Phys. A **340**, 287 (1991); B. Blättel, V. Koch, W. Cassing, and U. Mosel, Phys. Rev. C **38**, 1767 (1988).

[32] M. Belkacem *et al.,* Phys. Rev. C **58**, 1727 (1998); A. Dumitru *et al.,* Phys. Rev. C **57**, 3271 (1998)

[33] K. A. Waged, Phys. Rev. C **67**, 064610 (2003); *ibid.* **70**, 014605 (2004); *ibid.* **71**, 044607.

[34] R. K. Puri, E. Lehmann, A. Faessler, and S. W. Huang, Z. Phys. A **351**, 59 (1995).

[35] L. Jianye and Z. S. Guang, Z. Phys. A **348**, 31 (1994).

[36] M. Trefz, A. Faessler, and W. H. Dickhoff, Nucl. Phys. A **443**, 499 (1985); N. Ohtusuka, R. Linden, A. Faessler, and F. B. Malik, Nucl. Phys. A **465**, 550 (1987) and references therein.

[37] K. A. Waged, Phys. Rev. C **63**, 024618 (2001); J. of Phys. G **28**, 2951 (2002).

[38] A. Ono and H. Horiuchi, Phys. Rev. C **53**, 2958 (1996).

[39] N. Itagaki *et al.,* Phys. Rev. C **70**, 054307 (2004).

[40] M. Papa, T. Maruyama, and A. Bonasera, Phys. Rev. C **64**, 024612 (2001).

[41] M. Hoffmann *et al.,* Phys. Lett. B **478**, 161 (2000); Y. Akimura *et al.,* Eur. Phys. J. A **25**, 405 (2005).

[42] D. Lacorix, A. V. Lauwe, and D. Durand, Phys. Rev. C **69**, 054604 (2004).

[43] *Total cross-sectios for reactions of High Energy particles*, edited by A. Baldini, V. Flaminio, W. G. Moorhead, and R. R. O. Morrison (Springer-Verlag, Berlin, 1988).

[44] B. Remaud, C. Grëgoire, F. Sebille, and P. Schuck, Nucl. Phys. A **488**, 423c (1988); M. Farine, T. Sami, B. Remaud, and F. Sebille, Z Phys. A **339**, 363 (1991); L. G. Sobotka, Phys. Rev. C **50**, R1272 (1994).

[45] P. E. Hodgson, *Nuclear Reactions and Nuclear Structure* (Clarendon, Oxford, 1971), Chap. 9.3.

[46] M. Colona *et al.,* in *Critical Phenomena and Collective observables,* edited by S. Costa *et al.,* (World Scientific, Singapore, 1997), p. 369.

[47] C. Hartnack, H. Oeschler, and J. Aichelin, Phys. Rev. Lett. **90**, 102302 (2003); J. Phys. G: Nucl. and Part. Phys. **35**, 044021 (2008).

[48] C. Hartnack and J. Aichelin, J. Phys. G: Nucl. and Part. Phys. **28**, 1649 (2002); *ibid.* **30**, s531 (2004)

[49] S. A. Bass, C. Hartnack, H. Stocker, and W. Greiner, Phys. Rev. C **51**, 3343 (1995); B. J. VerWest and R. A. Arndt, Phys. Rev. C **25**, 1979 (1982).

[50] P. Danielewicz and G. F. Bertsch, Nucl. Phys. A **533**, 712 (1991).

[51] J. Cugnon, T. Mizutani, and J. Vandermeulen, Nucl. Phys. A **352**, 505 (1981).

[52] J. Huber and J. Aichelin, Nucl. Phys. A **573**, 587 (1994).

[53] S. A. Bass, C. Hartnack, H. Stocker, and W. Greiner, Z. Phys. A **352**, 171 (1995).

[54] P. B. Gossiaux and J. Aichelin, Phys. Rev. C **56**, 2109 (1997).

[55] J. Singh, S. Kumar, and R. K. Puri, Phys. Rev. C **62**, 044617 (2000); *ibid.* **65**, 024602 (2002); R. K. Puri and S. Kumar, *ibid.* **57**, 2744 (1998); S. Kumar and R. K. Puri, *ibid.* **58**, 2858 (1998); S. Kumar, S. Kumar, R. K. Puri, *ibid.* **78**, 064602 (2008); S. Kumar, S. Kumar, and R. K. Puri, Phys. Rev. C**81**, 014601 (2010).

[56] S. Kumar and R. K. Puri, Phys. Rev. C **58**, 320 (1998); J. Singh and R. K. Puri, *ibid.* **62**, 054602 (2000); S. Kumar, S. Kumar, and R. K. Puri, Phys. Rev. C **81**, 014611 (2010)

[57] R. K. Puri, C. Hartnack, and J. Aichelin, Phys. Rev. C **54**, R28 (1996); P. B. Gossiaux, R. K. Puri, C. Hartnack and J. Aichelin, Nucl. Phys. A **619**, 379 (1997); Y. K. Vermani and R. K. Puri, Eur. Phys. Lett. **85**, 62001 (2009); S. Kumar and S. Kumar, Pramana J. of Phys. **74**, 731 (2010).

Chapter 3

Importance of the momentum dependent interactions and system size effects in multifragmentation

3.1 Introduction

The last gem in the field of heavy-ion collisions, namely, multifragmentation has always attracted theoreticians as well as experimentalists [1-5]. Primarily due to the several hidden phenomena that need deeper investigations and secondary due to its connection with nuclear equation of state - *a question which always has captured a central place in the research of nuclear physics*. The knowledge of the nuclear compressibility is not only relevant for the nuclear physics, it is also vital for other branches such as astrophysics. One should, however, note that the compressibility depends not only on the density but also the entire momentum plane. In other words, equation of state apart from the population of nucleons also depends upon their relative velocities. This can also been seen from the optical potential where strong momentum dependence was reported in the literature[6].

It is argued by many authors that momentum dependent nature of equation of state can have a significant effect in those situations where nuclear matter is mildly and weakly excited. If matter is highly compressed, the nucleon-nucleon correlations are already broken due to violent nucleon-nucleon collisions. However, if matter is either weakly or mildly excited, the momentum dependent interactions (MDI) can have sizable effects. The momentum dependence of the nuclear equation of state has been reported to affect the collective flow and particle production drastically [1, 6-16]. In Ref. [6], pion yield was found to suppressed by 30% once momentum dependent interactions were included in the evolution of

reaction. Moreover, the MDI's also suppressed the nucleon-nucleon collisions by the same amount. Similarly, if one goes from soft to hard equation of state, the decrease in pion yield is $\approx$ 10 %. Interestingly, a soft equation of state with momentum dependent interactions (SMD) yields the same transverse momentum as static hard equation of state[1, 6-8]. It was also shown in Ref.[17] that SMD explains the data better than the hard equation of state. Later on, in Ref. [13-16], the importance of MDI in the determination of symmetry potential and balance energy is discussed. Some initial investigations also point toward its important role in multifragmentation [9, 10, 18, 19]. These investigations reveal: (i) fragments production is strongly influenced by the MDI's at peripheral geometries (ii) universal dependence of the effect of MDI on the asymmetry of the reaction and (iii) momentum fluctuations are useful in determining the symmetry energy in neutron/proton rich systems. From the above discussion, it is clear that the momentum dependence of the nuclear mean field plays a major role in determining the nuclear dynamics and is an important feature for the fundamental understanding of nuclear matter properties over a wide range of densities and temperatures

One has to keep in mind that the response of MDI also depends on the system size. A lot of efforts are available in the literature to pin down the importance of system size effects without momentum dependent interactions. These includes the temperature as well as density, flow of nucleons/fragments, disappearance of nuclear flow, particle production and multifragmentation etc. The study of the mass dependence in the evolution of the density and temperature reveals that maximum temperature is insensitive towards the mass of the system. However, the maximum density scales with the size of the interacting system [11, 20-23]. The hot and dense matter formed in heavy ion collision lasts longer in heavier colliding nuclei compared to lighter colliding nuclei [20, 21]. Interestingly, equation of state also depends on the size of the system. Due to less compression in lighter colliding nuclei, the different equations of state do not yield different results. On the other hand, a clear difference can be seen with heavier colliding nuclei[11, 20].

Hartnack *et al.* [24] studied the system size dependence of kaon production, indicating, the probability of kaon production can be parameterized in term of the power law. On the other hand, the kaon production probability per participant was independent of the

projectile-target combination[25]. In a experiment[25], the KAOS group reported the K^+ production per nucleon which increases with the size of the system. Contrary, the pion production per nucleon decreases in the same measurement. The unique observation was that the multiplicity of the high energy pion was nearly independent of the size of the interacting system and beam energy [25]. In an other experimental analysis, the entropy of the system was found to depend weakly on the size of the system[26]. The system mass dependence of collective flow has been investigated extensively during last few years[11, 22, 23, 27]. The disappearance of collective flow at a certain energy, known as balance energy is found to depend strongly on the size of the system. It is now clear that the balance energy scales as $A_{tot}^{-1/3}$. Recently, the system size effects on the collective flow in the presence of momentum dependent interactions is studied by Sood and Puri[11]. They observed that momentum dependent interactions push energies of the vanishing flow to significant lower level for $C^{12} + C^{12}$ system, whereas for heavier systems, the trend is just opposite.

A very few attempts exist in the literature which deals with the systematic study of the mass dependence of the multifragmentation [28-32]. Most of the reported studies are without momentum dependent interactions and involve the asymmetric colliding nuclei at a fixed velocity[30, 31]. The recent reports from the FOPI experiment [28] depict the dependence of the multiplicity of heavy fragments on the size of the interacting system. This was carried out for symmetric nuclei like $Ni^{58} + Ni^{58}$, $Ru^{96} + Ru^{96}$, $Xe^{129} + Cs^{133}I^{127}$ and $Au^{197} + Au^{197}$. The above study was based on the participant-spectator model where yields are analyzed separately for the participant and spectator fragments [28]. The universality in the production of the spectator fragments was achieved in the above study which confirms the results of ALADIN experiments[31]. However, a strong mass dependence was seen for the participant fragments[28]. The systematic theoretical attempt was made to study the role of the masses of colliding nuclei in multifragmentation [12, 32], but, unfortunately, no system mass dependence study for the multifragmentation process is done in the presence of momentum dependent interactions[33].

3.2 The Momentum Dependent Interactions (MDI)

In chapter 2, we have shown that the static interactions V_{Skyrme} reduces to simple density dependent parts ($\propto \ \rho$)[eqn. 2.33. The parameter γ in eqn. 2.33 leads to different incompressibility which represent different equations of state. It is widely accepted that the static equation of state, which depends on the density only, can not describe the heavy-ion reaction adequately. The contribution in the reaction is not only due to density, but due to momentum also. In the framework of G-matrix, the momentum dependence comes in a natural way [34]. However, the numerical utility of the G-matrix is limited due to its time consuming mechanism. In this case, one uses the parametrized momentum dependent potential which takes care of the momentum dependence.

The momentum dependent interactions can be obtained by parameterizing the momentum dependent part of the optical potential which reads as [6]

$$V_{MDI}^{ij} \ = \ t_4 \ln^2[t_5(p_i{}' - p)^2 + 1]\delta(r' - r). \tag{3.1}$$

For the momentum dependent interactions, which may optionally be used in QMD/IQMD, is fitted to experimental data [35] on the real part of the nucleon optical potential[1, 6], which yields:

$$U_{mdi} \ = \ \delta \cdot ln^2\left(\epsilon \cdot (\Delta p)^2 + 1\right) \cdot \left(\frac{\rho}{\rho_0}\right) \tag{3.2}$$

These momentum dependent interactions, interestingly, give rise to two new equations of state, namely, hard momentum dependent (HMD) and soft momentum dependent (SMD), having same compressibility as static hard and soft equations of state (discussed in table 2.1). The equation of state (EOS) in its standard Skyrme-type parameterization including momentum dependence then reads:

$$U \ = \ \alpha\left(\frac{\rho}{\rho_0}\right) \ + \ \beta\left(\frac{\rho}{\rho_0}\right)^{\gamma} \ + \ \delta \cdot ln^2\left(\epsilon \cdot (\Delta\vec{p})^2 + 1\right) \cdot \left(\frac{\rho}{\rho_0}\right) \tag{3.3}$$

The parameters $t_1....t_5$ are uniquely related to the corresponding values of α, β, γ, δ and ϵ. The standard values of these parameters can be found in Ref. [1].

The momentum dependent interactions without isospin dependence in QMD/IQMD is shown by eqn. 3.1 which comes from the optical potential. Liu *et al.* [36] considered an isospin degree of freedom in MDI to obtain an isospin momentum dependent interac-

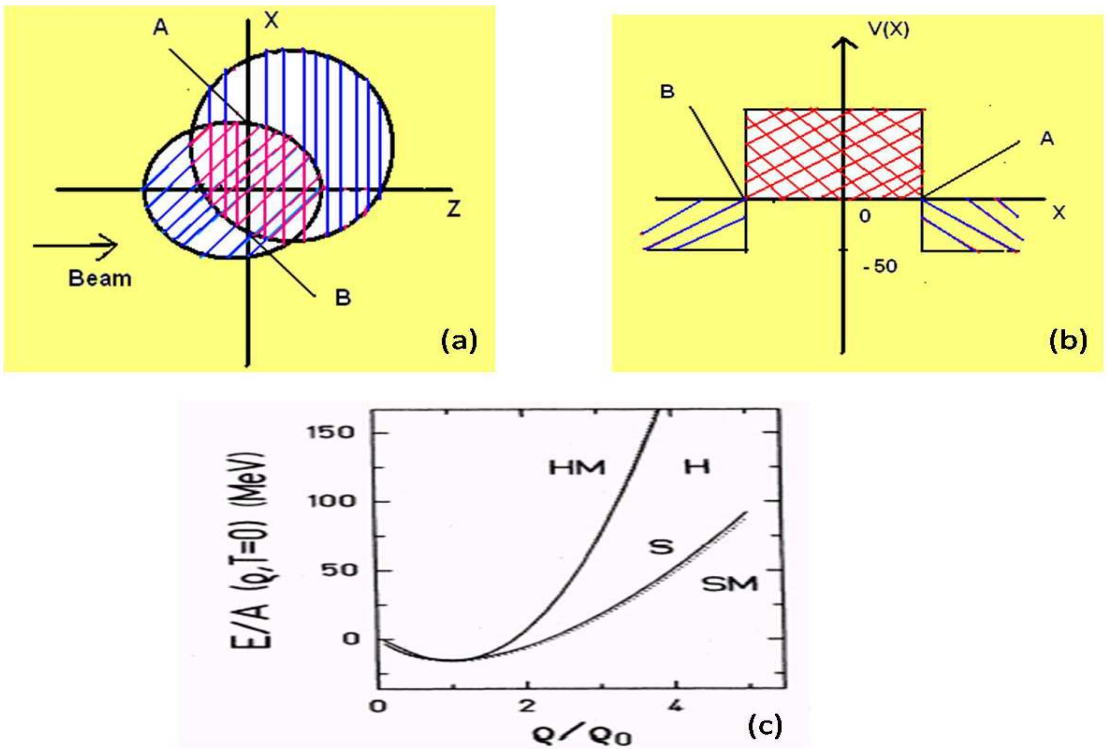

Figure 3.1: Transverse momentum caused by momentum dependent forces. (a) The reaction in the beam-impact parameter plane. (b) Graphical view of the potential produced in the reaction. We see in the overlap region strong repulsive and outside it an attractive potential. (c) The density dependence of the compression energy per nucleon. The hard, soft, HMD and SMD interactions are shown by solid, dash-dot-dash, dashed double dotted and dashed lines, respectively. The figure is taken from the Ref. [1].

tions (IMDI). In this case, an isospin degree of freedom is inserted into MDI to obtain IMDI which includes a neutron's IMDI

$$\begin{aligned} V_n^{IMDI}(\rho, k_n, p) = \quad & t_4 \ln^2[t_5(p_n{}' - p_n)^2 + 1] C_{nn} \frac{\rho_n}{\rho_0} \\ & + t_4 \ln^2[t_5(p_n - p_p)^2 + 1] C_{np} \frac{\rho_p}{\rho_0}. \end{aligned} \tag{3.4}$$

and the proton's one

$$\begin{aligned} V_p^{IMDI}(\rho, k_p, n) = \quad & t_4 \ln^2[t_5(p_p{}' - p_p)^2 + 1] C_{pp} \frac{\rho_p}{\rho_0} \\ & + t_4 \ln^2[t_5(p_p - p_n)^2 + 1] C_{pn} \frac{\rho_n}{\rho_0}. \end{aligned} \tag{3.5}$$

In the above, $p_n{}'$ indicates the momentum of other neutrons besides p_n of neutron n and $p_p{}'$ shows the momentum of other protons besides p_p of proton p and $\rho = \rho_n + \rho_p$. Finally,

an isospin momentum dependent interaction is written as:

$$V_\tau^{IMDI}(\rho, k_\tau, \tau') = \quad t_4 \ln^2[t_5(p_\tau{}' - p_\tau)^2 + 1]C_{\tau\tau}\frac{\rho_\tau}{\rho_0} \\ t_4 \ln^2[t_5(p_\tau - p'_\tau)^2 + 1]C_{\tau\tau'}\frac{\rho_{\rho'}}{\rho_0}, \tag{3.6}$$

where $\rho = \rho_\tau + \rho_{\tau'}$. Here $C_{nn} = C_{pp} = C_{\tau\tau}$ and $C_{np} = C_{pn} = C_{\tau\tau'}$. For the detailed knoweldge of the parameters, reader is suggested to the Ref.[36].

As discussed earlier, the momentum dependence of mean field potential has a crucial role to play in the description of heavy-ion collisions[1]. The individual momentum of the particle has a negligible role until the projectile and target nuclei overlap with each other. As soon as the projectile and target begin to overlap (see Fig.3.1[a]), the interaction takes place between the nucleons of projectile and target, which has a large relative momentum. Due to such a large relative momentum, the projectile nucleons feel a strong repulsion due to target nucleons in the overlap region and vice versa (see Fig.3.1[b]), while the nucleons in the spectator zone are either from the target or projectile, and hence potential is still attractive in that region(see Fig.3.1[b]). This deflects the nucleons in transverse direction during early phase of the reaction, resulting in the transfer of the momentum in the radial direction. This can result in decrease in density as well as number of collisions. The compressional energy per particle for soft, SMD, hard and HMD as a function of the nucleonic density is plotted in Fig. 3.1(c). We see that the no difference is observed in the soft, hard, SMD and HMD equations of state at normal nuclear matter density. On the other hand, the difference between different equations of state goes on increasing with increase in density above normal nuclear matter density. This motivated us to perform the study with momentum dependent interactions in intermediate energy heavy-ion collisions. In view of the above facts, it is challenging to investigate the role of momentum dependent interactions with respect to multifragmentation & see how system size affects the outcome. Our present aim, therefore, is three fold at least:

(i) to understand the role of momentum dependent interactions in multifragmentation,

(ii) to study the system size effects in the presence of momentum dependent interactions and (iii) to find a scaling to these system size effects.

3.3 Method of analysis

3.3.1 Minimum Spanning Tree (MST) Algorithm

The *MST* method is the most extensively used to clusterize the nucleons[1, 12, 33, 37]. In *MST* method, two nucleons share the same fragment if their centroids are closer than a distance d_{min},

$$|\vec{r_i} - \vec{r_j}| \ \leq \ d_{min} \tag{3.7}$$

where $\vec{r_i}$ and $\vec{r_j}$ are the spatial positions of both nucleons. The value of d_{min} can vary between 2-4 fm. The fragments production with $d_{min} \ = \ 4fm$ is shown in Fig.3.2. As reported, it has small effect on multifragmentation [37]. However, this method cannot address the question of time scale as it will give a big fragment during the early stage of the reaction where the density is quite high and the interactions between the nucleons are still active. It is worth mentioning that this method can only be used to analyze asymptotic configurations in which the fragmenting system can be viewed as a very dilute mixture of free particles and almost equilibrated fragments. To study the time of fragment formation, one needs to device a method which should be able to detect the overlapping fragments.

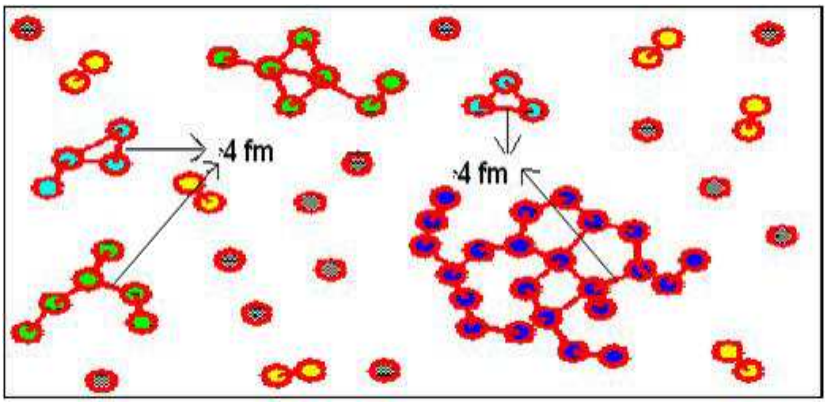

Figure 3.2: This figure is representing the fragments production with MST method where the distance between the nucleons is $\leq d_{min}$, here, $d_{min} = 4fm$.

3.4 Results and discussion

Here we simulate 100 events involving the symmetric reactions of $_{20}Ca^{40}$ + $_{20}Ca^{40}$, $_{28}Ni^{58}$ + $_{28}Ni^{58}$, $_{41}Nb^{93}$ + $_{41}Nb^{93}$, $_{54}Xe^{131}$ + $54Xe^{131}$, $_{68}Er^{167}$ + $_{68}Er^{167}$, $_{79}Au^{197}$ + $_{79}Au^{197}$ and $_{92}U^{238}$ + $_{92}U^{238}$ at incident energies between 50 and 1000 MeV/nucleon using different collision geometries. For the present analysis, soft as well as soft momentum dependent (SMD) equation of state with compressibility K = 200 MeV is used. The entire calculation is performed in the presence of a standard energy dependent nucleon-nucleon cross section due to Cugnon[1]. By using the symmetric (colliding) nuclei, system size effects can be analyzed without varying the asymmetry (and excitation energy) of the system. It is worth mentioning that the experimental studies by the MSU mini ball and ALADIN [2, 30] groups, varied the asymmetry of the reaction whereas FOPI experiments [28] are performed for the symmetric colliding nuclei only. In the following, we first discuss the phase space of nucleons followed by the time evolution of different reactions and then shall address the question of momentum dependent interactions and system size effects.

3.4.1 Phase space of nucleons

We display in Figs.3.3 and 3.4, the phase space of nucleons for X-Z and P_x − P_z plane for the reaction of $_{79}Au^{197}$ + $_{79}Au^{197}$ at semi-peripheral geometry. The panels from top to bottom are representing the position of nucleons of projectile and target at different times, while right and left panels are with and without momentum dependent interactions, respectively. The phase space remain unaffected by the momentum dependent interactions until the projectile and target overlap with each other. During and after the overlapping (above $t = 30fm/c$), more repulsion is observed in the projectile as well as target nucleons in x-z as well as $P_x - P_z$ plane. Moreover, more radial expansion of the matter is observed in the presence of momentum dependent interactions in the reaction plane. This is due to the fact that more is the repulsion, more is the squeeze-out of the particles and more is the transfer of the momentum in the radial direction. This picture is clear from the Fig.3.4, where the phase space of the $P_x - P_z$ plane is displayed. This will increase the mean free path, which will further lead to the decrease in the density as well as collisions in the presence of mo-

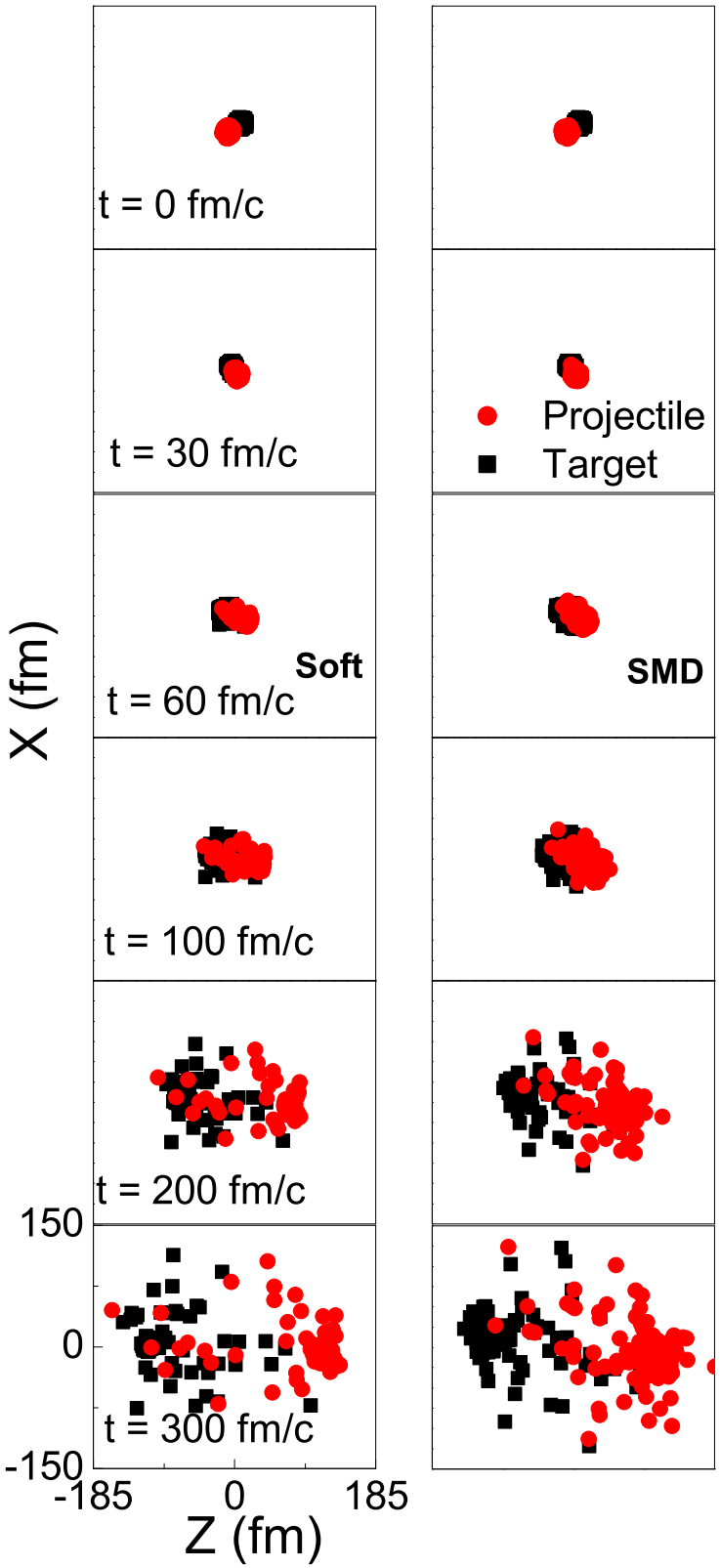

Figure 3.3: Phase space distribution of the projectile and target nucleons without (left) and with momentum dependent interactions (right) in X-Z plane. The reaction under study is ${}_{79}Au^{197}$ + ${}_{79}Au^{197}$ at incident energy $E = 400$ MeV/nucleon for semi-peripheral geometry. The panels from top to bottom are representing the positions at different times.

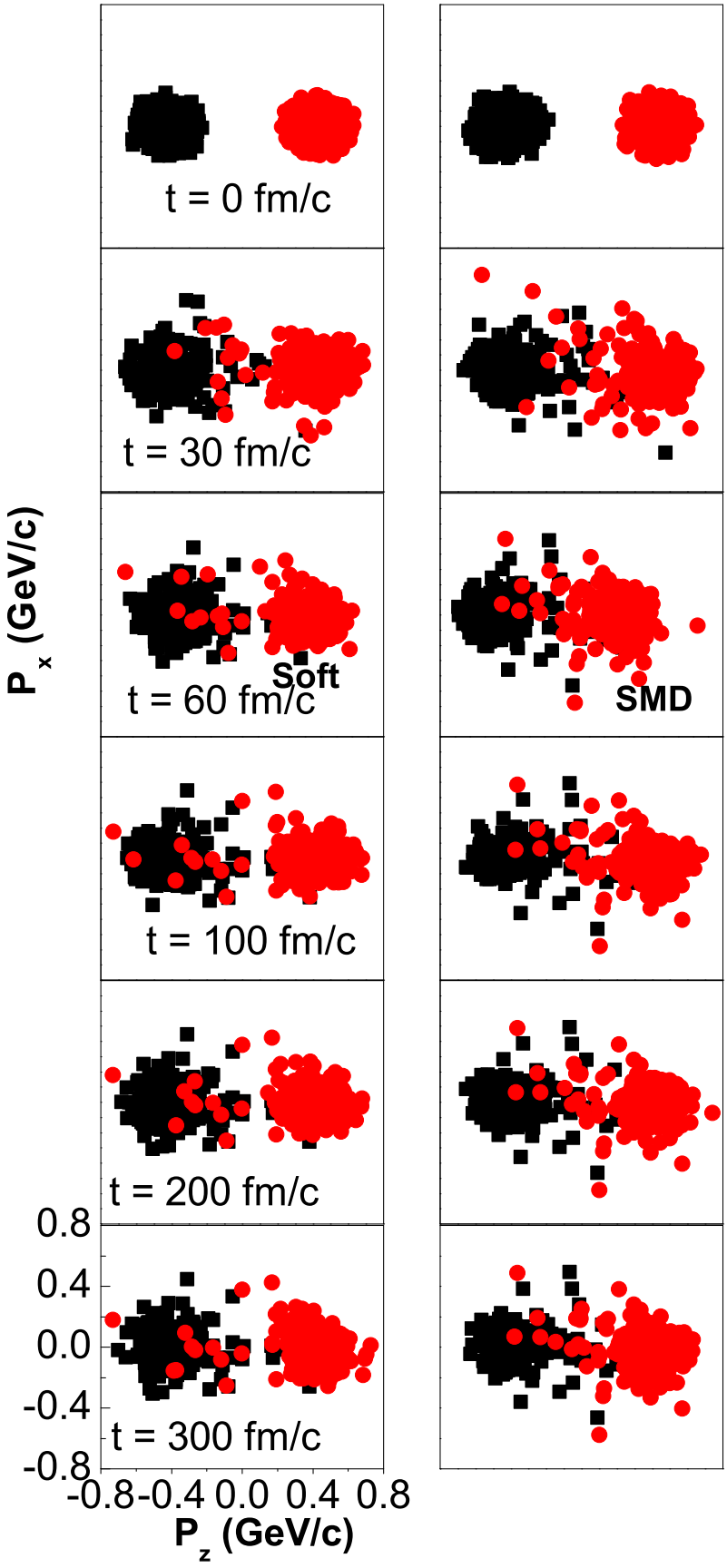

Figure 3.4: Same as in Fig.3.3, but for the $P_x - P_z$ Plane.

mentum dependent interactions. To check this, in the following, time evolution of density and number of collisions is displayed.

3.4.2 Time evolution of the density and nucleon-nucleon collisions

The density of the environment surrounding the nucleons of a fragment plays crucial role in deciding the physical process behind their formation. In Fig.3.5, we display the average density $< \rho/\rho_0 >$ reached in a typical reaction as a function of the time. The average nucleonic density $< \rho/\rho_0 >$ is calculated as [1]

$$< \rho/\rho_0 > \; = \langle \frac{1}{A_T \; + \; A_P} \quad \sum_{i=1}^{A_T \; + \; A_P} \sum_{j=1}^{A_T \; + \; A_P} \frac{1}{(2\pi L)^{3/2}} \cdot exp[-(\vec{r_i} - \vec{r_j})^2/2L] \rangle, \tag{3.8}$$

with $\vec{r_i}$ and $\vec{r_j}$ being the position coordinates of i^{th} and j^{th} nucleons, respectively. We here display the average density at incident energies of 50 and 400 MeV/nucleon. In addition, two colliding geometries corresponding to $\hat{b} \; = \; 0$ and $\hat{b} \; = \; 0.6$ are also taken. The central as well as peripheral collisions (at low incident energy) preserves most of the initial correlations and hence a small change in the density profile occurs. This trend turns to a sharp decrease at higher incident energies. This is due to the fact that higher incident energies destroy most of the initial correlations among nucleons, leading to highly unstable compressed zone, which does not sustain for a longer time and as a result fast emission of nucleons occur. It is also observed experimentally that a little change in fragmentation yield takes place beyond 400 MeV/nucleon[28, 29, 31]. From the Figure, it is also observed that heavier colliding nuclei are more compressed as compared to lighter one. This compression stage also sustains for a longer time in heavier nuclei as compared to lighter one. In other words, the heaviest fragment A^{max} will remain for a longer time. Moreover, the freeze-out density is more for the heavier systems indicating the existence of heavier fragments at later times for low energies, while, the universality is observed in freeze out density after 400 MeV/nucleon. This is supportive in nature with experimental findings [28, 29, 31]. The major aspect of the study, momentum dependent interactions, are found to affect the density profile drastically. The density is found to decrease by 35% (at low incident energies say E = 50 MeV/nucloen) and 25% (at higher incident energies say E = 400 MeV/nucleon)

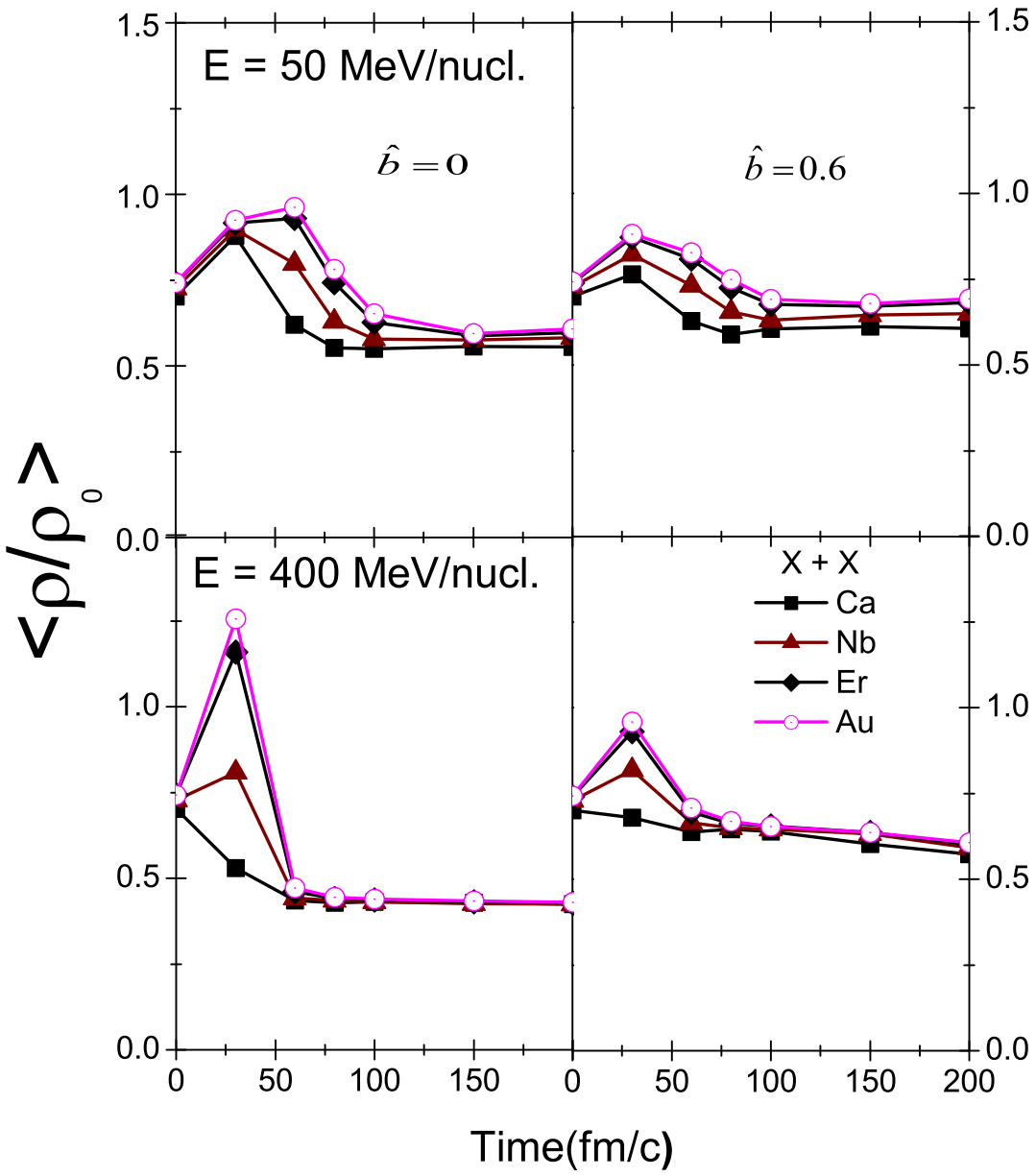

Figure 3.5: Average density $\langle \rho/\rho_0 \rangle$ as a function of the time. The top panel is at 50 MeV/nucleon, whereas bottom panel represents the reaction at 400 MeV/nucleon. The left and right hand sides represent, respectively, the central collision $\hat{b} = 0$ and peripheral collision $\hat{b} = 0.6$. All reactions represent symmetric colliding nuclei $X + X$, where X represents the reacting elements.

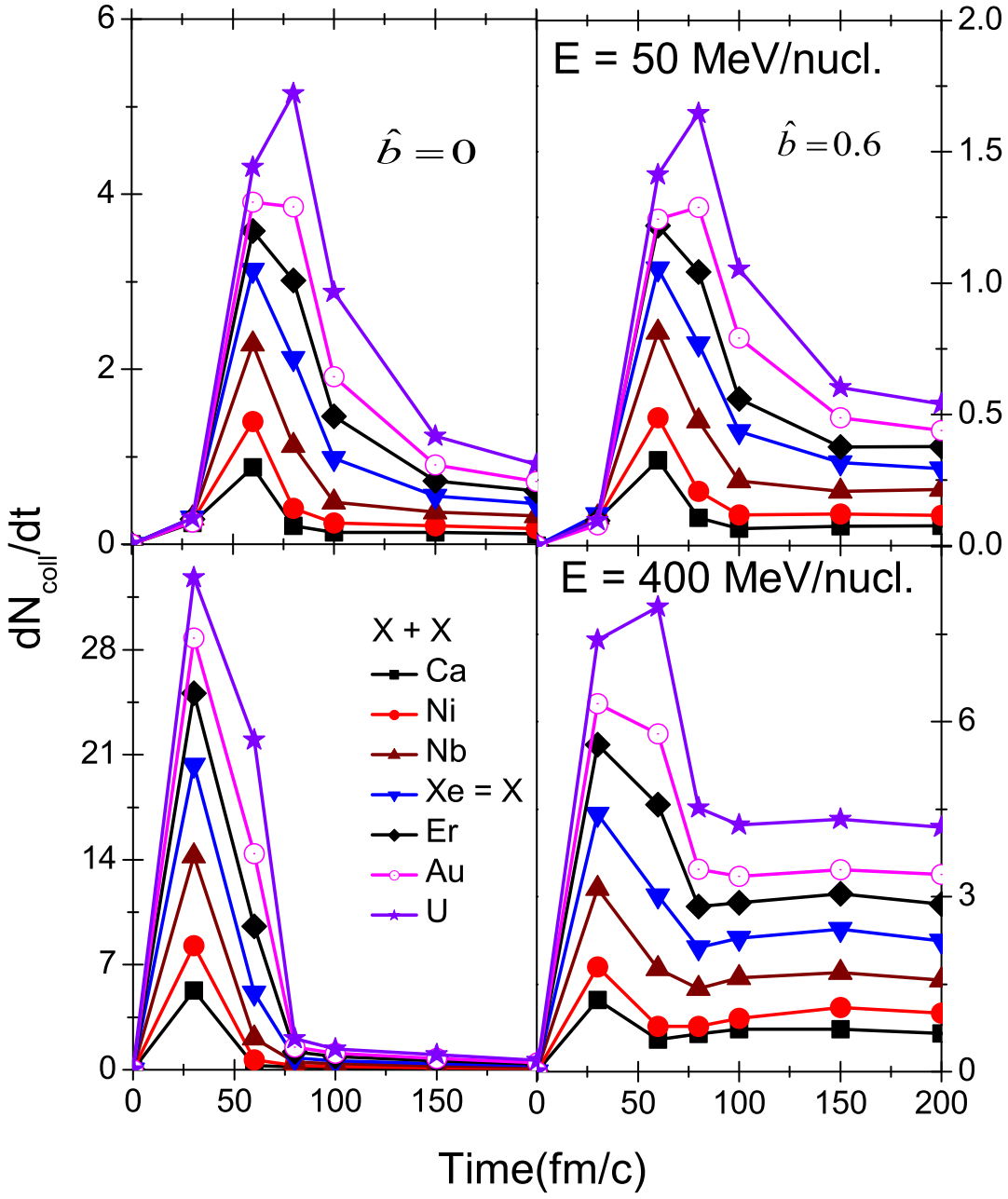

Figure 3.6: Same as Fig.3.5, but for the time evolution of collision rate $\frac{dN_{coll}}{dt}$

in the presence of MDI, when compared with the findings in Ref.[12]. To know this decrease in density profile, we must have exact knowledge of the collision profile in the presence of the MDI's.

In Fig.3.6, the time evolution of the allowed collisions is displayed under the same conditions as density profile was displayed in Fig.3.5. The collision profile is in one to one ratio with the density profile. Generally, collision rate depends on the participant zone and incident energy. At semi-peripheral geometries, the participant zone decreases and hence decrease is observed in the number of collisions at low as well as high incident energies compared to central geometries. This also supports the findings in the Fig.3.5, that density is less at semi-peripheral geometries as compared to central one. On the other hand, with increase in incident energy, collision rate is found to increase with the probability of break-up of initial correlations among the nucleons. For example, the maximum collision rate for central $U + U$ system at 400 MeV/nucleon is about 33, whereas it is 5.1 at 50 MeV/nucleon. Moreover, the momentum dependent interactions are found to suppress the number of collisions at all incident energies as well as at all impact parameters. This is due to the transfer of the momentum of the particles in the radial direction in the presence of momentum dependent interactions, which makes the system dilute and hence less number of collisions are observed. This decrease in number of collisions in the presence of MDI, supports our finding of decrease in density in Fig.3.5. These findings motivated us to see the effect of MDI on the fragments production.

3.4.3 Time evolution of various fragments and momentum dependent interactions

It is clear from the above results that MDI's are affecting the matter at semi-peripheral geometries as compared to the central one. This is due to the transfer of energy from the participant zone to spectator zone in the presence of MDI, which was not possible in the presence of static equation of state[12]. In order to see the effect of MDI's on the fragments production, in Fig. 3.7, we have displayed the time evolution of light charged particles (LCP's) [$2 \leq A \leq 4$] and medium mass fragments (MMF's) [$5 \leq A \leq 9$] with and without momentum dependent interactions for different systems at semi-peripheral geom-

etry and at incident energies 50 and 400 MeV/nucleon. From the figure it is clear that enhanced production of LCP's and MMF's takes place in the presence of momentum dependent interactions as compared to static one. This is due to the repulsive nature of the MDI's, which helps in breaking the heavier fragments into LCP's and MMF's. The universal behavior of increase in multiplicity of fragments with the size of the system is observed in the presence of static as well as momentum dependent interactions. Moreover, the effect of MDI is more for the MMF's as compared to LCP's at semi-peripheral geometries. This is clear from the relative percentage at t = 200 fm/c. The relative percentage at E = 50 MeV/nucleon for LCP's and MMF's is 83% and 105%, respectively, while it is 95% and 400% at E = 400 MeV/nucleon. This motivated us to study the time evolution of heaviest fragment (A^{max}) and MMF's at central as well as semi-peripheral geometries.

In Fig.3.8, we display the heaviest fragment A^{max} survived in a reaction. The medium mass fragments (MMF's) are displayed in Fig.3.9. The top panel in both figures is for 50 MeV/nucleon, whereas bottom panel is at 400 MeV/nucleon. The time evolution of the fragments reveals many interesting points: The heaviest fragment A^{max} survived in the reaction of heavier systems struggles for a longer time. The soft momentum dependent (SMD) equation of state destroy most of the nucleon-nucleon correlations, therefore, A^{max} obtained with SMD EOS is lighter than corresponding soft equation of state [12]. Consequently, there is an enhanced emission of the free nucleons, LMF's (light mass fragments) and MMF's. We also see an appreciable enhancement in the nucleonic emission (not shown here) at all incident energies and impact parameters. For heavier systems, emission of nucleons continues till the end of the reaction. This is due to the finite collisions happening at the later stage as well as due to the longer reaction time at these incident energies.

It takes longer time for A^{max} in heavy systems to be stabilized compared to lighter nuclei, where saturation time for A^{max} is much less. The excited A^{max} in heavier system continues to emit the nucleons till the end of the reaction. This time is, however, much shorter in lighter nuclei.

The multiplicity of MMF's has a different story to tell. We now see more fragments in central collisions at 50 MeV/nucleon compared to peripheral collisions. As we increase the energy, the MMF's production decreases considerably. This is valid for the central colli-

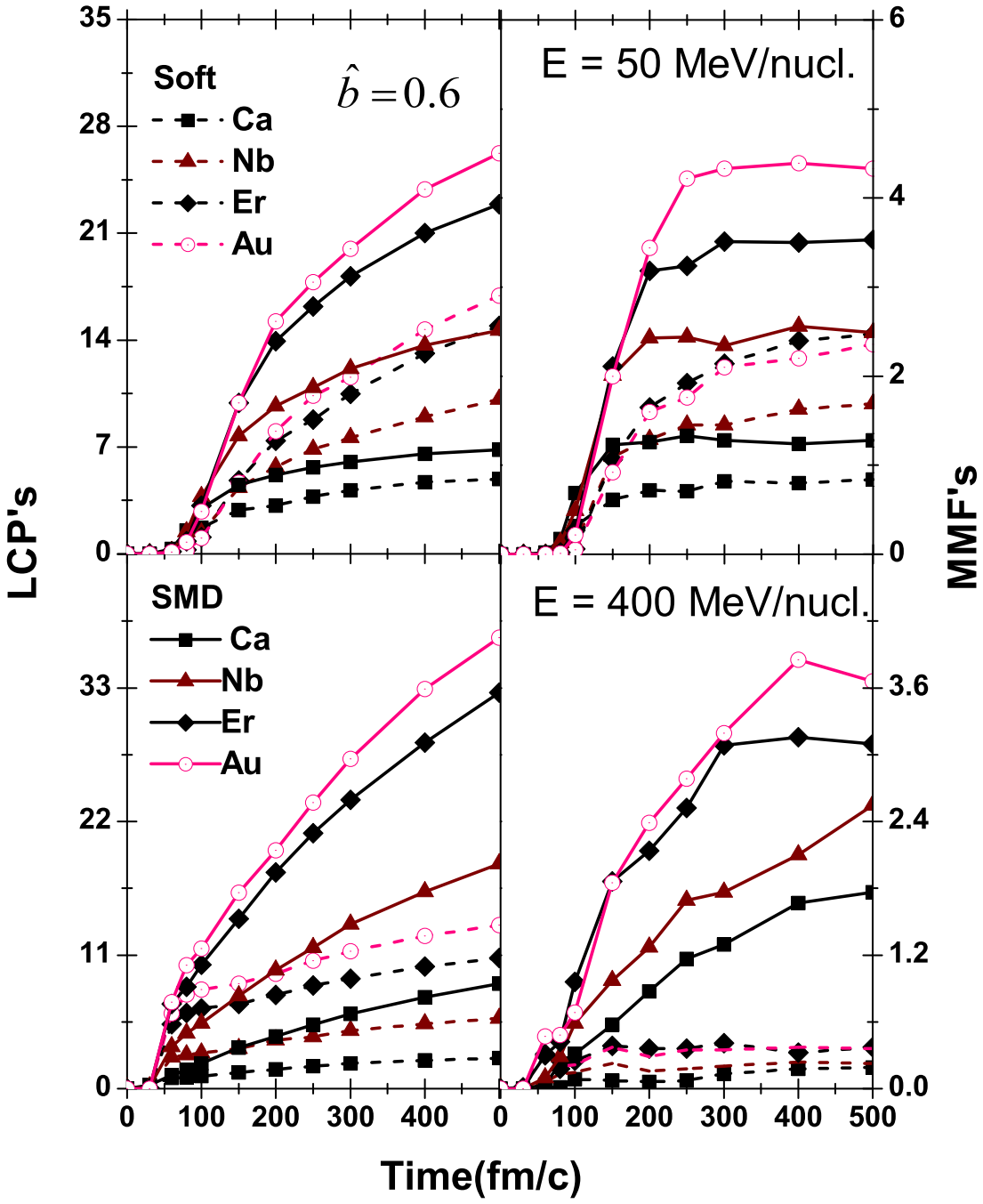

Figure 3.7: Time evolution of LCP's and MMF's for different symmetric systems at semi-peripheral geometry with static soft and soft momentum dependent interaction (SMD). The results are displayed at E = 50 (upper panel) and 400 MeV/nucleon (lower panel), respectively.

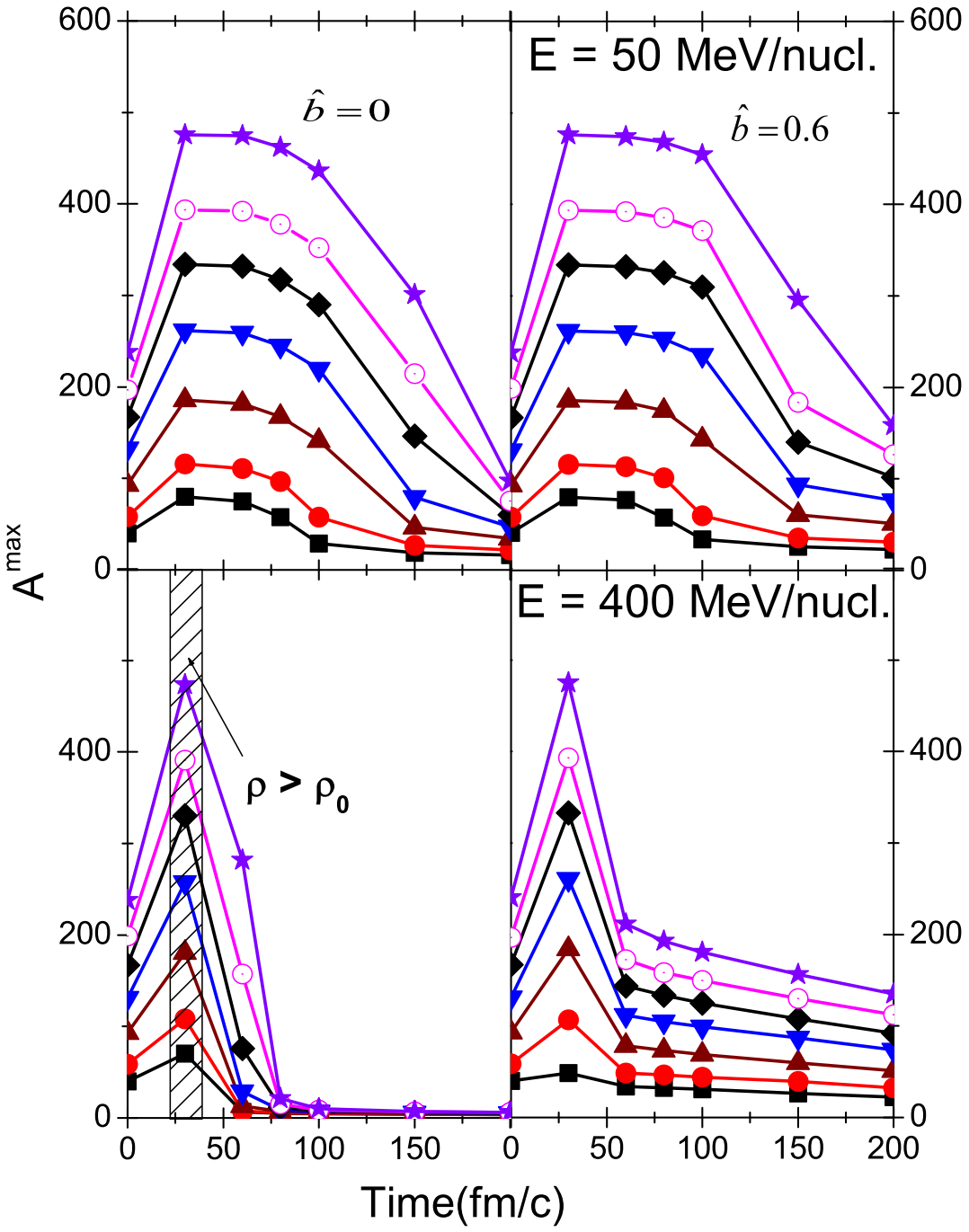

Figure 3.8: Same as in Fig. 3.5, but for the time evolution of the heaviest fragment A^{max} as a function of time. The shaded area corresponds to density higher than normal nuclear matter density ρ_0

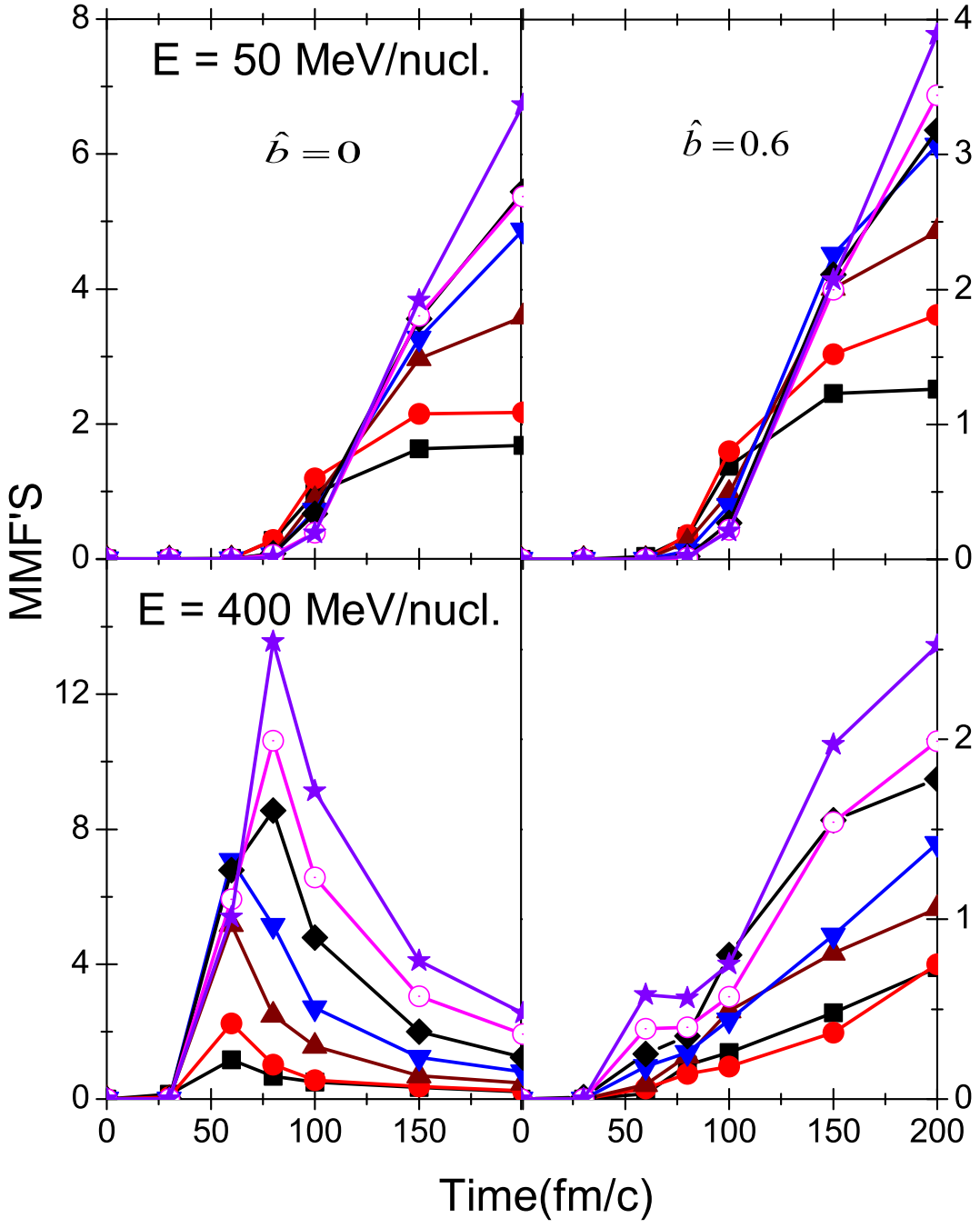

Figure 3.9: Same as in Fig.3.5, but for the time evolution of multiplicity of MMF's.

sions only. The peripheral collisions yield almost same MMF's. As noted in Ref. [12], the static soft EOS is not able to break the initial correlations among the nucleons in peripheral collisions. As soon as momentum dependence is taken into account, the initial correlations among the nucleons are destroyed, resulting in large number of MMF's. The simple static EOS fails to transfer the energy from the participant to spectator matter. In other words, MDI suppresses the production of free nucleons and LMF's while the production of MMF's is enhanced. This increase in MMF's production in the presence of momentum dependent interactions at semi-peripheral geometries is well justified by the decrease in the production of A^{max} in Fig.3.8. Overall, we observe enhancement in the multiplicity of medium mass fragments with MDI compared to static equation of state.

3.4.4 Final state medium mass fragments distribution

As we know, measurements are always done at the end of the reaction. The reaction time is chosen to be $t = 200$ fm/c. It is based on the fact that directed flow saturates by this time. Therefore, it will be of interest to see whether the final state fragment distribution has momentum and system size dependence or not.

We display in Fig.3.10, the reduced multiplicity (multiplicity/nucleon) of medium mass fragments (MMF's) with the mass of the projectile. It must be clear that system mass dependence of reduced multiplicity must have opposite trend in comparison to system mass dependence of average multiplicity of MMF's. In experimental observations (e.g. FOPI and ALADIN), the nuclear matter is divided into spectator and participant parts [38]. In our calculations, this division is made by splitting the reaction into different impact parameter zones that can be related with the spectators/participant matter. The top panel in Fig.3.10 displays the multiplicity of MMF's at 50 and 100 MeV/nucleon, whereas bottom panel is at 600 and 1000 MeV/nucleon, respectively. The middle panel represents the outcomes at 200 and 400 MeV/nucleon. Each window of the panel contains four different curves that correspond, respectively, to the scaled impact parameter values of $\hat{b} = 0.0, 0.3, 0.6, 0.9$. The wide range of incident energy between 50 and 1000 MeV/nucleon and impact parameter between zero and b_{max} gives opportunity to study the different dynamics emerging at low, intermediate and higher energies.

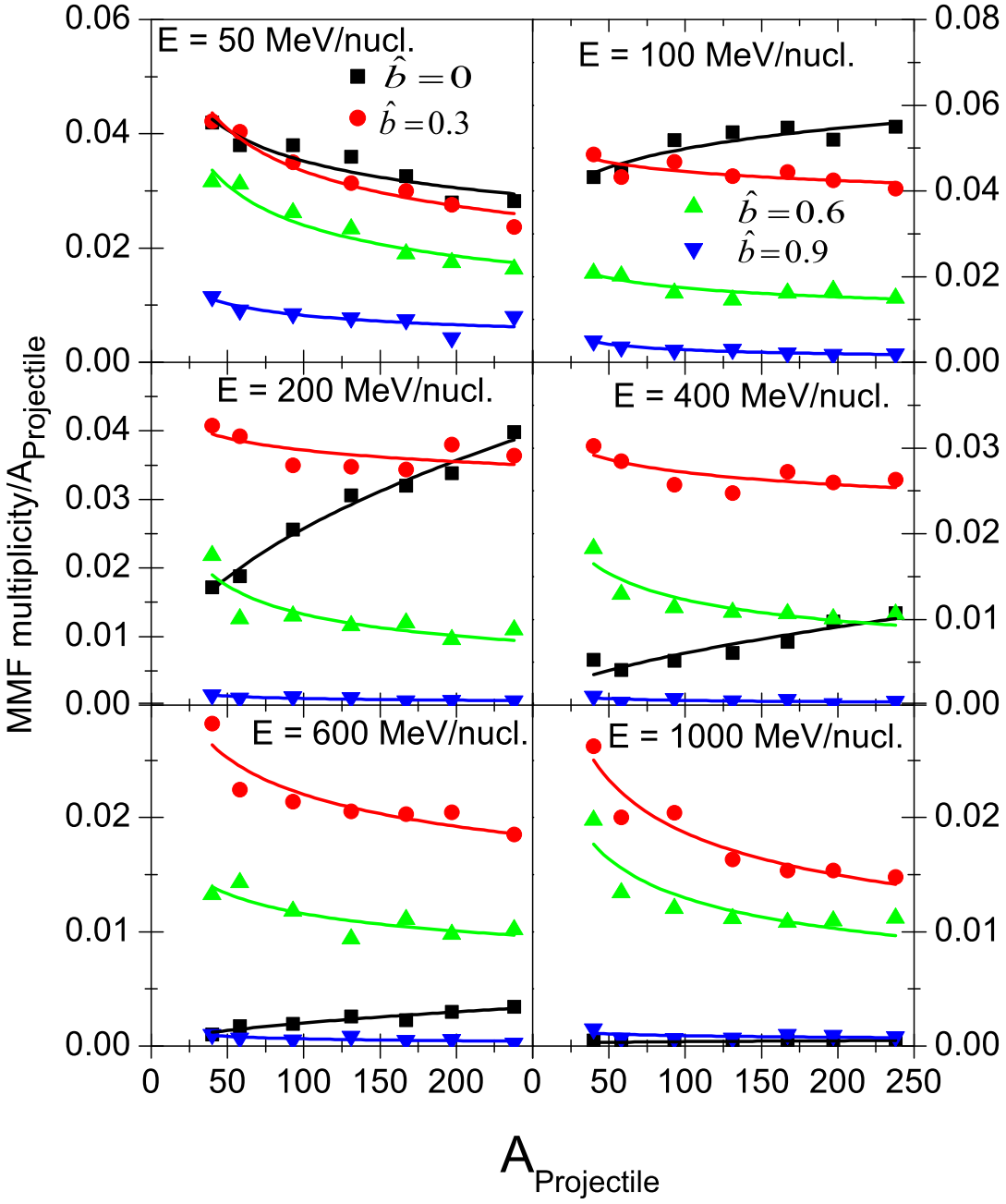

Figure 3.10: Final state multiplicity of the medium mass fragments per projectile nucleon as a function of projectile mass A_P. The top, middle and bottom panel at left side represent, respectively, the reactions at 50, 200, 600 MeV/nucleon. The corresponding right hand side represent, respectively, the reactions at 100, 400, 1000 MeV/nucleon. All curves are fitted using function $Y = CA_P^{\tau}$.

The energy received by the target in peripheral collisions in the presence of momentum dependent interactions is not too enough to excite the matter above the Fermi level, resulting in fewer light fragments. As a result, the break-up of heaviest fragment into MMF's takes place (discussed in Fig. 3.8 and 3.9). Moreover, the projectile mass dependence of $MMF's/A_{Projectile}$ is universal at all energies as well as at all impact parameters except $\hat{b} = 0$. For the central geometry, the dynamics at $E = 50$ MeV/nucleon is different as compared to all other incident energies under consideration. This is due to the reason that at $E = 50$ MeV/nucleon the mean field is dominating, while above energies 100 MeV/nucleon, the influence of nucleon-nucleon collisions goes on increasing. That's why trend for the MMF's production at central geometry is different at $E = 50$ MeV/nucleon compared to all higher incident energies. Irrespective of the incident energy and impact parameter, the multiplicity of medium mass fragments ($5 \leq$ A ≤ 9) scales with the size of the projectile that can be parameterized by a power law of the form $C(A_P)^{\tau}$; A_P is the mass of the projectile. The values of C and τ depends on the size of fragments as well as on the incident energy and impact parameter of the reaction. Now, it also becomes equi-important to see the comparative study of static and momentum dependent interactions over the whole periodic table.

For this in Fig.3.11, we display the relative effects of the soft momentum dependent (SMD) equation of state over the static equation of state. These relative effects are displayed with the parameter $\Delta M_c\%$ (Relative multiplicity difference), which is defined as:

$$\Delta M_c\% \;=\; \frac{[(Multiplicity)_{SMD} - (Multiplicity)_{Soft}]}{(Multiplicity)_{Soft}}\% \tag{3.9}$$

Here we have displayed the $\Delta M_c\%$ of MMF's for $Ca^{40} + Ca^{40}$, $Ni^{58} + Ni^{58}$, $Nb^{93} + Nb^{93}$, $Xe^{131} + Xe^{131}$, $Er^{167} + Er^{167}$, $Au^{197} + Au^{197}$ and $U^{238} + U^{238}$ at $\hat{b} = 0.6$ and $E = 50$, 400 and 1000 MeV/nucleon. It is observed form the figure that effect of momentum dependent interactions is constant throughout the periodic table upto 400 MeV/nucleon, while for the higher incident energy (say 1000 MeV/nucleon), the relative yield is found to decrease for the heavier systems. This is due to the fact that for the heavier systems at sufficient higher energies, the population of nucleon-nucleon collisions increases to a such extent that even static equation of state is able to break-up the initial correlations among nucleons, which is not possible upto 400 MeV/nucleon. This indicates the need of momentum dependent

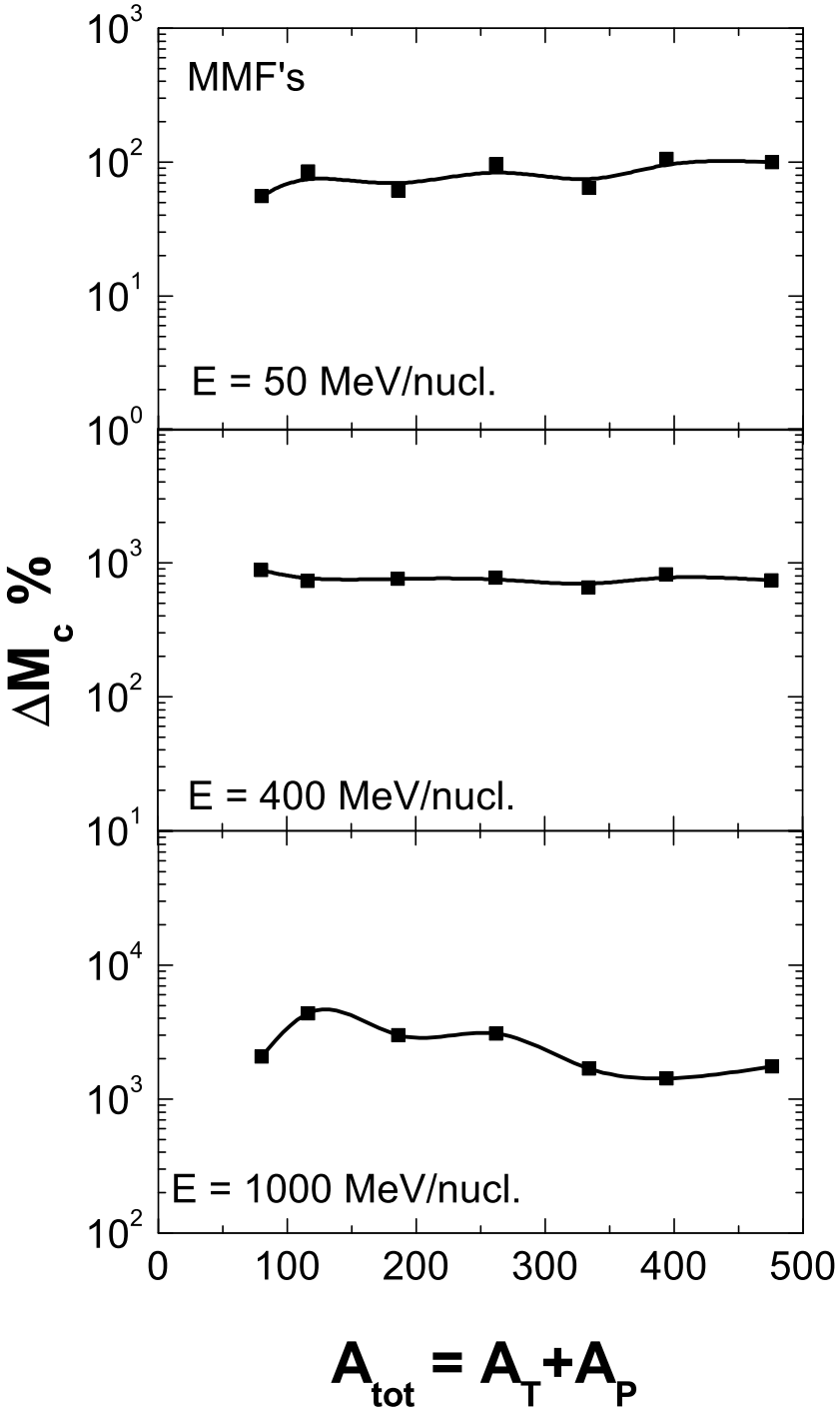

Figure 3.11: Relative multiplicity of MMF's $\Delta M_c\%$ in the presence of momentum dependent interactions with composite mass of system $A_{tot} = A_T + A_P$. The results are displayed at incident energies $E = 50$ (top), 400 (middle) and 1000 (bottom) MeV/n for semi-peripheral collisions $\hat{b} = 0.6$.

interactions upto certain incident energy in intermediate energy heavy-ion collisions.

3.4.5 Energy and impact parameter dependence of the parameter τ for MMF's

As discussed earlier in Fig.3.10, the multiplicity of MMF's can be parameterized with mass of the projectile in term of power law $Y = CA_p^{\tau}$ at all incident energies and impact parameters. Now we are interested to observe the variation of parameter τ between incident energies 50 and 1000 MeV/nucleon at all impact parameters. For this in Fig.3.12, we plot the power law parameter τ as a function of incident energy and impact parameter. Although, no unique dependence occurs for τ, we can correlate some of its values. For all the collision geometries, the value of the parameter τ is close to $-1/3$ at 50 MeV/nucleon. The total multiplicity of the fragments will be proportional to $A \times A^{-1/3} = A^{2/3}$ which is like a surface of the colliding nuclei representing the mean field. Therefore, it is clear that the mass dependence at low incident energy is like that of mean field. At higher incident energy (say 1000 MeV/nucleon), the value of parameter τ tends to approach a unique value except for central geometry. This is perhaps due to the complete destruction of initial correlations, moreover, as a result, even no collective flow has been observed in central collisions [27]. It has been stated by a number of authors that the repulsive nucleon-nucleon interactions at high energies scale like A [39]. However, no physical correlation can be observed from the parameter τ at high incident energies.

3.4.6 Energy and asymmetry dependence of MMF's

Asymmetry of the reaction in term of excess number of neutron is also supposed to play an important role in fragments production in intermediate energy heavy-ion collisions [40]. To observe this effect, incident energy dependence of medium mass fragments at different asymmetry has been explored in Fig.3.13. Here we display the isotopic yield of MMF's as a function of incident energy of colliding partners. We define $\delta = (N-Z)/A$ as a parameter [40], which is a measure of isotopic asymmetry of the colliding nuclei. $\delta = 0$ means isotopically symmetric colliding partner and $\delta \neq 0$ means isotopically asymmetric colliding

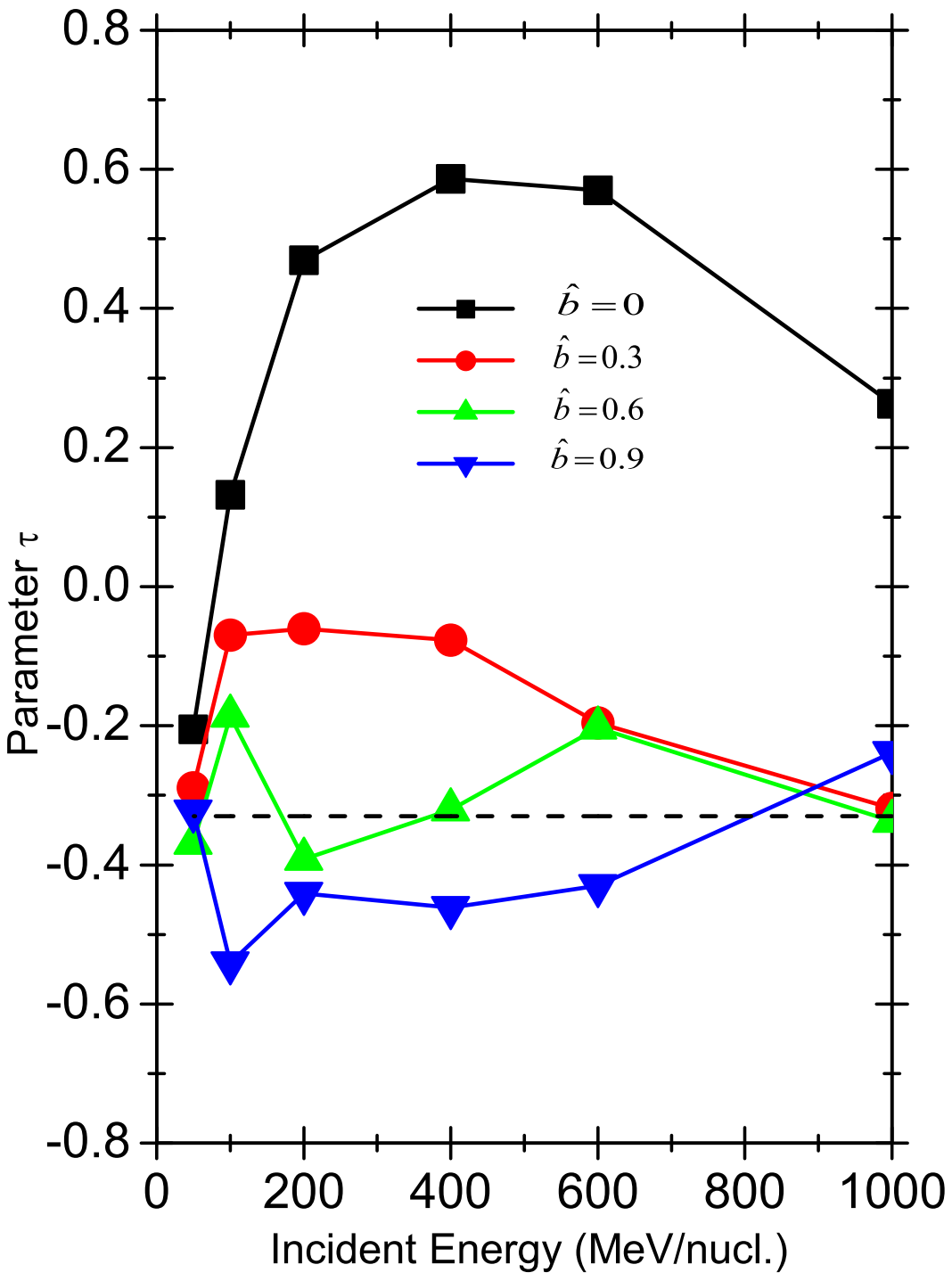

Figure 3.12: Parameter τ (appearing in the power law function A_P in Fig.3.10) as a function of incident energy. The panel displays the value of τ for medium mass fragments.

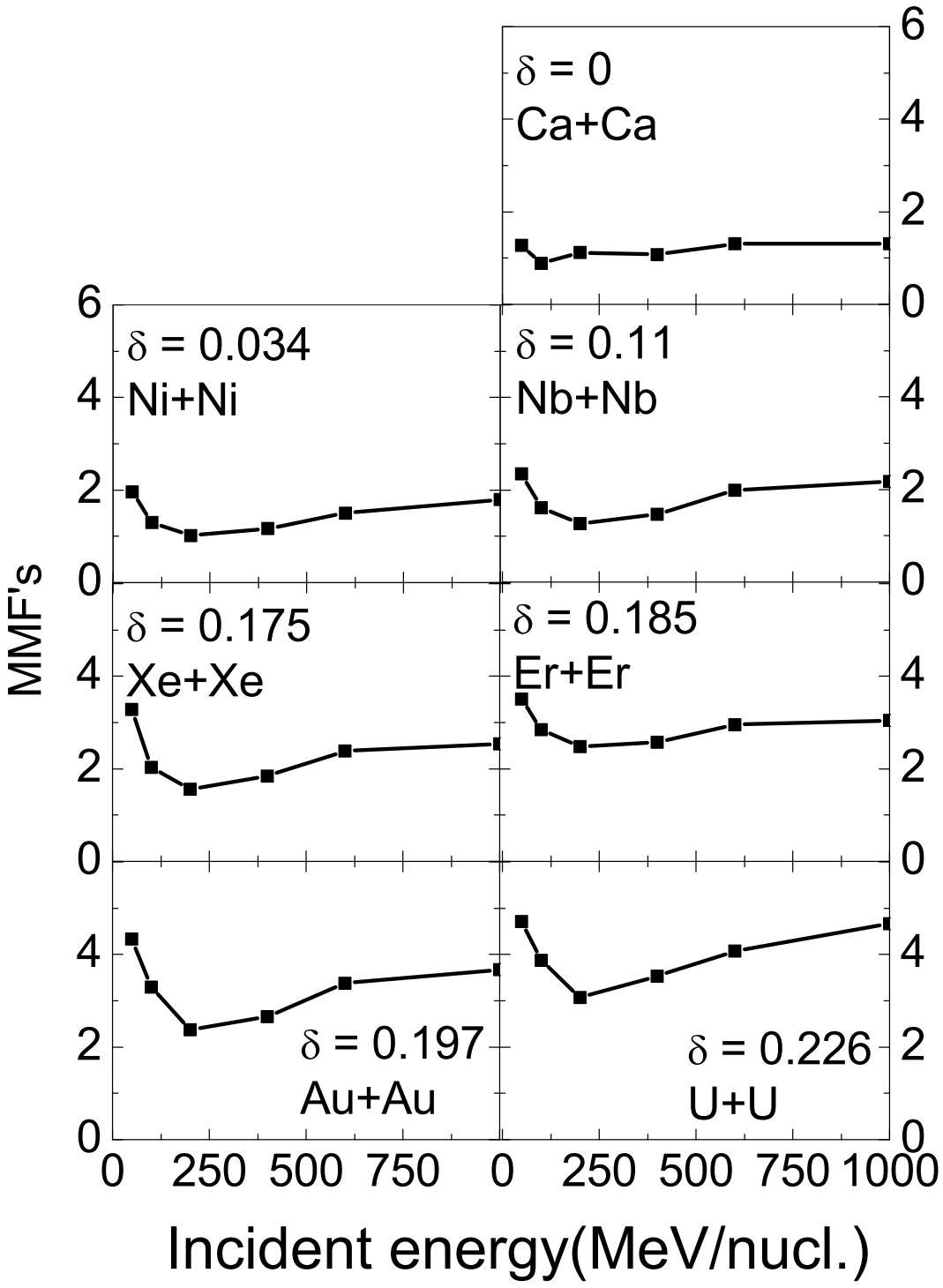

Figure 3.13: Incident energy dependence of the multiplicity of medium mass fragments from symmetry $\delta = 0$ to asymmetry $\delta = 0.226$ for symmetric reactions from Ca to U at $t = 300$ fm/c.

partners. One can see that while we move from symmetry to asymmetry, the production of medium mass fragments increases. Interestingly, the production of MMF's is almost constant for $\delta = 0$ throughout the incident energy range, while, the fall and rise is observed in multiplicity of MMF's with increase in asymmetry $\delta \neq 0$ and incident energy. This rise and fall is due to the strong mean field at low energies and increase in the frequency of the violent nucleon-nucleon collisions at high incident energies. This shows that isotopic asymmetry also play a significant role in the production of medium mass fragments. This phenomena can be understood in detail by taking the isospin degree of freedom into account.

3.5 Summary

Using quantum molecular dynamics (QMD) model, we have studied the role of momentum dependent interactions in fragmentation by systematically analyzing various reactions at incident energies between 50 and 1000 MeV/nucleon and over full collision geometry. The phase space obtained with in the framework of QMD model is analyzed with minimum spanning tree (MST) method. The lighter colliding nuclei generates less density whereas higher density is achieved by heavier nuclei. Moreover, momentum dependent interactions create more repulsion inside the compressed nuclear matter. This gives ample space for compression-decompression as well as radial expansion. For this, we have performed the detailed analysis of density evolution, number of collisions, multiplicity of fragments as well as system size dependence of fragments.

We find that the inclusion of momentum dependent interactions leads to less freeze-out density and number of collisions in all colliding systems as well as at all colliding geometries. This is due to the repulsive nature of the momentum dependent interactions, which further leads to the radial expansion of the matter. Moreover, it is also observed that at higher incident energies momentum dependent interactions are able to break-up the initial correlations among nucleons, which was earlier not possible with static equation of state. This is leading to the decrease in the production of heaviest fragment A_{max} and enhancement in the production of medium mass fragments in the presence of momentum dependent interactions.

The system size effects are found to vary with reaction parameters, incident energies and momentum dependent interactions. The multiplicity of medium mass fragments can be parameterized in term of a power law. This is true for a wide range of impact parameters and incident energies considered here. However, the parameter τ does not have unique value. At low incident energies, the parameter τ is close to 2/3 suggesting the dominance of mean field that scales as $A^{2/3}$. On the other hand, no physical correlation is observed at higher incident energies for central collisions. This dependence of the parameter τ at higher incident energies can be improved by varying the model ingredients such as equations of state, method of clusterization etc., provided the power law dependence of the system size effect should exhibit.

Interestingly, the fragments production is found to be influenced by the asymmetry of the reaction $((N-Z)/A)$ to a great extent at all incident energies. This asymmetry dependence can be better understood by using the more sophisticated models like IQMD [22] in which neutron and proton can be separated on the basis of charges, which is not possible in QMD model [1].

Bibliography

[1] J. Aichelin, Phys. Rep. **202**, 233 (1991).

[2] C. A. Ogilvie *et al.*, Phys. Rev. Lett. **67**, 1214 (1991); M. B. Tsang *et al.*, *ibid.* **71**, 1502 (1993); R. T. de Souza *et al.*, Phys. Lett. B **268**, 6 (1991); G. F. Peaslee *et al.*, Phys. Rev. C **49**, R2271 (1994); C. Williams *et al.*, *ibid.* **55**, R2132 (1997); K. Hagel *et al.*, Phys. Rev. Lett. **68**, 2141 (1992); N. T. B. Stone *et al.*, *ibid.* **78**, 2084 (1997); B. Jakobsson *et al.*, Nucl. Phys. A **509**, 195 (1990); M. Bagemann-Blaich *et al.*, Phys. Rev. C **48**, 610 (1993); J. Hubble *et al.*, *ibid.* **46**, R1577 (1992); J. Hubble *et al.*, Z. Phys. A **340**, 263 (1991).

[3] B. A. Li and D. H. E. Gross, Nucl. Phys. A **554**, 257 (1993); H. M. Xu, C. A. Gagliardi, R. E. Tribble, and C. Y. Wong, *ibid.* **569**, 575 (1994); F. Daffin, K. Haglin, and W. Bauer, Phys. Rev. C **54**, 1375 (1996); V. De la Mota, F. Sebille, M. Farine, B. Remaud, and P. Schuck, *ibid.* **46**, 677 (1992); G. F. Bertsch and S. D. Gupta, Phys. Rep. **160**, 189 (1988).

[4] T. Maruyama, K. Niita, and A. Iwamoto, Prog. Theor. Phys. **98**, 87 (1997).

[5] Q. Li, Z. Li, S. Soff, M. Bleicher, and H. Stöcker, J. Phys. G: Nucl. Part. Phys. **32**, 151 (2006).

[6] J. Aichelin, A. Rosenhaur, G. Peilert, H. Stöcker, and W. Greiner, Phys. Rev. Lett. **58**, 1926 (1987).

[7] C. Gale, G. F. Bertsch, and S. D. Gupta, Phys. Rev. C **35**, 1666 (1987); C. Gale, G. M. Welke, M. Prakash, S. J. Lee, and S. D. Gupta, Phys. Rev. C **41**, 545 (1990).

[8] S. W. Huang, A. Faesseler, G. Q. Li, R. K. Puri, E. Lehmann, D. T. Khoa, and M. A. Matin, Phys. Lett. B **298**, 41 (1993).

[9] S. Kumar and R. K. Puri, Phys. Rev. C **60**, 054607 (1999); Y. K. Vermani and Rajeev K. Puri, DAE symposium on Nuclear Physics, IIT Roorkee (India), 22-26 December (2008).

[10] J. Singh, S. Kumar, and R. K. Puri, Phys. Rev. C **63**, 054603 (2001).

[11] A. D. Sood and R. K. Puri, Eur. Phys. J. A **30**, 571 (2006).

[12] J. Singh and R. K. Puri, Phys. Rev. C **65**, 024602 (2002).

[13] W. Zuo, J. Y. Chen, B. A. Li, P. Y. Luo, and U. Lombardo, High Eng. Phys. and Nucl. Phys. **29**, 885 (2005).

[14] B. A. Li, C. B. Das, S. D. Gupta, and C. Gale, Phys. Rev. C **69**, 011603 (2004).

[15] J. Y. Chen, W. Zuo, L. Ma, and B. A. Li, Chin. Phys. Lett. **24**, 76 (2007).

[16] P. Danielewicz, Nucl. Phys. A **673**, 375 (2000).

[17] Q. Pan and P. Danielewicz, Phys. Rev. Lett. **70**, 2062 (1993); J. Zhang, S. D. Gupta, and C. Gale, Phys. Rev. C **50**, 1617 (1994).

[18] M. Colonna, J. Rizzo, P. Comaz, and M. D. Toro, nucl-th/0707.3902; V. Baran, M. Colonna, M. D. Toro, and V. Greco, Phys. Rev. Lett. **86**, 4492 (2001); J. Rizzo, M. Colonna, and A. Ono, Phys. Rev. C **76**, 024611 (2007).

[19] A. Ono, P. Danielewicz, W. A. Friedman, W. G. Lynch, and M. B. Tsang, Phys. Rev. C **70**, 041604(R) (2004).

[20] D. T. Khoa, N. Ohtsuka, A. Faessler, M. A. Martin, S. W. Huang, E. Lehmann, and Y. Lofty, Nucl. Phys. A **542**, 671 (1992); D. T. Khoa, N. Ohtsuka, M. A. Matin, A. Faessler, S. W. Huang, E. Lehmann, and R. K. Puri, Nucl. Phys. A **548**, 102 (1992).

[21] R. K. Puri, N. Ohtsuka, E. Lehmann, A. Faessler, M. A. Martin, D. T. Khoa, G. Batko, and S. W. Huang, Nucl. Phys. A **575**, 733 (1994); R. K. Puri, E. Lehmann, N. Ohtsuka, A. Faessler, and S. W. Huang, *Proceedings of the international workshop XXII on Gross properties of Nuclei and Nuclear Excitations, Hirschegg, Austria (1994)*

p.262; R. K. Puri, J. Singh, A. Kumar, J. Aichelin, and A. Faessler, *Horizon of Physics, Narosa Publication* (2001).

[22] C. Hartnack, Ph.D Thesis, GSI Report, **93**, 5 (1993).

[23] A. D. Sood and R. K. Puri, Phys. ReV. C **70**, 034611 (2004).

[24] C. Hartnack, J. Jaenicke, L. Sehn, H. Stocker, and J. AIchelin, Nucl. Phys. A **580**, 643 (1994); C. Hartnack, H. Oeschler, and J. AIchelin, Phys. Rev. Lett. **96**, 012302 (2006).

[25] C. Sturm *et al.,* Phys. Rev. Lett. **86**, 39 (2001).

[26] K. G. R. Doss *et al.,* Phys. Rev. C **32**, 116 (1985); K. G. R. Doss *et al.,* Phys. Rev. C **37**, 163 (1988).

[27] W. Reisdorf and H. G. Ritter, Annu. Rev. Nucl. Part. Sci. **47**, 663 (1997)

[28] B.de Schauenburg *et.al.*, GSI Rep. No.**98-1**, 1997 (unpublished); G. S. Wang *et.al.*,*ibid.* **96-1**, 1995 (unpublished); **97-1**, 1996 (unpublished); W. Reisdorf *et.al.*,*ibid.* 2000, 1999 (unpublished); W. Reisdorf in *Proceedings of the international workshop XXVII on cross properties of nuclei and nuclear exitations*, Hirschigg, Austria,1999, edited by H. Feldmeir, J. Knoll, W. Neorenberg and J. Wampach p82.

[29] J. Konopka *et al.,* GSI Rep. **96-1**, 65 (1995); J. P. Alard *ibid* **97-1**, 54 (1996); N. Bastid *et al., ibid.* **98-1**, 54 (1997); A. Andronic *et al., ibid.* **98-1**, 55 (1997).

[30] D. R. Bowman *et al.,* Phys. Rev. C **46**, 1834 (1992); E. Piasecki *et al.,* Phys. Rev. Lett. **66**, 1291 (1991).

[31] A. Schuttauf *et al.,* Nucl. Phys. A **607**, 457 (1996); M. B. Tsang *et al.,* Phys. Rev. Lett. **71**, 1502 (1993).

[32] J. K. Dhawan and R. K. Puri, Phys. Rev. C **75**, 057901 (2007); Phys. Rev. C **75**, 057601 (2007); Phys. Rev. C **74**, 054610 (2006).

[33] S. Kumar, S. Kumar, and R. K. Puri, Phys. Rev. C **78**, 064602 (2008); NCETEM2007, Thapar University, Patiala (Punjab), **p33**, Feb 1-3, (2007); INPC2007, Tokyo, Japan,

QW-236, June 3-8, (2007); CITICOMS2007, CIT, Coimbatore, Vol.1, 30, Aug. 27-29 (2007). Y. K. Vermani, S. Goyal and, R. K. Puri, Phys. Rev. C **79**, 064613 (2009).

[34] L. Zhuxia, C. Hartnack, H. Stocker and W. Greiner, phys. Rev. C **44**, 824 (1991).

[35] G. F. Arnold *et al.,* Phys. Rev. C **25**, 936 (1982); G. Passatore, Nucl. Phys. A **95**, 694 (1967).

[36] J. Y. Liu, W. J. Guo, Z. Y. Xing, and X. G. Lee, Chin. Phys. Lett. **22**, 65 (2005).

[37] J. Singh, S. Kumar, and R. K. Puri, Phys. Rev. C **62**, 044617 (2000); R. K. Puri and S. Kumar, *ibid.* **57**, 2744 (1998); S. Kumar and R. K. Puri, *ibid.* **58**, 2858 (1998); S. Kumar, S. Kumar, and R. K. Puri, Phys. Rev. C **81**, 014601 (2010).

[38] K. Zbiri, A. Le Fevre, J. Aichelin, W. Reisdorf, and F. Gulminelli, Phys. Rev. C **75**, 034612 (2007).

[39] G. D. Westfall *et al.,* Phys. Rev. Lett. **71**, 1986 (1993); R. Pak *et al.,* Phys. Rev. C **53**, R1469 (1996); D. J. Magestro *et al.,* Phys. Rev. C **61**, 021602 (2000)

[40] Ad. R. Raduta and F. Gulminelli Phys. Rev. C **75**, 044605 (2007).

Chapter 4

A comparative study of different nucleon-nucleon cross sections and model ingredients in multifragmentation

4.1 Introduction

The study of heavy-ion collisions at intermediate energies ($50 \leq E \leq 1000\ MeV/nucleon$) provides a rich source of information for many rare phenomena such as multifragmentation, collective flow as well as particle production[1, 2]. It can also shed light on the mechanism behind the fragmentation in highly excited nuclear systems. In this energy region, multifragmentation appears to be a dominant de-excitation channel apart from the other less populated channels of manifestation of liquid gas phase transition in finite nuclear systems [1, 3, 4]. In the literature, multifragmentation has also been considered as a gateway to nuclear equation of state [5, 6]. Numerous investigations are cited in the literature which handle the de-excitation of nuclear system in multifragmentation [7-13]. In chapter 3, the importance of momentum dependent interactions in multifragmentation in the presence of energy dependent cross section is studied in detail. In this chapter, we shall focus on the importance of nucleon-nucleon cross sections and model ingredients in multifragmentation in the presence of momentum dependent interactions (MDI) in intermediate energy heavy-ion collisions.

Experimentally, multifragmentation can be studied in term of intermediate mass fragments (IMF's). The experimental analysis of the emission of intermediate mass fragments (IMF's), ($5 \leq A \leq A_{tot}/6$), has yielded several interesting observations: De Souza et al.[10] observed

a linear increase in the multiplicity of IMF's with incident energies for central collisions. In this study, incident energy was varied between 35 and 110 MeV/nucleon. On the other hand, Tsang et al. [11] reported a rise and fall in the production of IMF's. The maximal value of the IMF's shifts from nearly central to peripheral collisions with the increase in the incident energy. More refined results were reported by Peaslee et al. [12] for the reaction of $_{36}Kr^{84}$ + $_{79}Au^{197}$ for incident energy between 35 and 400 MeV/nucleon. Their analysis revealed that IMF's multiplicity first increases till 100 MeV/nucleon and then decreases slowly. These findings pose a stringent test for any theoretical model designed for the study of multifragmentation.

Theoretically, multifragmentation can be studied by statistical [2] as well as semi-classical [5] models, respectively. The relation between multifragmentation process and nuclear equation of state was extensively studied by several authors within the statistical approach for intermediate energy heavy-ion collisions [2, 4, 6]. On the other hand, semi-classical dynamical models [5] are very useful for studying the reaction from the start to final state where matter is fragmented and cold. In addition, these models also give possibility to extract the information about the nuclear equation of state [13] and nucleon-nucleon cross section[1, 5, 14]. The interaction among nucleons (in a heavy-ion reaction) can be studied within the G-matrix, with its real part representing the mean field and complex part denotes the nucleon-nucleon cross section [1, 5, 14]. Note that the contribution of imaginary part of the interaction is nearly absent in the low energy process such as fusion, fission and radioactivity[15]. One often uses a parameterized form for the real and imaginary parts of the G-matrix. It is well accepted to use a density dependent Skyrme type interactions for the real part of the G-matrix. However, heavy-ion dynamics depends not only on the density but also on the entire momentum plane [7]. Therefore, it is advisable to use momentum dependent interactions additionally.

The exact nature of nucleon-nucleon cross section, on the other hand, is still an open question [7, 14]. A large number of calculations exist in the literature suggesting different strength and forms of the nucleon-nucleon cross sections [14, 16]. In a simple assumption of hard core radius of nucleon-nucleon potential, one has often used a constant and isotropic cross section of 40 mb. In other calculations, a constant and isotropic cross section with

magnitude between 20 and 55 mb is also used [14]. The most sensitive observable to pin down the nucleon-nucleon cross section is collective flow. Recent calculations advocated its strength between 35-40 mb[14]. We shall concentrate here on multifragmentation. Our present study will be based on the semi-classical model, namely, quantum molecular dynamics (QMD). In semi-classical model, one has to face the problem of the stability of nuclei. Several model ingredients such as width of the Gaussian (L), has been used as free parameter. It varies between 4.33 fm^2 to 8.66 fm^2[5]. At the same time, one needs to identify the clusters with the help of clusterization algorithm. Different cluster recognization algorithms can also influence the fragmentation. Our present interest is to perform a comparative study of different model ingredients along with different nucleon-nucleon cross sections and to see whether it is possible to pin down the strength of nucleon-nucleon cross sections by QMD model or not [17]. In the following section, we will discuss different type of nucleon-nucleon cross sections and clusterization algorithms.

4.2 Different nucleon-nucleon cross sections

During the propagation, two nucleons can collide if they come closer than a certain distance. The scattering of these nucleons is decided by a Monte Carlo procedure which is a stochastic scattering and hence is different from the Rutherford scattering. For nucleon-nucleon cross section σ, one can use a simple parameterization which depends on the center of mass energy of nucleons [18]. In most of parameterizations of nucleon-nucleon cross section, the following processes are always there:

$$\begin{array}{lll} N + N \rightarrow N + N & (a), & \\ N + N \rightarrow N + \Delta & (b), & \\ N + N \rightarrow \Delta + \Delta & (c), & \\ N + \Delta \rightarrow N + N & (d), & \\ \quad \Delta \rightarrow N + \pi, & & \\ N + \Delta \rightarrow N + \Delta & (e), & \\ \Delta + \Delta \rightarrow \Delta + \Delta & (f). & \end{array} \tag{4.1}$$

The phase space of scattered nucleons is checked with so called *classical Pauli-blocking* method. If the phase space of scattered nucleons is already occupied, the scattering is forbidden. The pictorial view of effect of cross sections on the trajectory of projectile and target nucleons is shown in Fig.4.1. In the literature, three type of cross sections, namely,

energy dependent[19], in-medium [20] and constant cross sections [14] are discussed. Since we are interested in energy dependent and constant cross sections, so, in the following subsections, they are discussed in detail.

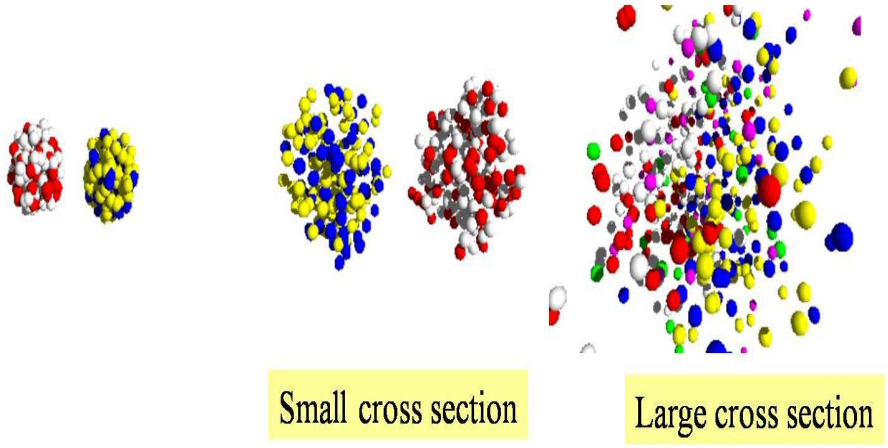

Figure 4.1: A pictorial view of effect of different cross sections on the trajectory of projectile and target nucleons in intermediate energy heavy-ion collisions. At sufficiently small cross sections, nuclei will pass each other without doing the reaction, while at large cross sections, hydro-dynamical behavior is obtained and nuclei will repel each other.

4.2.1 Energy dependent nucleon-nucleon cross section

The energy dependent cross section is a parametric fit on the experimental data, which is derived by Cugnon *et al.*[19]. Here cross section is divided into elastic and inelastic parts which depend on the center-of-mass energy available to the colliding pair of nucleons. For elastic channels, we use the total and differential cross section as [19]:

$$\sigma_{nn}^{(el)}(\sqrt{s}) = \begin{cases} 55(mb) & if\sqrt{s} < 1.8993 \\ \frac{35}{1+100(\sqrt{s}-1.8993)} + 20 & if\sqrt{s} \geq 1.8993, \end{cases} \tag{4.2}$$

with $\sqrt{s}$, the nucleon-nucleon center of mass energy given by:

$$\sqrt{s} = \sqrt{(E_1 + E_2)^2 - (P_1 + P_2)^2}. \tag{4.3}$$

Here E_i and P_i $(i,\ j = 1,\ 2)$ are, respectively, the energy and momentum of a nucleon. The angular distribution for these channels is given by

$$\frac{d\sigma}{dt} = ae^{bt}\ ; \qquad t = -2p^2(1 - cos\theta). \tag{4.4}$$

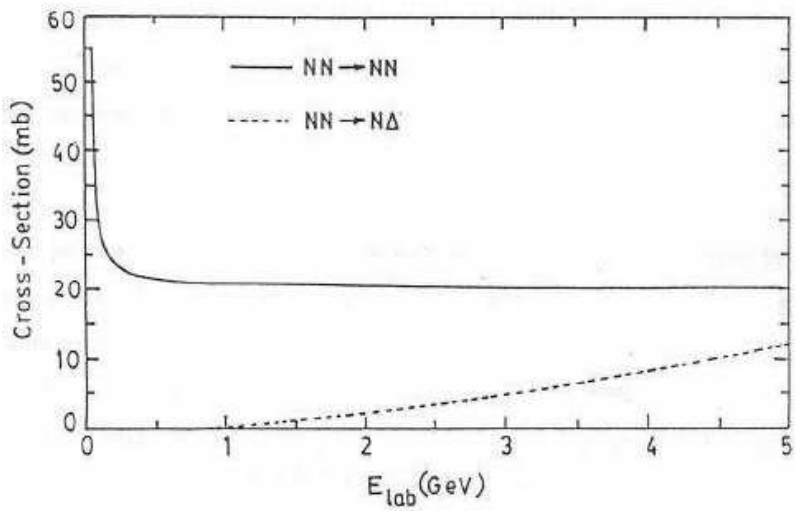

Figure 4.2: The Cugnon parameterization for the elastic (solid line) and inelastic (dashed line) cross sections of nucleon-nucleon scattering as a function of the incident energy E_{lab}. Figure is taken from Ref.[21]

.

For inelastic channels, the total cross section is parameterized as

$$\sigma^{(in)}_{nn\to n\Delta}(\sqrt{s}) = \begin{cases} 0 & if\sqrt{s} < 2.015 \\ \frac{20(\sqrt{s}-2.015)^2}{0.015+(\sqrt{s}-2.015)^2} & if\sqrt{s} \geq 2.015. \end{cases} \tag{4.5}$$

The angular distribution for in-elastic channels is assumed to be isotropic. The cross section for Δ absorption, i.e. channel (d) can be obtained from eqn. (4.5) using detailed balance principle.

$$\sigma_{n\Delta\to nn} = \frac{1}{8}(p_f^2/p_i^2)\sigma_{nn\to n\Delta}, \tag{4.6}$$

These parameterized forms of the cross sections are in fact a fit to the experimental measurements. The limit of $\sqrt{s}$=1.8993 GeV (in eqn. 4.2) is based on the fact that the mass of two nucleons is roughly equal to 1.876 GeV. Therefore, for two colliding nucleons with very small velocity, a constant cross section (= 55 mb) is used. The mass limit of the inelastic channel (i.e. Δ formation in eqn. 4.5) is based on the fact that mass of $\Delta(= N + \pi)$, is 1.076 GeV. Therefore, for $NN \to N\Delta$ channel, the outgoing mass should be at least 1.076+0.938 GeV.

The graphical representation of the elastic and in-elastic parts of the cross section is displayed in Fig.4.2. One sees clearly that the elastic cross section falls sharply in its initial stage and then saturate around 20 mb. Whereas, the in-elastic cross section starts increasing with increase in the bombarding energies. At very high energies, the nucleon-nucleon cross section is fully dominated by the in-elastic channel.

It is well known that the scattering cross section between two nucleons depends on their isospin. Fig.2.3 compares the free-space cross sections for neutron-proton and proton-proton or neutron-neutron scattering as a function of bombarding energy. The data in the energy range of 10 MeV $\leq E_{lab} \leq$ 1000 MeV can be parameterized by[22]

$$\sigma_{np}^{free} \;=\; -\,70.67 \;-\; 18.18\beta^{-1} \;+\; 25.26\beta^{-2} \;+\; 113.85\beta \;(mb), \tag{4.7}$$

$$\sigma_{pp}^{free} \;=\; 13.73 \;-\; 15.04\beta^{-1} \;+\; 8.76\beta^{-2} \;+\; 68.67\beta^{4} \;(mb), \tag{4.8}$$

where $\beta \;=\; v/c$ is the velocity of the projectile nucleon.

Because of the differences in the transition matrices of the isospin $T \;=\; 1$ and $T \;=\; 0$ channels, and the fact that both the iso-singlet and iso-triplet channels contribute to neutron-proton (np) scattering, their cross sections (σ_{np}^{free}) in free space are higher in free space are higher that those for protons-proton (pp) or neutron-neutron (nn) scatterings (σ_{pp}^{free}) where only iso-triplet channels are involved. It is seen from the figure that neutron-proton cross section is about a factor of 2 to 3 larger that the proton-proton or neutron-neutron cross section.

4.2.2 The in-medium nucleon-nucleon cross section

The first attempt to derive the in-medium nucleon-nucleon cross section was made by Faessler and collaborator [20]. At low incident energies (E$\leq$ 400 MeV/nucleon), the Pauli-blocking of intermediate states is quite important. This effect is reduced at higher incident energies. The Pauli-principle blocks about 4% collisions at 2 GeV/nucleon. Therefore, at low incident energies it is very important to take care of the in-medium effects. The nucleon-nucleon cross section in nuclear medium can be calculated from the G-matrix [20, 23, 24, 25] which is a solution of the Bethe-Goldstone equation [20]:

$$\langle \acute{k}_1,\; \acute{k}_2 | G(W) | k_1,\; k_2 \rangle \;\;=\;\; \langle \acute{k} | G(W,K) | k \rangle$$

$$= \langle \acute{k}|V|k\rangle + \int \frac{d^3k^{"}}{(2\pi)^3}\langle \acute{k}|V|k^{"}\rangle \times \frac{Q_F(k^{"},K)}{W - E(k^{"},K) + i\eta}\langle k^{"}|G(W,K)|k\rangle, \quad (4.9)$$

where $K = \frac{1}{2}(k_1 + k_2)$, $k = \frac{1}{2}(k_1 - k_2)$, and

$$E(k,K) = \epsilon(k_1,\rho_1) + \epsilon(k_2,\rho_2),$$
$$\epsilon(k,\rho) = \frac{\hbar^2\ k^2}{2m} + ReU(k,\rho). \quad (4.10)$$

The Q_F in eqn. 4.9 is the Pauli operator for two (colliding) nuclear matters whose momentum distribution F is given by two overlapping Fermi spheres. The mean field potential U of the single-particle energy ϵ is calculated from the G-matrix in a self-consistent way:

$$U(k,\rho) = \frac{1}{4}\sum_{spin,isospin}\int_F \frac{d^3\acute{k}}{(2\pi)^3}\ \langle k,\acute{k}|G|k,\acute{k}\rangle. \quad (4.11)$$

The mean field potential derived from the G-matrix is a momentum dependent. This dependence is usually approximated by an effective nucleon mass.

By using the standard angle averaging procedure for the Pauli operator and for the single particle energy, one can obtain the decoupled partial wave Bethe-Goldstone equation [20]:

$$\langle \acute{k},\acute{L}SJ|G|k,LSJ\rangle = \langle \acute{k},\acute{L}SJ|V|k,LSJ\rangle + \frac{2}{\pi}\sum_{L^{"}}\int dk^{"}\ k^{"2}\langle \acute{k},\acute{L}SJ|V|k^{"},L^{"}SJ\rangle \times \frac{\bar{Q_F}(k^{"},K)}{W\ - \bar{E}(k^{"},K) + i\eta}\langle k^{"},L^{"}SJ|G|k,LSJ\rangle, \quad (4.12)$$

where $\bar{Q_F}$ and $\bar{E}$ are the angle-averaged quantities. The Bethe-Goldstone equation has the same structure as the Lippmann-Schwinger equation for the free two-body scattering. In this sense, the G-matrix (which is a solution of the Bethe-Goldstone equation) can be regarded as the two-body scattering amplitude in the presence of a nuclear medium. The differential scattering cross section can then be calculated in a straight forward way:

$$\frac{d\sigma}{d\omega} = \frac{1}{4}\sum_{m_s,\acute{m_s}}|T^{S=1}_{\acute{m_s},m_s}(\theta)|^2\ - |T^{S=0}(\theta)|^2, \quad (4.13)$$

with

$$T^S_{\acute{m_s},m_s}(\theta) = \sum_{L\acute{L}J}\sqrt{\frac{2L+1}{4\pi}}Y^{\acute{L}}_{m_s,-\acute{m_s}}(\theta,0)\langle L0Sm_s|Jm_s\rangle \times \langle \acute{L}\ m_s - \acute{m}_sS\acute{m}_s|Jm_s\rangle\langle k,\acute{L}SJ|G|k,LSJ\rangle. \quad (4.14)$$

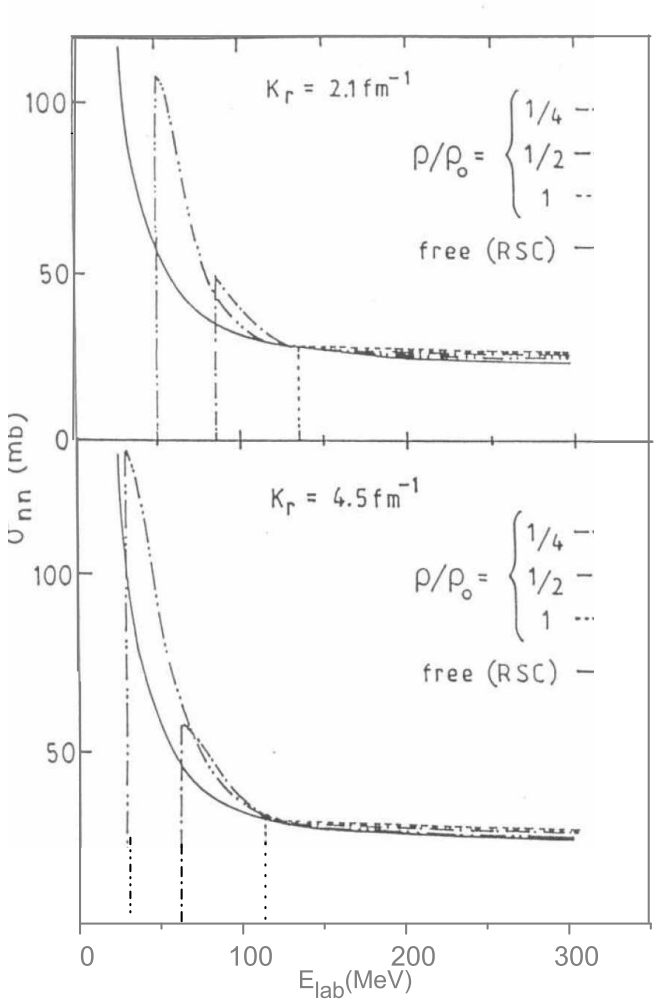

Figure 4.3: The in-medium nuceon-nucleon cross section based on the G-matrix for different incident energies (represented by the relative momentum K_r) and densities. The dashed, dash-dot-dashed and dash-double-dotted lines represents, respectively, the total density $\frac{\rho}{\rho_o}$ = 1, 1/2 and 1/4. Figure is taken from the Ref. [25].

The in-medium nucleon-nucleon cross section obtained from the G-matrix is shown in the Fig. 4.3 as a function of the nucleon energy (in the laboratory frame) for two different bombarding energies represented by the relative momentum K_r. We here display the results at three different densities ρ/ρ_o [25]. The solid line shows the free nucleon-nucleon cross section calculated using Reid soft core potential. The dashed, dash-dotted and dash-double-dotted lines represents, respectively, the total density ρ/ρ_o=1, 1/2 and 1/4. Puri and co-workers studied the importance of in-medium nucleon-nucleon cross sections many time in the literature[26].

As discussed above, in microscopic models medium effects appear in the Bethe- Goldstone

equation mainly through the Pauli blocking factor for intermediate states and the self energies of two the two nucleons in the denominator of the propagator. However, results from these studies differ significantly, with some models predicting a decrease of the in-medium NN cross sections compared to their free space values while others predict an increase. For instance, in the Dirac- Brueckner approach of Refs[16], in which the model parameters are fixed by fitting free space NN scattering data and deuteron properties, the NN cross sections in nuclear medium at zero temperature have been predicted to decrease with increasing density. For example, at the normal nuclear matter density and a bombarding energy of 50 MeV, both σ_{np} and σ_{pp} are reduced by a factor of two. The results of the calculations in Ref.[16] has been parameterized by

$$\sigma_{np}^{medium} = \left[31.5 + 0.092abs(20.2 - E_{lab}^{0.53})^{2.9}\right] \cdot \frac{1.0 + 0.0034E_{lab}^{1.51}\rho^2}{1.0 + 21.55\rho^{1.34}} \ (mb), \quad (4.15)$$

$$\sigma_{pp}^{medium} = \left[23.5 + 0.0256(18.2 - E_{lab}^{0.5})^4\right] \cdot \frac{1.0 + 0.1667E_{lab}^{1.05}\rho^3}{1.0 + 9.704\rho^{1.2}} \ (mb). \quad (4.16)$$

In this study, respective effects of Pauli blocking and the self-energy corrections on the in-medium NN cross sections have not been carried out[16]. Opposite results have been found by Bohnet *et al.*[25] in studying the in-medium NN cross sections during the collisions of two slabs of nuclear matter at zero temperature. The Pauli blocking factor has been estimated using two Fermi spheres separated by the beam momentum, and it is found that the in-medium cross sections generally increases with density.

Experimentally, strong evidences supporting reduced in-medium NN cross sections at intermediate energies[27]. An empirical density-dependent expression for reduced in medium NN cross sections is given as[27]:

$$\sigma_{NN}^{med} = \left(1 + \alpha\frac{\rho}{\rho_0}\right)\sigma_{NN}^{free} \quad (4.17)$$

with the parameter $\alpha \approx -0.2$ has been found to better reproduce the data compared to transport model calculations using the free space NN cross sections. By using eqn. 4.17 one can obtain the medium effects in the nucleon-nucleon collisions. Very recently, in the study of stopping power and collective flow in heavy-ion collisions at SIS/GSI energy, there were indications that the in-medium NN cross sections were reduced at low energies but enhanced at high energies[16]. Furthermore, no information about the isospin dependence

of the in-medium NN cross sections has been extracted from these experiments.

The basic physical picture of this approach is that the heavy-ion collision at any point in space and time can be represented by the collision of two Fermi sphere nuclear matter (with relative momentum between two Fermi spheres k_R) whose densities are the local densities of the target and projectile as a result of which the equation of state depends on the momentum configuration of the heavy-ion system, hence leads to the difference between the equation of state for the nuclear matter formed in heavy-ion collisions and that for nuclear matter which one has , for example, in a supernova explosion.

4.2.3 A constant nucleon-nucleon cross section

During early attempts, one has used a constant nucleon-nucleon cross section to study heavy-ion collisions through transport models. Several calculations based on a constant cross section were applied to study the disappearance of flow and multifragmentation[14]. One has used isotropic and energy independent nucleon- nucleon cross sections with magnitude between 20 and 55 mb. It has also been shown by Zheng *et al.*[16] that a stiff equation of state with free nucleon-nucleon cross section and a soft equation of state with reduced cross section yield nearly the same results. Following these Ref.[14], we also use a constant energy independent cross section. For comparison, we shall also use an energy dependent cross section as fitted by Cugnon[19].

On the other hand, the choice of the method of clusterization is also quite important in multifragmentation (specially for IMF's or at Peripheral geometries). The method of clusterization, MST, is discussed in chapter 3 in detail. This methods have one or more shortcomings: e.g. (1) the simple spatial correlation method can not address the question of the time scale of formation of fragments. This leads to a single cluster at the time of high density. (2) Less transfer of energy from the participant to spectator zone and hence the spectator nucleus does not break into fragments as shown experimentally in Ref.[28]. To overcome these shortcomings, MST with momentum cut (MSTM) [26] and Stimulated Annealing Clusterization Algorithm (SACA)[1] are developed to identify the fragments. These methods are discussed in detail in the following section. In this chapter, we will perform a comparative study with MST and SACA algorithm.

4.3 Methods of clusterization

4.3.1 Minimum Spanning Tree with Momentum cut (MSTM)

An improvement over the *MST* algorithm, is to put additional cut in momentum space [26]. It will help to get rid of fragments that although close in spatial space are far in momentum space. The *MSTM* method also takes care of the relative momentum of nucleons. Along with the restriction in the spatial space of nucleons, another restriction is put in the momentum space of nucleons i.e.

$$|\vec{p_i} - \vec{p_j}| \ \leq \ p_{min} \tag{4.18}$$

$$|\vec{r_i} - \vec{r_j}| \ \leq \ d_{min} \tag{4.19}$$

where p_{min} = 150 MeV/c in QMD, while, 268 MeV/c in IQMD. The value of cut (in the relative momentum of two nucleons) is about the average Fermi momentum of nucleons (i.e $\approx$ 150 MeV/c in QMD and 268 MeV/c in IQMD, respectively) as reported in [5].

4.3.2 Stimulated Annealing Clusterization Algorithm (SACA)

It was a first ever novel algorithm to detect the fragments at early stage of the reaction. To find a realistic fragment configuration, Puri *et al.* [1], assumed that a configuration is realized in the nature (at any time) which gives the largest binding energy. To find the most bound configuration one confronts with two problems:

a) The huge number of possible configurations.

b) The fact that the number of entities changes. The number of nucleons is constant, whereas the number of free nucleons and fragments are variable.

One may approach this problem by simple iterative methods. They, however, do not guaranty that a global minimum is obtained but may arrive at a local minimum [29]. First attempt to overcome this problem has been advanced in Ref. [30].

In new approach, the pattern can be summarized as follows.

It is assumed that:

1 The nucleons from target and projectile are grouped into fragments (of any size) and into free nucleons.

2 Though the nucleons inside a fragment can interact with each other, they do not interact with the nucleons from other fragments or free nucleons.

3 That pattern of nucleons and fragments is realized in nature which gives the highest binding energy.

To avoid the creation of too many fragments at intermediate times, an additional binding energy check has been employed. In the approach [1], a group of nucleons can form a fragment if the total fragment energy/nucleon ζ is below a minimum binding energy:

$$\begin{aligned} \zeta &= \sum_{i=1}^{N^f} \left[\sqrt{(\mathbf{p}_i - \mathbf{P}_{N^f}^{cm})^2 + m_i^2} - m_i + \frac{1}{2} \sum_{j \neq i}^{N^f} V^{ij}(\mathbf{r}_i, \mathbf{r}_j) \right] \\ &< L_{be} \times N^f, \end{aligned} \tag{4.20}$$

with L_{be} = -4.0 MeV if $N^f \geq 3$ and $L_{be} = 0$ otherwise. In this equation, N^f is the number of nucleons in a fragment, $\mathbf{P}_{N^f}^{cm}$ is the center-of-mass momentum of the fragment. The requirement of a minimum binding energy excludes the loosely bound fragments which will decay after a while.

One is tempted to start the search for the most bound cluster configuration by an iterative minimization method (also known as neighborhood search or local search). In this method, starting from a given configuration a new one is constructed. The new configuration is accepted only if it lowers the binding energy. The drawback of this procedure is that it may terminate at a local minimum. To improve this limitation, several modifications can be imagined [31]:

1. To execute the algorithm for a large number of the initial configurations. This will finally allow to reach the global minimum. This is very time consuming.

2. To use an algorithm which can jump over local minima and hence one can reach the global minima. This clearly depends strongly on the problem. Therefore its applications are limited.

3: To generalize the iterative method so that the transitions which yields a higher binding energy are always accepted. In addition, the transitions which yield a lower binding energy are also accepted with a certain probability. This algorithm is known as simulated annealing method [31]. Its name is based on the fact that this algorithm is akin to the one used for cooling the solids. The simulated annealing method is a sequence of metropolis algorithms [32] with decreasing control parameter ϑ. The control parameter ϑ can be interpreted as a *temperature*. For each metropolicity at a given temperature, one has to perform a sequence of steps until the binding energy does not change anymore. Each step is executed as follows:

1: Given some initial configuration a with energy ζ_a, a new configuration b with energy ζ_b is generated in the neighborhood of a using a Monte-Carlo procedure.

2: Let the energy difference between a and b is $\Delta\zeta = \zeta_b$ -ζ_a.

3.: If $\Delta\zeta$ is negative, the new configuration is always accepted. If $\Delta\zeta$ is positive, it is accepted with a probability $\exp(-\Delta\zeta/\vartheta)$.

At the start, the control parameter ϑ is taken to be large enough so that almost all attempted transitions are accepted. This is to overcome any kind of the local minima. After the binding energy remains constant, a gradual decrease in the control parameter ϑ is made and the Metropolis algorithm is repeated.

To start with, a random configuration a (which consist of fragments and free nucleons) is chosen. The total energy associated with configuration a is given by

$$\begin{aligned}
\zeta_a = &\sum_{i=1}^{N_1^f}\left\{\sqrt{(\mathbf{p}_i - \mathbf{P}_{N_1^f}^{cm})^2 + m_i^2} - m_i + \frac{1}{2}\sum_{j\neq i}^{N_1^f} V_{ij}(\mathbf{r}_i,\mathbf{r}_j)\right\}_1 \\
&+\cdots\sum_{i=1}^{N_\nu^f}\left\{\sqrt{(\mathbf{p}_i - \mathbf{P}_{N_\nu^f}^{cm})^2 + m_i^2} - m_i + \frac{1}{2}\sum_{j\neq i}^{N_\nu^f} V_{ij}(\mathbf{r}_i,\mathbf{r}_j)\right\}_\nu \\
&+\sum_{i=1}^{N_\mu^f}\left\{\sqrt{(\mathbf{p}_i - \mathbf{P}_{N_\mu^f}^{cm})^2 + m_i^2} - m_i + \frac{1}{2}\sum_{j\neq i}^{N_\mu^f} V_{ij}(\mathbf{r}_i,\mathbf{r}_j)\right\}_\mu \\
&+\cdots\sum_{i=1}^{N_n^f}\left\{\sqrt{(\mathbf{p}_i - \mathbf{P}_{N_n^f}^{cm})^2 + m_i^2} - m_i + \frac{1}{2}\sum_{j\neq i}^{N_n^f} V_{ij}(\mathbf{r}_i,\mathbf{r}_j)\right\}_n .
\end{aligned}$$

Here N_μ^f is the number of nucleons in a fragment μ, $\mathbf{P}_{N_\mu^f}^{cm}$ is the center-of-mass momentum of the fragment μ and $V_{ij}(\mathbf{r}_i, \mathbf{r}_j)$ is the interaction energy between nucleons i and j in a given fragment μ. Note that the total energy is the sum of the energies of individual fragments in their respective center-of-mass system. Therefore, ζ_a differs from the (conserved) total energy of the system because (i) the kinetic energies of fragments calculated in their center-of-masses and (ii) the interactions between fragments/free nucleons are neglected.

A new configuration is generated using Monte-Carlo procedure by either a) transferring a nucleon from some randomly chosen fragment to another fragment or by b) setting a nucleon of a fragment free or c) absorbing a free nucleon into a fragment. Let the new configuration b be generated by transferring a nucleon from fragment ν to fragment μ. Then the energy of new configuration b is given by:

$$\begin{aligned}
\zeta_b = &\sum_{i=1}^{N_1^f} \left\{ \sqrt{(\mathbf{p}_i - \mathbf{P}_{N_1^f}^{cm})^2 + m_i^2} - m_i + \frac{1}{2} \sum_{j \neq i}^{N_1^f} V_{ij}(\mathbf{r}_i, \mathbf{r}_j) \right\}_1 \\
+ \cdots &\sum_{i=1}^{N_\nu^f - 1} \left\{ \sqrt{(\mathbf{p}_i - \mathbf{P}_{N_\nu^f - 1}^{cm})^2 + m_i^2} - m_i + \frac{1}{2} \sum_{j \neq i}^{N_\nu^f - 1} V_{ij}(\mathbf{r}_i, \mathbf{r}_j) \right\}_\nu \\
+ &\sum_{i=1}^{N_\mu^f + 1} \left\{ \sqrt{(\mathbf{p}_i - \mathbf{P}_{N_\mu^f + 1}^{cm})^2 + m_i^2} - m_i + \frac{1}{2} \sum_{j \neq i}^{N_\mu^f + 1} V_{ij}(\mathbf{r}_i, \mathbf{r}_j) \right\}_\mu \\
+ \cdots &\sum_{i=1}^{N_n^f} \left\{ \sqrt{(\mathbf{p}_i - \mathbf{P}_{N_n^f}^{cm})^2 + m_i^2} - m_i + \frac{1}{2} \sum_{j \neq i}^{N_n^f} V_{ij}(\mathbf{r}_i, \mathbf{r}_j) \right\}_n
\end{aligned}$$

Note that in this procedure, the individual energies of all fragments except for the donor fragment (ν) and the receptor fragment (μ) remain the same. The change in the energy from $a \longrightarrow b$ is given by

$$\Delta\zeta = \zeta_b - \zeta_a. \tag{4.21}$$

Between the Metropolis algorithms, the system is cooled by decreasing the control parameter ϑ. A decrease in the temperature means that we narrow the energy difference which is accepted in a metropolis step. After many Metropolis steps, one would arrive at a minimum i.e. the most bound configuration. The problem is, however, that one usually arrive at a local minimum only. Between the local minimum, we find huge maxima. Let us give an

example: assume we have two fragments, but the most bound configuration would be one single fragment which combines both. Now each exchange of a single nucleons raises the binding and only the exchange of all nucleons at the same time lowers the total binding energy. This effect is well known in chemistry, where it is called Activation energy. In order to avoid this, one add, therefore, a second simulated annealing algorithm in which not anymore the nucleons are considered as the particles which are exchanged in each Metropolis step (like in the first simulated annealing), but also the entities (fragments or nucleons) obtained after the first step. This second stage of minimization is called fragment exchange procedure.

Note that even in this stage, the free nucleons can be exchanged as before. The total energy associated with any configuration c during the second stage of iterations is given by

$$\begin{aligned}\zeta_c = &\left\{\sum_{i=1}^{N_{S_1}}\left[\sqrt{(\mathbf{p}_i-\mathbf{P}^{cm}_{N_{S_1}})^2+m_i^2}-m_i+\frac{1}{2}\sum_{j\neq i}^{N_{S_1}}V_{ij}(\mathbf{r}_i,\mathbf{r}_j)\right]\right\}_1\\ &+\cdots\left\{\sum_{i=1}^{N_{S_\nu}}\left[\sqrt{(\mathbf{p}_i-\mathbf{P}^{cm}_{N_{S_\nu}})^2+m_i^2}-m_i+\frac{1}{2}\sum_{j\neq i}^{N_{S_\nu}}V_{ij}(\mathbf{r}_i,\mathbf{r}_j)\right]\right\}_\nu\\ &+\left\{\sum_{i=1}^{N_{S_\mu}}\left[\sqrt{(\mathbf{p}_i-\mathbf{P}^{cm}_{N_{S_\mu}})^2+m_i^2}-m_i+\frac{1}{2}\sum_{j\neq i}^{N_{S_\mu}}V_{ij}(\mathbf{r_i},\mathbf{r}_j)\right]\right\}_\mu\\ &+\cdots\left\{\sum_{i=1}^{N_{S_n}}\left[\sqrt{(\mathbf{p}_i-\mathbf{P}^{cm}_{N_{S_n}})^2+m_i^2}-m_i+\frac{1}{2}\sum_{j\neq i}^{N_{S_n}}V_{ij}(\mathbf{r}_i,\mathbf{r}_j)\right]\right\}_n .\end{aligned}$$

Here N_{S_μ} is the number of nucleons in a super-fragment $S_\mu=\sum_{k=1}^{N^f_{S_\mu}}N^k_{S_\mu}$, where $N^k_{S_\mu}$ is the number of nucleons in the k-th fragment contained in the super-fragment. S_μ and $N^f_{S_\mu}$ is the number of pre-fragments contained in the super-fragment S_μ. The $\mathbf{P}^{cm}_{N_{S_\mu}}$ is the center-of-mass momentum of the super fragment S_μ and $V_{ij}(\mathbf{r}_i,\mathbf{r_j})$ is the interaction energy between nucleons i and j in a given super-fragment. Note that now the particle i interacts with its fellow nucleons in the same pre-fragment and also with the nucleons of other pre-fragments which are contained in a new given super fragment S_μ.

The new configuration is generated using Monte-Carlo procedure by either a) transferring a pre-fragment from some randomly chosen super-fragment to another super-fragment or by b) setting a pre-fragment free or c) absorbing a single isolated pre-fragment into a super-fragment. Let us suppose that a new configuration d is generated by transferring a pre-

fragment $\mathbf{k}$ (with mass $N_{S_\nu}^k$) from super-fragment ν to super-fragment μ. The associated energy of new configuration d reads as :

$$\zeta_d = \left\{ \sum_{i=1}^{N_{S_1}} \left[\sqrt{(\mathbf{p}_i - \mathbf{P}_{N_{S_1}}^{cm})^2 + m_i^2} - m_i + \frac{1}{2} \sum_{j \neq i}^{N_{S_1}} V_{ij}(\mathbf{r}_i, \mathbf{r}_j) \right] \right\}_1$$
$$+ \cdots \left\{ \sum_{i=1}^{N_{S_\nu} - N_{S_\nu}^k} \left[\sqrt{(\mathbf{p}_i - \mathbf{P}_{N_{S_\nu} - N_{S_\nu}^k}^{cm})^2 + m_i^2} - m_i + \frac{1}{2} \sum_{i \neq j}^{N_{S_\nu} - N_{S_\nu}^k} V_{ij}(\mathbf{r}_i, \mathbf{r}_j) \right] \right\}_\nu$$
$$+ \left\{ \sum_{i=1}^{N_{S_\mu} + N_{S_\nu}^k} \left[\sqrt{(\mathbf{p}_i - \mathbf{P}_{N_{S_\mu} + N_{S_\nu}^k}^{cm})^2 + m_i^2} - m_i + \frac{1}{2} \sum_{j \neq i}^{N_{S_\mu} + N_{S_\nu}^k} V_{ij}(\mathbf{r}_i, \mathbf{r}_j) \right] \right\}_\mu$$
$$+ \cdots \left\{ \sum_{\alpha=1}^{N_{S_n}} \left[\sqrt{(\mathbf{p}_i - \mathbf{P}_{N_{S_n}}^{cm})^2 + m_i^2} - m_i + \frac{1}{2} \sum_{j \neq i}^{N_{S_n}} V_{ij}(\mathbf{r}_i, \mathbf{r}_j) \right] \right\}_n .$$

The only difference between the particle and the fragment exchange procedure occurs for the bound nucleons. Now the bound nucleons cannot change their identity neither by being absorbed nor by becoming free. They will remain bound in a pre-fragment. The pre-fragment itself can change its identity by either getting transferred to a new super-fragment, or be set free. As in the first stage, one calculate the energy difference between the new and the old configurations $\Delta\zeta$ and the metropolis procedure is continued till the most favored configuration is obtained.

The simulated annealing algorithm has several parameters to be determined : the initial and the final value of the control parameter ϑ, the number of metropolis steps to be executed at a given value of control parameter (i. e. length of Markov chain) , the decrease of the control parameter and the termination of the algorithm. This set of the parameters is also referred as cooling schedule in the literature [31]. One needs to choose the following parameters explicitly:

1.: The initial value of the control parameter ϑ_l. This will be referred as temperature.

2.: The final value of the control parameter ϑ_f [i.e. the termination procedure].

3.: The length of the Markov chain M_{ch}.

4.: A rule to fix the decrement in the control parameter σ.

For the details of these parameters, we refer the reader to Ref. [1]. In Ref. [1], a detail investigation of role of these parameters was made & after extensive analysis, the most economical set of parameters was given.

Using above discussed various nucleon-nucleon cross sections along with MDI (discussed in chapter 3), we shall present a role of different type of cross sections and momentum dependent interactions in multifragmentation for symmetric and asymmetric reactions using minimum spanning tree method. Moreover, we shall see the role of different model ingredients like Gaussian width, clusterization distance, method of clusterization (MST and SACA) and equations of state (Hard and Soft) on multifragmentation. At last, we will compare the results of different nucleon-nucleon cross sections with experimental findings as well as with different model ingredients.

4.4 Results and discussion

We here simulate the symmetric reactions of $_{79}Au^{197}$ + $_{79}Au^{197}$ at incident energies of 100, 400, 600 and 1000 MeV/nucleon and over complete range of the impact parameter using QMD model. The system size and asymmetry effects will be analyzed by further studying the reactions of $_{10}Ne^{20}$ + $_{13}Al^{27}$, $_{18}Ar^{40}$ + $_{21}Sc^{45}$, $_{36}Kr^{84}$ + $_{41}Nb^{93}$ and $_{54}Xe^{131}$ + $_{57}La^{139}$ at energies between 20 and 150 MeV/nucleon. The incident energy, colliding nuclei as well as impact parameters are chosen on the basis of the available experimental data from the ALADIN [33] and NSCL collaborations[34]. The comparison with experimental findings is done by varying the nucleon-nucleon cross section from Cugnon to constant (say 40 and 55 mb)in the presence of soft momentum dependent (SMD) equation of state. The cross section values are represented in the superscript. The clusterization at first instance is made using the minimum spanning tree (MST) method, in which, nucleons are bound if $R_{Clus} = |\vec{r_1} - \vec{r_2}|$ $\leq$ 4 fm. On the other hand, to understand the relative effects of different cross sections with model ingredients, the detailed analysis of model ingredients like Gaussian width, clusterization distance, method of clusterization and equations of state is performed.

4.4.1 Phase space of nucleons

To understand the role of different nucleon-nucleon cross sections on the projectile and target nucleons, in Fig.4.4, we have displayed the phase space for $_{79}Au^{197}$ + $_{79}Au^{197}$ reaction

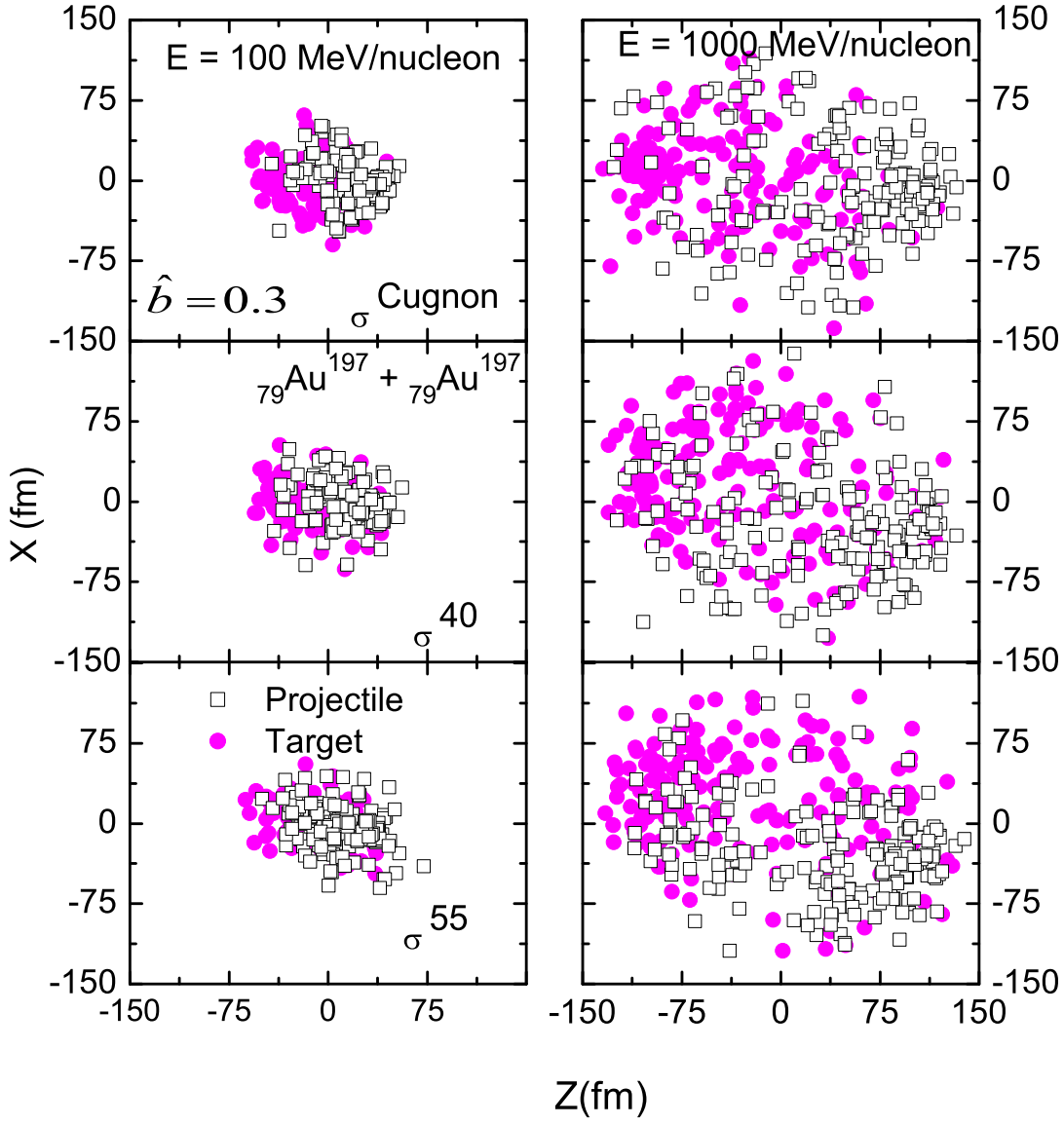

Figure 4.4: Phase space of projectile and target nucleons at t = 200 fm/c at different nucleon-nucleon cross sections in the presence of momentum dependent interactions. The left panel is at relatively low incident energy E = 100 MeV/nucleon, while, right panel is at relatively high incident energy E = 1000 MeV/nucleon.

in X-Z plane at semi-central geometry. The top, middle and bottom panels are at σ^{Cug}, σ^{40} and σ^{55}, respectively, while the left and right panels are at relatively low (say E = 100 MeV/nucleon) and high (say E = 1000 MeV/nucleon)incident energies. A heavy fragment is observed at incident energy E = 100 MeV/nucleon which disappears at energy E = 1000 MeV/nucleon. This is true for all the cross sections under consideration. Moreover, with increase in cross section, more expansion of the matter takes place at low incident energy, while negligible effect is at higher incident energy. As the role of momentum dependent interactions and cross sections is same: break up of the initial correlation among nucleons. Due to this reason, at low incident energy where mean field is dominating, the cross section is helping to break up the initial correlations among the nucleons and hence expansion of the matter. However, more expansion of the matter is observed at E = 1000 MeV/nucleon as compared at E = 50 MeV/nucleon. This expansion is further found to be affected by the nucleon-nucleon cross sections. This feature of heavy-ion collisions further can be strengthen by studying the time evolution of different kind of fragments.

4.4.2 Time evolution of free nucleons and fragments

The role of nucleon-nucleon cross sections on the fragments production is studied in the literature many times. One or more shortcomings were observed in these studies. In some studies, the static equation of state was used[7], while other studies were performed in the presence of momentum dependent interactions, but upto 200 MeV/nucleon[7]. To overcome these shortcomings, we have performed the present work in the presence of momentum dependent interactions upto 1 GeV/nucleon.

From Figs.4.5-4.8, the time evolution of free nucleons (FN) [$1 \leq A \leq 1$], light charged particles (LCP's)[$2 \leq A \leq 4$], medium mass fragments (MMF's) [$5 \leq A \leq 9$] and intermediate mass fragments (IMF's)[$5 \leq A \leq A_{tot}/6 = 65$ for Au + Au] is displayed for the collisions of ${}_{79}Au^{197}$ + ${}_{79}Au^{197}$ at semi-central (left panel) and semi-peripheral (right panel) geometries in each figure. The panels from top to bottom are at E = 100, 400, 600 and 1000 MeV/nucleon, respectively. The 200 fm/c is taken as freeze out time in view of the fact the nuclei, generated in molecular dynamical model, are no longer stable after 200 fm/c. In some cases, the multiplicity of fragments continues to change even at 200 fm/c. In these cases, the reaction takes longer time. We in fact do not know whether the contribution

after 200 fm/c is a real one or just spurious yield due to the de-stabilization of fragments. Therefore, we stop the reaction at 200 fm/c.

Free nucleons as well as LCP's have been the similar scenario at semi-central and semi-peripheral geometries except E = 100 MeV/nucleon (shown in Figs.4.5 and 4.6). At semi-central geometry, the production of free nucleons as well as LCP's is found to increase with increase in the nucleon-nucleon cross section. This is true at all incident energies under consideration. The free nucleon and LCP's generates from the participant zone. With increase in the cross section value, the participant zone will get more compressed and hot and hence more is the production of free and LCP's. The scenario of the free nucleons and LCP's is different with increase in incident energy. The free particles are found to increase with increase in incident energy, while, LCP's are found to decrease after certain incident energy (say E = 400 MeV/nucleon). This is due to the reason that after this energy LCP's starts breaking into free nucleons in the participant zone.

At semi-peripheral geometry, the different trend is observed for free as well as LCP's at E = 100 MeV/nucleon as compared to semi-central geometry. The production of free and LCP's at this energy is followed by SMD+σ^{40}, SMD+σ^{Cugnon} to SMD+σ^{55}, while, the trend was from SMD+σ^{Cugnon}, SMD+σ^{40} to SMD+σ^{55} at semi-central geometry. It means that tendency of break up of the initial correlation among nucleons, which is not possible with SMD+σ^{Cugnon}/σ^{40} is fulfilled by SMD+σ^{55}. This is showing the importance of momentum dependent interactions as well as large cross section at low incident energy in the semi-peripheral geometry. On the other hand, at all other incident energies the universal behavior is followed by free and LCP's as was followed at semi-central geometry.

Lets move towards the multiplicity of MMF's and IMF's (shown in Figs.4.7 and 4.8). The MMF's and IMF's have different story to tell in comparison to free nucleons and LCP's. At semi-central geometry, with increase in incident energy, the role of different nucleon-nucleon cross section on the multiplicity of MMF's and IMF's is found to decrease. This is more pronounced for IMF's as compared to MMF's. It is also shown in chapter 3 that SMD equation of state is able to break up the initial correlation among the nucleons. Moreover, larger cross section has also ability to break up the initial correlations. In the presence of MDI, with increase in the cross section value, more transfer of incident energy takes place

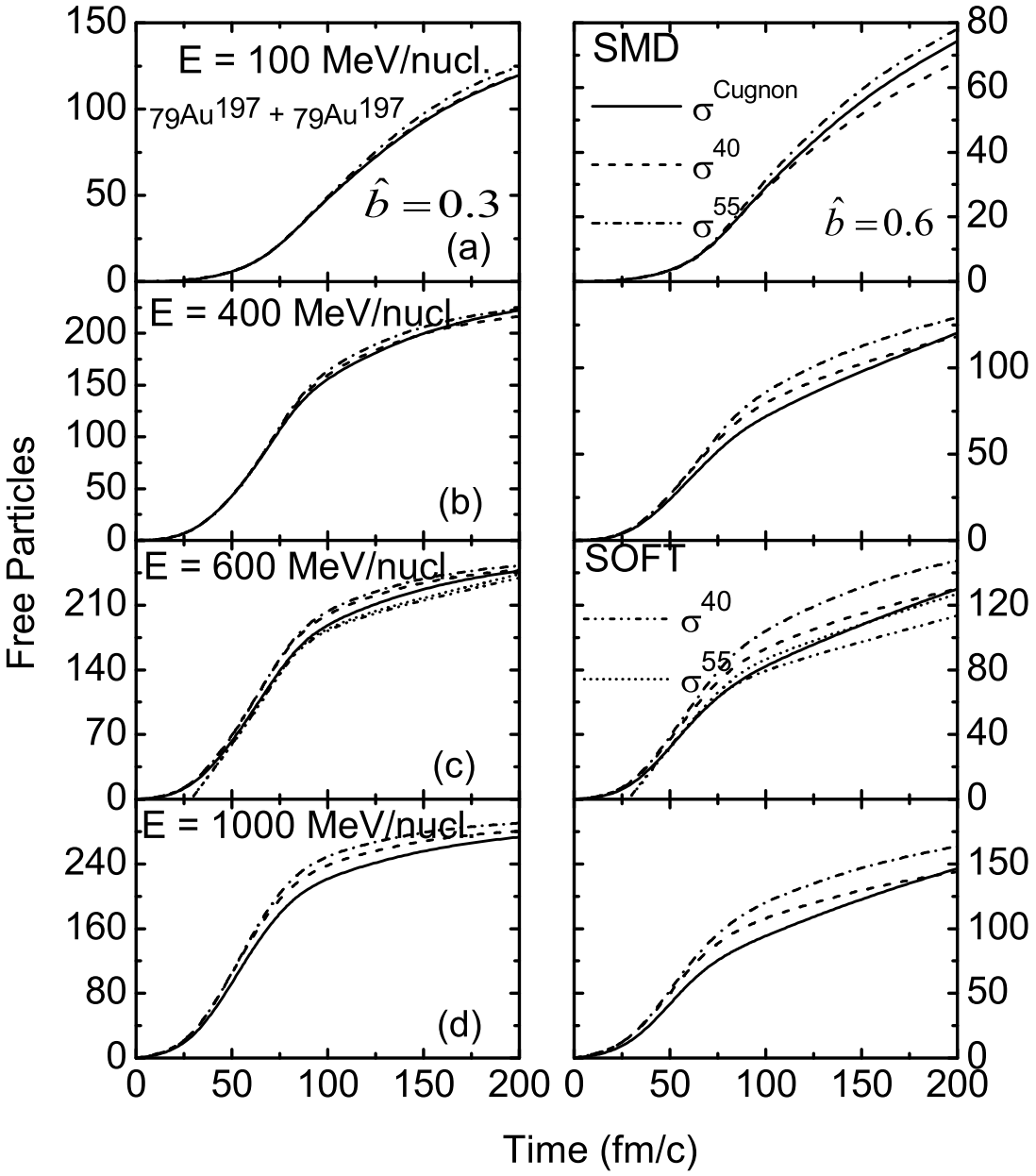

Figure 4.5: The time evolution of multiplicity of free nucleons in the presence of nucleon-nucleon cross sections and momentum dependent interactions. The panels from top to bottom are at E = 100, 400, 600, 1000 MeV/nucleon, respectively, while left and right panels are for semi-central and semi-peripheral geometries. In addition, the results with static equation of state are also displayed at E = 600 MeV/nucleon with σ^{40} and σ^{55}.

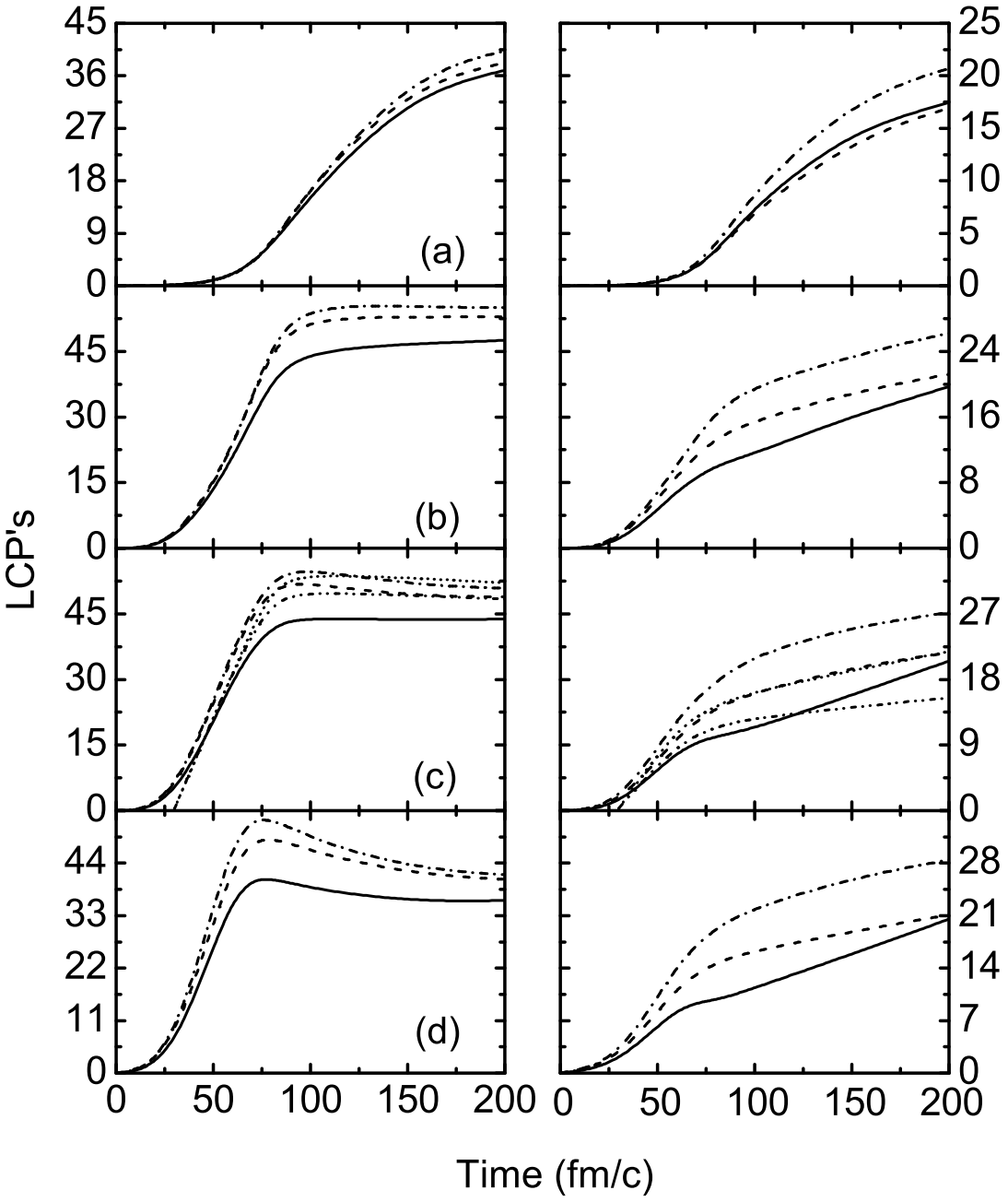

Figure 4.6: Same as in Fig.4.5, but for the time evolution of LCP's.

from participant to spectator zone and hence break up of the heavy fragments into MMF's. MMF's further will decay into LCP's and free nucleons at sufficient high incident energy (say E = 1000 MeV/nucleon). This will lead to decrease in the production of heavy fragments (like MMF's and IMF's) with cross section.

Moreover, at semi-peripheral geometry ($\hat{b} = 0.6$), the production of MMF's as well as IMF's found to increase with increase in cross section. The spectator zone at this geometry (which is more than half part of the projectile and target nucleus) will need high incident energy and larger cross section to break up the initial correlations as compared to semi-central geometry (where spectator is very less than half part of the projectile and target nucleus). As a result of this, the spectator matter at $\hat{b} = 0.3$, will break up into LCP's and free nucleons with increase in incident energy and cross section. On the other hand, the spectator matter at $\hat{b} = 0.6$ will break up into IMF's and MMF's. Interestingly, it is also observed that the chances of break up into IMF's is more as compared to MMF's. That's why the production of MMF's and IMF's at semi-peripheral geometry is found to increase with increase in the cross section at all incident energies.

To make the study more interesting, in the 3^{rd} panel from top to bottom the results are also displayed with soft equation of state at σ^{40} and σ^{55} at E = 600 MeV/nucleon. At semi-central geometry, increase is observed in the production of free and LCP's at σ^{40} and σ^{55} in the presence of momentum dependent interactions, while, decrease is observed in the production MMF's and IMF's. On the other hand, at semi-peripheral geometry, increase is observed in the production of free, LCP's, MMF's and IMF's at σ^{40} and σ^{55}. This study is indicating the need of momentum dependent equation of state with large cross section for free and LCP's at semi-central geometry, while for the free, LCP's, MMF's and IMF's at semi-peripheral geometry.

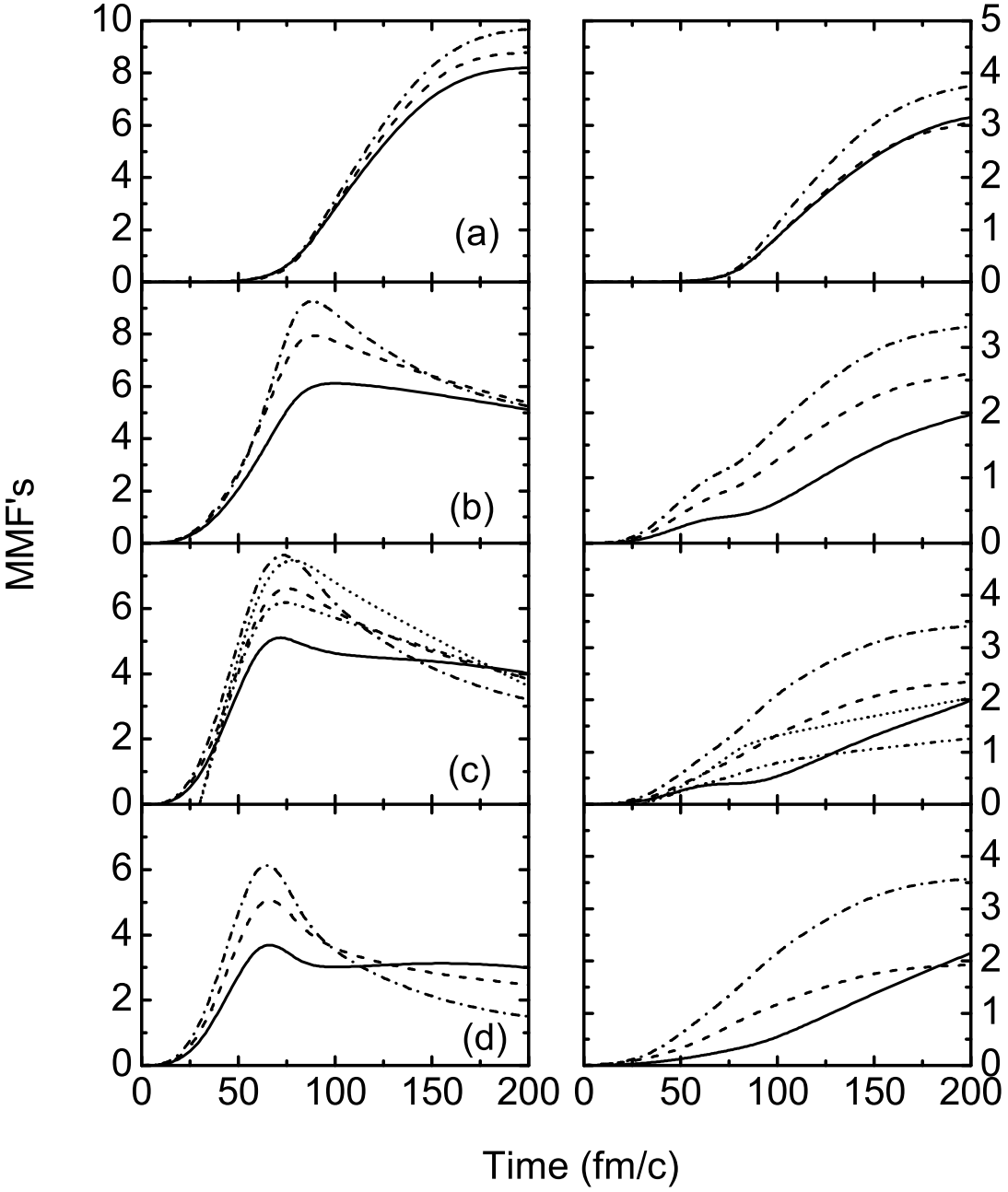

Figure 4.7: Same as in Fig.4.5, but for the time evolution of MMF's.

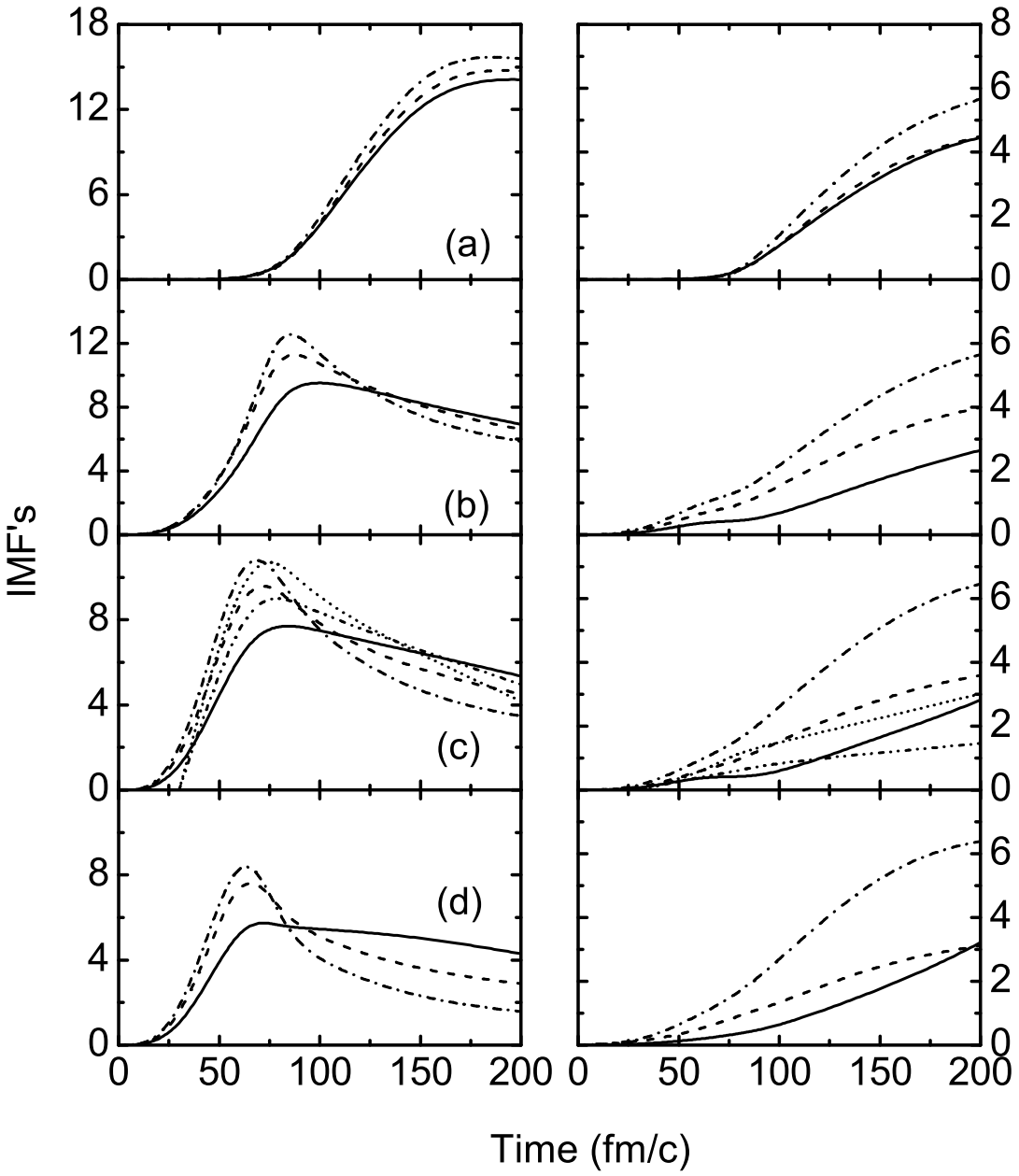

Figure 4.8: Same as in Fig.4.5, but for the time evolution of IMF's.

4.4.3 Effect of large nucleon-nucleon cross sections on fragments production

To see the relative effect of large cross sections on the multiplicity of different kind of fragments, we rather define a relative probability factor :

$$Rel_{frag}^{mult.}\% \;=\; \left(\frac{(mult.)^{\sigma^{55}} \;-\; (mult.)^{\sigma^{Cugnon}}}{(mult.)^{\sigma^{Cugnon}}}\right) \times 100 \tag{4.22}$$

Here mult. stands for the multiplicity of some kind of particles (free nucleons or fragments) with Cugnon and with σ^{55} using the SMD equation of state. The beam energy dependence of relative fragments probability is plotted in Fig.4.9 for free nucleons, LCP's, MMF's and IMF's, respectively. From the figure, many interesting points revealed out, which we were not able to detect at the instant of time evolution study.

i The relative role of large cross section is more at semi-peripheral geometry as compared to semi-central geometry. This is true for all kind of fragments as well as at all incident energies.

ii The relative role at semi-peripheral geometry goes on increasing as one moves from the free nucleons towards intermediate mass fragments. This is due to the reason that at large cross section, possibility of transfer of energy from the participant to heavier spectator matter increases, leading to production of more IMF's at large cross sections.

iii At semi-central geometry, the relative role is in opposite sense for MMF's and IMF's as compared to free nucleons and LCP's. This further goes on decreasing for IMF's. It reveals that the role played due to Cugnon cross section leads to more MMF's and IMF's as compared to constant cross section σ^{55}. Further, it is also indicating that with increase in incident energy, large cross section leads to formation of LCP's and hence decrease in MMF's and IMF's. The IMF's are mostly affected by the influence of nucleon-nucleon cross section as the relative % indicating which is 6%, 14%, -58% and -75% for free LCP's, MMF's and IMF's, respectively.

iv The almost constant production of free nucleons is observed at E = 400 MeV/nucleon (semi-central) with Cugnon and large cross section σ^{55}. This may be due to the other interesting findings at E = 400 MeV/nucleon like the maximum stopping [35] as well as maximum squeeze out for ${}_{79}Au^{197} + {}_{79}Au^{197}$ [36]. Finding the importance of intermediate mass frag-

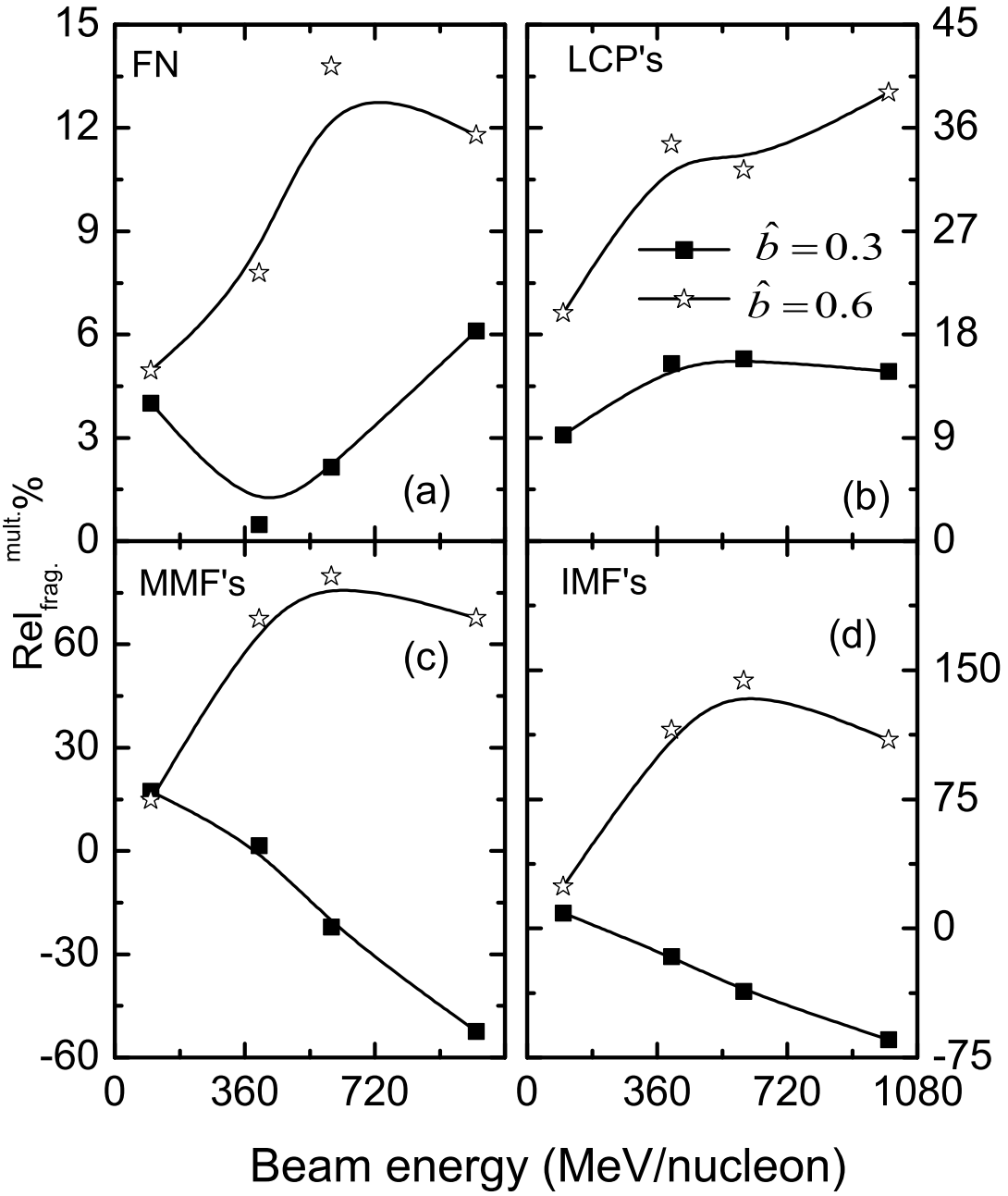

Figure 4.9: The relative fragment production as a function of the incident energy. The results in each panel are displayed for semi-central and semi-peripheral geometry.

ments in the presence of nucleon-nucleon cross section as well as with the availability of experimental data for IMF's, detailed analysis on the IMF's is performed in the following subsections.

4.4.4 Theory versus experiment

Impact parameter dependence of IMF's for symmetric system

In Fig.4.10, we display the multiplicity of intermediate mass fragments (IMF's) as a function of the impact parameter for the reaction of $_{79}Au^{197}$ + $_{79}Au^{197}$ at incident energies 100, 400, 600 and 1000 MeV/nucleon. Here soft momentum dependent interaction (SMD) is used with different cross sections. From the figure, the multiplicity of IMF's is maximal at 100 MeV/nucleon for smaller impact parameters, which decreases with the increase in the impact parameter. On the other hand, one sees a rise and fall in the multiplicity of the IMF's at higher incident energies. The dynamics at 100 MeV/nucleon, is mainly governed by the mean field or by the density of the reaction as compared to other higher incident beam energies under consideration (e.g. 400, 600 and 1000 MeV/nucleon). The incident energy of 30 MeV/nucleon is the lowest limit for any semi-classical model, where the effect of Pauli-blocking is $\approx 90\%$. Below this incident energy, quantum effects as well as Pauli-blocking need to be redefined. There are very little effects of different cross sections at 100 MeV/nucleon. Due to the low excitation energy, central collisions generate better repulsion and break the colliding nuclei into IMF's, whereas for the peripheral collisions, the size of the fragment is close to the size of the reacting nuclei, therefore, one sees a very few IMF's. In contrary, a rise and fall can be seen at other higher incident energies. For the central collisions, the frequent nucleon-nucleon collisions occurring at these energies do not allow any IMF's production, whereas, at peripheral collisions the energy transfer is from the participating matter to spectator matter is minimum, therefore, very few IMF's are seen.

In all the cases, some effects of different nucleon-nucleon cross sections are visible at higher incident energies. The use of the momentum dependent interaction yields better comparison with ALADIN setup [33] for $\sigma = 55$ mb. These findings are in agreement with the results reported in Ref.[1], where it was found that nucleon-nucleon cross section has sizable effect on reaction dynamics. Note that in these studies, static equation of state was

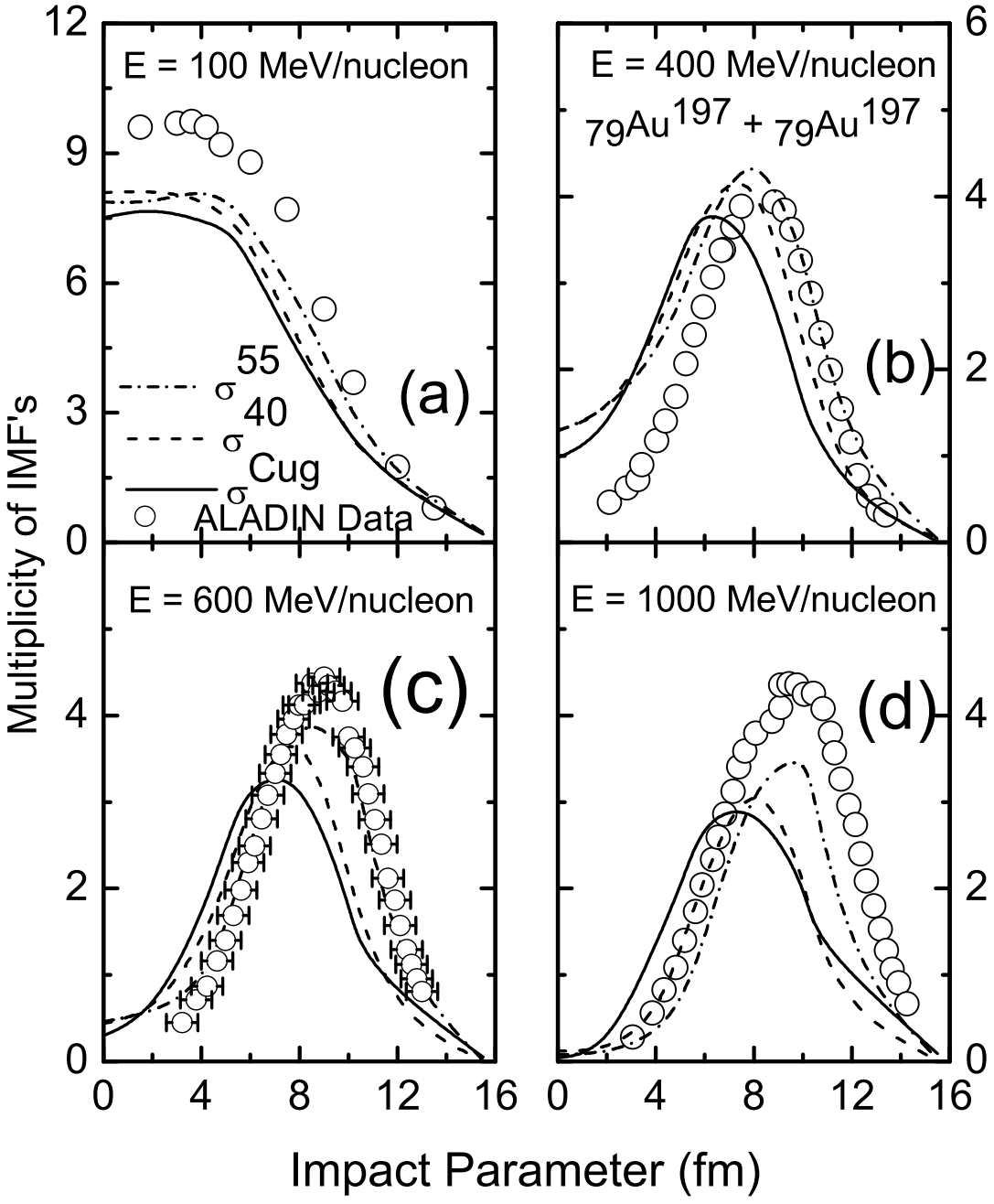

Figure 4.10: Comparison of average multiplicity of intermediate mass fragments (IMF's) with ALADIN data at incident energies of 100, 400 MeV/nucleon (top panel) and 600, 1000 MeV/nucleon (bottom panel) as a function of impact parameter. The results are displayed using soft momentum dependent (SMD) interactions.

used.

Incident energy dependence of IMF's for asymmetric systems

Let us now analyze the above facts in asymmetric reactions . In Fig. 4.11, asymmetric reactions of $_{10}Ne^{20}$ + $_{13}Al^{27}$, $_{18}Ar^{40}$ + $_{21}Sc^{45}$, $_{36}Kr^{84}$ + $_{41}Nb^{93}$ and $_{54}Xe^{131}$ + $_{57}La^{139}$ are displayed as a function of beam energy at scaled impact parameter $\hat{b} = 0.3$ (semi central collisions) using different cross sections. Final results are also compared with the NSCL experimental data [34]. Due to no access to filters, no direct comparison with data could be made. These comparisons are just indicating the trend within theoretical framework. From the figure, it is clear that the trends of our calculations with soft momentum dependent (SMD) interactions are in good agreement with experimental data. Again different nucleon-nucleon cross sections fail to make any significant impact on the cluster dynamics.

One further see that the multiplicity of IMFs in $_{10}Ne^{20} +_{13} Al^{27}$ decreases with increase in the beam energies. For the reaction of $_{18}Ar^{40} +_{21} Sc^{45}$, similar trends emerge above 55 MeV/nucleon, as in case of $_{10}Ne^{20} +_{13} Al^{27}$. For energies below 55 MeV/nucleon, we see dominated role of mean field and hence increase in the intermediate mass fragments. For the rest of the reactions, namely, $_{36}Kr^{84} +_{41} Nb^{93}$ and $_{54}Xe^{131} +_{57} La^{139}$, the multiplicity of IMF's increases with the increase in the beam energy and cross section. One should note that in the first two reactions, incident energy is much higher compared to the last two reactions.

4.4.5 Effect of model ingredients on the production of IMF's

As our aim is to see the influence of nucleon-nucleon cross sections as well as model ingredients on the multifragmentation. The effect of nucleon-nucleon cross sections is studied in the above sections on the multifragmentation, here we will try to see the effect of model ingredients. In Fig. 4.12, we display in the upper part, the effect of width of Gaussian wave packet. In the above sections, where role of different nucleon-nucleon cross sections is studied, a standard Gaussian width of nucleon $L = 4.33\ fm^2$ corresponding to root mean square radius of a nucleon $= 1.8\ fm$ has been implemented. As noted in Ref.[5], this value

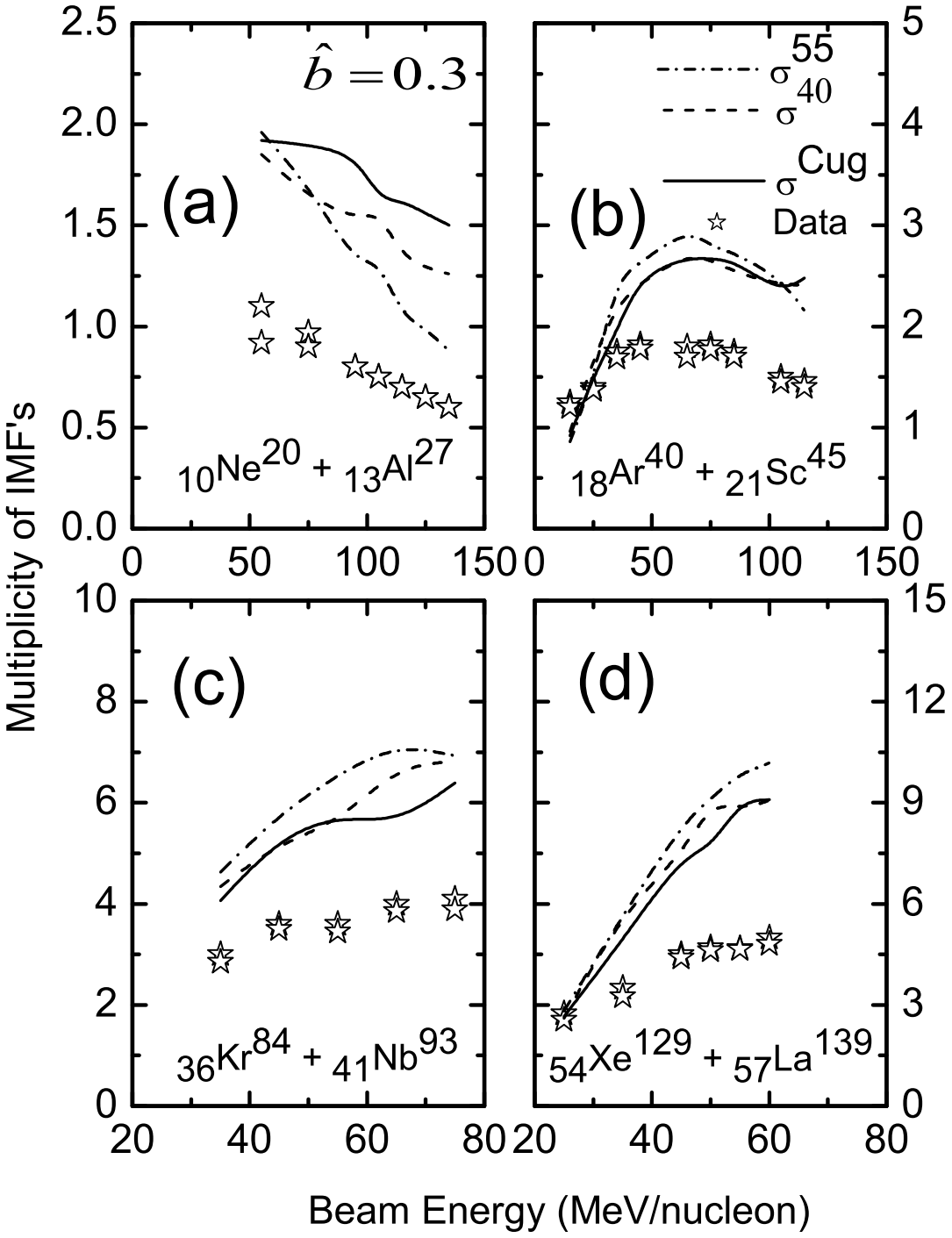

Figure 4.11: The average IMF's multiplicity versus beam energy in the reactions of $_{10}Ne^{20}$ + $_{13}Al^{27}$, $_{18}Ar^{40}$ + $_{21}Sc^{45}$, $_{36}Kr^{84}$ + $_{41}Nb^{93}$ and $_{54}Xe^{129}$ + $_{57}La^{139}$. The symbols represent the NSCL experimental results, while lines are representing the results obtained within QMD model using different cross sections σ^{55}, σ^{40} and σ^{Cug}.

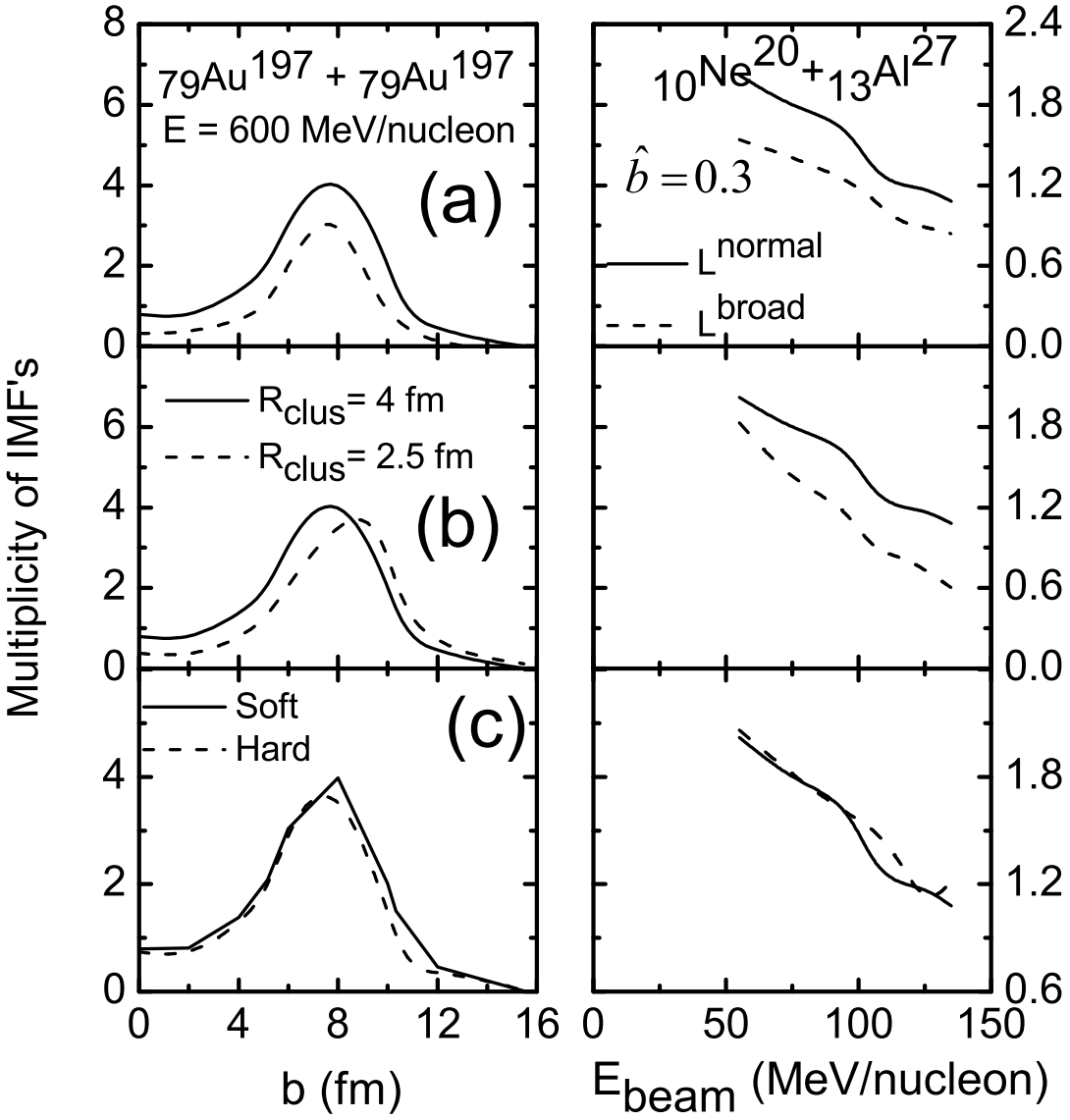

Figure 4.12: A Comparison of multiplicity of IMF's by employing different model ingredients like Gaussian width (upper panel), clusterization cut off distance R_{Clus} (middle) and equation of state (bottom). These results are displayed using soft (upper, middle, bottom) and hard (bottom) equation of state with σ^{55}.

of L determines the interaction range of particles and influences the density distribution of a finite system. In a semi-classical theory, this parameter is chosen by keeping in mind the stability of nuclei generated. A very small value of L is excluded because the nuclei would become unstable after initialization. On the other hand, very large value of L increases the effective range of interaction and thus lead to some smearing of fluctuations. Thus, the value of L represents the limit for a semi-classical theory. Ideally, a time dependent width of the Gaussian should be used. Some attempts (with limited success) have also been made in this direction [37]. Some authors have even used a system dependent Gaussian width[5]. The Gaussian width for a particular nucleon is chosen in a way so that maximum stability of the nucleonic density profile can be achieved. Hartnack and collaborators[5] used $L = 8.66\ fm^2$ for Au^{197} whereas it was $4.33\ fm^2$ for the Ca^{40} system. We, therefore, display the results with narrow width ($L = 4.33\ fm^2$), labeled as L^{normal}, and broad one ($L = 8.66\ fm^2$), labeled as L^{broad}. Naturally, a wider wave packet will connect large number of nucleons in a fragment, therefore, will lead to different fragmentation patterns depending upon energy and masses of the colliding nuclei. It is worth mentioning that the equation of state for finite matter depends strongly on the value of the width chosen and different Gaussian widths affect the fragmentation by 30-50%[5]. We see that the variation of the width has sizable effect on clusterization. A broader Gaussian results in extended interaction radius, therefore, binding more nucleons into a fragment. As a result, the fragment turns much heavier than the upper limit of IMF's (i.e 65 for (Au+Au) reaction) and hence there is net reduction in the production of IMF's. This result is in agreement with the findings in Ref.[1]. One should also note that larger Gaussian width will also result in more attractive nuclear flow and hence will push the energy of vanishing flow towards higher incident energies. In the middle panel, we display the effect of cut off distance or clusterization parameter R_{Clus} on fragmentation. If the system is dilute and nucleons are quite far from each other, then different clusterization parameters should have a small role to play. The problem, however, is that all transport models are semi-classical in nature where, most of the time, nuclei do not have a true ground state. As a result, the nuclei may emit nucleons and/or may disintegrate into clusters after some time. It has been reported by several authors[38] that the nuclei (generated in semi-classical transport model) are sta-

ble for a typical time of about 200 fm/c. This time is taken as the freeze-out time. The distribution obtained at the freeze-out time may not represent the final distribution which depends strongly on the incident energies. At low incident energies, it takes a very long time whereas a relatively smaller time is needed at higher incident energies. In other words, one can say that the nucleons and fragments at the freeze-out time may not be well separated and may still have interactions among themselves. The problem which arose from here is the choice of the value of the clusterization parameter representing the cutoff limit. This range of clusterization parameter will be different in different physical situations depending upon the excitation energy and density at freeze-out time. In a recent study, the longer interaction range in the quantum molecular dynamical model is reported to give much fewer fragments than detected in experiments [1, 7, 39]. Hence the range for the clusterization can play a important role in the formation of fragments. The most acceptable range of the clusterization parameter R_{Clus} is between 2 and 5 fm [1, 5, 7, 26, 38, 39]. In several earlier publications, the author have claimed that the role of different clusterization parameters is marginal whereas some others claim that the effect of doubling the range of the clusterization is less than 25%[26, 38, 39]. We have also display the results with $R_{clus} = 4$ fm and a narrower one 2.5 fm. We see that when we choose a narrow cut off distance, lesser number of fragments are formed. This is due to the reason that the particles which were in the range from 2.5 to 4 fm initial, were fragments, are now the free particles. In the bottom panel, we display the role of different equations of state by simulating the reactions with hard and soft equations of state. We see that different equations of state do not alter the results.

4.4.6 Nucleon-nucleon cross sections and model ingredients: A comparative study

To put the nucleon-nucleon cross sections and model ingredients on the same platform, we have displayed the variation due to cross sections and model ingredients in one figure. Two figures (4.13 and 4.14) are representing the variation of cross sections and model ingredients with different parameters. In Fig.4.13, the maximal number of intermediate mass fragments (N_{IMF}) as well as corresponding impact parameter as a function of the incident energy for the reaction of ${}_{79}Au^{197} + {}_{79}Au^{197}$ is displayed, while, in Fig.4.14, the mass yield is displayed

for the similar reaction at E = 600 MeV/nucleon and at semi-central geometry. Here apart from the different Gaussian widths, clusterization distance and equations of state, we also display the results with different clusterization algorithms (MST and SACA) and momentum dependent interactions.

From the Fig.4.13, we see that different cross sections yield quite similar trend. The maximum value of multiplicity of IMF's is found to decrease with increase in incident energy, while opposite trend of multiplicity is obtained with nucleon-nucleon cross sections. This type of findings were also obtained from the Fig.4.8. The lower panel of the figure is representing the impact parameter corresponding to the value at which maximum production of IMF's takes place. This impact parameter value is found to shift from semi-central to semi-peripheral values as the incident energy is increased, but not to extreme peripheral. This is due to the reason that as one moves from semi-central to semi-peripheral geometries, the spectator matter goes on increasing and needs more and more energy to even break up into IMF's.

Lets study the other aspect of this figure. The absolute value of multiplicity varies with nucleon-nucleon cross sections as well as with other model ingredients. For example, we see that at 600 MeV/nucleon, the SACA method with 20 mb yields results close to the MST method with 55 mb. In another example, results of MST method with 55 mb, in the presence of momentum dependent interactions are same with reduced clusterization distance $(R_{Clus}) = 2.5\ fm$ in the presence of static equation of state. A broader Gaussian scales down the number and so is the case with reduced cut off distance. In order to further strengthen our point, in Fig.4.14, the mass distribution is displayed for different nucleon -nucleon cross sections, different clusterization methods, different Gaussian width, different clusterization distance as well as different equations of state. The results are in supportive nature with the Fig. 4.14 that cross sections as well as different model ingredients have the same effect on the fragmentation pattern. For example : mass distribution is decreasing with increase in the nucleon cross section, which is due to the break up of the initial correlations among the nucleons with cross section. Similar decrease in mass distribution is observed when one moves from MST to SACA, L^{normal} to L^{broad}, $R_{Clus} = 4$ to 2.5 fm as well as Soft equation of state to SMD equation of state at constant cross section σ^{55}. From

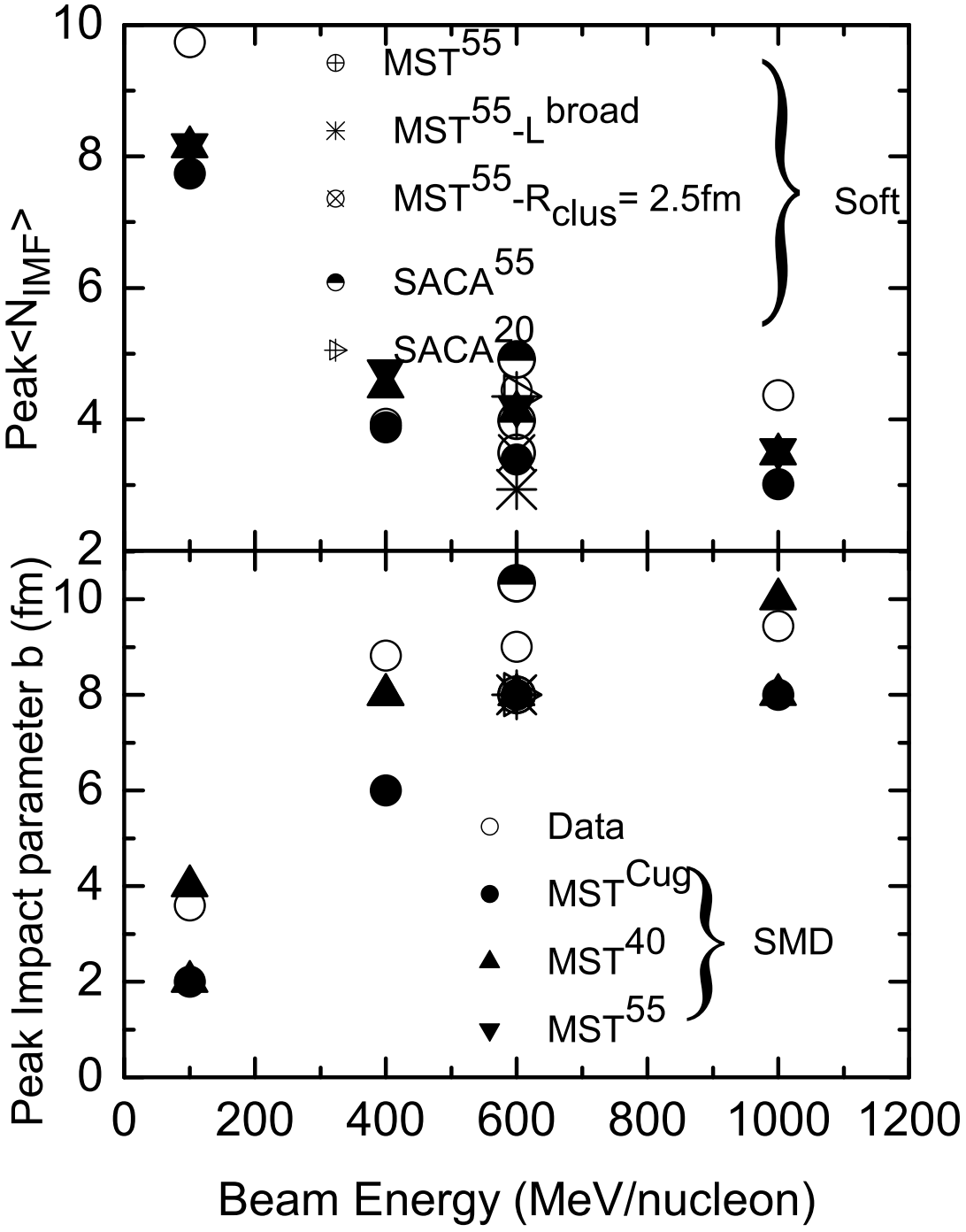

Figure 4.13: The Peak value of IMFs and corresponding impact parameter as a function of beam energy is compared with ALADIN data in the upper and bottom panels, respectively.

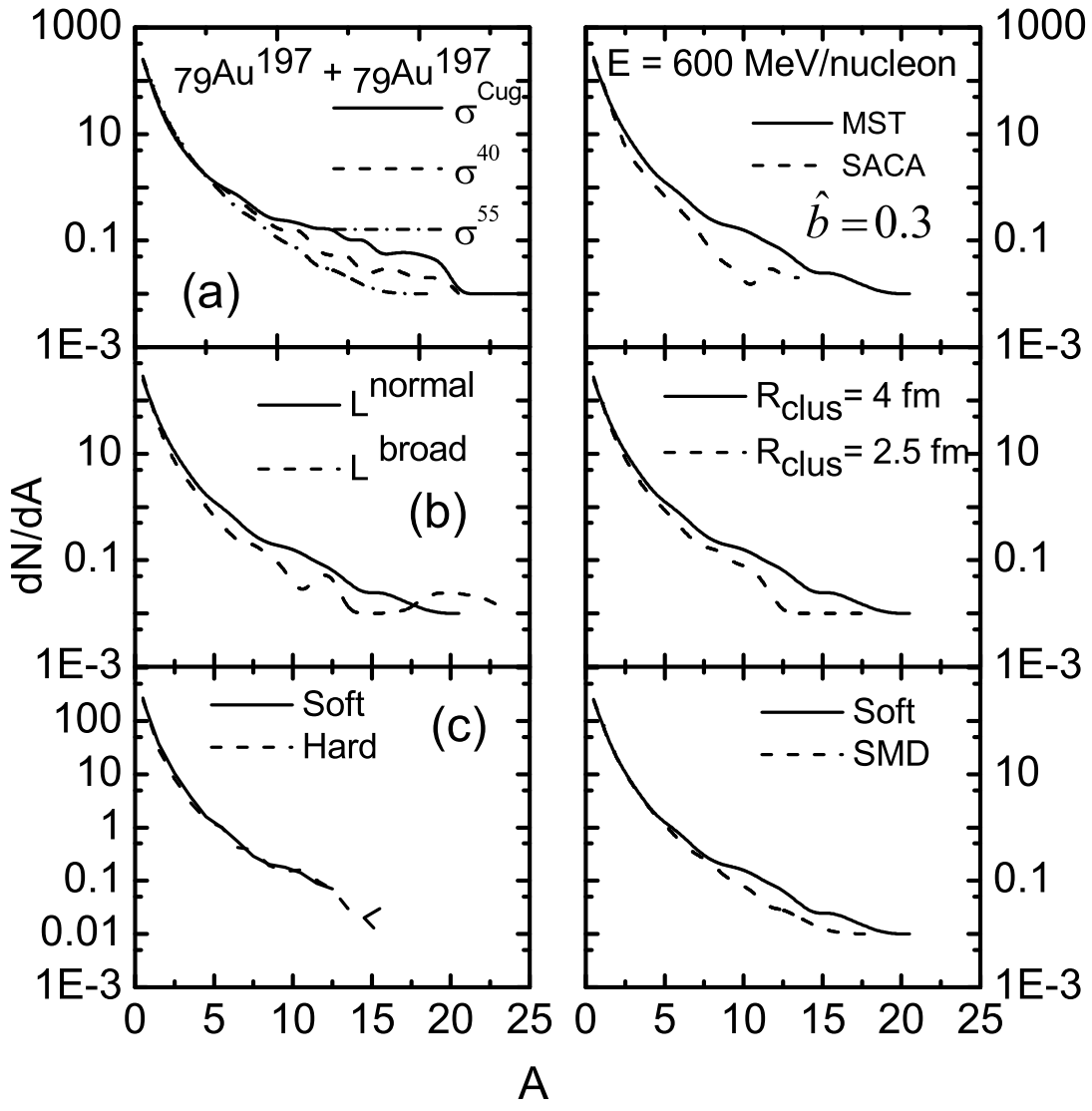

Figure 4.14: Mass distribution dN/dA with mass number A for the ${}_{79}Au^{197}$ + ${}_{79}Au^{197}$ at semi-central geometry. The top left panel is with SMD equation of state, while rest of the panels are in the presence of static equation of state with a constant cross section σ^{55}.

this discussion, it is clear that the effect of larger cross section (i.e. between 20 and 55 mb) is as large as effect of other model ingredients. Even a change of the clusterization algorithm affect the outcome sizeably. From this analysis, one conclude that it may not be possible to pin down the magnitude of cross section from multifragmentation since other technical parameters such as width of the Gaussian, clusterization range or even the change of the clusterization algorithm alters the results in similar fashion when semi-classical model such as quantum molecular dynamics is used.

4.5 Summary

We have performed the comparative study of nucleon-nucleon cross sections and technical parameters, known as model ingredients, in multifragmentation by studying the symmetric and asymmetric reactions [17] in the presence of momentum dependent interactions in Quantum Molecular Dynamical model. Our analysis, at the first instance, clearly indicates the importance of momentum dependent interactions and large cross sections for free nucleons and LCP's at semi-central as well as semi-peripheral geometries, while for MMF's and IMF's only at semi-peripheral geometries. Moreover, once the momentum dependent interactions are implemented, they tries to reduce the effect of nucleon-nucleon cross sections at higher energies as compared to static equation of state, where the effect of nucleon-nucleon cross section is large. In a comparative study with experimental findings of ALADIN and NSCL collaborations, better agreement is again obtained in the presence of momentum dependent interactions and large cross section for symmetric as well as asymmetric systems.

Interestingly when this study is extended with technical parameters, known as model ingredients, (like Gaussian width, clusterization algorithm, clusterization distance as well as equations of state) at constant nucleon-nucleon cross section, the results are found to vary in the same fashion as were with different nucleon-nucleon cross sections. We found that the effect of different cross sections is of the order of the one obtained from the model ingredients. All model ingredients affect the fragmentation pattern in a similar fashion. Lastly, one can conclude that it may not possible to pin down the magnitude of cross section from the multifragmentation until and unless the model ingredients are handled very carefully.

Bibliography

[1] R. K. Puri, C. Hartnack, and J. Aichelin, Phys. Rev. C **54**, R28 (1996); P. B. Gassiaux *et al.,* Nucl. Phys. A **619**, 379 (1997); R. K. Puri and J. Aichelin, J. Comp. Phys. **162**, 245 (2000); Y. K. Vermani, J. K. Dhawan, S. Goyal, R. K. Puri, and J. Aichelin, J. Phys. G: Nucl. and Part. **37**, 015105 (2010); Y. K. Vermani and R. K. Puri, Eur. Phys. Lett. **85**, 62001 (2009).

[2] J. P. Bondorf *et al.,* Phys. Rep. **257**, 133 (1995); J. P. Bondorf *et al.,*, Nucl. Phys. A **443**, 321 (1985); Nucl. Phys. A **444**, 460 (1985); A. S. Botvina *et al.,* Nucl. Phys. A **584**, 737 (1995); A. S. Botvina and I. N. Mishustin, Eur. Phys. J. A **30**, 121 (2006); A. S. Botvina *et al.,* Phys. Lett. B **668**, 414 (2008); G. Casini *et al.,* Nucl-ex/0905.4703 (2005); S. Pal, S. K. Samaddar, and J. N. De, Nucl. Phys. A **608**, 49 (1996), D. K. Srivastava *et al.,* Nucl-th/0506075 (2005); L. Satpathy, M. Mishra, A. Das, M. Satpathy, Phys. Lett. B **237**, 181 (1990); C. B. Das, A. Das, L. Satpathy, M. Satpathy, Phys. Rev. C **53**, 1833 (1996).

[3] J. B. Elliott *et al.,* Phys. Rev. C **49**, 3185 (1994); J. A. Hauger *et al.,* Phys. Rev. C **62**, 024616 (2000); P. F. Mastinu *et al.,* Phys. Rev. Lett. **76**, 2646 (1996); A. Bonasera *et al.,* Rivista del Nuovo Cimento **23**, 1 (2000); M. D'Agostino *et al.,* Phys. Lett. B **473**, 219 (2000).

[4] I. N. Mishustin, Nucl. Phys. A **630**, 111 (1998); M. Mishra, M. Satpathy, and L. Satpathy, J. Phys. G: Nucl and Part. **14**, 1115 (1988).

[5] C. Hartnack *et al.,* Eur. Phys. J. A **1**, 151 (1998); D. T. Khoa *et al.,* Nucl Phys. A **548**, 102 (1992); E. Lehmann, R. K. Puri, A. Faessler, G. Batko, and S. W. Huang, Phys. Rev. C **51**, 2113 (1995); R. K. Puri *et al.,* Nucl. Phys. A **575**, 733 (1994); C.

Fuchs *et al.,* J. Phys. G: Nucl and Part. **22**, 131 (1996); E. Lehmann *et al.,* Prog. Part. Nucl. Phys. **30**, 219 (1993); E. Lehmann *et al.,* Z. Phys. A **355**, 55 (1996).

[6] S. Pal, S. K. Samaddar, J. N. de, and B. Djerroud, Phys. Rev. C **57**, 3246 (1998); B. K. Srivastava *et al.,* (EOS collaboration) Phys. Rev. C **65**, 054617 (2002); A. Das, M. Mishra, M. Satpathy, and L. Satpathy, J. Phys. G: Nucl. and Part. **19**, 319 (1993).

[7] J. Singh, S. Kumar, and R. K. Puri, Phys. Rev. C **62**, 044617 (2000); S. Kumar and R. K. Puri, *ibid.* **58**, 1618 (1998); Y. K. Vermani, S. Goyal, and R. K. Puri, *ibid.* **79**, 064613 (2009).

[8] P. M. Milazzo *et al.,* Phys. Rev. C **66**, 021601(R) (2002).

[9] C. A. Ogilvie *et al.,* Phys. Rev. Lett. **67**, 1214 (1991); N. T. B. Stone *et al., ibid.* **78**, 2084 (1997); A. H. Raduta and A. R. Raduta Phys. Rev. C **65**, 054610 (2002).

[10] R. T. de Souza *et al.,* Phys. Lett. B **268**, 6 (1991).

[11] M. B. Tsang *et al.,* Phys. Rev. Lett. **71**, 1502 (1993); M. B. Tsang *et al., ibid.* **102**, 122701 (2009).

[12] G. F. Peaslee *et al.,* Phys. Rev. C **49**, R2271 (1994).

[13] Q. Li, Z. Li, S. Soff, M. Bleicher, and H. Stöcker, J. Phys. G: Nucl. Part. Phys. **32**, 151 (2006).

[14] A. D. Sood and R. K. Puri, Phys. Rev. C **70**, 034611 (2004); S. Kumar, M. K. Sharma, and R. K. Puri, *ibid.* **58**, 3494 (1998), A. D. Sood, R. K. Puri, and J. Aichelin, Phys. Lett. B **594**, 260 (2004); P. Danielewicz *et al.,* Science **298**, 1592 (2002).

[15] R. K. Gupta, S. Singh, R. K. Puri, and W. Scheid, Phys. Rev. C **47**, 561 (1993); R. K. Gupta *et al.,* J. Phys. G: Nucl and Part. **18**, 1533 (1992); S. S. Malik, S. Singh, R. K. Puri, S. Kumar, and R. K. Gupta, Parmana J. Physics **32**, 419 (1989); R. K. Puri, S. S. Malik, and R. K. Gupta, Eur. Phys. Lett. **9**, 767 (1989); R. K. Puri and R. K. Gupta, J. Phys. G: Nucl. and Part. **18**, 903 (1992); R. K. Puri, M. K. Sharma,

and R. K. Gupta, Eur. Phys. J. A **3**, 277 (1998); R. Arora, R. K. Puri and R. K. Gupta, Eur. Phys. J. A **8**, 103 (2000); R. K. Puri and R. K. Gupta, Phys. Rev. C **45**, 1837 (1992); R. K. Puri, P. Chattopadhyay, and R. K. Gupta, *ibid.***43**, 315 (1991); R. K. Puri *et al.,* Eur. Phys. J. A **23**, 429 (2005).

[16] G. Q. Li and R. Machleidt, Phys. Rev. C **48**, 1702 (1993); T. Alm, G. Ropke, W. Bauer, F. Daffin, and M. Schmidt, Nucl. Phys. A **587**, 815 (1995); Y. M. Zhang, C. M. Ko, B. A. Li, and B. Zhang, Phys. Rev. Lett. **83**, 2534 (1999); Q. Li, Z. Li, and G. Mao, Phys. Rev. C **62**, 014606 (2000); Q. Li, Z. Li, and E. Zhao, *ibid.* **69**, 017601 (2004); T. Gaitanos, C. Fuchs, and H. H. Wolter, Prog. Part. Nucl. Phys. **53**, 45 (2004); Y. Zhang, Z. Li, and P. Danielewicz, Phys. Rev. C **75**, 034615 (2007).

[17] S. Kumar and S. Kumar , Pramana J. of Phys. 74, 731 (2010); 52^{nd} DAE Symposium on Nuclear Physics, Sambalpur University, Orissa **52**, 491 (2007).

[18] G. F. Bertsch and S. D. Gupta, Phys. Rep. **160**, 189 (1988).

[19] J. Cugnon, T. Mizutani, and J. Vandermeulen, Nucl. Phys. A **352**, 505 (1981).

[20] A. Faessler, W. H. Dickhoff and M. Trefz, Nucl. Phys. **A 428**, 271c (1981); M. trefz, A. Faessler and W. H. Dickhoff, Nucl. Phys. **A 443**, 499 (1985).

[21] S. W. Huang, *Ph.D thesis*, Tubingen (Germany) (1994).

[22] S. K. Charagi and S. K. Gupta, Phys. Rev. C **41**, 1610 (1990). G. Alkahzov *et al.,* Nucl. Phys. A **280**, 365 (1977).

[23] T. Izumoto, S. Krewald and A. Faessler, Nucl. Phys. **A 341**, 319 (1980); **357**, 471 (1981).

[24] N. Ohtsuka, R. Linden, A. Faessler and F. B. Malik, Nucl. Phys. **A 465**, 550 (1987).

[25] A. Bohnet, N. Ohtsuka, J. Aichelin, R. Linder, and A. Faessler, Nucl. Phys. **A 494** , 349 (1989); R. K. Puri, N. Ohtsuka, E. Lehmann, A. Faessler, M.A. Matin, D.T. Khoa, G. Batko, and S.W. Huang, Nucl. Phys. **A 575** , 733 (1994).

[26] S. Kumar and R. K. Puri, Phys. Rev. **C 57**, 320 (1998); J. Singh and R. K. Puri, *ibid.* **62**, 054602 (2000).

[27] G. D. Westfall *et al.,* Phys. Rev. Lett. **71**, 1986 (1993); D. Klakow, G. Welke, W. Bauer, Phys. Rev. C **48**, 1982 (1993); M. J. Huang *et al.,* Phys. Rev. Lett. **77**, 3739 (1996).

[28] J. Hubele *et al.,* Phys. Rev. C **46**, R1577 (1992); Z. Phys. A **340**, 263 (1991).

[29] J. B. Garcia and C. Cerruti, Nucl. Phys. A **578**, 597 (1994).

[30] C. Dorso and J. Randrup, Phys. Lett. B **301**, 328 (1993).

[31] P. J. M. Laarhoven and E. H. L. Aarts, Simulated Annealing: theory and applications (Reidel, Dordrecht, 1987).

[32] N. Metropolis, A. W. Rosenblut, M. N. Rosenblut, A. H. Teller, and E. Teller, J. Chem. Phys. **21**, 1087 (1953).

[33] A. Schüttauf *et al.,* Nucl. Phys. A **607**, 457 (1996).

[34] W. J. Llope *et al.,* Phys. Rev. C **51**, 1325 (1995).

[35] W. Reisdorf *et al.,* Phys. Rev. Lett. 92, 232301 (2004); S. Kumar, S. Kumar, and R. K. Puri, Phys. Rev. C **81**, 014601 (2010).

[36] Y. Zhang and Z. Li, Phys. Rev. C **74**, 014602 (2006); S. Kumar, S. Kumar, and R. K. Puri, Phys. Rev. C **81**, 014611 (2010).

[37] H. Feldmeier, Nucl. Phys. A **515**, 147 (1990); J. Konopka, Ph. D thesis, University of Frankfurt, Frankfurt, Germany (1995).

[38] J. Aichelin, Phys. Rep. **202**, 233 (1991); G. Peilert *et al.,* Phys. rev. C **39**, 1402 (1989); S. R. Souza *et al.,* Nucl. Phys. A **571**, 159 (1994).

[39] R. Nebauer *et al.,* Nucl. Phys. A **658**, 67 (1999).

Chapter 5

Disappearance of elliptical flow in intermediate energy heavy-ion collisions and isospin effects

5.1 Introduction

In the preceding chapters, the multifragmentation is studied in detail. It is the need of the time to study the other aspects like collective flow and nuclear stopping parameters in intermediate energy heavy-ion collisions. In the following chapter, we will deal with the elliptical flow, while, the nuclear stopping is studied in the chapter 6.

The information about the nature of equation of state is still one of the burning topic of present day nuclear physics research in general and heavy-ion collisions in particular. A quite good progress has been made in the recent years in determining the nuclear equation of state from heavy-ion reactions [1, 2]. Among different observables, collective flow enjoys a special status. This is due to its sensitive response to the model ingredients that define equation of state. A lot of theoretical and experimental efforts have been made in studying the collective flow in heavy-ion collisions [3-9]. This collective motion of the particles in heavy-ion collision can be studied via directed and elliptical flows. The directed flow, which measures the collective motion of the particles in the reaction plane, has been studied extensively at BEVALAC, SIS and AGS energies [10]. This flow is reported to diminish at higher incident energies due to the large beam rapidity. Therefore, elliptical flow [11] is much more suited at these incident energies. The elliptical flow describes the eccentricity of an ellipse like distribution. Quantitatively, it is the difference between the major and minor axis. The orientation of the major axis is confined to azimuthal angle ϕ or $\phi+\frac{\pi}{2}$ for ellipse

like distribution. The major axis lies within the reaction plane for ϕ; while $\phi+\frac{\pi}{2}$ indicates that the orientation of the ellipse is perpendicular to the reaction plane, which is the case for squeeze out flow and may be expected at mid rapidity [12]. Therefore, the elliptical flow is defined by the second order Fourier coefficient from the azimuthal distribution of detected particles at mid rapidity. Mathematically,

$$\frac{dN}{d\phi} = p_0(1 + 2v_1 Cos\phi + 2v_2 Cos2\phi). \tag{5.1}$$

Here ϕ is the azimuthal angle between the transverse momentum of the particle and reaction plane. The positive value of the elliptical flow $< Cos2\phi >$ reflects an in-plane emission, whereas, out-of plane emission is reflected by its negative value. The reason for the anisotropic flow is orthogonal asymmetry in the configuration space (non-central collisions) and re-scattering. In the case of elliptical flow, the initial " ellipticity" of the overlap zone is usually characterized by a quantity $\epsilon = \frac{(<y^2-x^2>)}{(<y^2+x^2>)}$, assuming the reaction plane being xz. As the system expands, spatial anisotropy decreases. From the above discussion, it is clear that the second order flow (elliptical flow) is better candidate for determining the nuclear equation of state compared to first order sideward flow (directed flow).

In recent years, several experimental groups have measured the elliptical flow. The FOPI, INDRA and PLASTIC BALL collaborations [4, 5] are actively involved in measuring the excitation function of elliptical flow from Fermi energies to relativistic energies. In most of these studies, ${}_{79}Au^{197}$ + ${}_{79}Au^{197}$ reaction has been taken [4, 5]. Interestingly, a change in the elliptical flow was reported from positive to negative values around 100 MeV/nucleon. Both the mean field and two-body binary collisions play an important role in this energy domain. The mean field is supposed to play a dominant role at low incident energies. The binary collisions starts dominating the physics gradually. A detailed study of the excitation function of elliptical flow in entire energy region can provide a useful information about the nucleon-nucleon interactions related to the nuclear equation of state.

As discussed above, lots of attempts have already been made in the literature to explore different aspects of directed sideward flow. In this chapter, we attempt to study the different aspects of elliptical flow v_2.

For the present study, Isospin-dependent Quantum Molecular Dynamics (IQMD) model [13] is used to generate the phase space of nucleons and clusterization is done by minimum span-

ning tree with spacial (MST) and momentum cut(MSTM).

5.2 Elliptical flow

5.2.1 Origin of the elliptical flow

Elliptical flow refers to the anisotropy of the ϕ distribution at mid rapidity and its value indicates whether the particle emission is in-plane or out-of-plane. The pictorial view of the in-plane emission and out-of-plane emission is shown in Figs. 5.1 and 5.2. In the, Fig. 5.1 is collectively representing the in-plane as well as out-of-plane directions, while Fig. 5.2 is indicating separately the both of the emission (in-plane [right side] and out-of-plane [left side]). Azimuthal distributions which are peaked at 0^o and 180^o exhibit predominantly in-plane emission, while ϕ distributions peaked at $\pm 90^o$ signify out-of-plane emission. The term elliptical, initially, was known with the names like "Squeeze-out", "rotational motion", or "anisotropic flow", because the shapes of ϕ distributions at mid rapidity resemble ellipse with a major axis along the x-axis (in-plane emission) or y-axis (out-of-plane emission). The term "elliptical flow" was introduced in 1997 by H. Sorge[11], a theoretician at SUNY-Stony Brook.

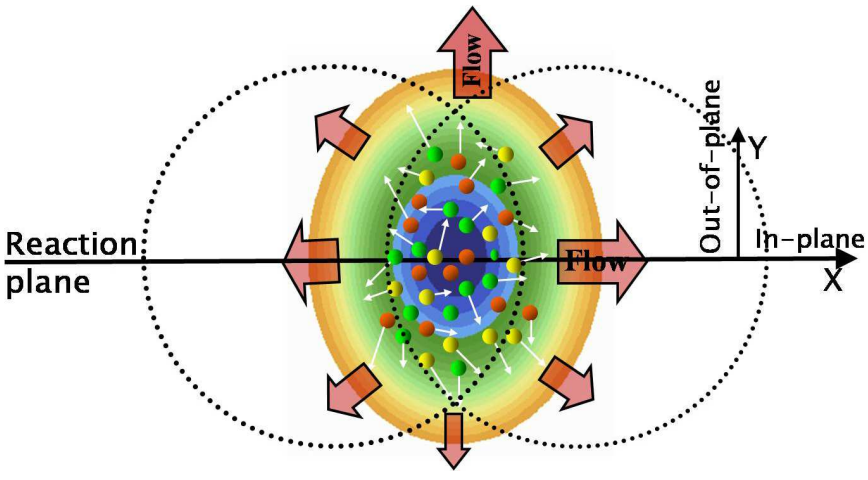

Figure 5.1: Pictorial view of the possible movement of the nucleons in the compressed zone. The directions of in-plane and out-of-plane emission is shown in the figure.

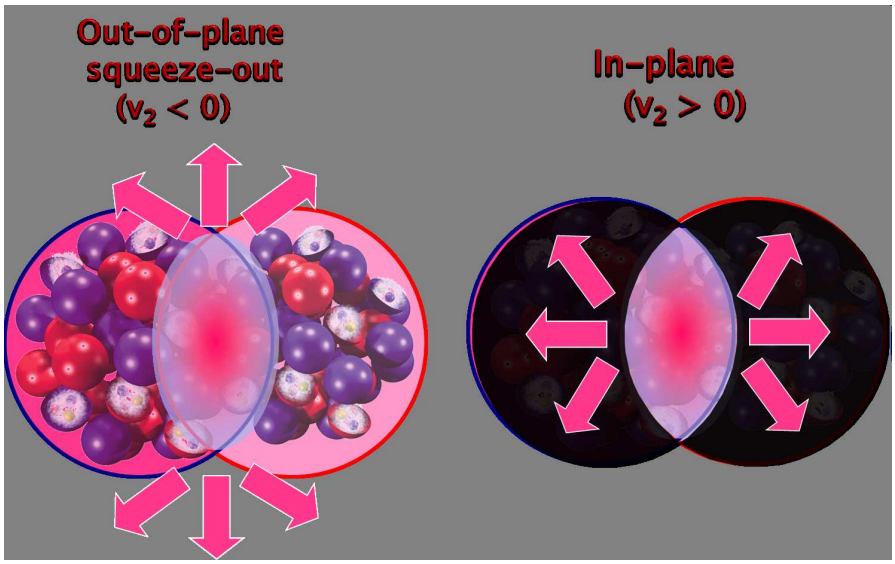

Figure 5.2: In-plane (right side) and out-of-plane (left side) emission of nucleons in the reaction plane and perpendicular to reaction-plane, respectively, is represented. This concept will give rise to transition energy at certain incident energy.

Out-of-plane elliptical flow, which can occur in non-central collisions, is an interesting phenomena which has been observed at incident energies ranging from 100 MeV/nucleon to $\approx$ 4 GeV/nucleon. The two factors are responsible for out-of-plane emission at mid rapidity:

1 The pressure build up in the compression stage compared to the energy density, and

2 The passage time for removal of the projectile- and target-like spectator of the Fireball model. If the participant zone emit particles at an early stage of the collision, the spectator pieces may still be close enough to cause pressure gradients in the out-of-plane direction.

Theoretically, the elliptical flow concept was originated in 1982 in term of the mid rapidity emission perpendicular to the "reaction plane". This concept was given by Stocker[14] by calculating the angular distributions of the protons emitted from near central collisions show out-of-plane jet structures at $\theta = 90^o$, $\phi = \pm 90^o$ in a Fluid dynamical model. The cause for this out-of-plane emission was the hindering of the compressed matter perpendicularly emitted in reaction plane by the spectator matter. On the other hand, a kinetic energy tensor was also employed first time to analyze the flow patterns[10]. For this, a 3×3 tensor is constructed from the emitted particles momentum components, weighted inversely by the mass of the fragments. The eigenvectors of the tensor represent the principal axes of the

flow ellipsoid. Its shape and orientation relative to the reaction plane and the beam axis can be used to measure in-plane and out-of-plane emission.

Experimentally, the out-of-plane emission, termed as squeeze-out, was first observed in 1989 by the two competing groups, namely, *Diogene Collaboration* at Sature Synchrotron in Saclay [15] and the *Plastic Ball/Wall group* at Bevalac in Berkeley [16]. They also characterized the emission pattern in term of the kinetic energy flow ellipsoid, which could account for directed as well as elliptical flow.

In fact, directed and elliptical flow can be treated as the first and second order harmonics of a Fourier expansion of ϕ:

$$F(\phi) \; = \; c_0 \; + \; c_1 cos(\phi) \; + \; c_2 cos(2\phi), \tag{5.2}$$

where coefficients c_1 and c_2 corresponds to the strength of the directed and elliptical flow contributions, respectively. The Fourier expansion is discussed in the detail in the following section.

5.2.2 Fourier expansion's second harmonic as elliptical flow

The elliptical flow is expected to be symmetric about the reaction plane as well as the perpendicular plane, fitting a ϕ distribution with a cos(2ϕ) term could characterize the strength of the elliptical flow. To account for both the cos(ϕ) nature of directed flow and the cos(2ϕ) nature of the elliptical flow in the azimuthal distributions, a Fourier expansion of the form:

$$\frac{dN}{d\phi} \; = \; a_0^{exp} \left[1 + a_1^{exp} cos(\phi) + a_2^{exp} cos(2\phi)\right], \tag{5.3}$$

is used, where dN/dϕ represents the azimuthal distribution of the emitted fragments at mid rapidity. In the eqn. 5.3, a_0^{exp} is a normalization factor, a_1^{exp} is related to the in-plane directed flow component and a_2^{exp} to the elliptical flow component. The superscript "exp" on the coefficients is to keep in mind that the coefficients extracted from fitting the ϕ distribution and are not corrected for reaction plane dispersion. This correction for the directed and elliptical flow depend on the azimuthal angle between the reaction plane and the particle whose flow is being measured, the data must be corrected for the effects of reaction plane

dispersion. The form of the correction is

$$Flow \;=\; \frac{Observed\ Flow}{\langle cos(\phi_m - \phi_r)\rangle}, \tag{5.4}$$

where ϕ_m and ϕ_r are the measured and true reaction plane angles, respectively, and the brackets signify the mean over all events. The mean cosine values are less than one and thus this correction always increases the measured flow. The correction term $\langle cos(\phi_m - \phi_r)\rangle$ in its current form contains the unknown ϕ_r. Therefore, this can be obtained by an indirect method. One method is to recognize the angle, when flow is present, a correlation exists between the azimuthal angles of the particles from a particular collisions. This method relies on the fact that the reaction plane resolution is directly related to the flow.

On the basis of this correction formula, the correction is made for a_2 by dividing the experimental coefficient by the correction factor:

$$a_2 \;=\; \frac{a_2^{exp}}{\langle cos(\Delta\phi_{rp})}. \tag{5.5}$$

Therefore,

$$\frac{dN}{d\phi} \;=\; a_0\left[1 + a_1 cos(\phi) + a_2 cos(2\phi)\right], \tag{5.6}$$

after the dispersion corrections are made. As the dispersion correction to a_2^{exp} is made after fitting the Fourier expansion to the ϕ distribution, the other coefficients can be ignored in the rest of the analysis.

The elliptical flow is quantified in term of the a_2 coefficient. The ratio of out-of-plane to in-plane emission, called the number squeeze-out ratio by Gutbroad *et al.*[17], is defined by the particles emitted perpendicular to the reaction plane divided by the number of the particles emitted in the reaction plane at mid rapidity and is given by

$$R_N \;=\; \frac{N(90^o) + N(-90^o)}{N(0^o) + N(180^o)}, \tag{5.7}$$

where N(ϕ) represents the summed number of particles in a 90^o wedge centered at ϕ. More explicitly, it can be written as:

$$R_N \;=\; \frac{\int_{45^o}^{135^o} \frac{dN}{d\phi} d\phi \;+\; \int_{-135^o}^{-45^o} \frac{dN}{d\phi} d\phi}{\int_{-45^o}^{45^o} \frac{dN}{d\phi} d\phi \;+\; \int_{135^o}^{225^o} \frac{dN}{d\phi} d\phi} \tag{5.8}$$

According to this definition, $R_N \;<\; 1$ and $>\; 1$ are related to a preferential emission of the matter in the reaction plane and out-of-plane, respectively, while $R_N \;=\; 1$ corresponds to

a perfect azimuthally isotropic distribution.

Interestingly, R_N can be expressed in term of a_2 coefficient from the Fourier expansion taking into account that directed flow coefficient a_1 should be zero at mid rapidity ($y_{c.m.} = 0$). Therefore, inserting eqn.5.6 into 5.8:

$$R_N = \left(\frac{[1 + a_2 cos(180^o)] + [1 + a_2 cos(-180^o)]}{[1 + a_2 cos(0^o)] + [1 + a_2 cos(360^o)]} \right)_{y_{c.m.}=0}, \tag{5.9}$$

which further reduces to

$$R_N = \frac{1 - a_2}{1 + a_2} \tag{5.10}$$

Further for the elliptical flow, in term of particle momentum, it is determined from the average difference between the square of the x and y components of particle transverse momentum provided the beam direction along z axis and the reaction plane on the x-z plane as usual:

$$v_2 = \langle \frac{p_x^2 - p_y^2}{p_x^2 + p_y^2} \rangle, \tag{5.11}$$

where p_x is in the reaction plane, while p_y is perpendicular to the reaction plane. This v_2 is a measure of the aspect ratio of the flow ellipsoid. A positive value of the elliptical flow describes the in-plane enhancement of the particle emission i.e. a rotational behavior. On the other hand, a negative value of v_2 shows the squeeze-out effects perpendicular to reaction plane.

v_2 can be related to the Fourier coefficient a_2 by recognizing that

$$\langle \frac{p_x^2 - p_y^2}{p_x^2 + p_y^2} \rangle = \langle cos(2\phi) \rangle \tag{5.12}$$

and since $\langle cos(2\phi) \rangle$ corresponds to $a_2/2$ in the Fourier expansion of eqn. 5.6,

$$v_2 = \frac{a_2}{2}. \tag{5.13}$$

On the basis of this, R_N can be expressed in term of v_2 as:

$$R_N = \frac{1 - 2v_2}{1 + 2v_2} \tag{5.14}$$

Eqns.5.10, 5.13 and 5.14 give the expressions for relating the Fourier coefficient a_2 to other methods for measuring anisotropy. In the present analysis, v_2 is the chosen elliptical flow representation.

5.2.3 Disappearance of elliptical flow

A promising and useful feature of the elliptical flow is the existence of transitions between two forms of the observable. These transitions amount to measuring "zeros" in the flow excitation functions, or the energy dependence of the flow variables.

Fig. 5.3 is a schematic representation of the elliptical flow excitation functions for nucleons over a wide range of beam energies. Dashed area of the curve at higher energies represent studies that are currently underway, and the dashed area in the NSCL energy regime represents the energy range studied in this chapter. The following transitions are believed to be present in the excitation functions, indicated by stars($\star$):

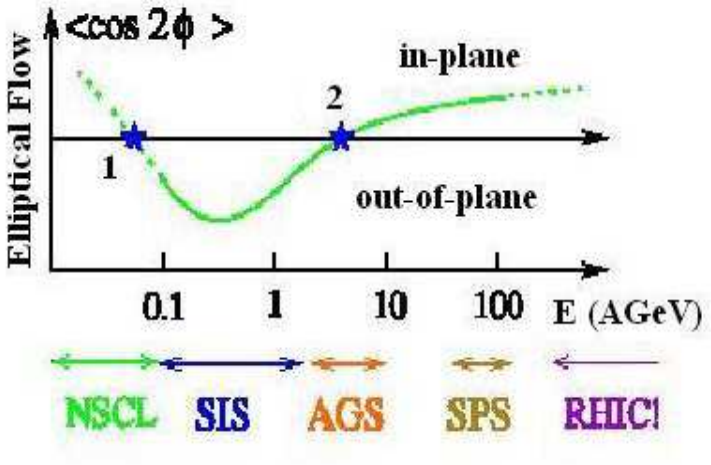

Figure 5.3: Schematic behavior of the elliptical flow as a function of the beam energy. The figure is taken from the Ref[18].

1. transition from in-plane to out-of-plane elliptical flow in the NSCL and near SIS energy region;

2. transition from out-of-plane to in-plane elliptical flow at AGS beam energies.

The first one is the object of study in this thesis and will be explained in detail in results

and discussion section.

Transition **2** in the Fig. 5.3 has been studied extensively in the past couple of years by

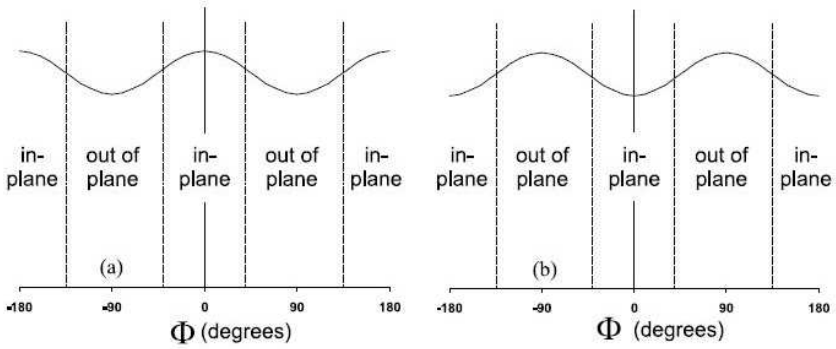

Figure 5.4: Schematic representation of ϕ distributions for (a) predominantly in-plane and (b) predominantly out-of-plane emission. The figure is taken from the Ref[18].

experimental groups at the AGS energy. The most interesting results are from the E895 collaborations, which measured the proton elliptical flow in ${}_{79}Au^{197}$ + ${}_{79}Au^{197}$ collisions for beam energies of 2-8 GeV/nucleon [19]. They observed the elliptical flow excitation exhibits a cross-over at $\approx$ 4 GeV/nucleon.

Transition **1** in Fig. 5.3 corresponds to the change in the direction of preferred fragment emission from the compressed participant region. The energy in this energy region at which elliptical flow reduces to zero is known as transition energy. At energies below the transition energy, emission is primarily in the reaction plane (ϕ distribution is peaked at $0^o, 180^o$). Above the transition energy, a maximum emission in the direction perpendicular to the reaction plane on both sides (known as squeeze-out) appears because of the compressed matter in the interaction region can escape preferentially in directions unhindered by the presence of the projectile and target spectators. In other words, one can say that the azimuthal emission pattern is primarily out-of-plane, signified by peaks at $\pm 90^o$. Fig. 5.4 is a schematic representation of the ϕ distributions for both elliptical flow regions.

The transition energy for ${}_{79}Au^{197}$ + ${}_{79}Au^{197}$ is one of the topics in chapter 5[20]. The mass dependence of transition energy is also measured for light charged particles. This energy is further compared with the findings of INDRA, FOPI and PLASTIC BALL collaborations

for ${}_{79}Au^{197}$ + ${}_{79}Au^{197}$ for protons and $Z \leq 2$ particles.

5.3 Results and discussion

We, here, perform a complete systematic study for the mass range between 80 and 394 units and over full range of the impact parameters. We here simulate the reactions of ${}_{20}Ca^{40} + {}_{20}Ca^{40}$, ${}_{28}Ni^{58} + {}_{28}Ni^{58}$, ${}_{41}Nb^{93} + {}_{41}Nb^{93}$, ${}_{54}Xe^{131} + {}_{54}Xe^{131}$ and ${}_{79}Au^{197} + {}_{79}Au^{197}$ at incident energies between 50 and 1000 MeV/nucleon. In addition, the reactions of ${}_{40}Zr^{96}$ + ${}_{40}Zr^{96}$ and ${}_{44}Ru^{96}$ + ${}_{44}Ru^{96}$ are also simulated to check the isospin effects explicitly. The choice of equation of state (or compressibility) is still a controversial one. Many studies advocate softer matter, whereas many more believe the matter to be harder in nature[21]. Moreover, in Ref.[22], it is shown that elliptical flow is unaffected by the choice of equation of state. For the present analysis, a hard (H) and hard momentum dependent (HMD) equation of state has been employed along with the standard energy-dependent cross section. As noted in Ref.[23], the relativistic effects do not play role at these incident energies and the intensity of sub-threshold particle production is very small. The phase space generated by the IQMD model has been analyzed using the minimum spanning tree (MST) [2, 24] method. The MST method binds two nucleons in a fragment if the distance between them is less than 4 fm. In recent years, several improvements have also been suggested [25]. One of the improvements is to also imply momentum cut of the order of Fermi momentum. This method is dubbed as MSTM method. The entire calculations are performed at $t = 200$ fm/c. This time is chosen by keeping in view the saturation of the collective flow [8].

The definition of elliptical flow used in the present analysis is the one displayed in eqn.5.11. A positive value of the elliptical flow describes the eccentricity of an ellipse like distribution and indicates in-plane enhancement of the particle emission i.e. a rotational behavior. On the other hand, a negative value of v_2 shows the squeeze out effects perpendicular to the reaction plane. Obviously, zero value corresponds to an isotropic distribution in the transverse plane. The v_2 is generally extracted from the mid rapidity region. The particles corresponding to $(Y_{c.m.}/Y_{beam} > 0.1)$ has been defined as projectile like (PL), whereas, $(Y_{c.m.}/Y_{beam} < -0.1)$ constitutes the target like (TL) particles.

5.3.1 Transverse momentum dependence of elliptical flow

In Fig. 5.5, the final state elliptical flow is displayed for the free particles (upper panel), light charged particles (LCP's) [$2 \leq A \leq 4$](middle), and intermediate mass fragments (IMF's) [$5 \leq A \leq A_{tot}/6$](lower panel) as a function of transverse momentum (P_t). A Gaussian type behavior is observed in all cases. Note that this elliptical flow is integrated over entire rapidity range. This Gaussian type behavior is quite similar to the one obtained by Colona and Toro *et al.*[26]. One sees that elliptical flow is positive in the whole range of P_t. The collective rotation is one of the main mechanism to induce the positive elliptical flow [27]. It is also evident from the figure that the peaks of the Gaussian shifts toward lower values of P_t for heavier fragments. This is due to the fact that the free and light charged particles feel the mean field directly, while heavy fragments have weaker sensitivity [28]. Furthermore, the peak values of v_2 for the free nucleons and LCP's at 50 MeV/nucleon is 0.70, 0.411, 0.126 and 0.27, 0.20, 0.059 for the reactions of ${}_{79}Au^{197} + {}_{79}Au^{197}$, ${}_{54}Xe^{131} + {}_{54}Xe^{131}$ and ${}_{20}Ca^{40} + {}_{20}Ca^{40}$, respectively and the corresponding ratios are $\approx$ 5.0, 3.3 and 1. The mass ratio of these reactions is 4.93, 3.27 and 1, whereas, N/Z ratio is 1.49, 1.42 and 1. The v_2 ratios are in closer agreement with the system mass ratios. The results, however, are different at E = 100 MeV/nucleon. Note that the peak values for the free nucleon are 0.48, 0.34, 0.134 and for LCP's numbers, are 0.132, 0.125, 0.058. Their corresponding ratios are $\approx$ 2.92, 2.36 and 1, indicating a clear deviation from the mass ratio.

To further strengthen our interpretation of the estimated v_2 ratios, we display in Fig. 5.6, the reactions of ${}_{40}Zr^{96} + {}_{40}Zr^{96}$ and ${}_{44}Ru^{96} + {}_{44}Ru^{96}$ under the same conditions for LCP's in the presence of Coulomb interactions and symmetry energy. These reactions are analyzed within MST method with momentum cut. Interestingly, the N/Z effect is more visible at E = 100 MeV/nucleon, indicating that this difference is not due to the mass dependence alone, but may be due to Coulomb interactions and isospin effects. To see the effect of Coulomb interactions and symmetry energy (leading to isospin), in Fig. 5.7, we have displayed the effect of Coulomb interactions (top panel), symmetry energy (middle panel) and no Coulomb + no symmetry on the transverse momentum dependence of elliptical flow. The black solid line is for ${}_{44}Ru^{96} + {}_{44}Ru^{96}$, while, shaded region is showing the effect on the

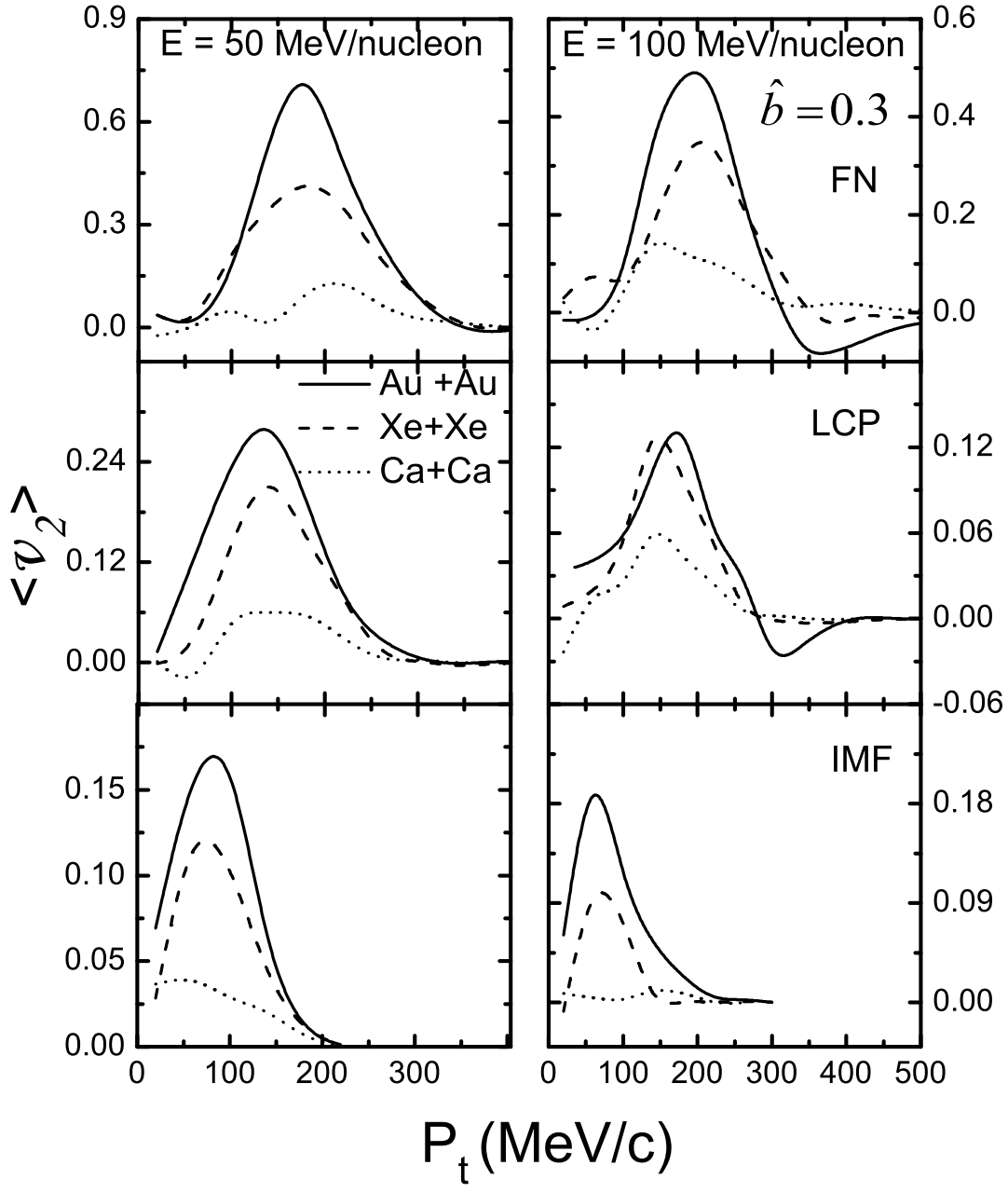

Figure 5.5: The transverse momentum dependence of the elliptical flow, summed over entire rapidity distribution, at $\hat{b} = 0.3$ for different symmetric reactions at 50 (left) and 100 MeV/nucleon (right) respectively. The top, middle and bottom panels are representing the free nucleons (FN), light charged particles (LCP's) and intermediate mass fragments (IMF's), respectively.

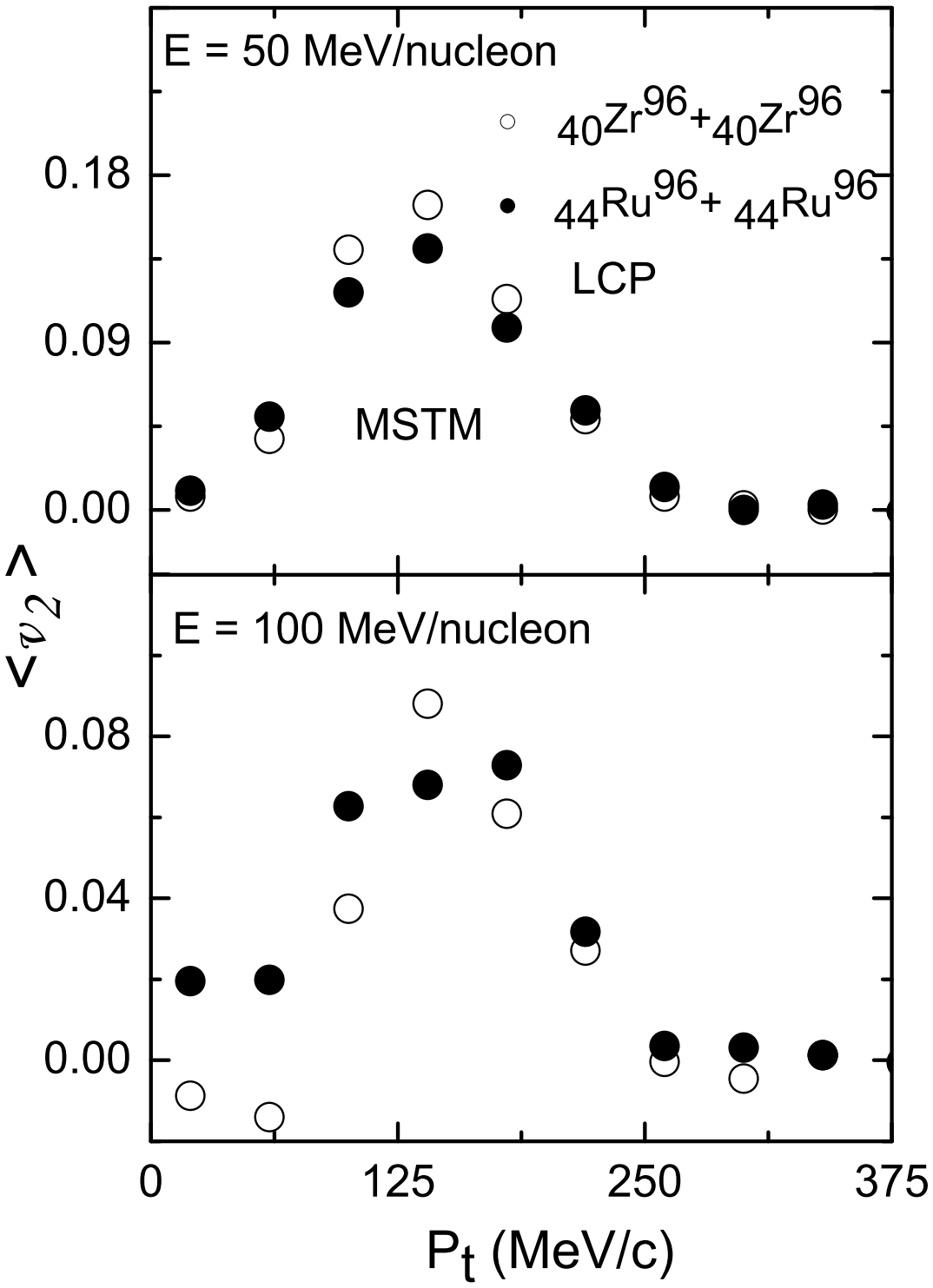

Figure 5.6: The transverse momentum dependence of the elliptical flow, summed over entire rapidity distribution, for LCP's at 50 (top) and 100 MeV/nucleon (bottom), respectively. The reactions under study having same mass number and different atomic number. The reactions are analyzed with MSTM algorithm.

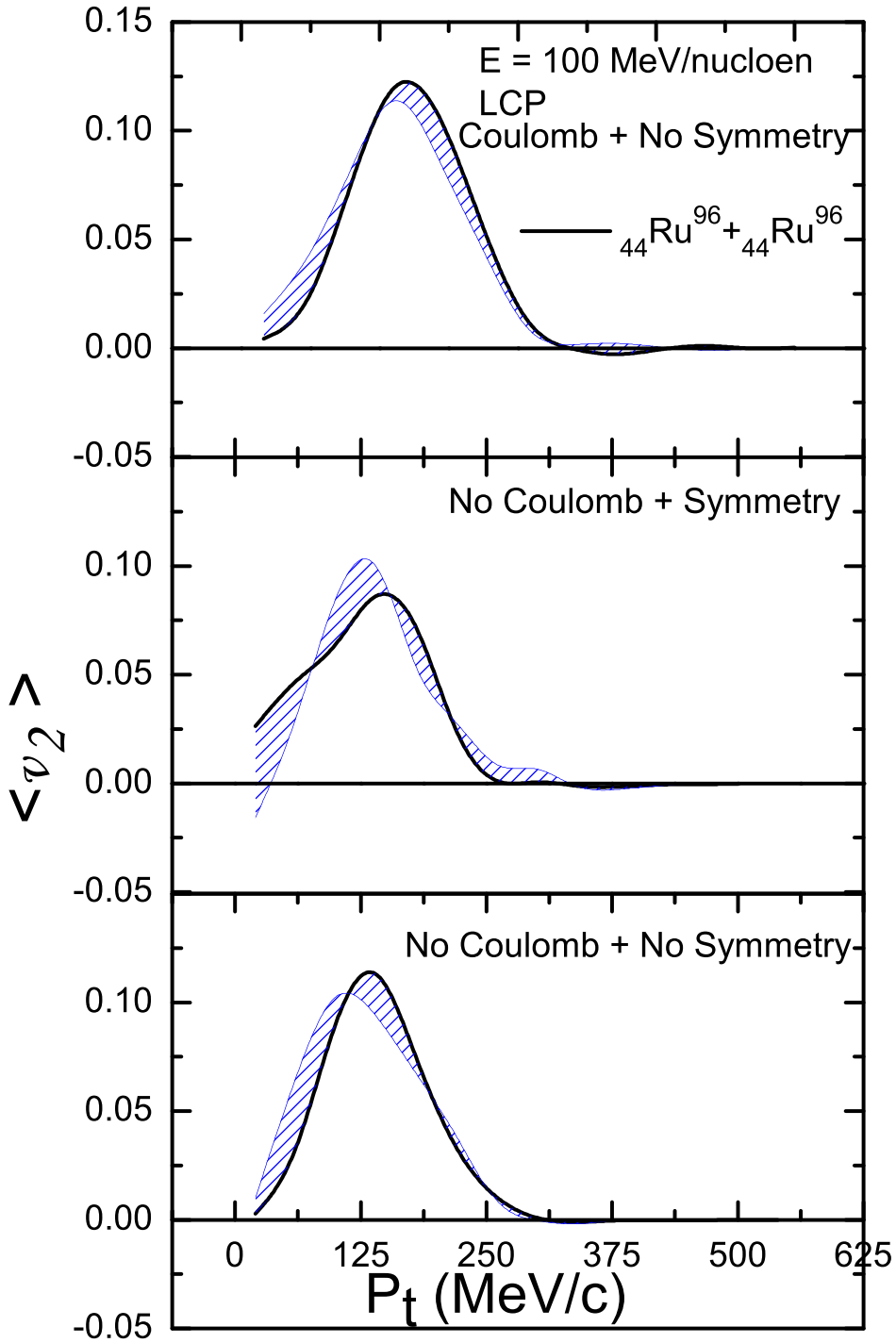

Figure 5.7: The transverse momentum dependence of the elliptical flow, summed over entire rapidity distribution, for LCP's at 100 MeV/nucleon for $_{40}Zr^{96}$ + $_{40}Zr^{96}$ and $_{44}Ru^{96}$ + $_{44}Ru^{96}$. The top, middle and bottom panels are representing the effect of Coulomb interactions, symmetry energy and no Coulomb + no symmetry, respectively.

$_{40}Zr^{96}$ + $_{40}Zr^{96}$ reaction. It is clear from the figure that marginal difference is obtained on transverse momentum dependence of the elliptical flow in the absence of symmetry energy and Coulomb interactions (bottom panel). The same is true in the presence of Coulomb interactions (top panel). The interesting results are in the middle panel (where Coulomb is absent and symmetry is present), indicating the visible effect of symmetry energy on the elliptical flow values for the systems having same mass number and different atomic number. This is further indicating that difference in Fig. 5.6(bottom panel) is supported by the difference in the middle panel of the Fig. 5.7. Our findings in Fig. 5.6 are also supported by Zhang *et al.* [29], where they showed that neutron-rich system exhibits weaker squeeze-out flow. At low incident energy (say 50 MeV/nucleon), binary collisions are rare, therefore isospin in the mean field does not play role. On the other hand, around 100 MeV/nucleon, both isospin of the mean field and binary collisions contribute, making isospin maximum. At higher incident energies, the role of mean field reduces. This situation is similar to the intermediate mass fragments, where maximum value is obtained around 100 MeV/nucleon [30]. It is clear now that symmetry energy is more responsible for the deviation in elliptical flow value as compared to coulomb interactions.

To understand the origin of this isospin effect, the transverse momentum dependence of elliptical flow for target-like, mid-rapidity and projectile-like distributions is displayed in Fig. 5.8. As discussed earlier, the projectile like, target like and mid-rapidity regions are specified according to the rapidity $Y_{c.m.}/Y_{beam}$ distribution. We know that the maximum contribution in projectile like and target like region comes from the spectator zone of the projectile and target nucleus, respectively. It is well explained earlier that elliptical flow originates from the compressed participant zone. That's why, from the figure, one can see that isospin effect originates from the mid-rapidity region or in other words from the participant zone. It is also clear that the isospin effects are stronger for LCP's compared to other fragments. This is due to the fact that heavier fragments have weak sensitivity towards mean field [28]. This weak sensitivity of the mean field is due to the indirect pairing between the nucleons of the projectile and target in the compressed participant zone for heavier fragments compared to LCP's, where direct pairing takes place between the nucleons. This leads to the more pronounced effect of the symmetry energy on the LCP's as compared to free and IMF's.

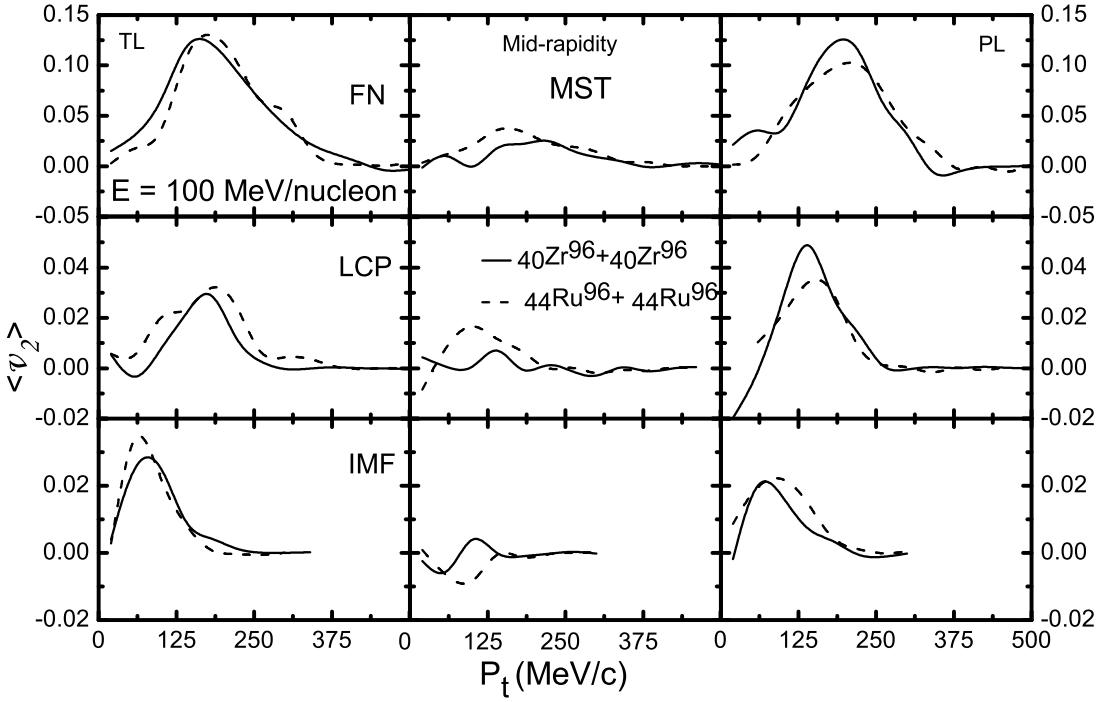

Figure 5.8: The transverse momentum dependence of the elliptical flow at $E = 100$ MeV/nucleon for the reactions displayed in Fig. 5.6. The left, middle and right panels are representing target-like, mid-rapidity and projectile like distributions, respectively, while, top, middle and and bottom panels have same meaning as that of Fig. 5.5. The reactions are analyzed with MST algorithm.

One point which still striking the mind is what will be the effect of the symmetry energy and Coulomb interactions on the individual system under the study. For this, in Fig.5.9, we display the transverse momentum dependence of elliptical flow for LCP's in the mid-rapidity region (a) with and without symmetry energy (top panel), (b) with and without Coulomb interactions (middle panel) (c) without symmetry energy and Coulomb interactions (bottom panel) for $_{40}Zr^{96} + {}_{40}Zr^{96}$ reaction. More squeeze-out is observed in the presence of Coulomb interactions and symmetry energy. This is due to the repulsive nature of Coulomb interactions and additional push to the participant zone in out-of-plane direction in the presence of symmetry energy. Once again effect of symmetry energy is dominating as compared to Coulomb interactions. The percentage effect of symmetry energy (displayed in top panel) is 55%, while of the Coulomb interactions is 35 % (displayed in middle panel). Similar findings were also observed when these effects were studied for different systems

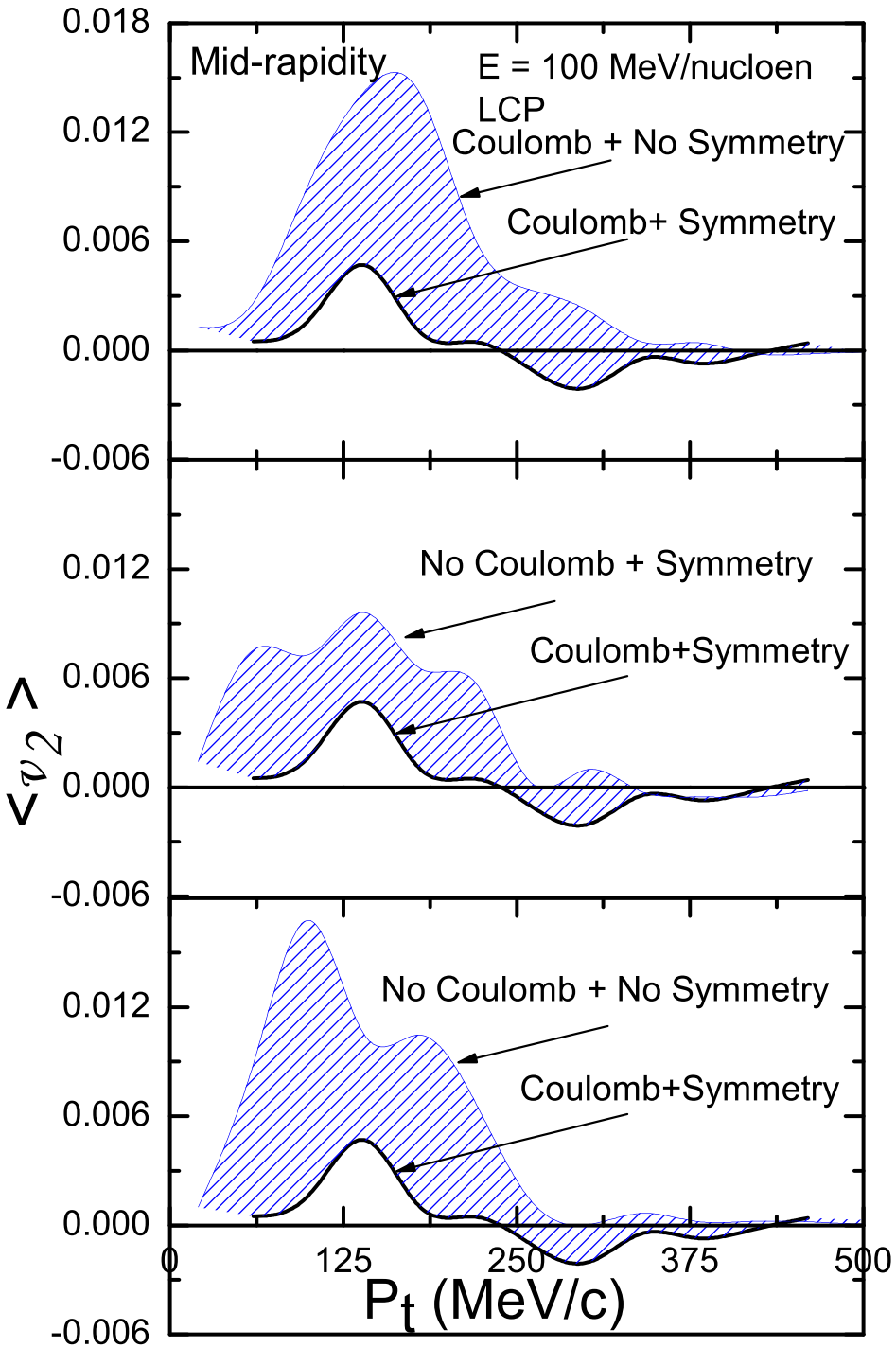

Figure 5.9: The transverse momentum dependence of elliptical flow for LCP's in the mid-rapidity region at E = 100 MeV/nucleon. The panel is exhibiting the effect of symmetry energy (top), Coulomb interactions (middle) and Symmetry+ Coulomb interactions (bottom) on the ${}_{40}Zr^{96} +_{40} Zr^{96}$ reaction.

in Figs. 5.6 and 5.7. This is in agreement with the findings of Chen *et al.* [31], where it was concluded that light clusters production acts as a probe for symmetry energy. This is strengthening our agreement that elliptical flow depends on the N/Z ratio or alternatively the isospin dependence rather than on the size of the interacting system.

5.3.2 Beam energy dependence of elliptical flow

In Fig. 5.10, we display the variation of the excitation function of elliptical flow v_2 for free, LCP's and IMF's over entire rapidity and mid-rapidity region. The elliptical flow is found to become less positive (entire rapidity) or more negative (mid-rapidity) with the increase in the beam energy, upto a certain energy, and then again becomes more positive or less negative. This is due to the fact that spectators move faster after the v_2 has reached a minimum value[5]. This energy, at which the behavior changes is found to decrease with the size of the fragment. It means that the flow of heavier fragments is larger compared to LCP's/free nucleons at all beam energies. These type of findings are also reported by different authors in Ref. [22]. This is true for entire rapidity region as well as for mid-rapidity region.

The interesting phenomena of transition from in-plane to out-of-plane is observed at mid-rapidity region[4, 32], while no transition is observed when integrated over entire rapidity region. The energy at which this transition is observed is dubbed as transition energy(E_{Trans}). It means that participant zone is responsible for the transition from in-plane to out-of-plane. That's why free particles and LCP's, which originate from the participant zone, are showing a systematic behavior with the beam energy as well as with the composite mass of the system. The elliptical flow for these particles is found to become more negative with the increase in the composite mass of the system. Heavier is the system, more is the Coulomb repulsion and more negative is the elliptical flow. This systematics of E_{Trans} with composite mass of the system is discussed later.

5.3.3 A comparison with experimental findings

In Fig. 5.11, we show v_2@mid rapidity ($|y| = |\frac{y_{c.m}}{y_{beam}}| \leq 0.1$) for $Z \leq 2$ (left panel) and for protons (right panel) as a function of the incident energy. The rapidity cut is in ac-

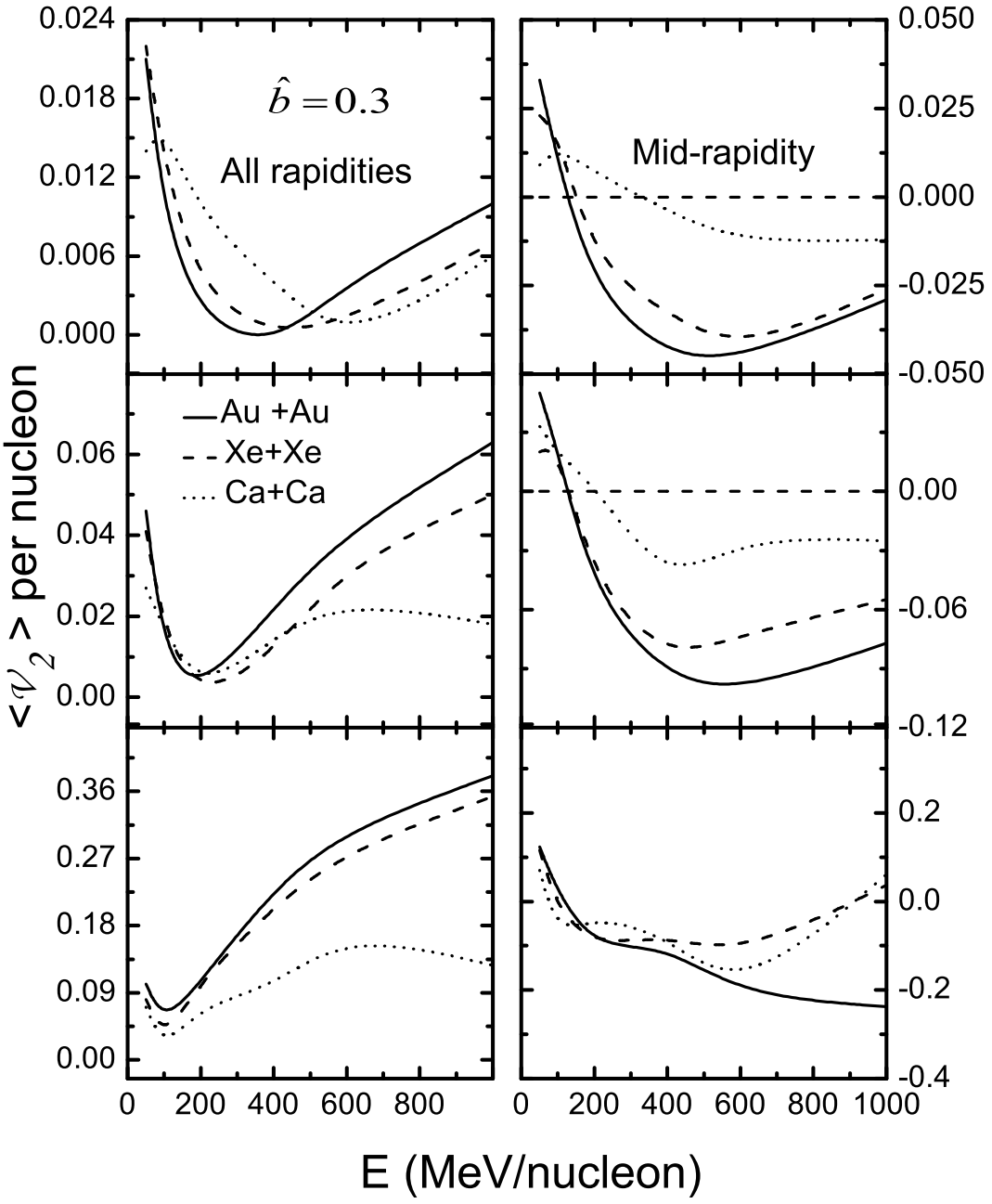

Figure 5.10: The variation of the elliptical flow, summed over entire transverse momentum, with beam energy at $\hat{b} = 0.3$ for different symmetric reactions over entire rapidity range and at mid-rapidity in the left and right panels, respectively. The top, middle and bottom panels have same meaning as that of Fig. 5.5.

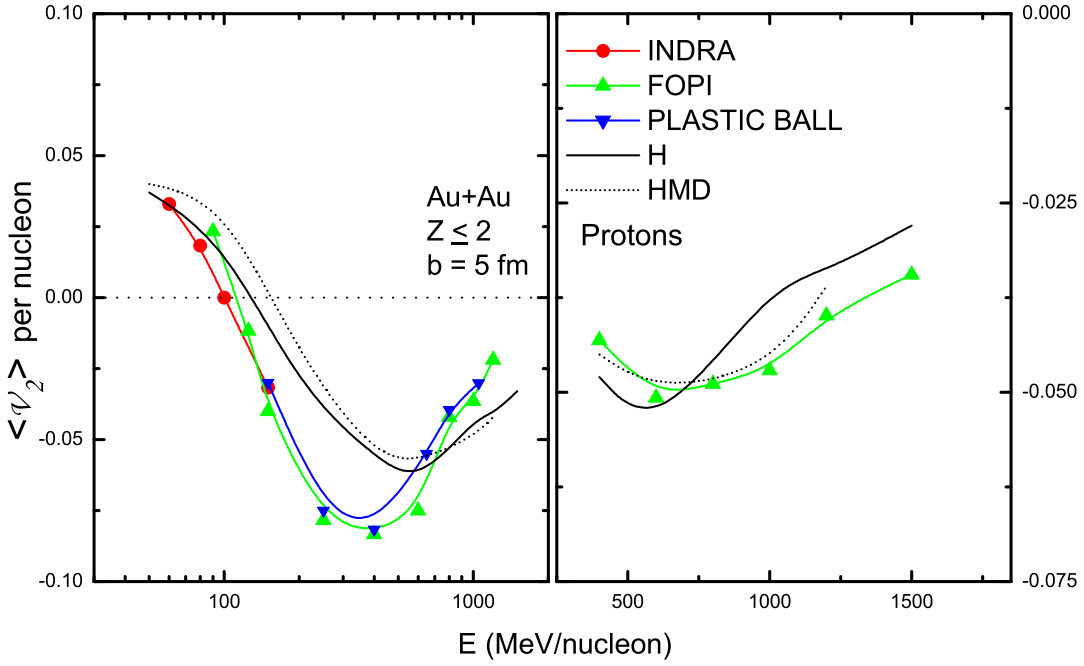

Figure 5.11: The variation of the elliptical flow, summed over entire transverse momentum, with beam energy at $|y| = |\frac{y_{c.m}}{y_{beam}}| \leq 0.1$ for ${}_{79}Au^{197} + {}_{79}Au^{197}$ reaction. Here comparison is shown with experimental findings of INDRA, FOPI and PLASTIC BALL Collaborations[4, 5, 6].

cordance with the experimental findings. The theoretical results are compared with the experimental data extracted by INDRA, FOPI and PLASTIC BALL collaborations[4, 5, 6]. With the increase in the incident energy, elliptical flow v_2 changes from positive to negative values exhibiting a transition from the in-plane to out-of-plane emission of nucleons. This is because of the fact that the mean field, which contributes to the formation of a rotating compound system, becomes less important and the collective expansion process based on the nucleon-nucleon scattering starts to be predominant. This competition between the mean field and N-N collisions depends strongly on the effective interactions that leads to the different transition energy due to different equations of state. Due to repulsive nature of the momentum dependent interactions, which leads to the suppression of binary collisions, less squeeze-out is observed in the presence of momentum dependent interactions (HMD) compared to static one (H). The maximal negative value of v_2 is obtained around $E = 500$ MeV/nucleon with hard (H) and hard momentum dependent (HMD) equations of state.

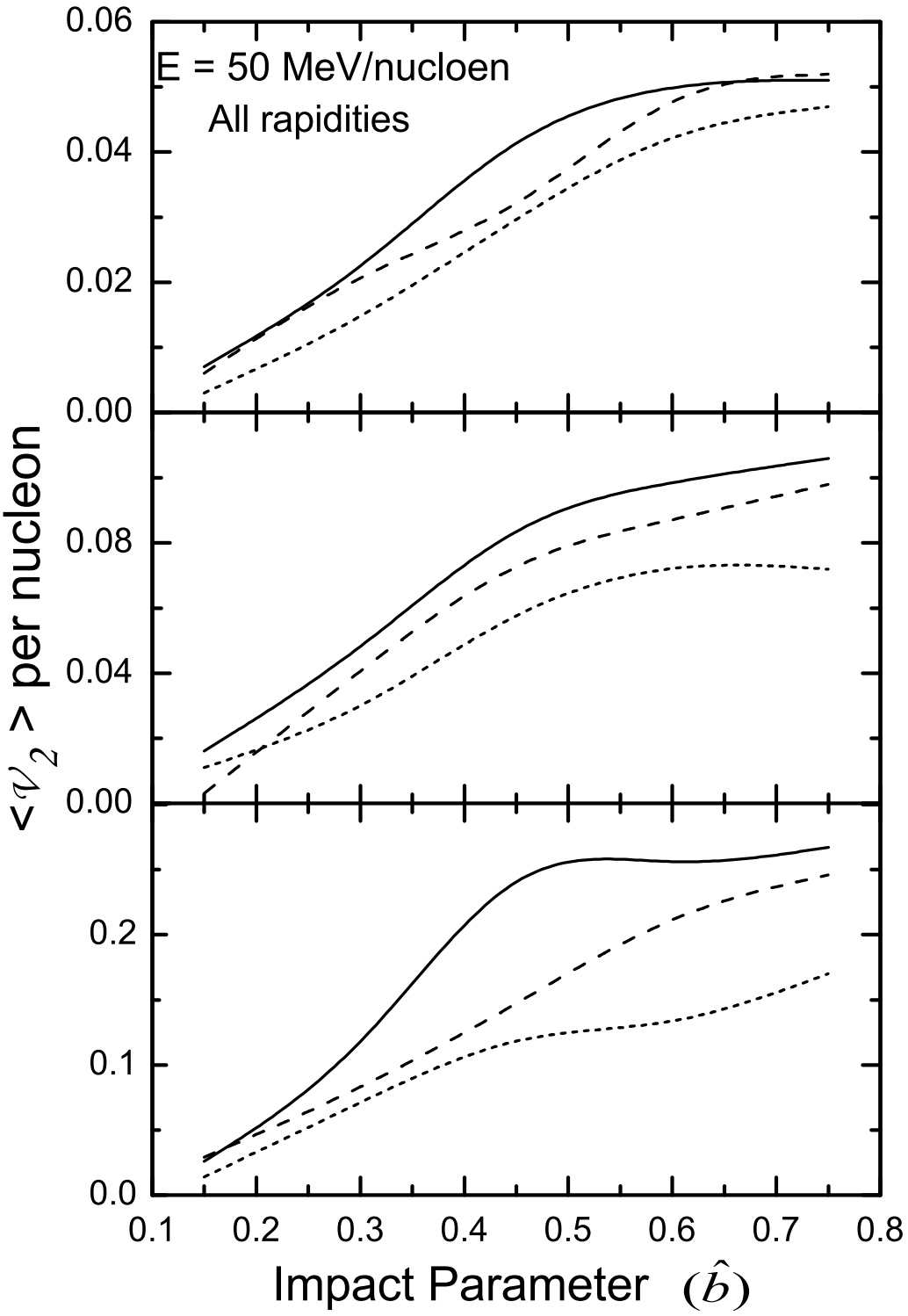

Figure 5.12: The impact parameter dependence of the elliptical flow, summed over entire transverse momentum and rapidity distribution, at incident energies 50 MeV/nucleon. The top, middle and bottom panels are for free particles, LCP's and IMF's, respectively.

This out-of-plane emission decreases again towards the higher incident energies. This happens due to faster movement of the spectator matter after v_2 reaches the maximal negative value [5]. This trend is in agreement with experimental findings. A close agreement with data is obtained in the presence of hard equation of state for $Z \leq 2$ particles, while, in the presence of momentum dependent interactions for protons. Similar results and trends have also been reported by Zhang et.al. in their recent communication [32].

5.3.4 Impact parameter dependence

The investigation of the elliptical flow with scaled impact parameter over entire rapidity range is displayed in Fig. 5.12. Here the top, middle and bottom panels represent the free nucleons, LCP's and IMF's. The value of the elliptical flow v_2 becomes more positive with the impact parameter and composite mass of the system at $E = 50$ MeV/nucleon, while at higher energies (not shown here), it is found to become less positive (entire rapidity) or more negative (mid-rapidity) with composite mass of the system. This is indicating the dominance of the in-plane flow at low incident energies with increasing impact parameter and composite mass of the system. Moreover, dominance of the out-of-plane flow at higher energies with small impact parameter and composite mass of the system is observed. With the increase in the beam energy, the expansion of the compressed zone becomes more vigorous, while, with an increase in the impact parameter, participant zone decreases, resulting an increases in the spectator region indicating dominance of azimuthal anisotropy with impact parameter. On the other hand, it reduces with beam energy. These observations are consistent with the experimental findings and with other theoretical works [22, 27, 33].

5.3.5 Power law dependence of transition energy

Finally, we carry out the system size dependence of the elliptical flow for free nucleons and LCP's. In Fig. 5.13, we show the transition energies E_{Trans} as a function of the composite mass of the system for free nucleons and LCP's, which are extracted from the Fig. 5.10. From the figure, we see that the transition energy decreases with the composite mass of the system as well as with the size of the fragment. The reason for this is that the pressure

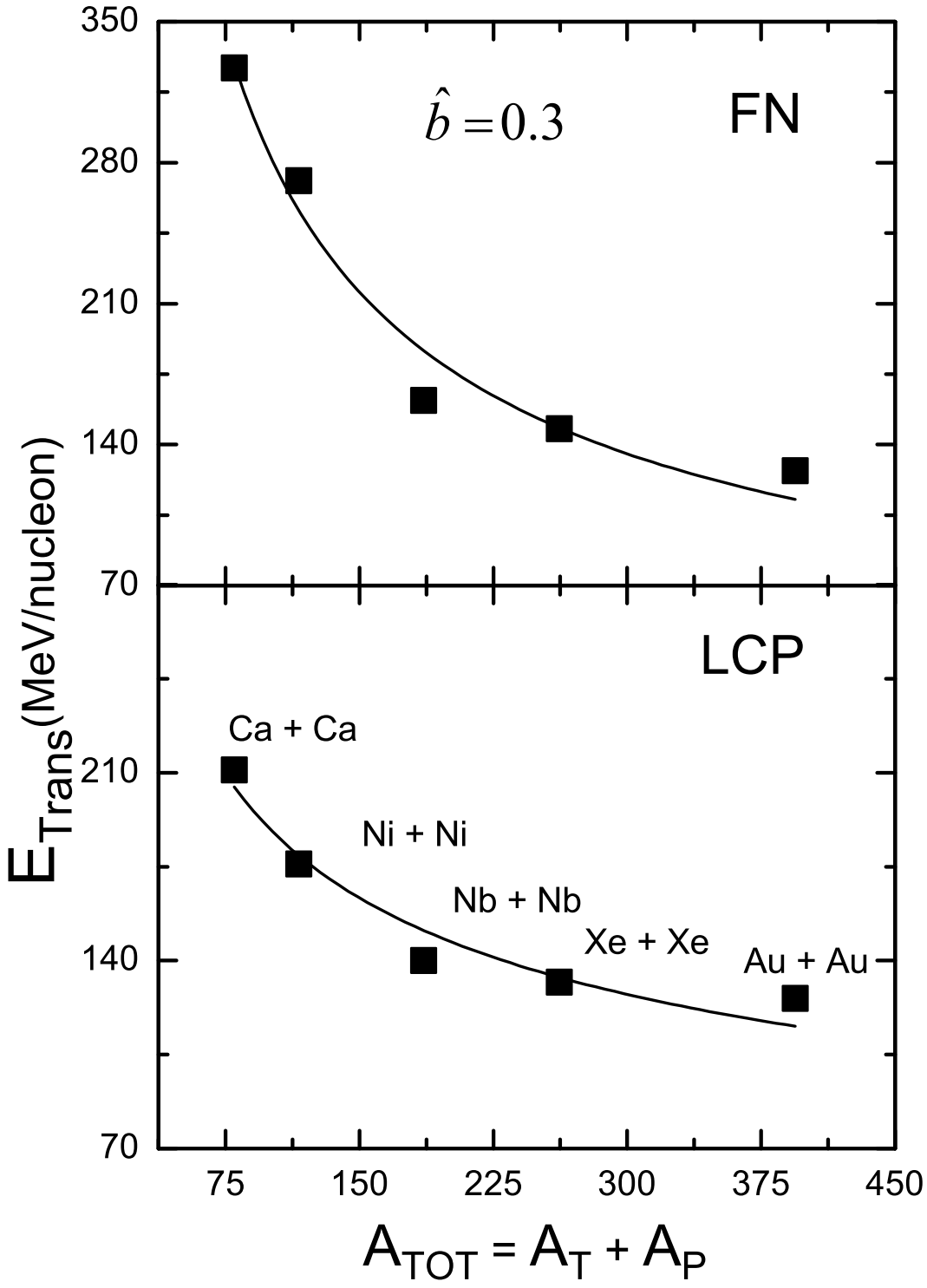

Figure 5.13: The transition energies for elliptical flow at intermediate energies as a function of the combined mass of the system. The upper panel is for the free nucleons, while, lower panel is for the LCP's.

produced by the Coulomb interactions increases with the system size. This dependence can be fitted using a power law of the kind:

$$E_{Trans} = C(A_{tot}^{-\tau}) \tag{5.15}$$

The exponent τ is found to be 2 times for free particles (0.67) compared to LCP's (0.35). This exponent is quite smaller compared the exponent of balance energy in directed flow [32]. This is due to the different origin of the balance and transition energy. The balance energy counter balances the mean field and N-N collisions, while transition energy is due to the more complex effects such as expansion of the compressed zone and shadowing of the cold spectator matter.

5.4 Summary

In this chapter, we have presented the isospin dependence (in term of symmetry energy) and the disappearance of elliptical flow in the presence of isospin-dependent quantum molecular dynamics (IQMD) model at intermediate energies for the several systems. The isospin dependence of the elliptical flow is studied in term of the transverse momentum dependence for different kind of fragments (free nucleons, LCP's and IMF's). The free nucleons and IMF's are found to be system mass dependent for the incident energies under consideration, while LCP's are found to be isospin dependent at relative high incident energy, where role of mean field and NN collisions is equal(say E = 100 MeV/nucleon). Moreover, these isospin effects due to symmetry energy are originating from the mid-rapidity region. In other words, one can say that LCP's acts as a probe to symmetry energy.

The disappearance of elliptical flow is observed at mid-rapidity region, while no transition is observed, when integrated over entire rapidity region. This is indicating the origin of squeeze-out or out-of-plane emission is from the participant zone and not from the spectator zone. The energy at which elliptical flow disappears is, dubbed as, transition energy. This transition energy is found to be strongly dependent on the size of the system as well as size of the fragment.

When comparison of excitation function of elliptical flow is made with experimental findings of INDRA, FOPI and PLASTIC BALL collaborations, the charged particles (Z $\leq$

2) are well explained by the static equation of state, while for the protons, good agreement with the inclusion of momentum dependent interactions is observed. This comparison can be explored to more accuracy by studying the effect of isospin-dependent cross sections on the excitation function of elliptical flow.

Finally, the transition energy for free nucleons and LCP's is parametrized in term of mass power law and is found to decrease with the composite mass of the system as well as with the size of the fragment. Further, one can elaborate the dependence of transition energy on the impact parameter, isospin-dependent cross sections, model ingredients, method of analysis, different rapidity cuts as well as different transverse momentum cuts. This can provide a challenge to the experimentalist to prove the theoretical findings.

Bibliography

[1] P. Danielewicz, R. Lacey, and W. G. Lynch, Science **298**, 1592 (2002); H. Stöcker and W. Greiner, Phys. Rep. **137**, 277 (1986); W. Reisdorf and H. G. Ritter, Ann. Rev. Nucl. Sci. **47**, 663 (1997); C. Hartnack and J. Aichelin, Phys. Rev. C **49**, 2801 (1994); S. Kumar, S. Kumar, and R. K. Puri, Phys. Rev. C **78**, 064602 (2008); A. R. Raduta and F. Gulminelli, *ibid.* **75**, 024605 (2007)

[2] J. Aichelin, Phys. Rep. **202**, 233 (1991).

[3] G. D. Westfall *et al.,* Phys. Rev. Lett. **71**, 1986 (1993); M. B. Tsang *et al.,* Phys. Rev. C **53**, 1959 (1996); Y. M. Zheng, C. M. Ko, B. A. Li, and B. Zhang, Phys. Rev. Lett. **83**, 2534 (1999); A. B. Larionov, W. Cassing, C. Greiner, and U. Mosel, Phys. Rev. C **62**, 064611 (2000); B. A. Li, A. T. Sustich, and B. Zhang, *ibid.* **64**, 054604 (2001); C. Alt *et al., ibid.***68**, 034903 (2003).

[4] J. Lukasik, G. Auger, and M. L. Begemann-Blaich *et al.,* Phys. Lett. B **608**, 223 (2005).

[5] A. Andronic *et al.,* Nucl. Phys. A **679**, 765 (2001); Phys. Lett. B **612**, 173 (2005).

[6] J. Lukasik, *et.al.,* INDRA Collaborations, Int. Workshop on Multifragmentation and related topics (IWM 2003) Caen, France (2003).

[7] S. Kumar, M. K. Sharma, R. K. Puri, K. P. Singh, and I. M. Govil, Phys. Rev. C **58**, 3494 (1998); A. D. Sood, R. K. Puri, and J. Aichelin, Phys. Lett. B **594**, 260 (2004).

[8] A. D. Sood and R. K. Puri, Phys. Rev. C **69**, 054612 (2004); Eur. Phys. A **30**, 571 (2006).

[9] L. W. Chen and C. M. Ko, Phys. Lett. B **634**, 205 (2006); Phys. Rev. C **73**, 014906 (2006).

[10] M. Gyulassy, K. A. Frankel, and H. Stöcker, Phys. Lett. B **110**, 185 (1982); P. Danielewicz and M. Gyulassy, Phys. Lett. B **129**, 283 (1983); C. M. Ko and G. Q. Li, J. Phys. G: Nucl. and Part. **22**, 1673 (1996); G. Q. Li, C. M. Ko, and B. A. Li, Phys. Rev. Lett. **74**, 235 (1995); G. Q. Li and C. M. Ko, Nucl. Phys. A **594**, 460 (1995); B. A. Li and C. M. Ko, Phys. Rev. C **52**, 2037 (1995); Phys. Rev. C **58**, R1382 (1998); Nucl. Phys. A **601**, 457 (1996).

[11] H. Sorge, Phys. Rev. Lett. **78**, 2309 (1997); J. Y. Ollitrault, Phys. Rev. D **46**, 229 (1992).

[12] S. Voloshin and Y. Zhang, Z. Phys. C **70**, 665 (1996).

[13] C. Hartnack *et al.,* Eur. Phys. J. A **1**, 151 (1998).

[14] H. Stocker *et al.,* Phys. Rev. C **25**, 1873 (1982).

[15] M. Demoulins *et al.,* Phys. Lett. B **241**, 476 (1990).

[16] H. H. Gutbrod *et al.,* Phys. Lett. B **216**, 267 (1989).

[17] H. H. Gutbrod *et al.,* Phys. Rev. C **42**, 640 (1990).

[18] D. J. Magestro, Ph. D thesis, NSCL, MSU, USA (2000).

[19] C. Pinkenburg *et al.,* Phys. Rev. Lett. **83**, 1295 (1999); A. Andronic *et al.,* Eur. Phys. J A **30**, 31 (2006).

[20] S. Kumar, S. Kumar and R. K. Puri, Phys. Rev. C **81**, 014611 (2010); 11^{th} Punab Science Congress, Thapar University, Patiala **p38**, Feb. 7-9, (2008); National Seminar on Advances in Physics, Panajb University, Chandigarh (India), Feb 28-March 1, (2008); Zakopane Conference on Nuclear Physics, Poland, Sep. 1-7, (2008); Int. Symposium on Nuclear Physics, BARC, Bombay Dec. 8-12, (2009).

[21] D. J. Magestro, W. Bauer, and G. D. Westfall, Phys. Rev. C **62**, 041603(R) (2000); E. Lehmann *et al.,* Z. Phys. A **355**, 55 (1996); A. D. Sood and R. K. Puri, Phys. Rev. C **73**, 067602 (2006); *ibid.* **70**, 034611 (2004).

[22] H. Y. Zhang *et al.,* J. Phys. G: Nucl and Part. **28**, 2397 (2002).

[23] E. Lehmann *et.al.,* Prog. Part. Nucl. Phys. **30**, 219 (1993); Phys. Rev. C **51**, 2113 (1995).

[24] Y. K. Vermani and R. K. Puri, Eur. Phy. Lett. **85**, 62001 (2009); Y. K. Vermani. S. Goyal, and R. K. Puri, Phys. Rev. C **79**, 064613 (2009); Y. K. Vermani, J. K. Dhawan, S. Goyal, R. K. Puri, and J. Aichelin, J. Phys. G: Nucl. and Part. **37**, 015105 (2010); S. Kumar and R. K. Puri, Phys. Rev. C **58**, 1618 (1998); R. K. Puri and J. Aichelin, J. Comp. Phys. **162**, 245 (2000); J. Singh, S. Kumar, and R. K. Puri, Phys. Rev. C **62**, 044617 (2000); R. K. Puri, C. Hartnack, and J. Aichelin, Phys. Rev. C **54**, R28 (1996).

[25] J. Singh and R. K. Puri, Phys. Rev. C **62**, 054602 (2000).

[26] M. Colona, M. D. Toro, G. Ferini, and V. Greco, *Catania workshop on nucleon and neutrino astrophysics*, 15-16 Feb., (2007); M. Di Toro, S. J. Yennello, and B. A. Li, Eur. Phys. J. A **30**, 153 (2006).

[27] Y. G. Ma, W. Q. Shen, J. Feng, and Y. Q. Ma, Phys. Rev. C **48**, 1492 (1993); Z. Phys. A **344**, 469 (1993); Y. G. Ma, W. Q. Shen, Z. Y. Zhu, Phys. Rev. C **51**, 1029 (1995); W. Q. Shen *et al.,* Nucl. Phys. A **551**, 333 (1993); R. Lacey *et al.,* Phys. Rev. Lett. **70**, 1224 (1993).

[28] T. Z. Yan *et al.,* Chin. Phys. **16**, 2676 (2007).

[29] F. S. Zhang, L. W. Chen, W. F. Li, and Z. Y. Zhu, Eur. Phys. J. A **9**, 149 (2000).

[30] M. B. Tsang *et al.,* Phys. Rev. Lett. **71**, 1502 (1993).

[31] L. W. Chen, C. M. Ko, and B. A. Li, Phys. Rev. C **68**, 017601 (2003).

[32] Y. Zhang and Z. Li, Phys. Rev. C **74**, 014602 (2006).

[33] J. Peter *et al.,* Nucl. Phys. A **519**, 611 (1990); Z. Y. He *et al., ibid.* **598**, 248 (1996).

Chapter 6

Fragmentation process as a indicator for nuclear stopping and momentum dependent interactions

6.1 Introduction

Nuclear reactions from low to relativistic energies provide variety of phenomena. As stated in chapter 1, Pauli principle blocks majority of scattering of nucleons at low incident energies. Therefore, attractive mean field dominates the physics in this energy regime[1]. The phenomena of interest in this energy region are structure of nuclei, phenomena of fusion-fission[2], cluster radioactivity[3] as well as halo nuclei [4]. At intermediate energies, however, a mixture of attractive mean field and repulsive nucleon-nucleon scattering exists[5, 6]. Both these regimes together, lead the matter from a fused state to total disassembly. One is also interested to understand the mechanism behind this. This mechanism has motivated the nuclear community to one of the goals of heavy-ion collisions (HIC) at intermediate energies, which is to extend the knowledge of hot and dense nuclear matter to the extreme conditions. In the past, these studies were focused on multifragmentation, that constitutes fragments of all sizes[7]. The process of multifragmentation is also studied in this thesis in chapter 3 and 4, indicating the importance of momentum dependent interactions and nucleon-nucleon cross-sections. Additional promising observable for the understanding of nuclear equation of state is the anisotropy in the momentum distribution that includes the directed in-plane flow (bounce off) as well as out of plane flow (squeeze out) [5, 6]. The absolute values of the flow results from the interplay between the attractive mean field and repulsive nucleon-nucleon scattering. This interplay is also responsible for the transition from a fused state to total

disassemble one. This transition between the in-plane and out-of-plane emission is studied in chapter 5 of this thesis. The another phenomena linked with the above interplay is the global stopping of nuclear matter. Recently, Puri and co-workers[8], tried to correlate the multifragmentation with global nuclear stopping. Their findings revealed that light charged particles (LCP's) acts in a similar fashion like anisotropy ratio. They, however, did not take isospin of the system into account. As discussed in chapter 5, the isospin degree of freedom is found to affect the light charged particles to a great extent. This makes the study of correlation between the nuclear stopping and LCP's uni-important.

The recent advances in the radioactive nuclear beam (RNB) physics is providing scientific community a unique opportunity to investigate the isospin effects in heavy-ion collisions (HIC's) [9] with respect to the above rare phenomena [10, 11]. Beside the many existing radioactive beam facilities, many more are being constructed or under planning, including the Cooling Storage Ring (CSR) facility at HIRFL in China, the Radioactive Ion Beam (RNB) factory at RIKEN in Japan, the FAIR/GSI in Germany, SPIRAL2/GANIL in France, and Facility for Rare Isotope Beam (FRIB) in the USA [12]. These facilities offer possibility to study the properties of nuclear matter or nuclei under the extreme conditions of large isospin asymmetries. Though at low incident energies, where fusion and related phenomena are dominant, systematic studies on isospin degree of freedom are available [13], such studies at intermediate energies are rarely available[9]. One of the cause could be the much more complex dynamics involved at intermediate incident energies. Among various above mentioned phenomena nuclear stopping of the colliding matter has gained a lot of interest since it gives us possibility to examine the degree of thermalization or equilibration or stopping of the nuclear matter.

Nuclear stopping in heavy-ion collisions has been studied by the means of rapidity distribution [14] or by the asymmetry of nucleonic momentum distribution [15]. As pointed out by Bauer [15], nuclear stopping at intermediate energies is determined by the mean field as well as by the in-medium NN cross-sections. Unfortunately, his calculations were silent about the symmetry potential. The recent work of many authors [9, 16, 17] suggest that the degree of approaching isospin equilibration helps to probe the nuclear stopping in heavy-ion collisions. In Ref.[16], isospin dependence of cross-section was investigated in nuclear stop-

ping. In a recent communication [17], authors studied the behavior of excitation function $Q_{zz}/nucleon$ and concluded that $Q_{zz}/nucleon$ can provide information about the isospin dependence in term of cross-section. Several more studies have also focused in the recent years on the isospin degree of freedom [18].

As is clear from the literature that the effect of isospin degree of freedom on the nuclear stopping is studied many times, but, no one has tried to correlate the LCP's production with the nuclear stopping or thermalization in the presence of symmetry energy [19].

Interestingly, no systematical study is available in the literature on the effect of isospin degree of freedom via symmetry energy on nuclear stopping. This becomes much more important if one acknowledges that the effect of symmetry energy could be altered in the presence of momentum dependent interactions [19], which has become essential part of the interaction for any reasonable dynamical model [9, 14]. Thus, our aim is at least three folds:

- To focus on the relation between LCP's and equilibration of the reaction i.e. nuclear stopping in the presence of symmetry energy using isospin-dependent quantum molecular dynamics (IQMD) model[20].

- We plan to understand the role of symmetry energy in the presence of momentum dependent interactions in a systematic way.
  and

- To further examine how mass dependence alter the above findings. It is worth mentioning that the study of the mass dependence is very essential for any meaningful conclusion.

This study is done in the presence of Isospin-dependent Quantum Molecular Dynamics (IQMD) Model. The isospin effects in the model are added in term of symmetry potential and isospin dependent cross sections. The isospin dependent cross sections are discussed in detail in chapter 2 and 4, while symmetry energy and symmetry potenial is discuused in the following section.

6.2 Symmetry energy and symmetry potential

A binding formula expresses the energy E of a nucleus in terms of nucleon numbers, $E = E(A, Z)$. Here, A and Z are the net nuclear nucleon and proton numbers, respectively, and the neutron number is $N = A - Z$. The basic[21], termed Bethe- Weizsacker [22](BW), formula represents the energy as a sum of five trms only:

$$E = -a_V A + a_s A^{2/3} + \frac{a_c Z(Z-1)}{A^{1/3}} + \frac{a_A (N-Z)^2}{A} + \delta. \tag{6.1}$$

For the details of these terms reader is referred to the Ref.[22]. The term of interest is the fourth term in formula, $a_A(N-Z)^2/A$, with $a_A \approx 21$ MeV, is commonly called a symmetry term although asymmetry would be a more adjective. This term accounts for the binding, under the sole influence of nuclear interactions, being stronger for more symmetric nuclei, with $N \approx Z$, than for more asymmetric nuclei with different N and Z. This term is, in particular, related to a stronger attraction between neutrons and protons than between like nucleons. In other words, it is the change in nuclear energy associated with changing neutron-proton asymmetry $(N-Z)/A$. The symmetry with respect to the np interchange in the symmetry term reflects the charge symmetry [21] of nuclear interactions.

This symmetry energy in term of symmetry potential V_{Sym} can be written in three different forms[9].

$$V^1_{Sym} = cF_1(u)\delta\tau_z, \tag{6.2}$$

$$V^2_{Sym} = cF_2(u)\delta\tau_z + \frac{1}{2}cF_2(u)\delta^2, \tag{6.3}$$

$$V^3_{Sym} = cF_3(u)\left[\delta\tau_z - \frac{1}{4}\delta^2\right], \tag{6.4}$$

with $\tau_z = 1$ for neutrons, and -1 for protons.

where $F_1(u) = u$, $F_2(u) = u^2$ and $F_3(u) = u^{1/2}$ and, $u = \frac{\rho}{\rho_0}$; δ is the relative neutron excess $\delta = \frac{\rho_n - \rho_p}{\rho_n + \rho_p} = \frac{\rho_n - \rho_p}{\rho}$; ρ, ρ_0, ρ_n and ρ_p are the total, normal, neutron and proton densities respectively. The strength of c is of the order of 32 MeV to reproduce the 4^{th} term of the Bethe Weizsacker mass formula.

The IQMD code [5] developed at Subatech, France by C. Hartnack and collaborators reduces the above symmetry potentials in the form as:

$$V_{Sym} = t_6 \frac{1}{\varrho_0} T_3^i T_3^j \delta(r_i' - r_j) \tag{6.5}$$

where, T_3^i, T_3^j are their respective T_3 components (i.e. 1/2 for protons and -1/2 for neutrons) and $t_6 = 100$ MeV. Here again the strength of symmetry energy is found to be of the order of 32 MeV.

It is clear from the Ref.[23] that the repulsive (attractive) mean field potential for neutrons (protons) depends sensitively on the form of $F(u)$, the neutron excess δ and the baryon density ρ. In collision of neutron-rich nuclei at intermediate energies, both δ and ρ can be appreciable in a large space-time volume where the isospin-dependent mean field potentials are strong. Since the symmetry potentials have opposite signs for neutrons and protons, they affect differently the reaction dynamics of neutrons and protons. For protons, the nuclear mean field potential also includes a Coulomb term. The competition between the Coulomb and the symmetry potential then leads to possible differences in the yield and energy spectra of protons and neutrons as well as other isospin effects.

In the present chapter, we have studied the effect of the strength of the symmetry energy of 32 MeV on the fragmentation and nuclear stopping, while the effect of coulomb and symmetry potential was discussed in the previous chapter.

6.3 Origin of nuclear stopping and light charged particles

If two nuclei collide three different scenarios are possible. These different scenarios are shown in Fig.6.1:

1 The nuclei are repelled by each other like in the collision of two hard spheres. (shown in Fig. 6.1[a]).

2 The nuclei are compressed and mix-up like in the collisions of two (compressible) droplets (shown in Fig. 6.1[b]).

3 The nuclei are passing each other without much interactions like two large crowds of bees (shown in Fig.6.1[c]).

The different scenario would cause different longitudinal momentum distributions for the projectile and target particles. The scenario shown in Fig. 6.1[b] is the one which happens in intermediate energy heavy-ion collisions. The global stopping is defined as the

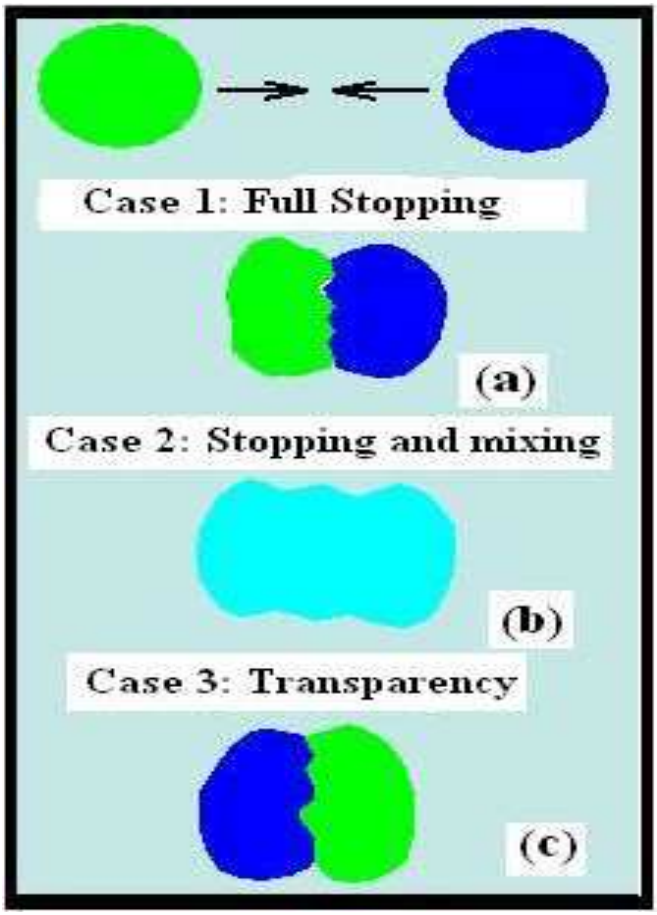

Figure 6.1: Schematic movement of the projectile and target nucleons. The figure is representing (a)Full stopping (b) Stopping and mixing (c) Transparency

randomization of one-body momentum space or memory loss of the incoming momentum or momentum transfer during the break up of the initial correlations among nucleons of projectile and target nuclei. The colliding nuclei not only compress each other, they also heat the matter[8, 14]. In addition, the destruction of initial correlations, makes the matter homogeneous and one can have global stopping. More the initial memory of nucleons is erased, better it is stopped and better one has average mixing of projectile and target momentum (shown in Fig. 6.1[b]). The degree of stopping however, may vary drastically with incident energies, mass of colliding nuclei and colliding geometry. The degree of global stopping has also been linked with the thermalization (equilibrium) in heavy-ion collisions. A complete knowledge about the degree of stopping is very important since it can be connected to the properties of the system, equation of state and in medium properties of the nucleon-

nucleon cross-section [24].

Theoretically, these happenings are followed by a variety of models. Some models assume a priori equilibrium (at least at local level) whereas others hunt for the degree of thermalization in a reaction. Several models which depend on the assumption of equilibrium, have been applied successfully to study the physics at low and intermediate energies [25].

On the other hand, light charged particles are the particles having the range $2 \leq A \leq 4$. The detailed analysis of production of different kind of fragments is studied in literature by taking into account different equations of state, different nucleon-nucleon cross sections as well as different methods of analysis[7, 10]. Any type of the fragment can be considered for the correlation with the nuclear stopping, provided both the quantities must have similar properties. Out of the different kind of fragments, light charged particles are expected to be an indicator for nuclear stopping because of their origin from the participant zone, pairing nature of the particles in LCP's, acts as a probe to symmetry energy. In the literature, the light and medium mass fragments (produced and emitted in reactions), have also been used to get information about the thermalization and stopping in heavy-ion collisions [8, 26, 27, 28]. This work was done without taking into account the effect of symmetry energy. The origin of light and medium mass fragments is still under debate [6, 8].

The global stopping in heavy-ion collisions has been studied with the help of many different variables. In earlier studies, one used to relate the rapidity distribution with global stopping. The rapidity distribution can be defined as [8, 29]:

$$Y(i) = \frac{1}{2} ln \frac{E(i) + p_z(i)}{E(i) - p_z(i)}, \tag{6.6}$$

where $E(i)$ and $p_z(i)$ are, respectively, the total energy and longitudinal momentum of i^{th} particle. For a complete stopping, one expects a single Gaussian shape. Obviously, narrow Gaussian indicate better thermalization compared to broader Gaussian.

The second possibility to probe the degree of stopping is the anisotropy ratio (R) [16]:

$$R = \frac{2}{\pi} \frac{(\sum_i |p_\perp(i)|)}{\left(\sum_i |p_\parallel(i)|\right)}, \tag{6.7}$$

where, summation runs over all nucleons. The transverse and longitudinal momenta are $p_\perp(i) = \sqrt{p_x^2(i) + p_y^2(i)}$ and $p_\parallel(i) = p_z(i)$, respectively. Naturally, for a complete stopping, R should be close to unity.

Another quantity, which is indicator of nuclear stopping and has been used recently, is the quadrupole moment Q_{zz}, defined as[16]:

$$Q_{zz} = \sum_i \left(2p_z^2(i) - p_x^2(i) - p_y^2(i)\right). \tag{6.8}$$

Naturally, for a complete stopping, Q_{zz} should be close to 0.

In this chapter, we will show the similarities in the different properties of LCP's and equilibration of the reaction i.e. nuclear stopping in the presence of symmetry energy and then understand the role of symmetry energy in the presence of momentum dependent interactions in a systematic way. Further we will examine, how mass dependence is altering the above findings.

6.4 Results and Discussion

In the present analysis, thousands of event were simulated for the neutron-rich reaction of ${}_{54}Xe^{131}$ + ${}_{54}Xe^{131}$ at incident energies between 50 and 1000 MeV/nucleon using hard equation of state along with isospin dependent free and constant nucleon-nucleon cross-sections[30]. Moreover, to see the effect of compressibility on nuclear stopping and fragmentation, soft equation of state is also used in Fig.6.6. The geometry of the collision was varied between the most-central to peripheral one. The role of symmetry energy is studied by simulating the above reaction with and without this term. In addition, the reactions of ${}_{20}Ca^{40} + {}_{20}Ca^{40}$, ${}_{28}Ni^{58} + {}_{28}Ni^{58}$, ${}_{41}Nb^{93} + {}_{41}Nb^{93}$, ${}_{79}Au^{197} + {}_{79}Au^{197}$, ${}_{20}Ca^{34}$ + ${}_{20}Ca^{34}$ (N/Z = 0.7), ${}_{20}Ca^{40}$ + ${}_{20}Ca^{40}$ (N/Z = 1), ${}_{20}Ca^{48}$ + ${}_{20}Ca^{48}$ (N/Z = 1.4) and ${}_{20}Ca^{57}$ + ${}_{20}Ca^{57}$ (N/Z = 1.85) are also simulated to see the system size and N/Z effects on the production of fragments and nuclear stopping. As stated above, we plan to study the degree of stopping and emission of fragments using symmetry energy and isospin-dependent cross-section. We shall also correlate the degree of stopping with the emission of light charged particles as is also done in Ref.[8]. The fragments are constructed within minimum spanning tree (MST) method [7], which binds nucleons if they are with in a distance of 4 fm. Finally, the effect of momentum dependent interactions on the nuclear stopping in the presence of symmetry energy is also studied.

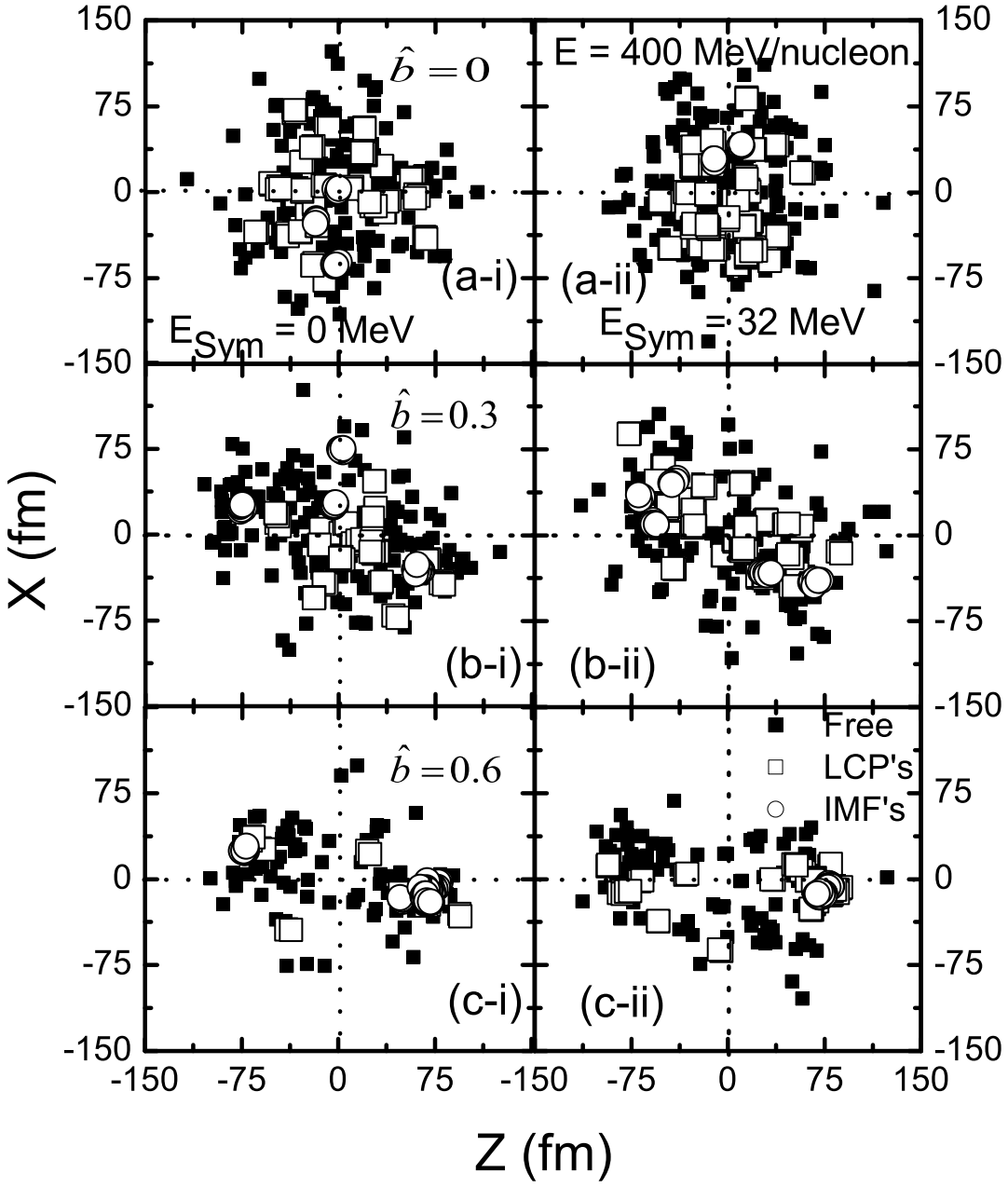

Figure 6.2: The final phase space of a single event for the reaction of ${}_{54}Xe^{131}$ + ${}_{54}Xe^{131}$ with(ii) and without symmetry energy(i). The top(a), middle(b) and bottom (c) panels are, respectively, for scaled impact parameters $\hat{b}$ = 0, 0.3, 0.6. Different symbols are for free nucleons, LCP's and IMF's.

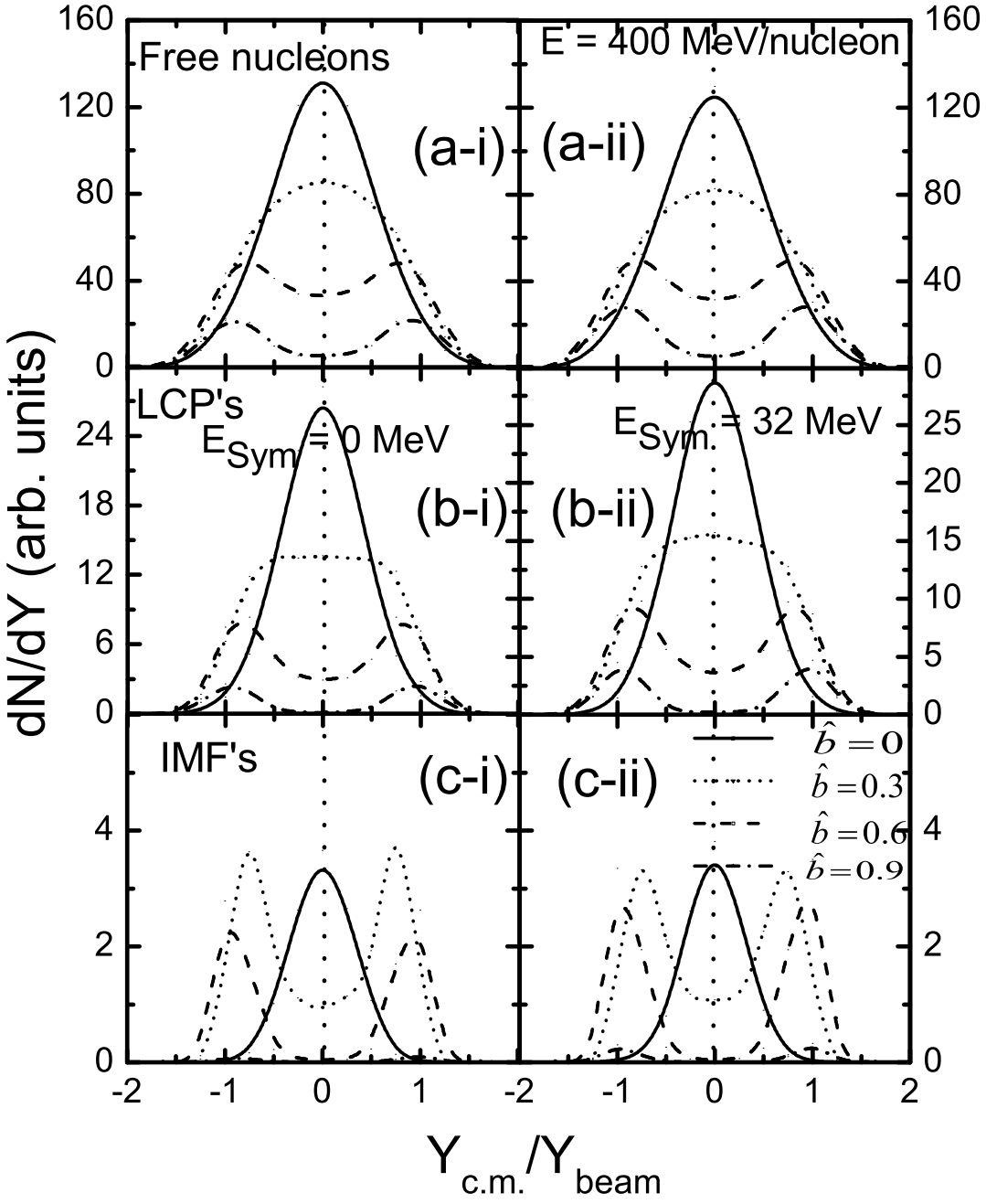

Figure 6.3: The rapidity distribution $\frac{dN}{dY}$ as a function of reduced rapidity for free nucleons(a), LCP's (b) and IMF's(c) at different impact parameters. The reaction under study is ${}_{54}Xe^{131}$ + ${}_{54}Xe^{131}$ at incident energy E = 400 MeV/nucleon. The left and right panels are with (ii) and without symmetry energy (i).

6.4.1 The phase space of fragments

In Fig.6.2, we display the final phase space of a single event of $_{54}Xe^{131}$ + $_{54}Xe^{131}$ at incident energy of 400 MeV/nucleon, with and without symmetry energy. The top, middle and bottom panels are at $\hat{b}$ = 0, 0.3 and 0.6, respectively. Here phase space of free particles [A =1], light charged particles (LCP's) [2≤A≤4] and intermediate mass fragments(IMF's)[5≤ A ≤ 44] is displayed. We note that irrespective of the symmetry energy, central collisions lead to complete spherical distribution of particles, indicating, spreading of the nucleons in all directions. It means that breaking of initial correlations among nucleons is maximal in this region and, as a result, more randomization and stopping in the hot and compressed nuclear matter occurs. This effect seems to decrease with impact parameter. Since free particles as well as LCP's originate from the mid-rapidity region, they are better suited for studying the degree of stopping reached in a heavy-ion collision. On the other hand, IMF's seems to originate either from the target or from the projectile region, therefore, are the remnant/residue of the spectator matter. This observation is in agreement with many other studies [7, 8, 31].

6.4.2 The rapidity distribution

To further quantify this observation, we display in Fig.6.3, the rapidity distribution $\frac{dN}{dY}$ for the emission of free nucleons as well as LCP's and IMF's. We see that free particles and LCP's emitted in the central collisions form a single narrow Gaussian shape, whereas, IMF's have broader Gaussian, indicating less thermalization. As we increase impact parameter, single Gaussian distribution splits into two Gaussian (at target and projectile rapidities), indicating correlated matter. From the shape of the Gaussian, one sees that free particles and LCP's are better indicator of thermal source. Obviously, this condition is necessary, but, not a sufficient one.

From the figure, it is also evident that the symmetry energy does not plays significant role for the rapidity distribution. The peak value of the Gaussian for LCP's is altered by about 10%, whereas, nearly no effect is seen in the case of intermediate mass fragments. The reason is that LCP's can feel the role of mean field directly, while, the heavy fragments have

weak sensitivity [32]. From the figure, one sees a one to one relation between the degree of stopping and emission of LCP's. These conclusions match with the findings of Fig.6.2 and Ref.[8].

6.4.3 Impact parameter dependence of fragments and nuclear stopping

In Fig.6.4, we display impact parameter dependence of global variables (R and $Q_{zz}/nucleon$), whereas, the multiplicity dependence of free nucleons and LCP's is displayed in Fig.6.5. The displayed results are at E_{Sym}= 0 and E_{Sym} = 32 MeV in each panel, while, in panel (b) the results are also displayed with isospin-dependent cross-section. The value of cross-section is denoted in the superscript. From Fig.6.4, We observe that R and $Q_{zz}/nucleon$ behave in opposite fashion i.e. R and $\frac{1}{Q_{zz}/nucleon}$ will behave in a similar fashion. For $R > 1$ and $Q_{zz}/nucleon < 0$, it can be explained by the preponderance of momentum flow perpendicular to the beam direction[33]. The maximum stopping is observed around 400 MeV/nucleon, which is in supportive nature with the findings of W. Reisdorf *et al.*[27]. In their work, they measured the nuclear stopping from 0.090 to 1.93 GeV/nucleon and maximal stopping was observed around 400 MeV/nucleon. It is clear that if the reaction reaches the maximal stopping around certain energies, the matter formed in the reaction should reach minimum transparency and thus most of the particles are preferentially out-of-plane. On the other hand, no visible effect is seen for symmetry energy term. We see both quantities are nearly independent of the symmetry energy, while, strongly depends on the isospin-dependent cross-section.

As we know, major contribution for the stopping of nuclear matter is from the hot and compressed region, where symmetry energy does not play any role. Some small spikes can be seen at lower beam energies, however, outcome is independent of the symmetry energy at higher incident energies. This is due to the fact that above the Fermi energy, incident energy itself is sufficient to break the initial correlations among the nucleons. On the other hand, isospin-dependent cross-section will lead to violent N-N collisions, which further cause the transformation of the initial longitudinal motion in other directions and hence thermalization of the system. This dominant role played by the isospin-dependent cross-section

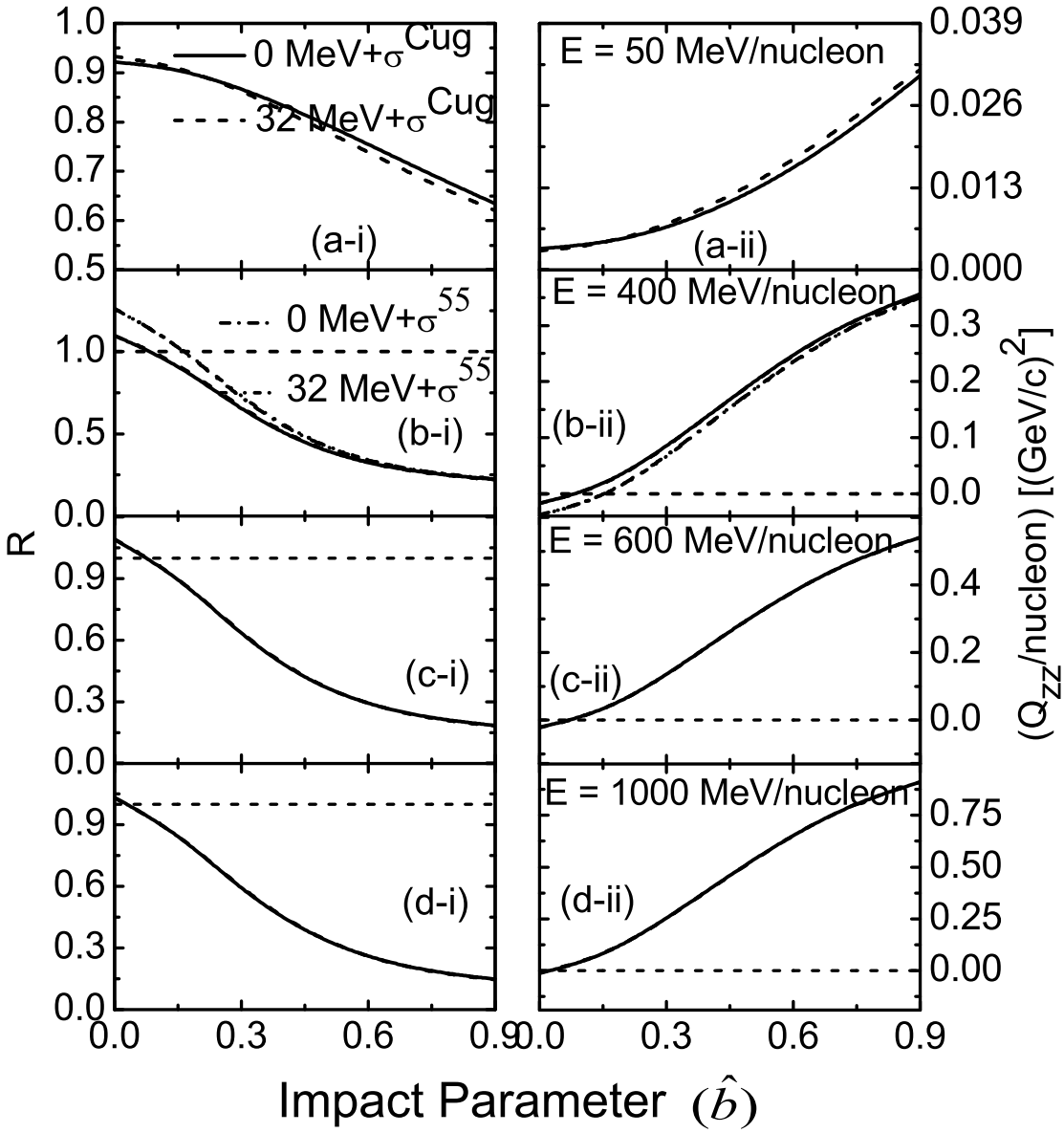

Figure 6.4: The anisotropy ratio R (i) and quadrupole moment ($Q_{zz}/nucleon$) (ii) as a function of normalized impact parameter with and without symmetry energy. In panel (b), the results are also displayed with isospin-dependent cross-section (55mb). The panels from top to bottom are at incident energy of 50 (a), 400 (b), 600 (c) and 1000 MeV/nucleon (d), respectively.

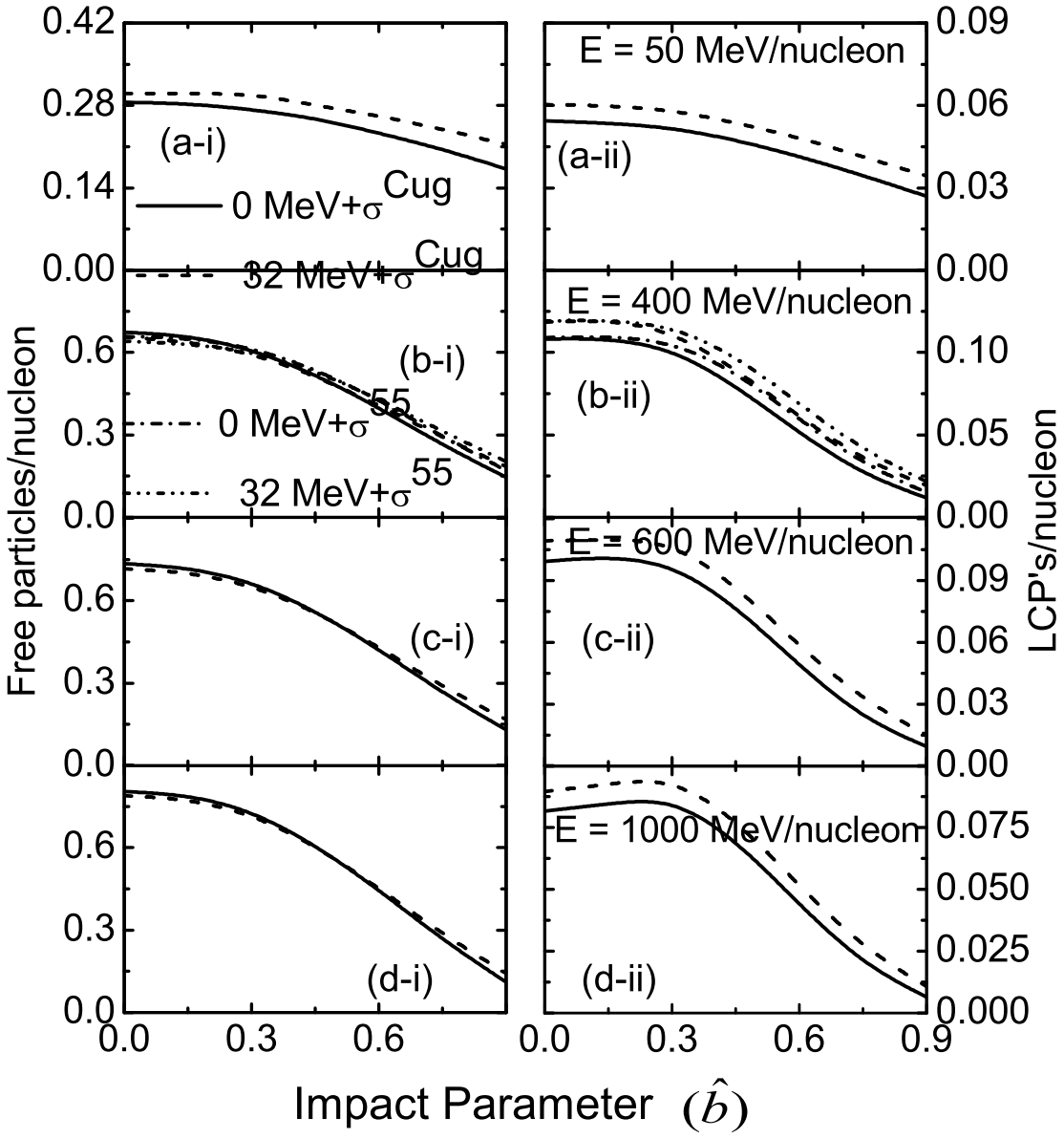

Figure 6.5: Same as in Fig.6.4, but for the multiplicity of free particles/nucleon and LCP's/nucleon.

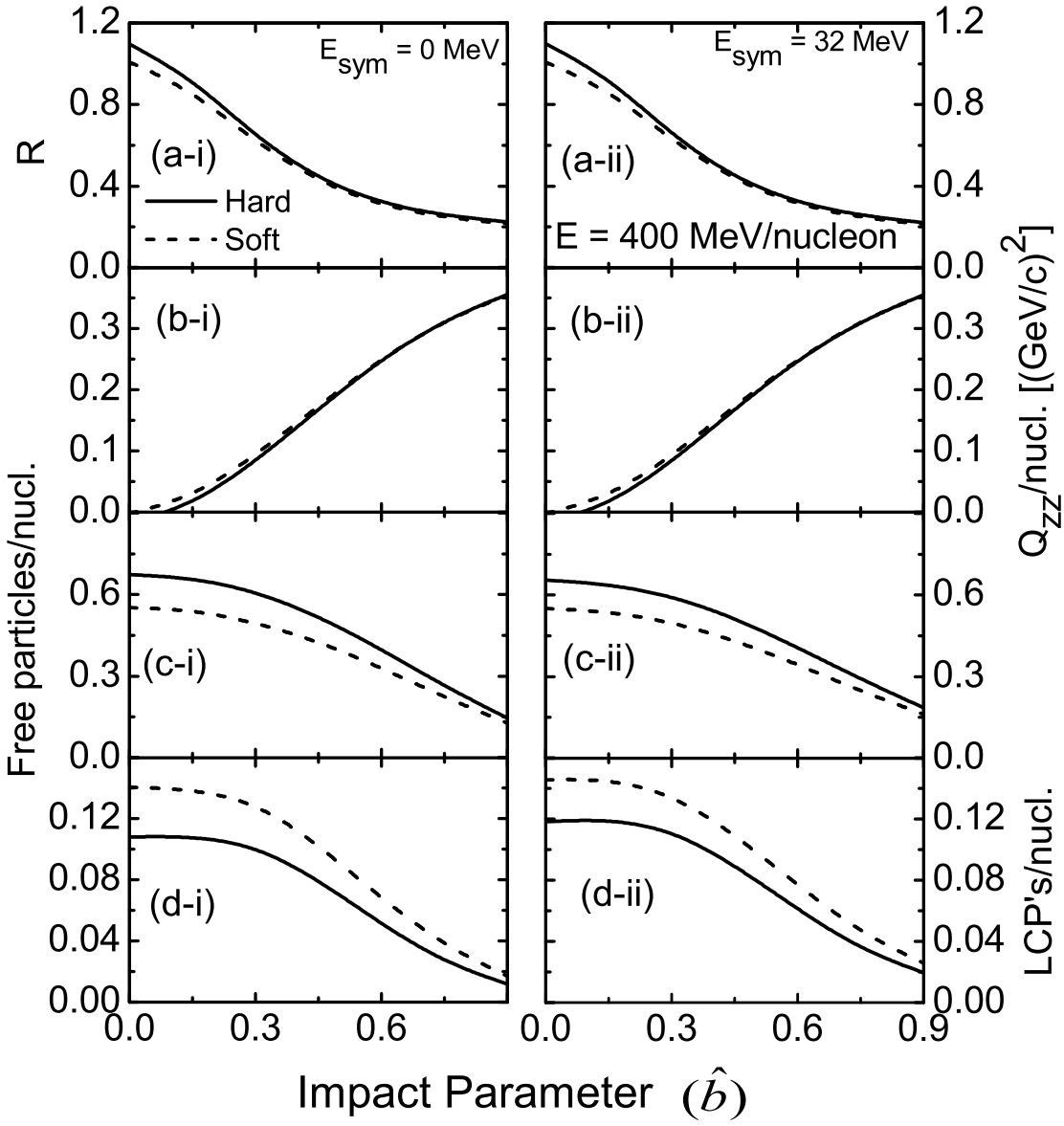

Figure 6.6: Impact parameter dependence of (a) R, (b) $Q_{zz}/nucleon$, (c) free particles/nucleon, (d) LCP's/nucleon, with hard (H) and soft (S) equations of state. The results are displayed at $E_{Sym} = 0$ (i) and 32 MeV (ii).

gradually disappears with increase in the impact parameter. As discussed earlier, stopping is the phenomena which originates from the participant zone and this zone goes on decreasing with increase in the impact parameter and hence the effect of cross-section on nuclear stopping. These findings are also in supportive nature with the findings of Liu *et al.,* [16].

To correlate the degree of stopping with the multiplicity of fragments, we display in Fig.6.5, the impact parameter dependence of the multiplicity of free nucleons as well as of LCP's. The behavior of all curves is similar to that of nuclear stopping parameters R and $\frac{1}{Q_{zz}/nucleon}$, as discussed in Fig.6.4. In addition, LCP's are more sensitive towards symmetry energy compared to free particles. Due to pairing nature of LCP's, symmetry energy term $\propto (N-Z)^2$ contributes considerably. The effect of isospin-dependent cross-section is more visible for the LCP's as compared to free particles. This also gives us clue that LCP's production can act as a indicator for the nuclear stopping. Moreover, free particles/nucleon are found to increase monotonically with the incident energy, while LCP's/nucleon behave in similar fashion as that of nuclear stopping i.e. maximum around 400 MeV/nucleon and then decreases. It is also evident from Ref.[8], LCP's production act as a barometer for nuclear stopping compared to the free particles.

In Fig.6.6, we have checked the sensitivity of nuclear stopping as well as fragment production with the nuclear equation of state (EOS). For this purpose, a hard (H) and soft (S) equations of state with compressibility κ = 380, 200 MeV are employed, respectively. The nuclear stopping is found to be weakly dependent on the equations of state, while, the fragments production is sensitive to different equations of state. It means that the fragment production with different equations of state can act as a global indicator for the nuclear stopping as it is weakly dependent on equations of state.

6.4.4 System mass and isospin asymmetry dependence

It also becomes important to study the system size dependence and isospin asymmetry of R, $\frac{1}{Q_{zz}/nucleon}$, free particles and LCP's. For this, in Fig.6.7, we have displayed the results for the reactions of ${}_{20}Ca^{40}$ + ${}_{20}Ca^{40}$, ${}_{28}Ni^{58}$ + ${}_{28}Ni^{58}$, ${}_{41}Nb^{93}$ + ${}_{41}Nb^{93}$, ${}_{54}Xe^{131}$ + ${}_{54}Xe^{131}$ and ${}_{79}Au^{197}$ + ${}_{79}Au^{197}$, in which Z as well as A is varied. On the other hand, results are displayed, in Fig.6.8, for the reactions of ${}_{20}Ca^{34}$ + ${}_{20}Ca^{34}$ (N/Z = 0.7), ${}_{20}Ca^{40}$ + ${}_{20}Ca^{40}$

(N/Z = 1), $_{20}Ca^{48}$ + $_{20}Ca^{48}$ (N/Z = 1.4) and $_{20}Ca^{57}$ + $_{20}Ca^{57}$ (N/Z = 1.85), having same Z and different A, in the presence of symmetry energy and isospin-dependent cross-section. The curves in Figs.6.7 and 6.8 are parametrized with the power law $Y = CX^{\tau}$, where C and τ are constants, while X and Y are the respective parameters on X and Y axis.

From the Fig.6.7, it is observed that the parameters R, $\frac{1}{Q_{zz}/nucleon}$, free particles as well as LCP's are in similar trend with the composite mass of the system. All the parameters are found to increase with the composite mass of the system. For a fixed geometry (semi-central here), more heavier is the composite system, more hot is the compressed zone, which further results in more thermalization or global stopping. Looking the parallel side, the free particles and LCP's will always originate from the participant zone. With an increase in the composite mass of the system, the participant zone goes on increasing for a fixed geometry (semi-central here) and hence the production of free particles and LCP's. Similar findings are also published in the Ref.[16, 28].

The dependence of these parameters on the isospin asymmetry (N/Z dependence) displayed, in Fig.6.8, is also found to be supportive in nature with the findings in Fig.6.7. An increase in the number of neutrons will increase the number of collisions and hence dominance of R, $\frac{1}{Q_{zz}/nucleon}$, free particles as well as LCP's is observed with increase in N/Z ratio. Nuclear stopping as well as LCP's are observed to be strongly dependent on the isospin-dependent cross-section. Similar results with isospin dependent cross-section are observed in Figs.6.4 and 6.5. From here, one may conclude that the nuclear stopping and LCP's can also be used as a tool to investigate the isospin-dependent cross-section.

6.4.5 Normalization of fragments production with stopping parameters

To further elaborate this point, we display in Fig.6.9, Multiplicity/nucleon (free and LCP's) as well as R and $\frac{1}{Q_{zz}/nucleon}$. Once free nucleons and LCP's are normalized with R at the starting point of impact parameter, we see that their behavior with respect to impact parameter is similar to that of anisotropy ratio, whereas, visible difference occurs with reference to quadrupole moment. As seen in Fig.6.2, the LCP's are emitted from the mid-rapidity where initial correlations and memory of nucleons is completely destroyed. In

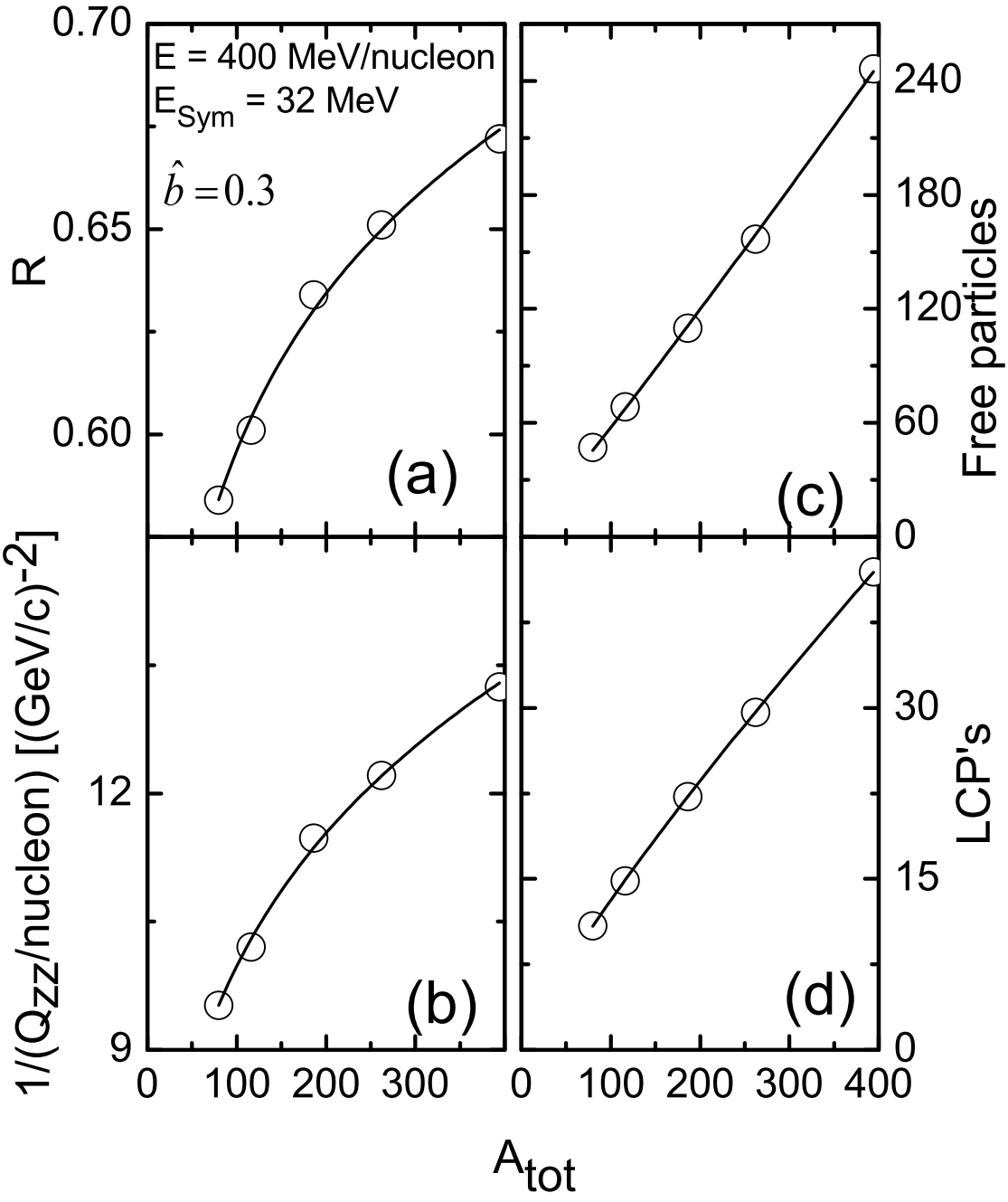

Figure 6.7: System size dependence of (a) R, (b) $\frac{1}{Q_{zz}/nucleon}$, (c) free particles, (d) LCP's, in the presence of symmetry energy. All the curves are fitted with power law.

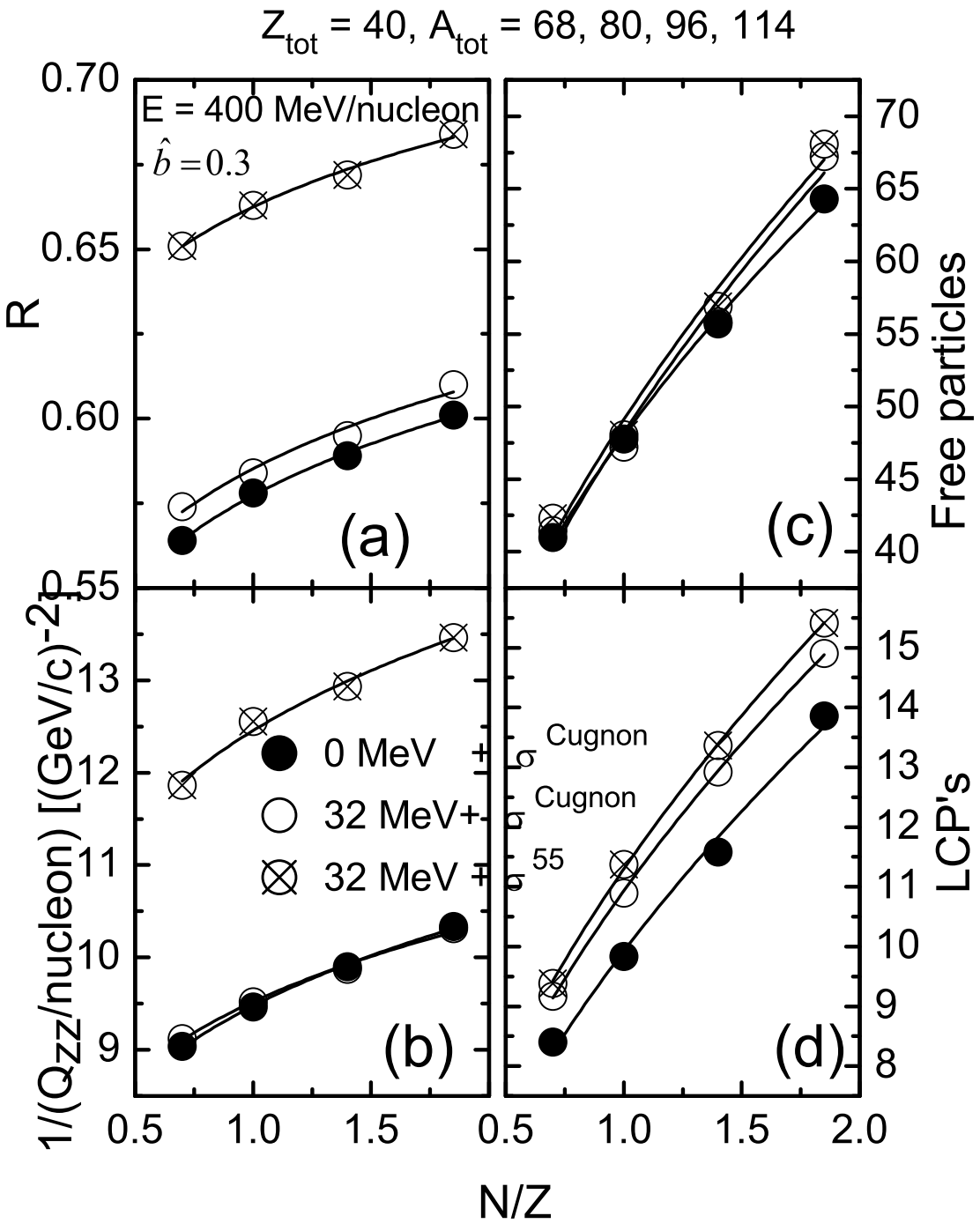

Figure 6.8: Isospin asymmetry of (a) R, (b) $\frac{1}{Q_{zz}/nucleon}$, (c) free particles, (d) LCP's, in the presence of symmetry energy and isospin-dependent cross-section (55 mb).

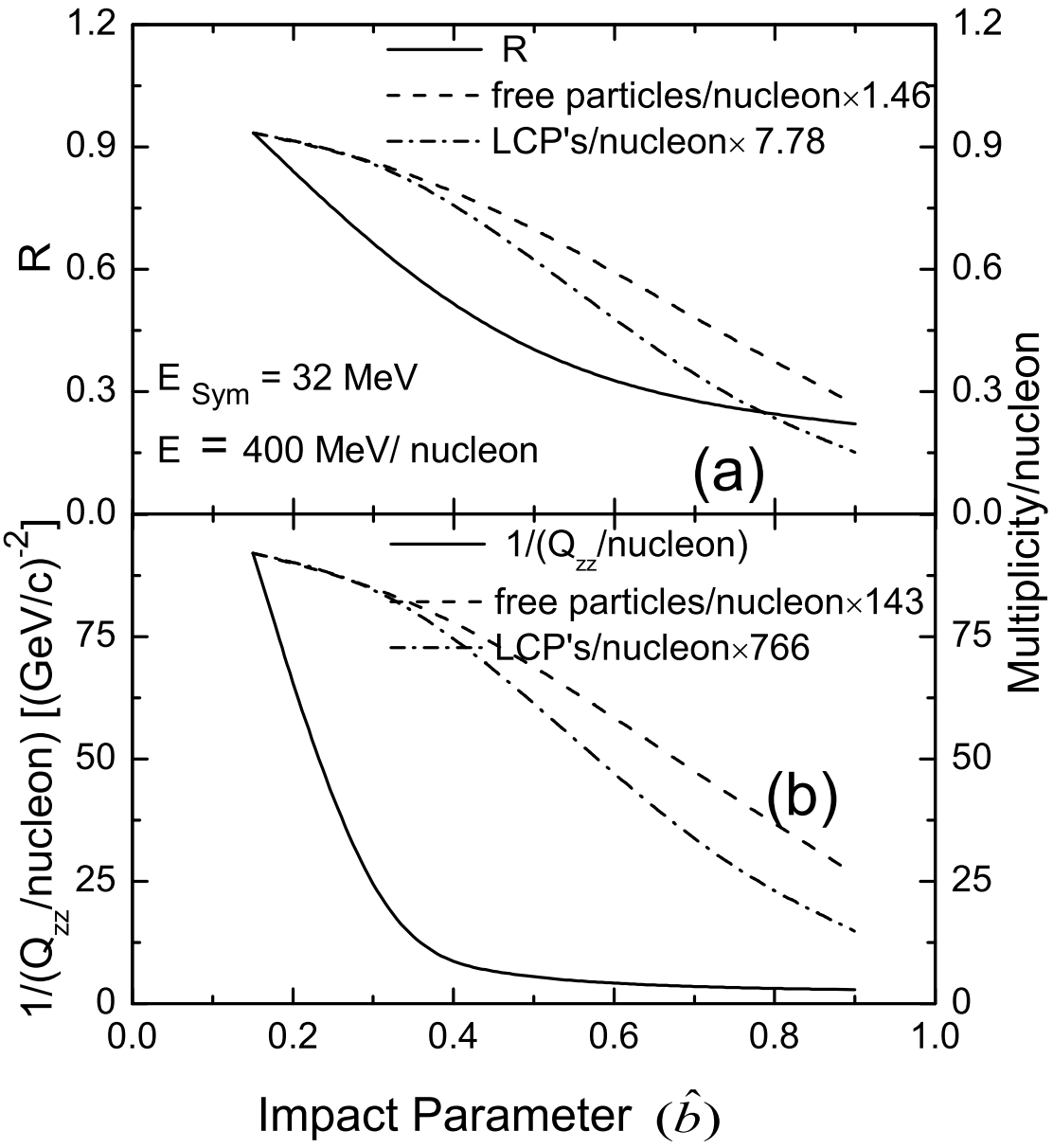

Figure 6.9: The scaled free particles/nucleon and LCP's/nucleon along with anisotropy ratio R (a) and $\frac{1}{Q_{zz}/nucleon}$(b) as a function of normalized impact parameter in the presence of symmetry energy. The reaction is at incident energy 400 MeV/nucleon.

the presence of symmetry energy, due to the pairing nature of LCP's, breakup of the initial correlations gets enhanced. The nuclear stopping (R and $1/Q_{zz}$) is also a direct indicator of breaking of the initial correlations and erasing the memory of nucleons. As is seen, in addition to impact parameter dependence, system mass and isospin asymmetry dependence is quite similar in all the cases. This similarity in all three quantities in the presence of symmetry energy makes LCP's good indicator of global stopping in heavy-ion collisions. Therefore all the three quantities in principle are general quantities to study the global stopping.

6.4.6 Effect of symmetry energy and momentum dependent interactions on nuclear stopping

For this particular study, simulations were carried out for the above mentioned reactions of $X + X$ (where X = Ca, Ni, Nb, Xe and Au) at different beam energies ranging between 30 and 1000 MeV/nucleon at central and semi-peripheral geometries. The incident energy of 30 MeV/nucleon is the lowest limit for any semi-classical model. Below this incident energy, quantum effects as well as Pauli blocking need to be redefined. A hard (H) and hard momentum dependent (HM) equation of state (EOS) has been employed with symmetry energy $E_{sym} = 0$ and 32 MeV. The corresponding values of the symmetry energy are indicated as subscript. It is worth mentioning that global stopping is insensitive toward the nature of static equation of state. Though MDI destabilizes the nuclei, a careful analysis is made by Puri *et al.* [34] and found that upto 200 fm/c, emission of the nucleons with momentum dependent interactions is quite small.

In Fig. 6.10, we display the time evolution of the anisotropy ratio R for the central collisions of ${}_{20}Ca^{40} + {}_{20}Ca^{40}$ (left panel) and ${}_{79}Au^{197} + {}_{79}Au^{197}$ (right panel). The incident energies of 30, 50, 400 and 1000 MeV/nucleon are employed using the four different equations of state H_0, H_{32}, HM_0 and HM_{32}. Interestingly, the anisotropy ratio R, though, is insensitive towards the symmetry energy, shows appreciable effect for the momentum dependent interactions. As we go higher in the incident energy, both effects (of momentum dependent interactions as well of symmetry energy) wash away. For further test, we simulated two reactions (i) ${}_{20}Ca^{40} +_{20} Ca^{40}$ and kept the same N/Z ratio by taking ${}_{100}X^{200} +_{100} X^{200}$

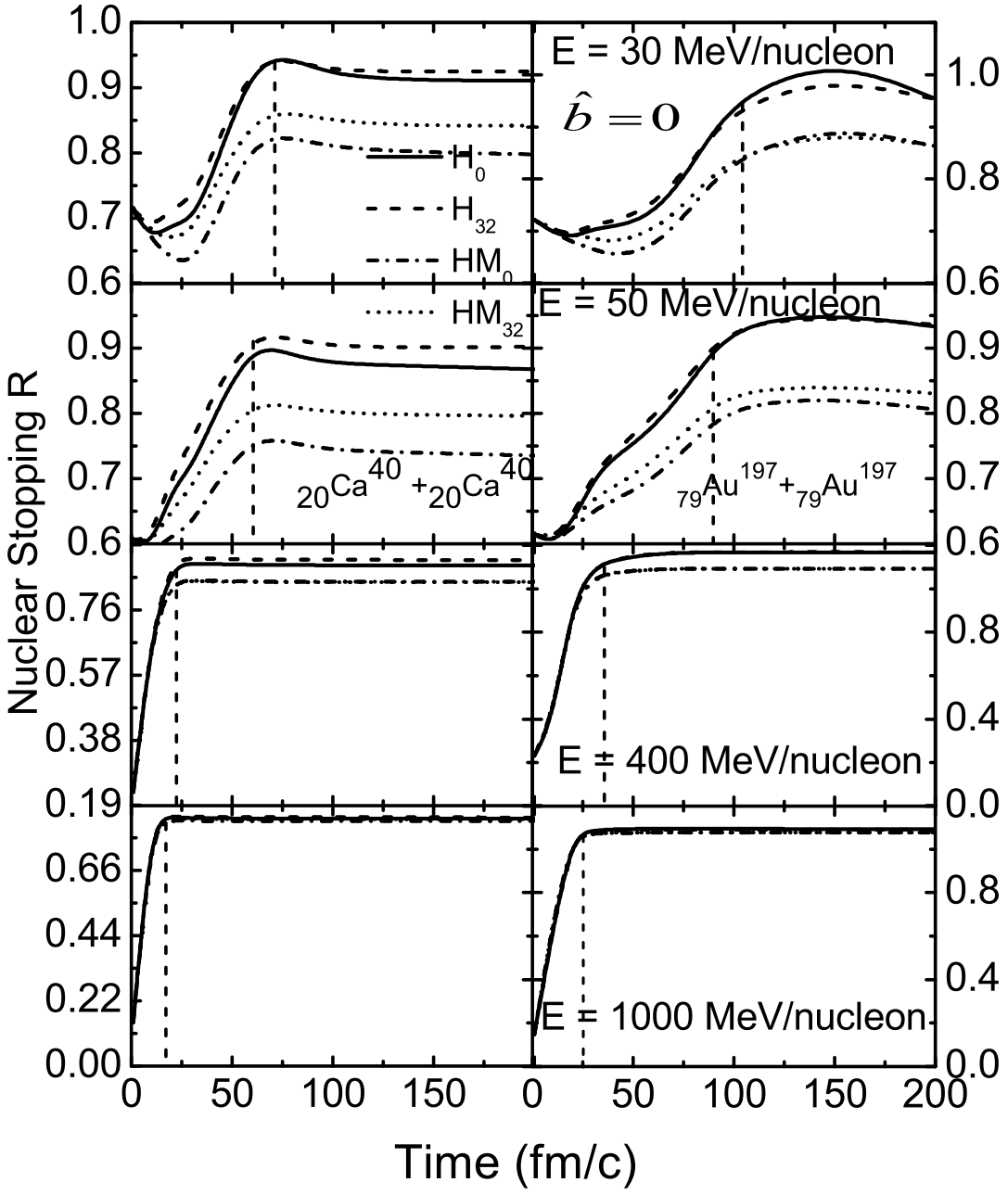

Figure 6.10: The time evolution of anisotropy ratio R for the reactions of $_{20}Ca^{40} +_{20} Ca^{40}$, and $_{79}Au^{197} +_{79} Au^{197}$. The panels from top to bottom represent the scenario at beam energies 30, 50, 400 and 1000 MeV/nucleon, respectively.

reaction. In other case (ii) we took neutron rich reaction ${}_{79}Au^{197} +_{79} Au^{197}$ and simulated the reactions of ${}_{16}X^{40} +_{16} X^{40}$ by keeping N/Z ratio again same. In both the cases, the above trend holds good. Therefore, indicating that the above behavior is universal. Even rapidity cuts to mid-rapidity region do not yield different results. Below the beam energy of 50 MeV/nucleon, collision dynamics is governed by the mean field. Therefore, interactions involving isospin particles like nn, np, pp dominate the outcome and hence symmetry effects are visible. Above the Fermi energy, dynamics is dominated by the NN collisions and hence these effects washes away.

As discussed earlier, R approaches to 1 at low incident energies, indicating the isotropic nucleon momentum distribution of the whole composite system. The behavior at 30 MeV/nucleon is little different due to the fact that binary collisions do not play any role and mean field will take larger time to thermalize the colliding nuclei. As beam energy increases above the certain energy, R starts decreasing from 1 towards the lower values, indicating partial transparency. This value of the beam energy, above which R starts decreasing, depends on the size of the system. In our observations for the reaction of ${}_{79}Au^{197} + {}_{79}Au^{197}$, it is close to 400 MeV/nucleon. This finding is similar to the one reported by W. Reisdorf *et al.* [28]. The value of $R > 1$, can be explained by the preponderance of momentum perpendicular to beam direction [33]. This is true for all equations of state. It is also seen that relaxation time decreases with the increase in the beam energy, while, increases with the increase in the mass of the colliding system. It shows that high beam energy and lighter systems lead to more violent NN collisions and faster dissipation. This is consistent with the isospin equilibrium process as shown by Li et.al. [9].

It will be of further interest to see whether the above findings have mass dependence or not. This is particularly important since the role of the momentum dependent interactions and the symmetry energy depends on the size of the system. For this, we display in Fig. 6.11, the anisotropy ratio R as a function of the composite mass of the system ($A_{tot} = A_T + A_P$) at different beam energies ranging from 30 to 1000 MeV/nucleon. The left panel represents the results at central geometry, while, right panel is at semi-peripheral geometry.

Our findings are:

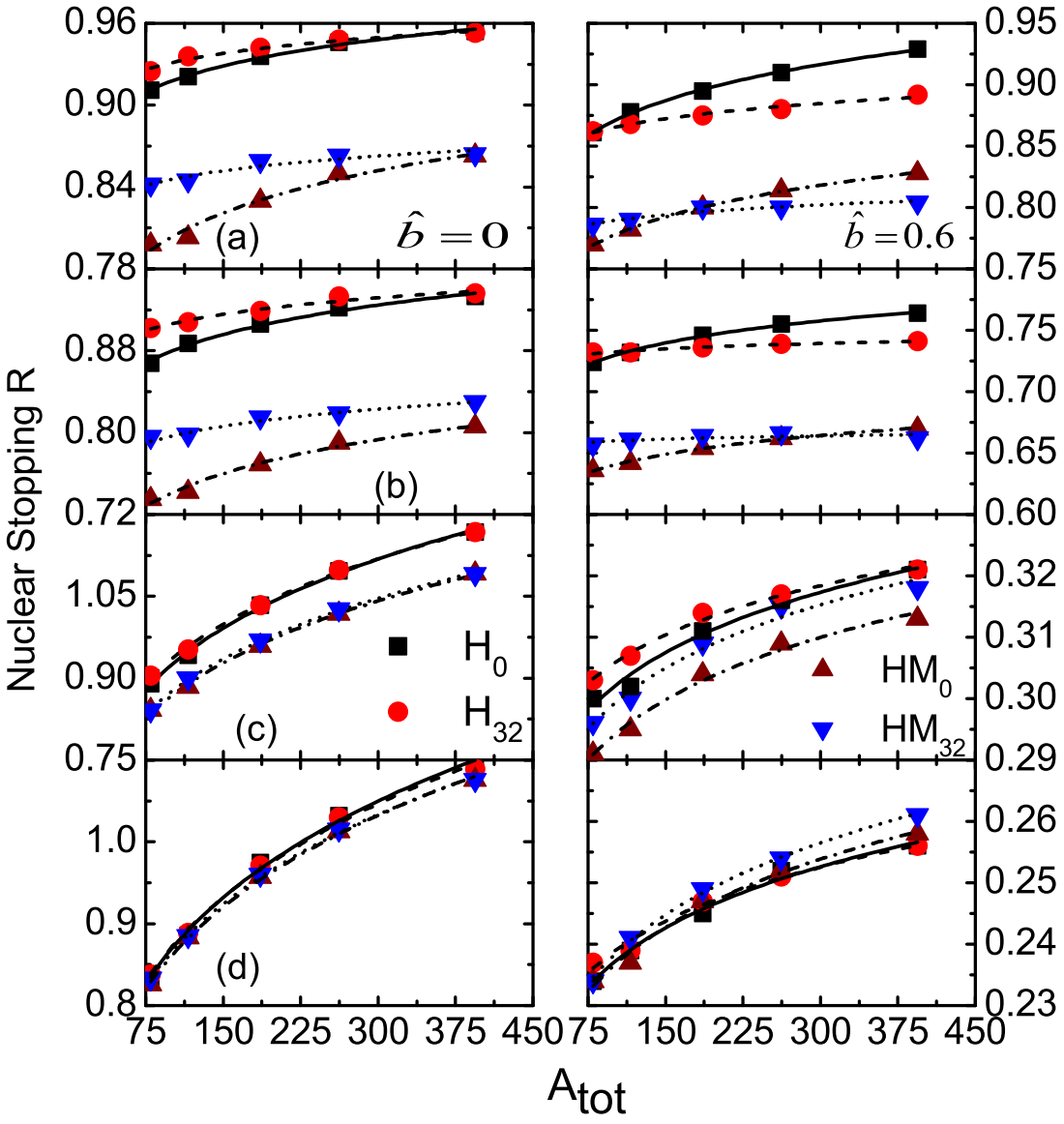

Figure 6.11: The final state anisotropy ratio R as a function of composite mass of the system A_{tot} for different equations of state (discussed in text). The left and right panels are at central and semi-peripheral geometries. The panels labeled with a, b, c and d are at E= 30, 50, 400 and 1000 MeV/nucleon, respectively. All the curves are fitted with power law.

- The anisotropy ratio R increases with the composite mass of the system. This is true for all incident energies and impact parameters. This dependence weakens as one moves from central to semi-peripheral geometry. It is due to the fact that nuclear stopping is governed by the participant zone only. This is further supported by the fact that at higher incident energies e.g. E = 1000 MeV/nucleon, stopping is almost independent of the composite mass of the system at semi-peripheral geometry and almost 50% decrease is observed in the nuclear stopping as compared to central geometry.

- The effect of the symmetry energy is visible below the Fermi energy. Same conclusion was also reported in Fig. 6.10. The effect of the symmetry energy diminishes in the absence of momentum dependent equation of state. Moreover, this effect weakens at semi-peripheral geometries.

- The importance of momentum dependent interactions is also visible in the nuclear stopping. This effect decreases as one moves from the low to higher incident energy and from central to peripheral geometry. At the higher incident energies e.g. at E = 1000 MeV/nucleon, the anisotropy ratio is independent of the equation of state and symmetry energy. It is worth mentioning that the inclusion of momentum dependent interactions is found to suppress the binary collisions and as a result is found to affect the sub threshold particle production as well as disappearance of collective flow [10, 14].

6.5 Summary

In summary, using the isospin-dependent quantum molecular dynamics (IQMD)model, we investigate the emission of free particles, LCP's, and degree of stopping reached in a heavy-ion collisions in the presence of symmetry energy and isospin dependent cross-section. In addition, impact of momentum dependent interactions in the presence of symmetry energy is also studied on the nuclear stopping. We observe that impact parameter dependence, equa-

tions of state dependence as well as system size and isospin asymmetry dependence have similar behavior for the light charged particles and nuclear stopping parameters. Nuclear stopping in term of anisotropy ratio and quadrupole moment depends weakly on the symmetry energy and strongly on the isospin-dependent cross-section. However, the symmetry energy and isospin-dependent cross-section has an effect of 10% on the LCP's production. This means nuclear stopping and LCP's production can be used as a tool to investigate the isospin-dependent cross-section. One can say that LCP's production is found to be highly correlated with the global stopping.

On the other hand, the role of symmetry energy and momentum dependent interactions on the nuclear stopping is observed at low incident energies. These effects are found to vanish at higher incident energies. The role of symmetry energy at low incident energy get enhanced in the presence of momentum dependent interactions. Further, we can conclude that maximum stopping is obtained for the heavier systems at low incident energies in central collisions in the absence of momentum dependent interactions implying that momentum dependent interaction suppresses the nuclear stopping.

Bibliography

[1] R. K. Puri, Ph.D Thesis, Panjab University, Chandigarh, India (1990) and refrences within.

[2] J. R. Birkelund, J. R. Huizenga, J. N. De, and D. Sperber, Phys. Rev. Lett. **40**, 1123 (1978); A. Bonasera, Phys. Rev. C **34**, 740 (1986); J. N. De and W. Stocker, Phys. Rev. C **42**, R819 (1990); M. M. Majumdar, J. N. De, C. Samanta, and S. K. Sammander, Phys. Rev. C **48**, 2093 (1993).

[3] P. B. Price *et al.,* Phys. Rev. C **46**, 1939 (1992); Z. Ren, C. Xu, and Z. Wang, Phys. Rev. C **70**, 034304 (2004).

[4] C. Yanhuang, A. Smerzi, and M. D. Toro, Phys. Rev. C **50**, 2809 (1994); Z. H. Liu, X. Z. Zhang, and H. Q. Zhang, Phys. Rev. C **68**, 024305 (2003); C. Beck, N. Keeley, and A. Diaz-Torres, Phys. Rev. C **75**, 054605 (2007).

[5] H. Stöcker and W. Greiner, Phys. Rep. **137**, 277 (1986); A. D. Sood and R. K. Puri, Phys. Rev. C **69**, 054612 (2004); D. J. Megestro *et al.,* Phys. Rev. C **61**, 021602(R) (2000); P. Danielewicz, R. Lacey, and W. G. Lynch, Science **298**, 1592 (2002); J. Lukasik *et al.,* Phys. Lett. B **608**, 223 (2005); X. F. Luo, M. Shao, X. Dong, and C. Li, Phys. Rev. C **78**, 031901 (2008).

[6] J. Aichelin, Phys. Rep. **202**, 233 (1991).

[7] J. Singh, S. Kumar, and R. K. Puri, Phys. Rev. C **62**, 044617 (2000); A. Le Fevre and J. Aichelin, Phys. Rev. Lett. **100**, 042701 (2008); Y. K. Vermani and R. K. Puri, Eur. Phys. Lett. **85**, 62001 (2009); S. Kumar, S. Kumar, and R. K. Puri, Phys. Rev. C **78**, 064602 (2008).

[8] J. K. Dhawan, N. Dhiman, A. D. Sood, and R. K. Puri, Phys. Rev. C **74**, 057901 (2006) and the refrences within; P. B. Gossiaux and J. Aichelin, Phys. Rev. C **56**, 2109 (1997).

[9] B. A. Li and S. J. Yennello, Phys. Rev. C **52**, R1746 (1995); H. Johnston, T. White, J. Winger, D. Rowland, B. Hurst, F. G. Nogues, D. Okelly, and S. J. Yennello, Phys. Lett. B **371**, 186 (1996); B. A. Li, C. M. Ko, and W. Bauer, Int. J. Mod. Phys. E **7**, 147 (1998); S. J. Yennello *et al.,* Phys. Lett. B **321**, 15 (1994); M. D. Toro *et al.,* Prog. Nucl. Part. Phys. **42**, 125 (1999).

[10] R. K. Puri *et al.,* Nucl. Phys. A **575**, 733 (1994); R. K. Puri *et al.,* Phys. Rev. C **54**, R28 (1996); R. K. Puri *et al.,* J. Comp. Phys. **162**, 245 (2000).

[11] P. B. Gossiaux *et al.,* Nucl. Phys. A **619**, 379 (1997); S Kumar *et al.* Phys. Rev. C **58**, 3494 (1998); C Fuchs *et al.,* J. Phys. G: Nucl and Part. **22**, 131 (1996).

[12] W. Zhan *et al.,* Int. J. Mod. Phys. E **15**, 1941 (2006); Y. Yano, Nucl. Inst. Meth. B **261**, 1009 (2007); http://www.gsi.de/fair/index_e.html; http://www.ganinfo.in2p3.fr/research/developments/spiral2; Whitepapers of the 2007 NSAC Long Range Plan Town Meeting, Jan., 2007, Chicago, http://dnp.aps.org.

[13] R. Arora *et al.,* Eur. Phys. J. A **8**, 103 (2000); R. K. Puri *et al.,* Phys. Rev. C **43**, 315 (1991); R. K. Puri *et al.,* Eur. Phys. J A **3**, 277 (1998); Phys. Rev. C **45**, 1837 (1992); J. Phys. G: Nucl. and Part. **18**, 903 (1992); Eur. Phys. Lett. **9**, 767 (1989); R. K. Puri *et al.,* Eur. Phys. J. A **23**, 429 (2005); S. S. Malik *et al.,* Parmana J. Phys. **32**, 419 (1989).

[14] D. T. Khoa *et al.,* Nucl. Phys. A **619**, 102 (1992); S. W.Huang *et al.,* Phys. Lett. B **298**, 41 (1993); G. Batko *et al.,* J. Phys. G: Nucl. and Part. **20**, 461 (1994); A. D. Sood *et al.,* Phys. Rev. C **70**, 034611 (2004); S. W. Huang *et al.,* Prog. Part. Nucl. Phys. **30**, 105 (1993); Y. K. Vermani *et al.,* J. Phys. G: Nucl. and Part. **37**, 015105 (2010); A. D. Sood *et al.,* Phys. Lett. B **594**, 260 (2004); E. Lehmann *et al., Z. Phys. A* **355**, 55 (1996).

[15] W. Bauer, Phys. Rev. Lett. **61**, 2534 (1988); G. F. Bertsch, G. E. Brown, V. Koch, and B. A. Li, Nucl. Phys. A **490**, 745 (1998).

[16] J. Y. Liu, W. J. Guo, S. J. Wang, W. Zuo, Q. Zhao, Y. F. Yang, Phys. Rev. Lett. **86**, 975 (2001).

[17] L. Q. Feng and L. Z. Xia, Chin. Phys. Lett. **19**, 321 (2002).

[18] J. Y. Liu, W. J. Guo, Y. Z. Xing, X. G. Li, and Y. Y. Gao, Phys. Rev. C **70**, 034610 (2004); B. A. Li, P. Danielewicz, and W. G. Lynch, *ibid.* **71**, 054603 (2005); X. F. Luo, X. Dong, M. Shao, K. J. Wu, C. Li, H. F. Chen, and H. S. Xu *ibid.* **76**, 044902 (2007); B. A. Li, W. Chen, and C. M. Ko, Phys. Rep. **464**, 113 (2008)

[19] S. Kumar and S. Kumar, Chin. Phys. Lett. **27**, 062504 (2010); S. Kumar, S. Kumar, and R. K. Puri, Phys. Rev. C **81**, 014601 (2010); 53^{rd} DAE Symosium on Nuclear Physics, IIT, Roorkee (India) **53**, 569 (2008); *ibid* 571 (2008); INS Seminar NSTD2009, Thapar University, Patiala, Oct. 10-11, (2009).

[20] C. Hartnack *et al.,* Eur. Phys. J. A **1**, 151 (1998).

[21] A. Bohr and B. R. Mottelson, Nuclear Structure **1**, (Benjamin, New York) (1969).

[22] C. F. Weizsacker, Z. f. Physik **96**, 431 (1935); H. A. Bethe and R. F. Bacher, Rev. Mod. Phys. **8**, 82 (1936)

[23] B. A. Li, C. M. Ko, and Z. Z. Ren, Phys. Rev. Lett. **78**, 1644 (1997); B. A. Li, L. W. Chen, and C. M. Ko, Phys. Rep (in press) (2010) **nucl-th 0804.3580**.

[24] P. Danielewicz, Acta Phys. Polon. B **33**, 45 (2002); B. Hong *et al.,* Phys. Rev. C **71**, 034902 (2005); T. Gaitanos, C. Fuchs, and H. H. Wolter, Phys. Lett. B **609**, 241 (2005).

[25] J. P. Bondorf *et al.,* Nucl. Phys. A **443**, 321 (1985); D. H. E. Gross, Rep. Prog. Phys. **53**, 605 (1990); L. G. Moretto and G. J. Wozniak, Annu. Rev. Nucl. Part. Sci. **43**, 379 (1993).

[26] J. Lukasik *et al.,* Phys. Rev. C **55**, 1906 (1997); *ibid* **61**, 014606 (1997); *ibid* **66**, 064606 (2002); T. Lefort *et al.,* Nucl. Phys. A **602**, 397 (2000); F. Rami *et al.,* Phys. Rev. Lett. **84**, 1120 (2000).

[27] W. Reisdorf *et al.,* Phys. Rev. Lett. **92**, 232301 (2004).

[28] W. Reisdorf *et al.,* Phys. Lett. B **595**, 118 (2004).

[29] C. Y. Wong, *Introduction to High-Energy Heavy-Ion Collisions* (World Scientific, Singapore, 1994).

[30] S. Kumar and R. K. Puri, Phys. Rev. C **58**, 1618 (1998); C. Liewen, Z. Fengshou, and J. Genming, Phys. Rev. C **58**, 2283 (1998); K. Chen, Z. Fraenkel, G. Friedlander, J. R. Grover, J. M. Miller, and Y. Shimamoto, Phys. Rev. **166**, 949 (1968).

[31] J. K. Dhawan and R. K. Puri, Eur. Phys. J. A **33**, 57 (2007).

[32] T. Z. Yan, X. G. Ma, X. Z. Cai, D. Q. Feng, W. Guo, C. W. Ma, W. Q. Shen, W. D. Tian, and K. Wang, Chin. Phys. **16**, 2676 (2007).

[33] R. E. Renforolt *et al.,* Phys. Rev. Lett. **53**, 763 (1984).

[34] J. Singh , S. Kumar, and R. K. Puri, Phys. Rev. C **63**, 054603 (2001); A. D. Sood and R. K. Puri, Eur. Phys. J. A **30**, 571 (2006); S. Kumar and R. K. Puri, Phys. Rev. C **60**, 054607 (1999); Y. K. Vermani *et al.,* Phys. Rev. C **79**, 064613 (2009).

Chapter 7

Summary and outlook

"I may not have gone where I intended to go, but I think I have ended up where I needed to be.".....*Douglas Adams* (1952-2001).

7.1 Summary

In this thesis, a theoretical study of multifragmentation and related phenomenas like elliptical flow and nuclear stopping in intermediate energy heavy-ion collisions was presented. The quantum molecular dynamics (QMD) and isospin-dependent quantum molecular dynamics (IQMD) model was used to generate the phase-space of nucleons. The phase space was, then, analyzed using the different clusterization algorithms to get the useful information about different phenomena's mentioned above.

After an introduction to the field of heavy-ion physics and various phenomena's like multifragmentation, elliptical flow, nuclear stopping and isospin physics, we discussed in **chapter 1**, the various experimental and theoretical attempts to study these phenomena's. The detail of various theoretical models was discussed in **chapter 2**. We discussed, in particular, the QMD and IQMD model, which were used for the present study.

In **chapter 3**, Using quantum molecular dynamics (QMD) model, we studied the role of momentum dependent interactions in fragmentation by systematically analyzing various reactions at incident energies between 50 and 1000 MeV/nucleon and over full collision geometry. The lighter colliding nuclei generates less density whereas higher density is achieved by heavier nuclei. Moreover, momentum dependent interactions create more repulsion in-

side the compressed nuclear matter. This gives ample space for compression-decompression as well as radial expansion. We have found that the inclusion of momentum dependent interactions leads to less freeze-out density and number of collisions in all colliding systems as well as at all colliding geometries. Moreover, it is also observed that at higher incident energies momentum dependent interactions are able to break-up the initial correlations among nucleons, which was earlier not possible with static equation of state. This is leading to the decrease in the production of heaviest fragment A_{max} and enhancement in the production of medium mass fragments in the presence of momentum dependent interactions. The system size effects are found to vary with reaction parameters, incident energies and momentum dependent interactions. The multiplicity of medium mass fragments is parametrized in term of a power law. This is true for a wide range of impact parameters and incident energies considered here. However, the parameter τ does not have unique value. At low incident energies, the parameter τ is close to $2/3$ suggesting the dominance of mean field that scales as $A^{2/3}$. On the other hand, no physical correlation is observed at higher incident energies for central collisions. This dependence of the parameter τ at higher incident energies can be improved by varying the model ingredients such as equations of state, method of clusterization etc., provided the power law dependence of the system size effect should exhibit.

In **chapter 4**, We have performed the comparative study of nucleon-nucleon cross sections and technical parameters, known as model ingredients, in multifragmentation by studying the symmetric and asymmetric reactions in the presence of momentum dependent interactions in Quantum Molecular Dynamical model. Our analysis, at the first instance, clearly indicates the importance of momentum dependent interactions and large cross sections for free nucleons and LCP's at semi-central as well as semi-peripheral geometries, while for MMF's and IMF's only at semi-peripheral geometries. Moreover, once the momentum dependent interactions are implemented, they tries to reduce the effect of nucleon-nucleon cross sections at higher energies as compared to static equation of state, where the effect of nucleon-nucleon cross section is large. In a comparative study with experimental findings of ALADIN and NSCL collaborations, better agreement is again obtained in the presence of momentum dependent interactions and large cross section for symmetric as well as asym-

metric systems. Interestingly when this study is extended with technical parameters, known as model ingredients, (like Gaussian width, Clusterization algorithm, clusterization distance as well as equations of state) at constant nucleon-nucleon cross section, the results are found to vary in the same fashion as were with different nucleon-nucleon cross sections. We found that the effect of different cross sections is of the order of the one obtained from the model ingredients. All model ingredients affect the fragmentation pattern in a similar fashion. Lastly, one can conclude that it may not possible to pin down the magnitude of cross section from the multifragmentation until and unless the model ingredients are handled very carefully.

In **chapter 5**, we have presented the isospin dependence (in term of symmetry energy) and the disappearance of elliptical flow in the presence of isospin-dependent quantum molecular dynamics (IQMD) model at intermediate energies for the several systems. The isospin dependence of the elliptical flow is studied in term of the transverse momentum dependence for different kind of fragments (free nucleons, LCP's and IMF's). The free nucleons and IMF's are found to be system mass dependent for the incident energies under consideration, while LCP's are found to be isospin dependent at relative high incident energy, where role of mean field and NN collisions is equal(say E = 100 MeV/nucleon). Moreover, these isospin effects due to symmetry energy are originating from the mid-rapidity region. In other words, one can say that LCP's acts as a probe to symmetry energy.

The disappearance of elliptical flow is observed at mid-rapidity region, while no transition is observed, when integrated over entire rapidity region. This is indicating the origin of squeeze-out or out-of-plane emission is from the participant zone and not from the spectator zone. The energy at which elliptical flow disappears is, dubbed as, transition energy. This transition energy is found to be strongly dependent on the size of the system as well as size of the fragment. When comparison of excitation function of elliptical flow is made with experimental findings of INDRA, FOPI and PLASTIC BALL collaborations, the charged particles ($Z \leq 2$) are well explained by the static equation of state, while for the protons, good agreement with the inclusion of momentum dependent interactions is observed. This comparison can be explored to more accuracy by studying the effect of isospin-dependent cross sections on the excitation function of elliptical flow. Finally, the transition energy for

free nucleons and LCP's is parametrized in term of mass power law and is found to decrease with the composite mass of the system as well as with the size of the fragment.

In **chapter 6**, using the isospin-dependent quantum molecular dynamics (IQMD)model, we investigated the emission of free particles, LCP's, and degree of stopping reached in a heavy-ion collisions in the presence of symmetry energy and isospin dependent cross-section. In addition, impact of momentum dependent interactions in the presence of symmetry energy is also studied on the nuclear stopping. We observed that impact parameter dependence, equations of state dependence as well as system size and isospin asymmetry dependence have similar behavior for the light charged particles and nuclear stopping parameters. Nuclear stopping in term of anisotropy ratio and quadrupole moment depends weakly on the symmetry energy and strongly on the isospin-dependent cross-section. However, the symmetry energy and isospin-dependent cross-section has an effect of 10% on the LCP's production. This means nuclear stopping and LCP's production can be used as a tool to investigate the isospin-dependent cross-section. One can say that LCP's production is found to be highly correlated with the global stopping. On the other hand, the role of symmetry energy and momentum dependent interactions on the nuclear stopping is observed at low incident energies. These effects are found to vanish at higher incident energies. The role of symmetry energy at low incident energy get enhanced in the presence of momentum dependent interactions. Further, we can conclude that maximum stopping is obtained for the heavier systems at low incident energies in central collisions in the absence of momentum dependent interactions implying that momentum dependent interaction suppresses the nuclear stopping.

Summarizing, we have attempted to understand the phenomena of multifragmentation, elliptical flow, nuclear stopping and symmetry energy in intermediate energy heavy-ion collisions. The influence of momentum dependent interactions and nucleon-nucleon cross sections have been investigated in detail. An attempt has been made to understand the effect of isospin degree of freedom in term of symmetry energy on the elliptical flow, nuclear stopping and light charged particles. At last, the disappearance of elliptical flow is studied

in detail. The comparison with experimental findings is performed, where the data was available in literature.

7.2 Outlook

The fragments production is found to be influenced by the asymmetry of the reaction $((N-Z)/A)$ to a great extent at all incident energies. This asymmetry dependence can be better understood by using the more sophisticated models like IQMD in which neutron and proton can be separated on the basis of charges, which is not possible in QMD model. One can have another possibility to study the effect of momentum dependent interactions on the multifragmentation in the presence of stimulated annealing clusterization algorithm (SACA), which is performed in the presence of minimum spanning tree (MST) in this thesis. The elliptical flow, which is discussed in **chapter 5**, has showed a transition from in-plane to out-of-plane at certain incident energy, known as transition energy. In this chapter, the dependence of transition energy on the system mass and size of the fragment is investigated. One can elaborate the dependence of transition energy on the impact parameter, isospin-dependent cross sections, model ingredients, method of analysis, different rapidity cuts as well as different transverse momentum cuts. This can provide a challenge to the experimentalist to prove the theoretical findings. Moreover, various other higher order flows such as hexadecupole v_4 etc. can be of further interest in the future.

The thermalization of the reaction i.e. nuclear stopping can be explored by studying the average kinetic energy of the fragments in the transverse direction ($ERAT$) or by the ratio of the longitudinal (z) and transverse (y) variances of the rapidity distributions(var_{tl}).